OPTIMISED CONFIGURATION OF SENSING ELEMENTS FOR CONTROL AND FAULT TOLERANCE APPLIED TO AN ELECTRO-MAGNETIC SUSPENSION SYSTEM

by
Konstantinos Michail

A doctoral thesis submitted in partial fulfilment of the requirements
for the award of Doctor of Philosophy of
Loughborough University

October 18, 2009

to my family
and the new member, Ioannis.

στην οικογένεια μου
και στο νέο μέλος της, Ιωάννη.

Ithaca

As you set out for Ithaka,
hope the journey is a long one,
full of adventure, full of discovery.
Laistrygonians and Cyclops,
angry Poseidondo not be afraid of them:
youll never find things like that on your way
as long as you keep your thoughts raised high,
as long as a rare excitement stirs your spirit and your body.
Laistrygonians and Cyclops,
wild Poseidonyou wont encounter them
unless you bring them along inside your soul,
unless your soul sets them up in front of you.

Hope the journey is a long one.
May there be many a summer morning when,
with what pleasure, what joy,
you come into harbors seen for the first time;
may you stop at Phoenician trading stations
to buy fine things,
mother of pearl and coral, amber and ebony,
sensual perfume of every kind
as many sensual perfumes as you can;
and may you visit many Egyptian cities
to learn, and learn more, from those who know.

Keep Ithaka always in your mind.
Arriving there is what you are destined for.
But do not hurry the journey at all.
Better if it lasts for years,
so you are old by the time you reach the island,
wealthy with all you have gained on the way,
not expecting Ithaka to make you rich.

Ithaka gave you the marvelous journey.
Without her you would not have set out.
She has nothing left to give you now.

And if you find her poor, Ithaka wont have fooled you.
Wise as you will have become, so full of experience,
you will have understood by then what these Ithakas mean.

Constantine P. Cavafy (1911)

Ιθάκη

Σαν βγείς στον πηγαιμό για την Ιθάκη,
να εύχεσαι νάναι μακρύς ο δρόμος,
γεμάτος περιπέτειες, γεμάτος γνώσεις.
Τους Λαιστρυγόνας και τους Κύκλωπας,
τον θυμωμένο Ποσειδώνα μη φοβάσαι,
τέτοια στον δρόμο σου ποτέ σου δεν θα βρείς,
αν μέν΄ η σκέψις σου υψηλή, αν εκλεκτή
συγκίνησις το πνεύμα και το σώμα σου αγγίξει.
Τους Λαιστρυγόνας και τους Κύκλώπας,
τον άγριο Ποσειδώνα δε θα συναντήσεις,
αν δεν τους κουβανείς μες στην ψυχή σου,
αν η ψυχή σου δεν τους στήνει εμπρός σου.

Να εύχεσαι νάναι μακρύς ο δρόμος.
Πολλά τα καλοκαιρινά πρωϊά να είναι
που με τι ευχαρίστησι, με τι χαρά
θα μπαίνεις σε λιμένας πρωτοειδώμενους·
να σταματήσεις σ΄ εμπορεία Φοινικικά,
και τες καλές πραγμάτειες ν΄ αποκτησεις,
σεντέφια και κοράλλια, κεχριμπάρια κ΄ έβενους,
και ηδονικά μυρωδικά κάθε λογής,
όσο μπορείς πιο άφθονα ηδονικά μυρωδικά·
σε πόλεις Αιγυπτιακές πολλές να πας,
να μάθεις και να μάθεις απ΄τους σπουδασμένους.

Πάντα στο νου σου νάχεις την Ιθάκη.
Το φθάσιμον εκεί ειν΄ ο προορισμός σου.
Αλλά μη βιάζεις το ταξίδι διόλου.
Καλλίτερα χρόνια πολλά να διαρκέσει·
και γέρος πια ν΄ αράξεις στο νησί,
πλούσιος με όσα κέρδισες στον δρόμο,
μη προσδοκώντας πλούτη να σε δώσει η Ιθάκη.

Η Ιθάκη σ΄ έδωσε το ωραίο ταξίδι.
Χωρίς αυτήν δεν θάβγαινες στον δρόμο.
Άλλα δεν έχει να σε δώσει πια.

Κι αν πτωχική την βρεις, η Ιθάκη δεν σε γέλασε.
Έτσι σοφός που έγινες, με τόση πείρα,
ήδη θα το κατάλαβες η Ιθάκες τι σημαίνουν.

Κωνσταντίνος Π. Καβάφης (1911)

Contents

Abstract

New technological advances and the requirements to increasingly abide by new safety laws in engineering design projects highly affects industrial products in areas such as automotive, aerospace and railway industries. The necessity arises to design reduced-cost hi-tech products with minimal complexity, optimal performance, effective parameter robustness properties, and high reliability with fault tolerance. In this context the control system design plays an important role and the impact is crucial relative to the level of cost efficiency of a product.

Measurement of required information for the operation of the design control system in any product is a vital issue, and in such cases a number of sensors can be available to select from in order to achieve the desired system properties. However, for a complex engineering system a manual procedure to select the best sensor set subject to the desired system properties can be very complicated, time consuming or even impossible to achieve. This is more evident in the case of large number of sensors and the requirement to comply with optimum performance.

The thesis describes a comprehensive study of sensor selection for control and fault tolerance with the particular application of an ElectroMagnetic Levitation system (being an unstable, nonlinear, safety-critical system with non-trivial control performance requirements). The particular aim of the presented work is to identify effective sensor selection frameworks subject to given system properties for controlling (with a level of fault tolerance) the MagLev suspension system. A particular objective of the work is to identify

the minimum possible sensors that can be used to cover multiple sensor faults, while maintaining optimum performance with the remaining sensors.

The tools employed combine modern control strategies and multiobjective constraint optimisation (for tuning purposes) methods. An important part of the work is the design and construction of a $25kg$ MagLev suspension to be used for experimental verification of the proposed sensor selection frameworks.

Acknowledgements

This research has been done after hard work, few holidays and many sleepless nights. I could never have done it without the support of all these people at Loughborough and the fully funded studentship from the department of Electronic and Electrical Engineering which I am thankful for.

Both my supervisors, Prof. Roger Goodall and Dr. Argyrios Zolotas were very patient and supportive throughout my PhD studies. One cannot find such easy going and friendly supervisors. I would particularly like to thank them for giving me both theoretical and practical knowledge in control systems engineering.

I would also like to thank Dr. John Pearson from Systems Engineering Innovation Centre at Loughborough University for his support during my PhD studies.

I am grateful to Dr. Thomas Steffen that was very supportive with all those technical problems with MATLAB and practical implementations.

I would like to thank both supervisors of the mechanical and electronics workshops Mr. Chandrakant Mistry and Mr. Gary Wagg, for being so supportive and always helpful with the experimental MAGLEV suspension rig.

Heartfelt thanks also got to my colleagues in the control systems group including Jessica Davies, Karmjit Grewal, Samir Khan, Dr. William Garlick,

Dr. Roger Dixon and the previous group members Pete Hubbard, Dr. Guy Charles, Dr. Hairi Zamzuri and Dr. Scott Halsey.

I cannot close the acknowledgement section without thanking Dr. Ralph Gottschalg and Dr. Chris Hibberd for introducing me to the new exciting field of the concentrated Photovoltaics systems during the last months.

Last but not least thanks to my good friends here at Loughborough always willing to cool me down during difficult periods: Nikolaos Roidos, Dr. Konstantinos Kyriakopoylos, Dr. Lian Zhou and Maha El Amin Abdelgalil Mahmoud.

Finally, my family in Cyprus have been continually beside me especially during the last year of my studies. Many thanks to my Mother, Father, Sister and Brother in law.

Konstantinos Michail
Loughborough, October 18, 2009

List of Tables

List of Figures

List of Acronyms and Symbols

$(z_t - z)$	Small air gap variations
$\alpha, \beta, \zeta, \rho$	Constant parameters
ϵ	Stability margin (LSDP)
$\eta_{(z_t - z)}$	Noise from air gap measurement
$\eta_{\ddot{z}}$	Noise from acceleration measurement
$\eta_{\dot{z}}$	Noise from velocity measurement
η_b	Noise from flux measurement
η_i	Noise from current measurement
$\mathcal{F}_L(P, K)$	Lower Linear Fractional Transformation
$\mathfrak{R}$	Field of real numbers
μ_o	Permeability of air
$\Omega(.)$	Overall constraint violation function
ω_i	Soft constraint violation
$\overline{\sigma}[.]$	Maximum singular value
Φ_k	k^{th} penalised objective function
ϕ_k	k^{th} objective function

ϕ_{d_i}	Objective function for stochastic closed-loop response
ϕ_{s_i}	Objective function for deterministic closed-loop response
ψ_i	Hard constraint violation
σ	Structure singular value
$\mathbf{F}$	Feasible region
$\mathbf{S}$	Search space
$\underline{\sigma}[.]$	Minimum singular value
ξ	Small tolerance value
A, B, C, D	State space linearisation of a system
A^*	Complex conjugate transpose
A^T	Transpose of a matrix/vector
A_p	Pole face area
A_r	Track Roughness
B	Flux density
b	Small variation in flux density
B_o	Nominal flux density
d	disturbance vector
d_i	Euclidian distance
$E\{.\}, E[.]$	Expected value
e_{ss}	Steady state error
F	Force
f	Small variation in force

F_d	Disturbance force
f_f	Faults vector
F_i	Pareto front
F_o	Nominal force
f_{c_i}	Controller(s) selection criteria
f_{u_i}	User's controller selection criteria
G	Air Gap
g	Gravity acceleration constant - $9.81 m/s^2$
G_I	Self zeroing integrator transfer function
g_i	i^{th} soft constraint
h_j	j^{th} hard constraint
I	Coil current
i	Small variation in current
I_o	Nominal current
K_i	Integral gain vector
K_p	Proportional gain vector
K_r	State feedback vector
K_{LQG}	Kalman filter matrix
L_c	Mutual inductance
M_s	Total mass of magnet and load
m_s	Total mass of passengers
N_c	Number of coil's turns

N_p	Parent population (for NSGA-II)
n_r	Number of variables
N_s	Total number of sensor combinations
n_s	Total number of sensors
n_u, n_y	Number of inputs and outputs
p_c	Crossover probability
p_m	Mutation probability
P_t	Parent population
P_{t_o}	Initial parent population
Q	State weight matrix (LQR)
Q_o	Output measurements weight matrix (LQR)
Q_t	Offspring population
Q_{t_o}	Initial offspring population
R	Control weight matrix (LQR)
R_c	Magnets resistance
R_k	Penalty parameter
R_t	Combined population
R_{t+1}	New parent population
S	Double-sided power spectrum density
S_f	Sum of objective functions
t_g	Current generation number (for NSGA-II)
t_s	Settling time

$tr(.)$	trace of a given expression
$u_{coil_{noise}}$	RMS value of the noise on the input voltage
u_{coil_p}	Peak value of small variation around the operating voltage
$u_{coil_{rms}}$	RMS value of small variation around the operating voltage
u_{coil}	Small variation around the operating voltage
V	Sensor noise weighting matrix (KBF)
V_{coil}	Coil voltage
V_v	Speed of vehicle
W	Process noise weighting matrix (KBF)
W_c	Controllability grammian
W_o	Observability grammian
y_i, u_i	System's output and input
y_{rms}	Root mean square value of the output function
$z, \dot{z}, \ddot{z}$	Electromagnets position,velocity,acceleration
Z_o	Nominal electromagnet position
$z_t, \dot{z}_t, \ddot{z}_t$	Track position,velocity,acceleration
EMS	Electromagnetic Suspension
FDI	Fault Detection and Isolation
FTC	Fault Tolerant Control
GA	Genetic Algorithms
IO	Input-Output
KF	Kalman Filter

LCF	Left Coprime Factorisation
LMI	Linear Matrix Inequality
LQG	Linear Quadratic Regulator
LQR	Linear Quadratic Regulator
LSDP	Loop Shaping Design Procedure
M.O.	Multi-Objective
MAGLEV	MAGnetic LEVitation
MIMO	Multiple Input Multiple Output
NP	Nominal Performance
NSGA-II	Non-dominated Sorting Genetic Algorithm-II
PI,P+I	Proportional Integral
PM	Phase Margin
PSD	Power Spectrum Density
RHP	Right Hand Plane
RMS,rms	Root Mean Square
RP	Robust Performance
RS	Robust Stability
SE	Single Ended
SISO	Single Input Single Output

Other symbols and acronyms are defined as they appear

Chapter 1

Introduction

In recent years, there is a high demand of technological needs with the automotive, aerospace as well as transport markets being highly affected. Due to rapid increment of technological demands the necessity of reducing the cost, the complexity and improving reliability of industrial products arises. In recent years there is a lot of research towards that area which aims to produce affordable, reliable and safe products.

In this context the control system design plays an important role and the impact is crucial for the final value of a product. Moreover, the control engineer has to take into account a lot of different parameters and requirements in order to achieve the best possible control system design with a number of characteristics that reduce complexity, cost and optimise performance. Furthermore, safety-critical control systems are highly sensitive under fault conditions. In fact, for safety-critical control systems either single or multiple sensor faults may lead to disaster and therefore the fault tolerance concept is introduced in order to recover the performance under fault conditions at the expense of higher cost and complexity. Additionally, for every stable or unstable plant the need to select the best possible sensors subject to optimum performance, cost, robustness and safety can be very complicated or even impossible to do, especially if optimum performance is required under any fault conditions.

In this thesis, three novel systematic frameworks are proposed by the author that simplify the sensor set selection subject to design requirements. This problem falls into the multiobjective constraint optimisation area because many objectives are required subject to design constraints. Metaheuristic approaches combined with modern control strategies (i.e LQG, $\mathcal{H}_\infty$) simplify the sensor selection of the control system subject to the performance requirements and sensor fault tolerance. In this thesis a **MAG**netic **LEV**itated (MAGLEV) suspension is used as example in order to create a baseline for more complex problems.

1.1 Problem setup

The overall block diagram to be used for the optimised sensor configurations for control and sensor fault tolerance setup is shown in Fig. 1.1. Any given plant has a number of control inputs (n_u) and a number of measurement outputs (n_y). The selection of inputs and outputs subject to optimum performance, robustness, cost and fault tolerance is very important and complex process. A typical flow chart of **I**nput/**O**utput (IO) optimisation algorithm is depicted in Fig. 1.2, page 4. The simplified IO optimisation algorithm optimally tune the closed-loop response of the control system subject to the aforementioned requirements for each feasible IO set following the selection of the best IO set at the end of the optimisation process. In this thesis only the combinations of the outputs are optimised since the MAGLEV suspension has only one control input. Although only the outputs are incorporated within the systematic framework (as illustrated in Fig. 1.1) the proposed systematic frameworks can be extended for plants with more inputs/outputs. Regardless the MAGLEV suspension has small number of IO sets the sensor optimisation process is complex because the design requirements of such system are not trivial.

The number of outputs defines the number of feasible sensor sets that is possible to use in order to control the plant as desired. For example,

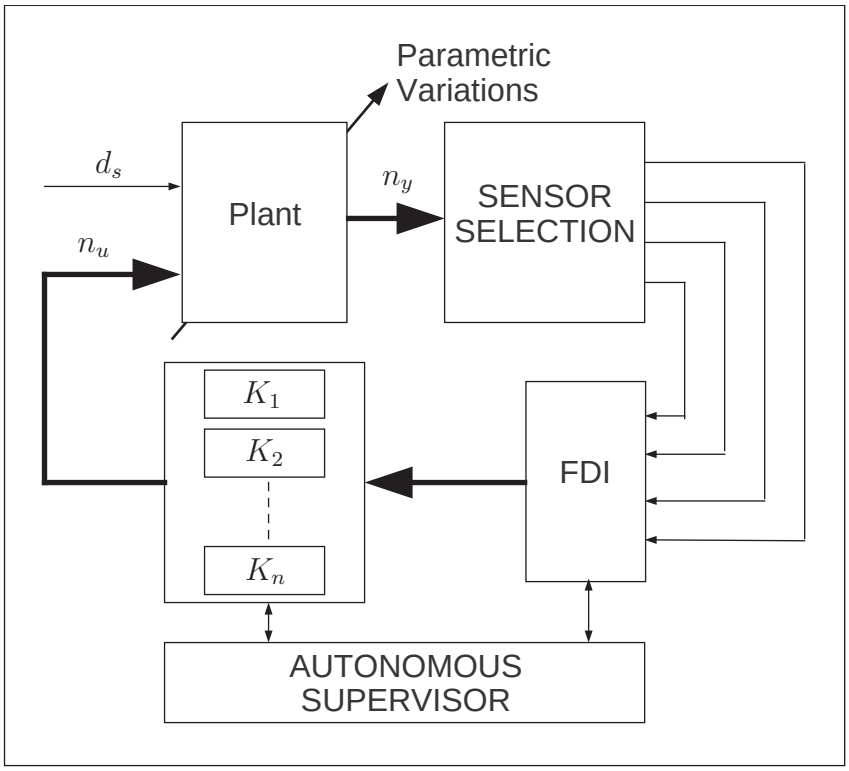

Figure 1.1: Block diagram of optimum sensor selection for control and fault tolerance.

if there are 3 measurements then 7 feasible sensor sets are available. For example, $[y_1]$, $[y_1\ y_2]$, $[y_1\ y_3]$ and $[y_1\ y_2\ y_3]$. From those sensor sets the best possible should be used subject to optimum performance, disturbance rejection, robustness, cost and fault tolerance. This problem is often not trivial and sometimes impossible to do manually if there are many outputs i.e. 10 sensors leads to $2^{10} - 1 = 1024$ sensor sets. Metaheuristic approaches can be used within the systematic framework in order to assist with the optimum tuning of the controller's parameters for each sensor set subject to the aforementioned desired requirements. At the end of the optimisation process the optimum sensor set that meets the requirements can be selected. To achieve the fault tolerance to any sensor(s) failure(s) a bank of controllers can be used. In fact, if there is(are) any sensor failure(s) the **F**ault **D**etection and **I**solation (FDI) detects and isolates the faulty sensor(s) and the autonomous

supervisor takes remedial actions by controller reconfiguration so that the performance is either fully recovered or degraded until the fault is repaired.

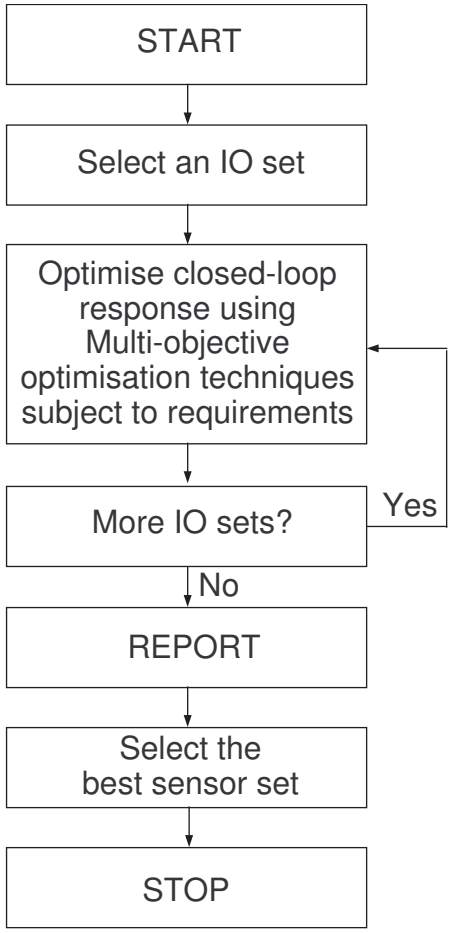

Figure 1.2: Generalised flow chart for a sensor optimisation systematic framework.

1.1.1 MAGLEV suspension

The MAGLEV suspension is used in this thesis as an example to demonstrate the systematic frameworks and as baseline for large scale complex plants. The Electromagnetic suspension system is used in MAGLEV trains in order to support the vehicle and the load (i.e passengers). The diagram of a single degree of freedom MAGLEV suspension is shown in Fig. 1.3. The

suspension consists of an electromagnet where the vehicle mass is supported by producing an attractive force onto the rail and, by controlling the circulated flux, the air gap can be controlled. The Electromagnetic (EMS) type of suspension that is used in MAGLEV technology is open-loop unstable, non-linear, safety-critical system with non-trivial requirements and a number of available measurements. This system can be used as a good example for the demonstration of the overall idea depicted in Fig. 1.1.

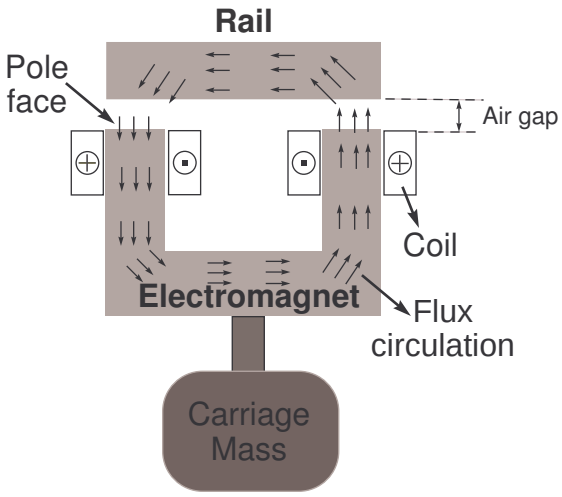

Figure 1.3: Typical diagram of a MAGLEV suspension.

1.2 Research objectives

This research project objectives are:

- to reduce the control system's complexity
- to simplify the sensor set selection process
- to optimise the performance for every possible sensor set with respect to working boundaries (i.e disturbance rejection, robustness etc)
- to find the minimum number of sensors that can be used to ensure optimum performance

- to extend the method so that the performance is recovered when one or more sensor fails i.e introduce sensor selection for sensor fault tolerance
- to apply the proposed systematic frameworks to an electromagnetic (EMS) MAGLEV suspension system
- and to design and construct a $25kg$ MAGLEV suspension test rig in order to verify the theoretical sensor optimisation frameworks mentioned above.

1.3 Thesis contributions

This thesis addresses a number of issues concerning sensor selection for control and fault tolerance with regards to the MAGLEV suspension application and makes contributions in the following areas:

1. Incorporation of the recently developed Non-dominated Sorting Genetic Algorithm in the context of tuning and constraint-handling functions within actuator/sensor selection for control and fault tolerance, in particular to take account of the complexity involved in the selection of sensor configurations for practical engineering systems;
2. Fundamental study of optimised sensor configurations using classical control strategies for a MagLev suspension system;
3. The development of practical systematic frameworks for sensor optimisation via modern control strategies using LQG and $\mathcal{H}_\infty$ robust control design [1];
4. The extension of the sensor selection framework to the particular concept of fault tolerance minimising the sensor hardware redundancy.

[1]The work is in fact proposing one main skeleton for sensor selection in control and fault tolerance, while extends this skeleton to accommodate the different control design methods. Thus the term "frameworks" is used (in this thesis) to distinguish between the different methodologies.

5. Experimental verification of controllers generated using the design framework using an experimental MAGLEV suspension rig.

1.4 Thesis structure

The thesis is laid out as follows:

- *Chapter 2*: The literature review is done related to sensor selection for control systems, Fault Tolerant Control and the MAGLEV technology.
- *Chapter 3*: The Multiobjective constrained optimisation concept with genetic algorithms is presented. The recently developed Non-Dominated Sorting Genetic Algorithm II is described along with two examples for the MATLAB code validation.
- *Chapter 4*: The MAGLEV suspension modelling is considered in this chapter. The non-linear model with the linear time invariant state space linearisation model are presented along with the feasible sensor sets and the design requirements.
- *Chapter 5*: Two optimised sensor configurations via classical control strategies are presented. The controller selection criterion is explained in this chapter that is used as a metric to select controllers among many that satisfy the closed-loop design requirements. Studies on noise suppression and uncertain operating point are undertaken as well as robustness to load variations.
- *Chapter 6*: Optimised sensor configurations systematic framework for control via linear quadratic gaussian control strategy is presented. The optimisation process combines the LQG strategy, the genetic algorithms and the MAGLEV suspension to demonstrate the concept.
- *Chapter 7*: Two optimised sensor configurations systematic frameworks via $\mathcal{H}_\infty$ robust control design methods are presented. In this chapter, the $\mathcal{H}_\infty$-multiobjective robust control and the loop-shaping design strategies are considered for the sensor optimisation. A comparison

of the sensor optimisation via LQG, and the two approaches presented in this chapter is carried out.

- *Chapter 8*: The Fault Tolerant Control (FTC) for sensor failures is considered where two approaches are studied. One considers single sensor failure via classical control and the second multiple sensor faults using the optimised sensor configurations via LQG control that was presented in Chapter 6. The concept is extended to sensor selection for Fault Tolerant Control covering multiple sensor failures in an attempt to minimise the sensor hardware redundancy. Appropriate simulations demonstrate the efficacy of this approach.

- *Chapter 9*: The design and construction of a $25kg$ MAGLEV suspension rig is described. The experimental rig has been designed and constructed from scratch and all necessary details including mechanical, electrical and electronics implementations are described. The purpose of the MAGLEV rig is to demonstrate the theoretical frameworks developed into the practical application.

- *Chapter 10*: In this chapter, conclusions as well as suggestions for future work are given.

- The following information is included in the Appendix:(A) Matlab code and Simulink diagrams for the theoretical frameworks are given, (B) Matlab code and Simulink diagrams for the $25kg$ MAGLEV suspension experiments are given, (C) Mechanical diagrams of the $25kg$ MAGLEV suspension, (D) Electronics circuits for the custom made circuit boards, (E)Published papers and other publications.

1.5 Publications

See Appendix E

Journal

K. Michail, A.C. Zolotas, R.M. Goodall. *Optimised sensor configurations for MAGLEV suspension systems.* Journal Facta Universitatis (FU) Series Mechanics, Automatic Control and Robotics (MACR), Invited paper for the Special Issue on Advanced Controls and Signal Processing in Active and Robotic systems, Published by the University of Niš, Serbia, Vol. 7, No. 1,pp.169-184, 2008.

K. Michail, A.C.Zolotas, R. M. Goodall and J. Pearson. *Sensor Optimisation via H_∞ applied to a MAGLEV suspension system.*, WASET, International Journal of Electrical, Computer, and Systems Engineering, Vol.3,No.3,pp.143-149 (selected to appear in the journal of WASET).

Conference

K. Michail, A. C. Zolotas and R. M. Goodall. *Optimised sensor configurations for a Maglev suspension.* Proceedings of the 17^{th} World Congress the International Federation of Automatic Control, Seoul, Korea, July 6-11, 2008, p.8385-8310.

K. Michail, A.C.Zolotas, R. M. Goodall and J. Pearson. *MAGLEV suspensions - a sensor optimisation framework.* IEEE 16^{th} Mediterranean Conference on Control and Automation, Ajaccio, Corsica, France, June 25-27, 2008, p. 1514-1519.

K. Michail, A.C.Zolotas, R. M. Goodall and J. Pearson. *Sensor Optimisation via H_∞ applied to a MAGLEV suspension system.* WASET ICCAS 2008: International Conference on Control and Automation Systems, Prague,

Czech Republic, July 25-27, 2008, p.171-177.

K. Michail, A.C.Zolotas, R.M.Goodall. *EMS systems: Optimised Sensor Configurations for Control and Fault Tolerance.* Japan Society of Mechanical Engineers, The International Symposium on Speed-up, Safety and Service Technology for Railway and Maglev Systems. Niigata, Japan, 16-19 June, 2009.

K. Michail, A.C. Zolotas, R.M. Goodall. *Fault Tolerant Control for EMS systems with sensor failure.* IEEE 17^{th} Mediterranean Conference on Control and Automation, Makedonia Palace, Thessaloniki, Greece, June 24-26, 2009.

Workshop

K. Michail, A.C.Zolotas, R.M.Goodall. *A Fault Tolerant Control system for electromagnetic suspension with sensor failure.* 23^{rd} IAR Workshop on Advance Control and Diagnosis, Coventry University,Coventry, UK, 27-28 Nov 2008.

Other

T. Steffen, **K. Michail**, R. Dixon, A.C. Zolotas, R.M. Goodall. Optimal Passive Fault Tolerant Control of a High Redundancy Actuator. 7^{th} IFAC Symposium on Fault Detection, Supervision and Safety of Technical Processes, Barcelona, Spain, 30^{th} june- 3^{rd} july, 2009.

Z. Li , A. C. Zolotas, I. M. Jaimoukha, K. M. Grigoriadis, **K. Michail** and J. T. Pearson. Output selection under control and fault detectability considerations. IEEE 15^{th} Mediterranean Conference on Control and Automation, Athens, Greece, June 27-29, 2007.

Chapter 2

Literature review

2.1 Introduction

Control system design involves Input/Output (IO) selection, that is, decision on the number, the place, and the type of actuators and sensors to be used subject to performance, robustness, stability etc. For plants with many inputs and outputs the selection of the IO with respect to a number of performance requirements can be complicated and time consuming (Mushini and Simon [2005]). In this thesis the focus is upon sensor set selection, for which it is very difficult to meet optimum performance, minimum cost, robustness and sensor fault tolerant requirements via manual procedures. However, the frameworks are equally applicable to actuator (input) set optimisation. For this reason systematic frameworks are developed that can actually simplify the sensor set selection with respect to multiple objectives. In this chapter, an overview is given with respect to sensor selection, fault tolerant control and magnetic levitated vehicles technology.

2.2 Sensor selection in control systems

The number of sensor elements and location affect the robustness, performance, complexity and cost of the control system. In the literature many papers are found with respect to sensor selection depending on the objective/s

required. Sensor selection is a procedure that in most cases is done via off-line methods like in this research work. Real-time sensor selection is done usually in continuous manufacturing industries (Fraleigh et al. [2003]).

Based on nominal performance, the closed-loop H_∞ norm of a nonlinear compressor system is minimised using different IO sets (Wal et al. [2002]). The results show that fewer sensors can be used resulting to the same or slightly degraded nominal performance. For an active vibration attenuation controller applied on the NASA Langley Mini-Mast experimental structure, H_2 optimal control is used with different IO sets to study the nominal performance of the system (Balas and Young [1999]). Results show that the system's performance can be satisfied using a specific IO set but it cannot be improved using a larger number of IO sets. This gives a control system with the minimum complexity and cost. The robust performance is considered in some cases, like the active vehicle suspension system by Wal et al. [1998] where the $\mu - synthesis$ controller is used for different IO sets and it was found that fewer sensors can be used, to achieve the same robust performance as with the full IO set. In these problems where the number of sensors is large, leading to large number of IO sets, long computational time is required to check all IO candidates. A method based on a feasibility test combined with a search strategy is proposed by Jager et al. [1998] to reduce the computational time for large-scale problems. The same approach used by Jager and Wal [1999] where a method is proposed to optimally select controller IO that assure desired level of robust performance. Another two IO selection methods are presented by Wal and Jager [1998] to achieve robust performance applied to an active suspension control problem for a tractor-semitrailer. Wal and Jager [1996] aimed at robust performance (RP) and robust stability (RS) for different IO sets where the minimum number of IO set was found to achieve RP and RS. Moreover, the sensor selection is considered in fault diagnosis (Debouk et al. [2002]) and supervisory control (Rohloff et al. [2006]).

There are a number of methods used for IO set selection in control system

design. A very detailed literature survey on IO selection is done by Wal and Jager [2001]. These methods are briefly summarised as follows:

IO selection methods for control systems

1. *Accessibility*: This is a qualitative technique for IO selection based on cause-and-effect graphs. The ideal is that a causal path must exist between the manipulated (u_i) and the controlled variables (z_i) as illustrated in Fig. 2.1 and the measured (y_i) and controlled variables (z_i).

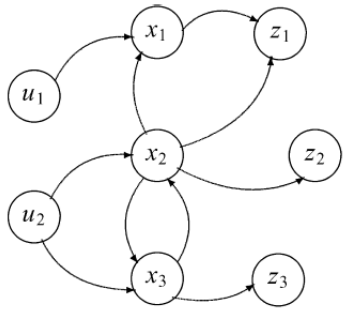

Figure 2.1: Simple cause-and-effect graph for IO selection.

2. *State controllability and state observability* can be used in two senses for a dynamic model described by a linear time invariant state space form with state space matrices given as: A - state matrix, B - Input matrix and C - output matrix. The binary sense where the candidate IO set causing uncontrollable (A,B) system and/or unobservable (C,A) system is rejected. When the system is controllable and observable, then the corresponding sensor set is kept and the procedure is repeated until the minimum number of sensors is recovered. The second approach is the qualitative sense where the controllability grammian $W_c(t)$ and the observability grammian $W_o(t)$ (den berg et al. [1999]) are evaluated

using the Lyapunov equations

$$\begin{aligned} AL_c + L_cA^T + BB^T &= 0 \\ A^TL_o + L_oA + C^TC &= 0 \\ Where: L_c = \lim_{t\to\infty} W_c(t) \quad &and \\ L_o = \lim_{t\to\infty} W_o(t) & \end{aligned}$$

Using these grammians actuator and sensor selection can be done because they show in quantified manner the states' controllability/observability.

3. *Right half-plane zeros* pose performance limitations to a control system (Skogestad and Postlethwaite [2005]). In this case the IO sets that introduce RHP zeros with magnitudes below a desired bandwidth are rejected.

4. The *Input-output controllability* is a selection method based on singular value (σ) decomposition. Different groups of controllability measures are considered.

   - The minimum singular value ($\underline{\sigma}$) can be used where the IO set that result to a large $\underline{\sigma}$ is the selected sensor/actuator set.
   - The maximum singular value ($\overline{\sigma}$) can be used but depending on the objective this may either required to be small or large.
   - The condition number in general should be small because it results to a good robustness against full-block (unstructured) multiplicative uncertainty. Therefore, the IO set that gives small condition number is used (Skogestad and Postlethwaite [2005]).
   - The left and right singular vectors from the singular value decomposition can be used for IO controllability measure. The idea is to find the best compromise between measurements y_i that are mutually independent and measurements that are sensitive to changes of the input u_i.

- The relative gain array is also used as IO selection method. That is, IO sets causing large RGA elements should be rejected since the corresponding plants difficult to be controlled.

5. *Efficiency of manipulation and estimation*: The objective of actuators is to manipulate the system as desired with the lowest possible energy consumption. From this point of view, the actuator selection can be based on the minimisation of an input-set-depend cost function (J_u) in terms of the input energy. Sensors are used to obtain the best-possible information on the system's behaviour. Therefore sensor selection can be based on the minimisation of an output-set-depended cost function (J_y) while depends on the estimation errors of variables, for example the system states. Both cost function can be combined as one (J_{uy}) input-output-set-depend functions and used to select the optimum IO set. That is minimise J_{uy} so that the minimum number of IO set is used to control the system with minimum energy consumption and minimum estimation error.

6. *Robust Stability* (RS) and *Nominal Performance* (NP): RS guarantees stability in the presence of uncertainties, whereas NP guarantees stability and performance in absence of uncertainties. SISO and MIMO systems are treated separately. For a MIMO system, the infinity norm of the closed-loop system is taken as a metric for this RS and NP criterion.

7. *Robust performance* (RP): IO set which results to an acceptable robust performance metric and low cost control system is selected for feedback. The structured singular value can be used as metric for the robust performance. This metric is used to verify that the performance of the control system, will be maintained in the presence of uncertainties.

8. Search methods. As it has been seen from previous criteria, all IO sets has to be checked in order to find the optimum IO set. This is done by checking one by one candidates and it requires a big computational

effort. The computational effort can be reduced rabidly by rejecting the nonviable IO sets using a search method.

Desirable properties of IO selection methods

An IO selection method has to be: Well-founded, Efficient, Effective, Generally applicable, Rigorous, Quantitative, Controller independent and Direct (see Wal and Jager [2001]). In the next paragraphs each property is briefly summarised.

1. Well-founded: The theory behind an IO selection method must be sound and complete. The method should be easy to use and transparent, i.e bearing the basic idea of the method in mind, the way in which the outcome is affected by changes in the control goals must be understandable. At least one convincing application should prove the method's practical relevance.

2. Efficient: An IO selection method should make it possible to quickly evaluate a large number of candidate IO sets. Algorithms are commonly called efficient if they solve problems in time polynomial in a measure of the problem size; if not, they are called inefficient.

3. Effectiveness: Implies that those candidate IO sets are eliminated for which the considered selection criterion cannot be achieved ("nonviable IO sets"), while those candidates are kept for which it can be achieved ("viable IO sets"). Necessary or sufficient condition may lead to the faulty rejection of viable IO sets. Hence, effectiveness calls for conditions which are necessary and sufficient.

4. Generally applicable: An IO selection method should deal with a wide variety of control problems. For instance, a method is preferably suitable or easy generalized to handle classes of nonlinear systems. General applicability requires a set-up which can describe a wide variety of control problems.

5. Rigorous: Viability should be addressed rigorously to cover a wide variety of issues that are important for control system design. For example an IO selection criterion based on robust stability is more rigorous that a criterion base on nominal stability. In general, a more rigorous criterion selects a smaller number of viable IO sets which may be manageable for more detailed further analysis.

6. Quantitative: An IO selection method preferably employs quantitative criterion for IO set viability to clearly distinguish between the prospectus of candidate IO sets. For instance, a qualitative criterion like state controllability only provides a 'yes' or 'no' answer to input set viability, while a quantitative controllability measure provides additional information on 'how strongly' an input set affects the state.

7. Controller independent: An IO selection method should eliminate IO sets for which there does not exist any controller meeting the intended control goal. Usually, it is undesirable to impose restrictions on the controller design method, because this yields biased conclusions on IO set viability. On the other hand, if restrictions on the controller design method or the maximum controller order do play a role, a controller-dependent IO selection method may be advantageous. For efficiency reasons, IO selection should not involve complete controller design.

8. Direct: For the purpose of efficiency or if the list of candidates is infinite (as is often the case for flexible structures), it is desired that an IO selection method directly characterises the viable IO sets, instead of performing a candidate-by-candidate test for a particular criterion. the latter, brute-force approach is indirect and not solvable in time polynomial in N_u and N_y.

2.3 Fault Tolerant Control systems

Fault-tolerant and fail-safe control system design is very important for safety-critical systems (i.e aircraft, MAGLEV trains, shuttles, satellites etc). In fact,

fail-safe systems are able to withstand any single point failure without any change in the functionality or performance, whereas FTC systems may have degraded performance in case of a fault, but are designed to prevent this fault from being developed into system instability. The aim of moving towards FTC systems is the cost reduction. In Table 2.1 the main characteristics for both control systems design approaches are tabulated. Generally it can be seen that the fault tolerant control systems can cost less because they do not require hardware redundancy (Blanke et al. [1997]). Nevertheless, FTC system may be complex and therefore reliability and robustness issues arise as mentioned by Wu [2001a,b] and Patton [1993] respectively. Performance analysis on FTC system for an aircraft vehicle is considered by Shin and Belcastro [2006].

Fault tolerance can be achieved using either active or passive methods. The first approach is based on controller reconfiguration but the second on the robustness of the controller design (i.e the controller can be designed to tolerate faults). Detailed description of Fault Tolerant Control concept is given by Blanke et al. [2001a].

Some applications are found in the literature based on Fault-Tolerance design such as the ship propulsion (Izadi-Zamanabadi and Blanke [1999]; Wu et al. [2006]), the Ørsted Satellite (Blanke et al. [1997]), three-tanks system and chemical process (Blanke et al. [2003]), a DC motor control (Campos-Delgado et al. [2005]), double inverted pendulum (Niemann and Stoustrup [2005]) and automotive vehicle longitudinal control (Seron et al. [2008]).

Table 2.1: Fault-tolerant and Fail-safe systems characteristics (Blanke et al. [1997]).

Fail-Safe System
The system continues to perform normally for any single point failure.
The hardware redundancy is triple, in case that a unit fails, another one will keep the system working.
The system uses voting scheme (eg. 2 out of 3) for sensor signals.
Use triple signal processing computers.
Use double or more actuators.
Fail safe systems are very expensive since they require hardware redundancy.
Fault tolerant System
Any single fault does not develop into system instability but degraded performance.
Use information redundancy to detect faults.
Use reconfiguration in programmable system components to accommodate faults.
Accept degraded performance due to a fault but keep plant availability.
Low cost because they do not required redundancy hardware.

2.3.1 A Fault Tolerant Control architecture

The design of a fault tolerant control system requires to consider many parameters and deep control system analysis. Some issues are taken into consideration like the fault propagation in the system and the end-effect of the fault. How serious a fault is as well as remedial actions to be taken for the specific fault are also taken into account.

A three layer architecture for Fault Tolerant Control system design is shown in Fig. 2.2 (Blanke et al. [2001b]). The lower layer is the control loop, the second layer is the detector functions and effectors to effect reconfiguration, and the third represents autonomous supervisor functionality. Each layer is summarised as follows:

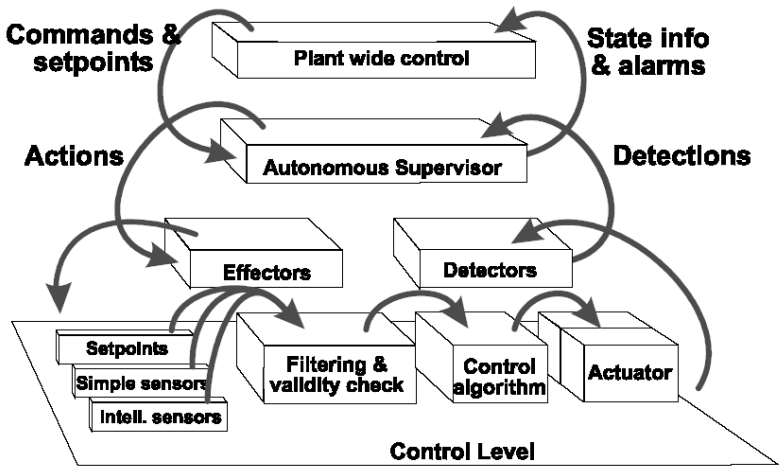

Figure 2.2: A Fault-tolerant control system architecture (Blanke et al. [2001b]).

1. The lowest layer represents the control loop with sensor and actuator interfaces, signal conditioning and filtering and the controller. For FTC design, the sensor interface should include detectability and validity checking. Three objectives have to be satisfied, i.e check the range, check for abrupt faults and check the RMS values for incipient faults.

2. The second level includes as many detectors as faults to be detected as well as link to the autonomous supervisor for fault alerts. The effectors are able to re-configure or apply remedial actions initiated from the autonomous supervisor. The functions of the modules are: Fault detection based on hardware or analytical redundancy using fault detection and isolation methods, detection of faults in control algorithms and application software and effector modules used for fault handling (i.e remedial actions).

3. The third level, the supervisor, is composed of state-event logic to describe the logical state of the controlled object. Transitions between states are driven by events. The autonomous supervisor system is able to interface to detectors for change detection, interface to upper level for mode change signals, demand re-configuration or other remedial actions to accommodate a fault and signal to plant-wide co-ordination or operator about current state.

2.3.2 Fault Tolerant Control methods

Diagram in Fig. 2.3 shows the taxonomy of the fault tolerance approaches. The passive approaches take into account the robustness of the system against faults. In fact, the robust controller is designed is such a way that the possible faults are taken into account. The closed-loop control system is designed to remain stable in case of a fault without any further controller action. In contrast, the active approaches are using reconfiguration of the controller in case of a fault. That is why this approach requires fault detection mechanism. Generally, there are two types of faults taken into account in FTC design (Frank [1990]):

- *Abrupt faults*: These faults play a role in safety-relevant systems where hard-failures have to be detected early enough so that catastrophic consequences can be avoided by early system reconfiguration.

- *Incipient faults*: Incipient faults are of major relevance in connection with maintenance problems where early detection of worn equipment is

required. In this case the faults are typically small and not as easy to detect, but the detection time is of minor importance and may therefore be large.

A good Fault-Tolerant control overview is given Patton [1997a].

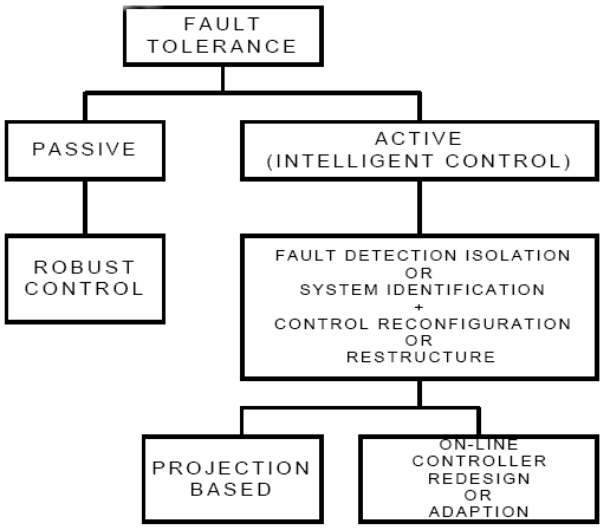

Figure 2.3: Decomposition of Fault Tolerant Control (Patton [1997a]).

2.3.3 Active Fault Tolerance

In active fault tolerance the control system is redesigned once a fault has occurred based on the performance and robustness of the original control system but with degraded capabilities. In order to achieve control system reconfiguration, the control system requires knowledge of the expected fault beforehand or a detection and isolation mechanism for fault detection.

Diagram in Fig. 2.3 shows that active fault tolerance approach is divided into two categories: the first is the projection-based method where a new pre-computed control law is selected depending on the type of the fault, and the second uses on-line automatic controller redesign methods (reconfiguration) where calculation of new controller parameters in response to a control

impairment (fault). A simple way to apply active fault tolerant is through control law rescheduling where the gain parameters are stored beforehand and, if a fault occurs, the gain is redesigned depending on the fault. An important part of the fault tolerance controller is the Fault Detection and Isolation (FDI) mechanism, particularly the aim is to detect, isolate and identify a fault before the controller reconfiguration.

Fault Detection and Isolation

The key problem for active fault tolerant control is on-line reconfiguration of the controller. For this to be possible detailed information about changes in the system parameters (or changes in the system operating point) due to either normal process changes or component failures is required. The major task of FDI is to acquire this information, whilst it is the task of a supervision system to manage the controller reconfiguration (for example, by model-selection based upon FDI unit information).

Often referred to as Diagnosis, Fault Detection and Isolation (FDI) is a method which Detects and Isolates a fault in an active FTC system. In detection part of FDI special emphasis is given in incipient, or developing, faults rather than large step faults, because incipient faults are harder to detect. The Fault isolation is the part of FDI which determines not only the faults' origin but also the fault type, size and time. When using direct redundancy, extra hardware channels or components provide additional signals, that can be used from FDI unit to generate residual signals by direct comparison and using voting techniques is able to identify and isolate a faulty component.

In case that analytical redundancy is used to produce additional (or back-up) signals, as well as the residual signals, the system is fault-free, and all of the residuals should are close to zero (for a healthy system). After a fault occurs, the FDI module that is used or residual generation and decision-making is responsible for finding out the location of the fault. The system

can then be reconfigured or restructured so that any non-impaired or healthy channel (or component), or signals will be chosen to take a role in system operation.

According to Patton [1997a] there are three FDI approaches. The Quantitative model-based approaches (Venkatasubramanian et al. [2003c]), the qualitative (Venkatasubramanian et al. [2003a]) and the knowledge based (Venkatasubramanian et al. [2003b]) approaches.

1. **Knowledge based FDI**: In knowledge or history based approaches there is no need to be supported by analytical functions. The knowledge can be gathered by the engineers working with the process. This approach is divided into two techniques. The shallow diagnostic reasoning techniques and the Deep diagnostic reasoning techniques (Frisk [1996]). No emphasis is given for this approach since model-based approaches are more important in this thesis.

2. **Qualitative based FDI**: These methods are based on Qualitative Reasoning (QR) which consists of relating to a non-numerical description of the system, preserving all its important behavioral properties and distinctions. Qualitative model aim to capture the fundamental aspects of a system or mechanism, while suppressing much of the detail. Methods such as abstraction and approximation are often used to build models based on qualitative rather than numerical aspects of a system.

   The values in Qualitative Reasoning divide the corresponding quantitative space into a finite number of regions and each interval is assigned a name. A simple example by Calderon-Espinoza [2003] shows the philosophy behind QR. Qualitative values for a quantity space representing temperature might be "cold", "warm" and "hot" with these three values mapped to quantitative intervals. In diagnosis very often qualitative signals take up three values: +,- and 0 for positive, negative and zero respectively. The example is illustrated in Table 2.2

Table 2.2: FDI using qualitative Reasoning about temperature (Calderon-Espinoza [2003]).

Quantitative intervals	Qualitative values		
$[17, 20]$	cold	-	negative
$[21, 25]$	warm	0	zero
$[26, 30]$	hot	+	positive

3. **Quantitative model-based FDI**: Controller design requires, precise knowledge about the plant dynamic model. The same information is required for reconfiguration of the control system. On considering these requirements, more emphasis has been traditionally placed upon quantitative model-based FDI approaches as these rely on detailed knowledge of system's dynamic model and may finally provide more details about the changes in system dynamics, in keeping with the requirements for reconfiguration and closed-loop adaption. The major emphasis therefore in the field of quantitative model-based FDI has been placed upon methods of detecting and isolating faults fast and accurately.

   The block diagram in Fig. 2.4 shows the general concept of the structure of model-based fault diagnosis system comprising two main stages of residual generation and decision making and the use of a knowledge-base for improving the decision-making and assisting in residual generation

FDI using analytical redundancy

The fault diagnosis using the analytical redundancy is a quantitative model-based method to detect and isolate faults. Consider the dynamic system in Fig. 2.5 (Frank [1990]) with input vector u and output vector y. The actual dynamic system consists of the actuators, the plant dynamics (components), and the sensors. For Fault detection and

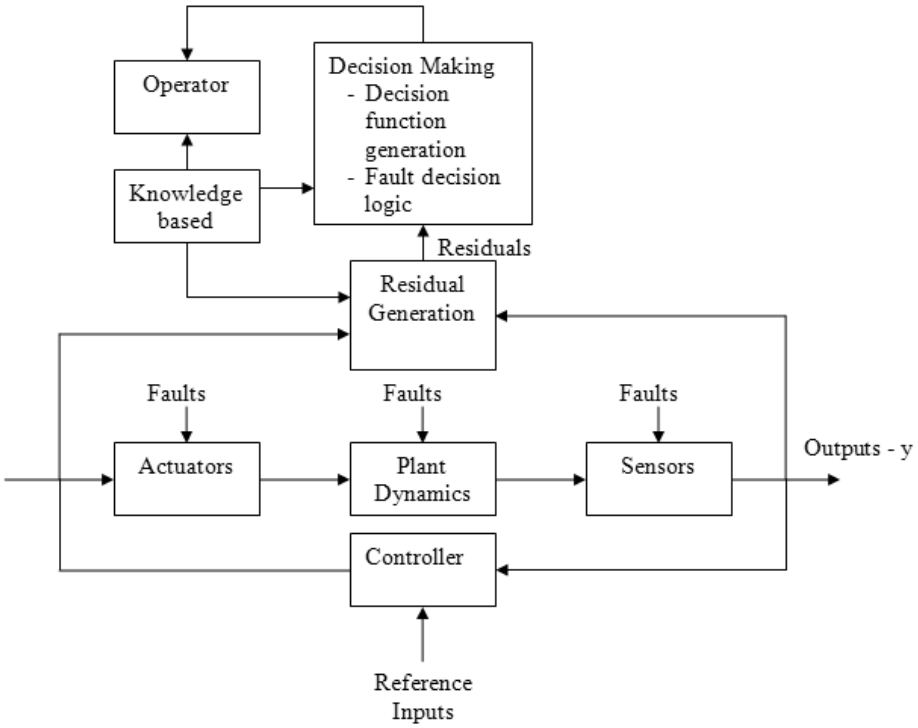

Figure 2.4: Block diagram of Quantitative model-based fault diagnosis (Patton [1993]).

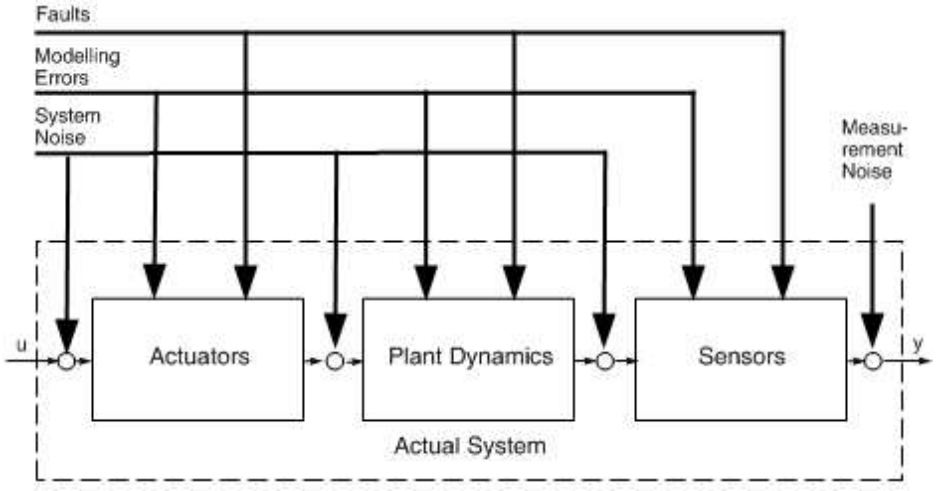

Figure 2.5: Realistic dynamic system block diagram with faults and uncertainties (Frank [1990]).

isolation considerations, it is important to model all effects that can lead to alarms or false alarms. Such effects are:

- Faults in the actuators, in plant components (dynamic system fault), or in the sensors.
- Modelling errors between the actual system and its mathematical model.
- Noise considerations i.e dynamic system noise and measurement noise.

All faults are considered in vector f_f and all unknown inputs (eg noise, modelling errors) are placed in vector d.

The realistic system may be given in continues time by the state space dynamic equations:

$$\dot{x} = Ax(t) + Bu(t) + E_d d(t) + H_f f_f(t) \tag{2.1}$$

$$y(t) = Cx(t) + F_d d(t) + G_f f_f(t) \tag{2.2}$$

where x is the $n \times 1$ state vector, u the $p \times 1$ known input vector, y the $q \times 1$ vector of measured outputs and $A^{n\times n}$, $B^{p\times 1}$, $C^{m\times n}$ known matrices describing the plant dynamics. A is the state matrix, B the input matrix and C the output matrix. The term $E_d d(t)$ models the unknown inputs to the actuators and the dynamic process, $H_f f_f(t)$ actuator and component faults, $F_d d(t)$ the unknown inputs to the sensors, and $G_f f_f(t)$ sensor faults. Notice that A, B, C are the nominal matrices of the dynamic system since the faults that are principally reflected in changes of A, B, C as well as modelling errors, are considered by f_f and d associated with proper choices of E_d, F_d, G_f, H_f. Whilst these matrices are usually given, the modes (i.e the evolutions) of f_f and d must generally be considered unknown.

The schematic structure of the FDI procedure using analytical redundancy (applied to a plant of a feedback control system) is illustrated in Fig. 2.6. The procedure of evaluation of the redundancy given by the mathematical model of the system, in (2.1) and (2.2), can be roughly divided into the following two steps:

- Generation of so-called residuals, i.e functions that are accentuated by the fault vector f_f.
- Decision and isolation of the faults (time, location, sometimes also type, size and source).

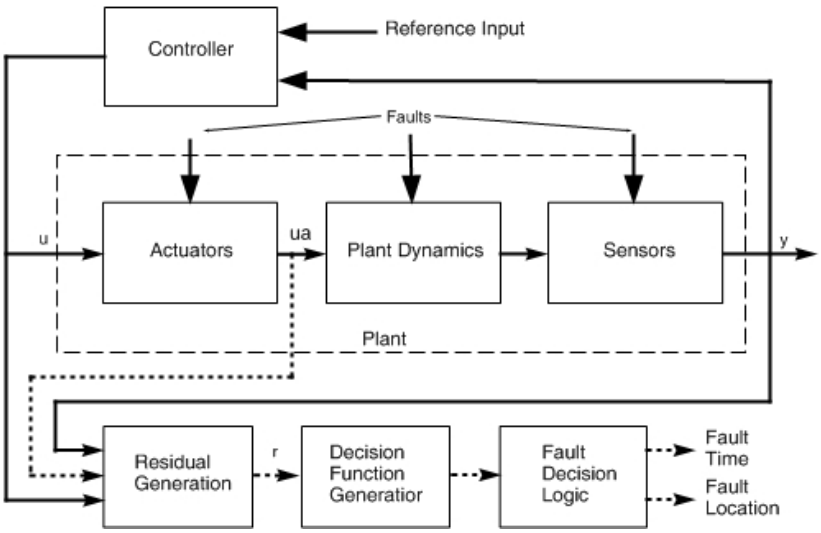

Figure 2.6: Structure of FDI using analytical redundancy (Frank [1990]).

The analytical redundancy approach requires that the residual generator performs some kind of validation of the nominal relationships of the system, using the actual input, u, and measured output, y. If a fault occurs, the redundancy relations are no longer satisfied and a residual, $r \neq 0$, occurs. The residual is then used to form appropriate decision functions. They are evaluated in the fault decision logic in order to monitor both the time of occurrence and location of the fault. For the residual generation three kinds of models are required: the nominal, actual (observed) and that of the faulty system. In order to

achieve a high performance of fault detection with low false alarm rate the nominal model should be tracked and updated by the observation model.
Different ways of producing residual signals are described by Frank [1990] as follows:

(a) The parity space approach,

(b) The dedicated observer approach and innovation-based approach,

(c) The fault detection filter approach and

(d) The parameter identification approach.

2.3.4 Passive Fault Tolerance

Passive approaches, use the robust control (Gu et al. [2005]) design methods, to achieve fault tolerance. That is, the closed-loop system remains insensitive to certain faults using constant controller parameters without any need for fault information (i.e time, location) like in the case of the active fault tolerance.

In any control system design robustness issues must be taken into consideration because the performance has to be maintained in case of unknown disturbance, uncertainties or modelling errors (mathematical model is never precise). Faults can be also taken into account for the controller design in such a way that the closed-loop response becomes insensitive to specific faults (i.e robustness against faults). Two types of faults are taken into account, the multiplicative faults that affect the system's dynamic parameters and the additive faults that affect the inputs and/or outputs. The 4-parameter controller structure depicted in Fig. 2.7 is an example of a passive fault tolerant control system (Patton [1997a]). The notation explanation is tabulated in Table 2.3.

The estimated control signal $u(s)$ given by the robust controller is shown

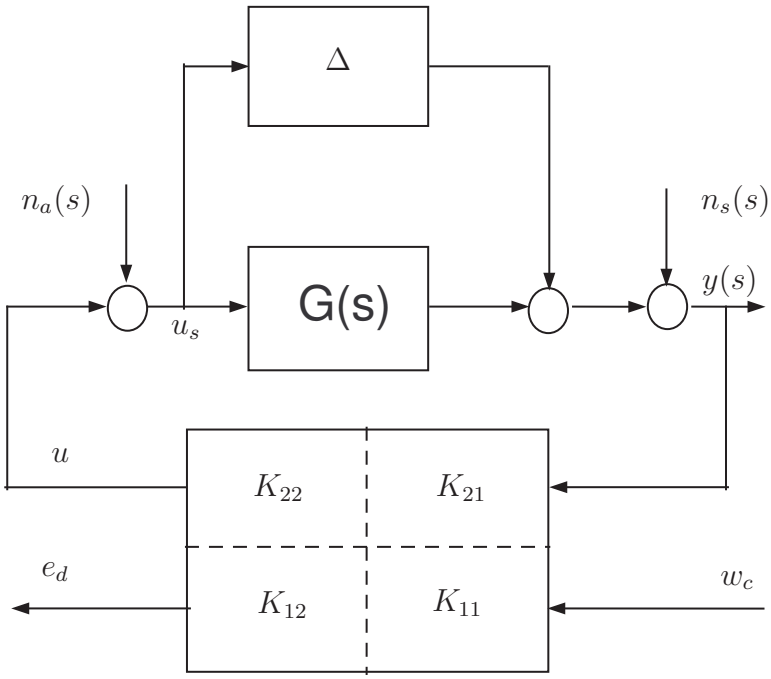

Figure 2.7: Passive FTC system with the 4-parameter controller structure (Patton [1997a]).

in (2.3) and the estimated fault signal $e_d(s)$ is given by (2.4).

$$u(s) = \begin{bmatrix} K_{21} & K_{22} \end{bmatrix} \begin{bmatrix} w_c(s) \\ y(s) \end{bmatrix} \tag{2.3}$$

$$e_d(s) = \begin{bmatrix} K_{11} & K_{12} \end{bmatrix} \begin{bmatrix} w_c(s) \\ y(s) \end{bmatrix} \tag{2.4}$$

Robustness can be achieved for example, using H_∞ robust control design (Zhou et al. [1996]). The objectives are:

1. The control system output is able to track the reference signal and not been affected by the actuators faults.

2. The $e_d(s)$ diagnostic output signal tracks actuator faults (abrupt and incipient faults).

3. The above two properties have to considered in the design so they

Table 2.3: Notations for the passive fault tolerant 4-parameter controller

Variable	Meaning
G(s)	Transfer function matrix of the plant
Δ	Additive uncertainty
w_c	Exogenous inputs
e_d	Diagnostic signal
$n_a = f_a + \eta_a$	Model actuator noise η_a and fault f_a
$n_s = f_s + \eta_s$	Model sensor noise η_s and fault f_s
$u(s)$	Control signal
$y(s)$	Output signal
K_{ij}	Control parameters

persist even in the presence of uncertainties (Δ).

When Passive fault tolerance is applied, there are three main disadvantages:

- No use of diagnostic information.
- No knowledge of fault occurrence.
- Lack of severity information about the fault.

Those disadvantages, limit, the ability of the controller to achieve a reliable fault tolerance against faults. Therefore, the passive approaches are not very practical.

2.4 MAGLEV train technology

MAGnetic **LEV**itated (MAGLEV) trains are being developed in practice since they offer a number of advantages over the conventional trains. This is a developing area that is being attractive to transport industry the last years. MAGLEV trains in contrast with the conventional wheel-on-rail trains do not have mechanical contact with the rails and therefore friction, mechanical losses, vibration and acoustic noise are reduced significantly. The MAGnetic

LEVitated train can be reasonably dated from 1934 when Hermann Kemper from Germany patented it. After this, development of the Maglev train went through the quicken period of the 1960s, the maturity of the 1970s and 1980s, and the test period of the 1990s. The first MAGLEV train to serve the public was operating from 1984 in Birmingham, UK (Pollard [1984]). A photo of the Birmingham MAGLEV train is shown in Fig. 2.8

Figure 2.8: Birmingham MAGLEV train photo (Pollard [1984]).

Although it was operating at low speed the Birmingham MAGLEV was operating for more than 10 years until 1996. High speed MAGLEV train, accomplished practical public service in 2003 in Shanghai, China. Different systems exist in practice for low speed MAGLEV trains (i.e HSST-High Speed Surface Transport) as well as for high speed MAGLEV trains (i.e Transrapid). Details are not given in this thesis about MAGLEV systems but a good review is done by Lee et al. [2006].

There are two main types of suspensions used in MAGLEV trains: The *Electromagnetic suspension* (EMS) where the vehicle is levitated by

producing an attractive force to the rail, and the *Electro-Dynamic suspension* (EDS) which is levitated via a repulsive force to the rail. A third type is the *Hybrid Electro-Magnetic Suspension* (HEMS) where permanent magnets are used in conjunction with the electromagnets in order to lift the vehicle (see Wai et al. [2005]). Using this type of suspension a power-saving electromagnetic suspension can be achieved (Morishita et al. [1989]). In this thesis the EMS suspension is considered. A picture of the German Transrapid MAGLEV suspension (Yan [2004]) used in Shanghai, China is illustrated in Fig. 2.9. In this picture the EMS suspension with air gap (point A) of around $10mm$ can perform up to a maximum speed of $500km/h$.

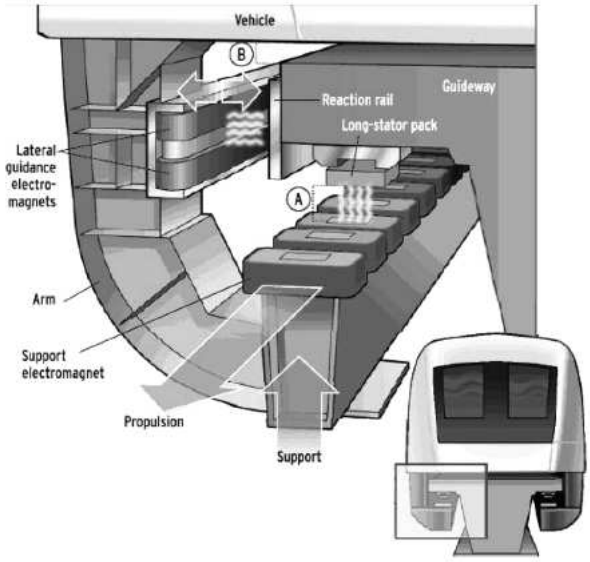

Figure 2.9: EMS system for the transrapid (Yan [2004]).

Because the MAGLEV train is not using wheels to run on the rails but attractive or repulsive forces it offers a number of advantages against the conventional wheel-on-rail trains. The advantages are listed in Table 2.4. It is clear that the MAGLEV train is less noisy, requires very low maintenance and it cannot derailed since it is supported on the guideway.

Table 2.4: MAGLEV Train advantages against Wheel-On-Rail systems (Yan [2004]).

	MAGLEV Train	Iron Wheel-On-Rail system
Vibration and Noise	No mechanical contact, 60-65dB	Contact between Wheels and Rails, 75-80dB
Safety	No possibility of derailment	Derails from a minor rail's defect
Guideway	Light vehicle and distributed load	Heavy and concentrated load
Maintenance	Very little	Periodic replacement of wheels, gear, rails, etc.
Grade	About 80-100/1000	About 30-50/1000
Curve	In 30[m] in radius	In 150 [m] in radius

The Electromagnetic suspension design is discussed in details by Goodall [1985, 2008]. This is a non-linear open loop unstable system with some non-linear control methods described by Zhao and Thornton [1992] and Sinha and Pechev [2004]. Since non-linear controllers are not favourite in practice many linear controller approaches have been found in the literature including Zhao and Thornton [1992]; Sinha and Pechev [2004]; Mohamed et al. [1997]; Morishita [1996]; Lane et al. [1997]; MacLeod and Goodall [1996]; Paddison [1995] and Goodall [2000]. The MAGLEV suspension has three requirements enumerated as follows:

- support the large weight of the vehicle and the load (i.e passengers)
- follow the intended variations in the position of the track
- provide isolation from the unintentional irregularities in the track position

These requirements cannot be fully met simultaneously because there is a trade-off between them. The MAGLEV suspension has to satisfy a number of requirements in order to perform satisfactorily with respect to the ride quality experienced by the passengers, fault tolerance, input power and the international transport rules. The performance requirements have to take into account the disturbances coming for the rails (i.e both deterministic and stochastic). The requirements and working limitations are described by Goodall [1994, 2004]. Because the system is open loop unstable the closed loop control system is very sensitive to sensor faults. In fact, if there is an air gap sensor failure, it is possible that the MAGLEV suspension will go unstable and therefore it will either fall-off or stick to the rail and probably result in catastrophic failure. Some active fault tolerant design approaches for sensor failures are discussed by Huixing et al. [2006]; Long et al. [2007] and Sung et al. [2005].

Since the EMS system is non-linear, open-loop unstable, safety-critical system with non-trivial performance requirements it can serve as a good example for the sensor optimisation frameworks aim to find the minimum

number of sensors for controlling the MAGLEV suspension with extension to sensor fault tolerance.

2.5 Summary

In this chapter, a literature survey based on the tools that can help in order to implement the optimised sensor configurations for control and fault tolerance theoretical frameworks is done. An overview of the sensor selections methods that exist is presented and the Fault Tolerant Control concept is described. In fact, FTC system design proves to be useful when hardware redundancy is to be minimised with consequent reduction of the overall cost although complexity may increase. Moreover, the MAGLEV suspension is to be used as example within the systematic frameworks. The MAGLEV suspension is a non-linear, open loop unstable, safety-critical system with non-trivial requirements. This practical problem can serve as a baseline for the systematic frameworks to be developed for more complicated plants.

Finally, the originality of this thesis is to combine the three concepts together within one framework in order to select the best sensor set with which the optimum performance is achieved while maintaining sensor fault tolerance according to design requirements. Evolutionary algorithms are merged within the systematic frameworks for the purpose of the performance optimisation for each sensor set. The next chapter describes the evolutionary algorithms along with detailed description of the Non-dominated Sorting Genetic Algorithm II (NSGA-II) to be used throughout this thesis.

Chapter 3

Multiobjective constraint optimisation

3.1 Introduction

Meta-heuristic approaches have become very popular in recent years since the optimisation field becomes more and more favoured within industry as well as science. In fact, Meta-heuristic approaches are divided into different optimisation methods including tabu search, simulated annealing, ant colony algorithms and evolutionary algorithms. A detailed description of the different Meta-heuristic approaches is given by Dreo et al. [2006]. Varieties of the aforementioned methods include particle swarm optimisation (PSO) and GRASP.

Survey and descriptions of existing evolutionary-based multiobjective optimisation techniques is found by Fonseca and Fleming [1995] followed by Coello [1999a] and Coello [1999c]. Another survey is presented by Kicinger et al. [2005]. Evolutionary algorithms have been used extensively compared to the other meta-heuristic approaches and the reason is as Jones et al. [2002] indicates: *'....the fact that genetic algorithms can naturally produce multiple solutions and therefore provide an ideal tool for generating a representation of the many solutions that comprise the efficient set.'*

Genetic algorithms (GAs) were inspired by Drawin's based on survival of biological reproduction, as described by Goldberg [1989]. Since the first version of GA a number of different versions of genetic algorithms invented and all summarised by Konak et al. [2006]. The first genetic algorithm for multiple objectives is the **V**ector **E**valuated **G**enetic **A**lgorithm (VEGA) that was presented by Schaffer [1985], followed by the multi-objective GA (MOGA) by Fonseca and Fleming [1993] which is a simple extension of VEGA but with slow population convergence due to problems related to niche size parameter. A new genetic algorithm is recently developed by Zou et al. [2008] but not encountered in this research work.

Based on the comparison of different multiobjective evolutionary algorithms by Zitzler et al. [2000] the **N**on-dominated **S**orting **G**enetic **A**lgorithm developed by Srinivas and Deb [1994] seams to converge fast but there are three disadvantages of the NSGA algorithm briefly summarised as (see Deb et al. [2002]):

- High computational complexity of non-dominated sorting.
- Lack of elitism
- Need to specify the sharing parameter.

An improved version of NSGA is developed by Deb et al. [2002] and is called NSGA-II. The latter genetic algorithm is able to deal with more complex and real-world multiobjective optimisation problems. The NSGA-II is used throughout this thesis and it proves to be very powerful tool for one more reason. Both, MOGA and NSGA are niche size parameter dependants. The niche parameter has to be set by the user and effectively affects the spread of the solutions onto the optimum Pareto front. In fact, if the algorithm has to optimally tune the controllers with different sensor sets this may need to be dynamically changed in order to incorporate with different dynamical systems. This problem is avoided using the recently developed **N**on-dominated **S**orting **G**enetic **A**lgorithm II where the niche

size parameter is avoided because the crowding distance mechanism (that is explained in details in Section 3.5.1) is used to spread the solutions evenly onto the optimum Pareto front.

3.2 Genetic algorithms

Genetic algorithms functionality is based on the principles of natural evaluation and population genetics. The differences between genetic algorithms and other traditional optimisation techniques such as the gradient method are briefly summarised as follows:

- the parameters to be optimised are encoded instead of using the real parameters
- genetic algorithms search for the potential solution based on the the number of trials (maximum generation) in a search space.
- each trial solution is guided through based on objective assessment using fitness functions to identify the best solution in each population.

Genetic algorithms search for the best solution based on the fitness value assigned to each population. The fitness value indicates how good the solution to solve the problem is by giving a higher value of fitness within all the solution. The population that consists of individuals known as *chromosomes* are paired and genetic algorithm operators are applied to them. For each chromosome in the population, the fitness value is assigned based on the evaluation of the fitness function.

In general the operations applied to the individual during evolution are mainly three:

1. selection,
2. crossover,
3. and mutation

For *selection*, a string of chromosomes is chosen randomly based on the magnitude of their normalised fitness value. Fitness is normalised with an average value, so the strings with above fitness will have more potential than those with below average fitness. This process will result in one or more copies of higher fitness values in order to reproduce in a new generation. The function of *crossover* is to produce a new trial solution by exchanging a part of the structure between two selected strings. By doing this, the weaker individuals in the population can be replaced with the best population. The *mutation* operator can be viewed as a secondary operator to ensure against loss of information in any chromosome and as a way of getting the algorithm out of stuck state (i.e local minimum). This operator makes a small random change in the chromosome with one or more chromosome changed at one time.

Initially, genetic algorithms start without any knowledge of the correct solutions (due to randomly generated chromosomes in the population), and implement an interacting environment and evolution operators through the process of searching for a better solution as shown in Fig. 3.1. The evolution process is completed when the population has converged or the maximum number of generations have been reached.

3.3 Genetic algorithms in control engineering

Genetic Algorithms (GA), introduced by Holland and further explained in detail by Goldberg [1989], have successfully been used in many control systems design areas such as controller design and/or parameter optimisation, stability analysis, fault diagnosis, robotic design and system reliability. Particularly, using genetic algorithms for controller parameter optimisation, it is possible to select values for a large number of controller parameters when attempting to obtain a number of control objectives with respect to satisfactory control performance.

Evolutionary algorithms have been widely used in control engineering as

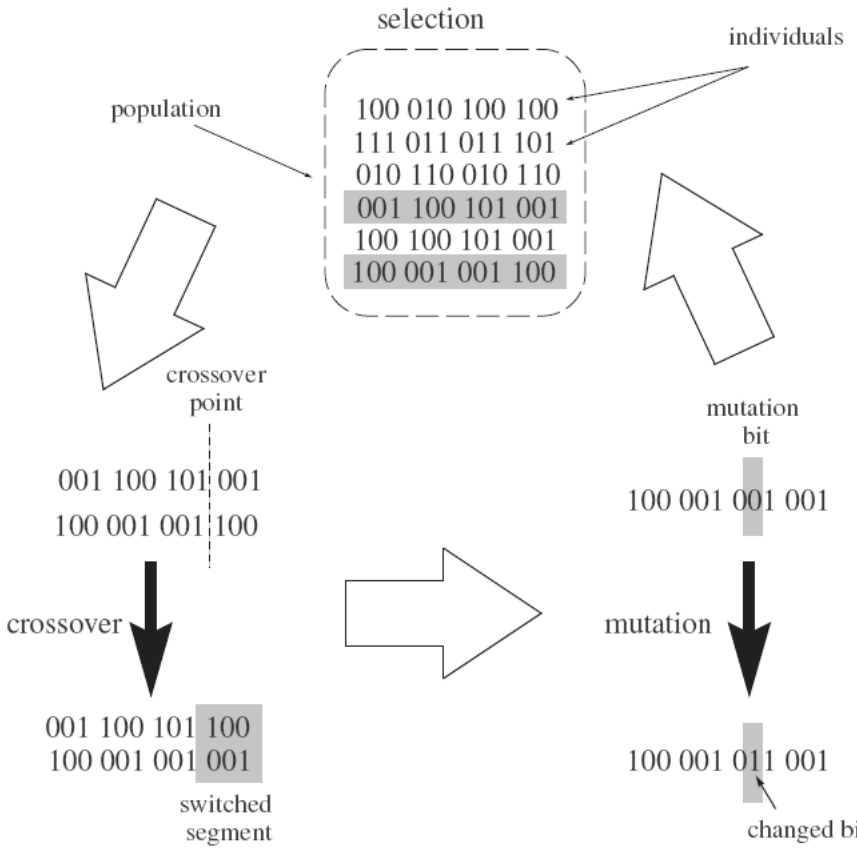

Figure 3.1: Basic genetic algorithm representation (Zamzuri [2008]).

mentioned by Fleming and Purshouse [2002], Fleming and Fonseca [1993] and Wang et al. [2003]. A number of applications have been found in control systems for classical control strategies optimisation (see Zhenyu and Pedersen [2006], Obika and Yamamoto [2005], Lin et al. [2003], Krohling et al. [1997], Kwok et al. [1993]) as well as for modern controller optimisation (Pereira and Araujo [2004], Sun et al. [2003], Neumann and Araujo [2004], Chellaboina and Ranga [2005]).

The structure and/or the controller parameters are included into the chromosome of the evolution procedure. The desired performance is assigned to the objective functions via different quantities (i.e. output settling time, overshoot, H_∞ robustness margins etc.). In fact, such problems are posed as

the minimisation of the objective functions with respect to optimal tuning of the controller's parameters.

Obviously, the controller parameters are real values but early genetic algorithms like NSGA-II convert them into binary forms. This method increases computational memory usage and a loss of precision occurs due to conversion from real to binary forms. When using real parameters the controller parameters are directly used to form the chromosomes without the need for transformation. Moreover, the feasibility of genetic algorithms can be seen when a case of mixed decision variables (binary and real parameters) needs to be used, and extra care should be taken to ensure the genetic operators use a function correctly over the decision variables.

A manually designed controller can achieve a certain desirable performance but is not the optimum. Moreover, the problem becomes more complex when there is a number of performance metrics within specific working boundaries to achieve. Further more its almost impossible to optimise the controller/s parameters for every sensor set that is available especially for systems with many outputs.

The applications of genetic algorithms in the control area can be categorised into two main areas:

- *On-line tuning and adaptation:* In this case, the genetic algorithm is used as adaptive control tuning for a known and unknown plant. However, this method is not widely applied due to time constraint since large computational effort is required until the maximum generation is reached.

- *Off-line design:* In this case the evolutionary process is applied to a particular control optimisation problem in order to achieve an optimum performance within given limits. Off-line optimisation is widely used since the time constraint is relaxed but not ignored. Some problems require huge computational effort and therefore time limit is

an important issue. In this thesis the *Off-line design* is implemented due to large computational effort.

3.4 Multiobjective constraint optimisation

In most practical applications, designing the controller requires considerations of multiple conflicting performance criteria. GAs performance criteria can be considered as objective functions to be achieved towards a better result (usually minimise). A trade-off often occurs between the objectives where a better result in one objective will cause a deterioration in other. The problem is posed as follows:

Find $\mathbf{X}$ which minimises the objective functions:

$$\phi_1(\mathbf{X}), \phi_2(\mathbf{X}), \phi_3(\mathbf{X}).....\phi_k(\mathbf{X}) \tag{3.1}$$

subject to:

$$g_i \leq 0, \quad i = 1, ..., n \tag{3.2}$$

$$h_j = 0, \quad j = 1, ..., p \tag{3.3}$$

where $\mathbf{X}$ is the vector of solutions ($\mathbf{X} = x_1, x_2, ...x_r$), k is the number of objective functions, n is the number of inequality constraints and p is the number of equality constraints (note that constraints can be linear or non-linear). Generally, constraints are separated into two categories: The inequalities that are called *soft constraints* and equalities are called *hard constraints*. Both types are widely used in the thesis since the closed-loop response of the MAGLEV suspension problem involves a lot of different constraints.

In Fig. 3.2 an example of two objective functions is given. Assume that $\mathbf{F}$ is the feasible region and $\mathbf{S}$ is the whole search space, then of course $\mathbf{F} \subseteq \mathbf{S}$.

The problem here is to minimise ϕ_1 and ϕ_2 subject to $g_1 \leq \phi_1(\mathbf{X}_1)$ and $g_2 \leq \phi_2(\mathbf{X}_2)$ respectively. The feasible region is defined from the constraints which in this example depends on the objective function values $\phi_1(\mathbf{X}_1)$ and $\phi_2(\mathbf{X}_2)$ with solution vectors $\mathbf{X}_1$ and $\mathbf{X}_2$ respectively. The optimum Pareto front with non-dominated solutions within the feasible region is shown with dark dots. Particularly, the best solution of $\phi_1(\mathbf{X})$ is the worst for $\phi_2(\mathbf{X})$ and viceversa (note that the functions are constrained by g_1 and g_2). Within the feasible region, the dominated solutions are also shown with $*$. The $\times$ mark shows solutions that although they are on the optimum Pareto front are lying on the infeasible solution area, while x_1 solutions are constrained from $\phi_2(\mathbf{X}_2)$ and x_3 from $\phi_1(\mathbf{X}_1)$. Solutions x_2 are penalised from both assigned constraints.

There exist many constraint handling techniques throughout the literature and they are all summarised by Coello [1999b]. In the next section a brief description is given along with the techniques used in this thesis.

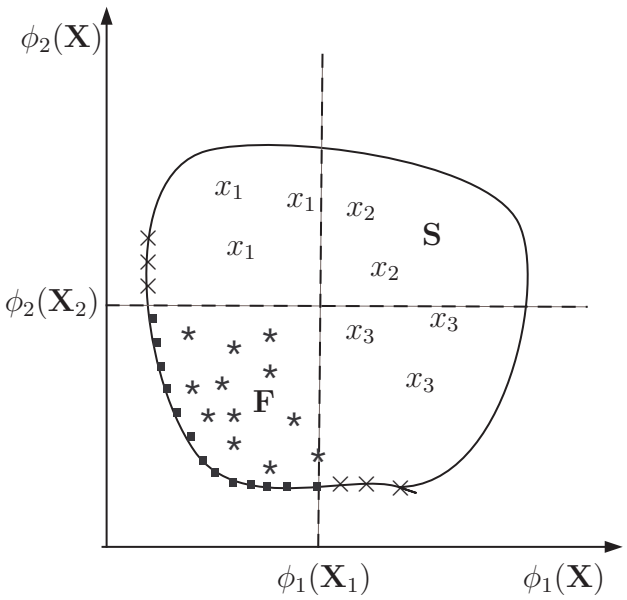

Figure 3.2: Mimisation of ϕ_1 and ϕ_2 subject to two constraints.

3.4.1 Constraint handling via penalty functions

In order to design the controller via genetic algorithms in such a way that the overall control system operates within desired boundaries, one or more combinations of the constraint-handling technique are required. A survey on constraint handling techniques is done by Coello [1999b] and a recent one is also found in Coello [2002].

The most popular efficient and simple technique is the penalty function approach. There are a number of penalty function methods used to avoid the infeasible regions within the search space and 'guide' the objective functions within the boundaries decided from the specifications (Coello [1999b]):

- Static penalties
- Dynamic penalties
- Annealing penalties
- Adaptive penalties
- Self-adaptive penalties
- Segregated genetic algorithm
- Penalty function based on feasibility
- Death penalty

In this thesis a combination of the static, dynamic and the death penalty methods are implemented depending on the current needs. Using the death penalty function is the easiest way but this is not suitable for all problems. It was found that the combination of static or dynamic with the death penalty is required.

3.4.2 Death penalty method

Rejection of infeasible individuals (also called 'death penalty') is the easiest and most efficient way to handle constraints because when a certain solution is not within the required limits it is assigned a fitness of zero. This solution will be rejected for the next generation. As the generations evolve the penalised individuals are rejected and the optimum individuals remain. This method is mainly used for the rejection of individuals that cause instability to the closed-loop response during simulations. It is not possible to quantify the objective functions since an unstable system behaves outside the modelled properties.

3.4.3 Static penalty method

The static penalty method mentioned by Coello [2002] is very well described by Deb [2001] and is summarised as follows:

The soft constraint violation for each constraint, k^i, is given as

$$\omega_i(k^i) = \{^{|g_i(k^i)|, \quad if \quad g_i(k^i)<0}_{0 \qquad otherwise} \tag{3.4}$$

Each soft constraint is normalised as in (3.5) g_{jlow} and g_{jhigh} for values less than the predefined level and values higher than the predefined respectively.

$$g_{ilow} = -\frac{k^i}{k^i_{des}} + 1 \geq 0 \quad g_{ihigh} = \frac{k^i}{k^i_{des}} - 1 \geq 0 \tag{3.5}$$

Where, k^i_{des} is the predefined constraint value and k^i is the measured value.

The hard constraint violation, ψ_j, is given as

$$\psi_j(f^j) = \{^{|h_j(f^j)| \quad if \quad h_j(f^j)\neq 0}_{0, \qquad otherwise} \tag{3.6}$$

This is transformed into a *soft constraint*, allowing a small tolerance value ξ

(see Coello [2002]). The hard constraint violation function is then given as

$$h_j =\mid f^j \mid -\xi < 0 \tag{3.7}$$

Where f^j is the desired constraint to be equal to zero.

The overall constraint violation function is then constructed and given in (3.8). This function is to be used as a metric for the controllers' performance towards the given constraints in the real control system design problem.

$$\Omega(k^{(i)}, f^{(j)}) = \sum_{i=1}^{i} \omega_i(k^{(i)}) + \sum_{j=1}^{j} \psi_j(f^{(j)}) \tag{3.8}$$

The overall constraint violation is then added to each of the objective functions values forming the following equation

$$\Phi_k = \phi_k + R_k\Omega(k^{(i)}, f^{(j)}) \tag{3.9}$$

Where ϕ_k is the objective function, Φ_k is the penalised objective function and R_k is the penalty parameter. It can be seen that if all constraints are satisfied the overall constraint violation function in (3.8) is zero therefore $\Phi_k = \phi_k$ while if $\Omega(k^i, f^j)$ is not zero, there is some constraint violation and this is added to the objective functions reducing the possibilities to survive the next generations.

The penalty parameter is defined by the user and is used to define the weight of the overall constraint violation on the objective function. The penalty parameter affects the end result (Optimum Pareto front) and the value of it depends on the problem nature. For more details on the effect of the penalty parameter to the final result see Deb [2001]. In some cases, while the constraints violations are getting smaller the effect of the Ω is getting less ending with solutions within the infeasible space. For this reason the dynamically updated penalty function is used and is described next.

3.4.4 Dynamically updated penalty function

In the case where the constraints violations are very small the dynamical updated penalty parameter is necessary. Particularly, while the constraint violations are getting smaller, the overall constraint violation function increases. This is useful in order to avoid infeasible solutions as described by Joines and Houck [1994]. The objective function in (3.9) is modified as follows:

$$\Phi_k = \phi_k + (\zeta \times t_g)^\alpha \times \Omega(\beta, k^{(i)}, f^{(j)}) \tag{3.10}$$

where ζ is defined here as the penalty parameter ($\zeta = R_k$), α,β are constants defined by the user and t_g is the current generation number. The overall constraint violation is then given as

$$\Omega(\beta, k^{(i)}, f^{(j)}) = \sum_{i=1}^{i} \omega_i^\beta(k^{(i)}) + \sum_{j=1}^{j} \psi_j(f^{(j)}) \tag{3.11}$$

The overall constraint violation function proves to be very useful for the sensor optimisation frameworks because it can be used as an indicator of whether a closed-loop configuration with the corresponding controller violates the preset constraints or not. Particularly, where we have a population of 50 individuals that represent the optimised parameters of 50 controllers, the overall constraint violation can easily be used as tool to select the controllers that do not violate any of the constraints. This concept is presented in Chapter 5.

3.5 Non-dominated Sorting Genetic Algorithm II

3.5.1 NSGA-II principle

In this section a description of the **N**on-dominated **S**orting **G**enetic **A**lgorithm II introduced by Deb et al. [2002] is presented. The first step in the overall evolutionary procedure is to create an initial parent population (P_{t_0}) of

size $2N_p$. The population is sorted according to the non-domination of the individuals. Each individual is assigned a fitness (or rank) equal to its non-domination level (1 is the best level, 2 is the next-best level and so on). In fact the solutions with rank one are spread on the first front with rank 2 to the second front and the rest accordingly. After non-domination sorting, the crowding distance is assigned to each individual. The next step is to create the offspring population Q_{t_0} of size N_p from the parent population P_{t_0} using genetic operators including crossover, mutation and binary tournament selection. After the initialisation the algorithm continues to produce the next generation in an iterative way that is described next.

The NSGA-II procedure is illustrated in Fig. 3.3. First the combined population R_t with size $2N_p$ is created from P_t and Q_t ($R_t = P_t \bigcup Q_t$). The population R_t is sorted according to non-domination. Elitism is ensured since all previous and current individuals are included in R_t. Once the non-domination sorting is done, and the crowding distance is assigned the new population P_{t+1} of size N_p start filling via binary tournament selection. The selection is done using the rank and the crowding distance. The

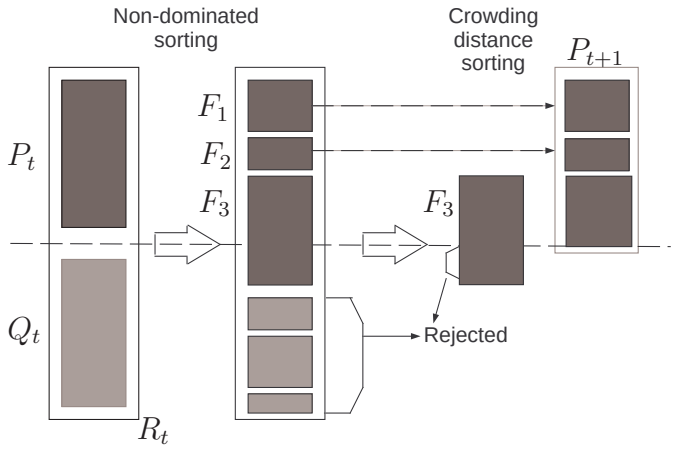

Figure 3.3: Diagram of NSGA-II optimisation procedure (Deb et al. [2002]).

best individuals that belongs to the fronts closer to the Pareto optimum $(F_1, F_2, ...F_n)$ starts filling the new parent population (R_{t+1}). From the

figure it can be seen that the fronts F_1 and F_2 are fitted into the new parent population P_{t+1} but the solution within F_3 front cannot fit all of them. In this case the individuals with the largest crowding distance are selected to complete the new parent population. After the creation of the new parent, the genetic operators crossover and mutation are implemented to create the next one. This procedure is repeated until the maximum generation is reached. If all the parameters assigned are correctly selected by the user then the Pareto optimality is ensure as well as uniform distribution of the solutions on the optimum Pareto front.

The overall procedure of the NSGA-II given by Deb et al. [2002] is summarised as follows:

1. Combine parent and offspring population to create $R_t = P_t \bigcup Q_t$
2. Set new population $P_{t+1} = \emptyset$. Set a counter $i = 1$. Until $|P_{t+1}| + |F_i| < N_p$, perform $P_{t+1} \bigcup F_i$ and i=i+1
3. Perform Crowding-sort $(F_i <_c)$ procedure and include most widely spread $(N_p - |P_{t+1}|)$ solutions by using crowding distance values sorted F_i to P_{P+1}.
4. Create offspring population Q_{t+1} from P_{t+1} by using binary tournament selection, crossover and mutation operators

Crowding distance

Once the non-dominated sorting is done, the crowding distance is assigned to each individual. Crowding distance is used by Deb et al. [2002] and the purpose is to uniformly distribute the solutions on the best Pareto front. The advantage of this method is that the user defined niches sharing method is not necessary anymore.

The basic idea is to find the Euclidian distance between each individual on a front based on their k^{th} objective in the k^{th} dimensional hyperspace. The

individuals within the boundary are always selected since they have infinity distance assignment. The technique is summarised as follows:

1. For each front F_i, initialise the distance (d_i) to be zero.

2. For each objective function ϕ_k, sort the individuals in front F_i based on objective k in ascending order. i.e sort(F_i, k)

3. for k=1,2,3,....,K assign a large distance to the boundary solutions ($d_{I_i^k} = d_{I_i^k} = \infty$) and all other solution $j = 2$ to $(l-1)$ assign:

$$d_{I_j^k} = d_{I_j^k} + \frac{\phi_k^{(I_j^k+1)} - \phi_k^{(I_j^k-1)}}{\phi_k^{max} - \phi_k^{min}} \tag{3.12}$$

   where I_j is the solution of the j^{th} member of the sorting list while ϕ_k^{max} and ϕ_k^{min} are the maximum and minimum population values in the k objective function.

3.5.2 NSGA-II code validation

In this section, two examples are given to test the selected evolutionary algorithm. Particularly, the evolutionary algorithm, is tested under a disjoint Pareto Optimum (KUR test function) and under constraints assignment (CONSTR test function). In the later problem, the static penalty approach is used as explained in Section 3.4.3.

The first problem is a non-convex problem named KUR with two objective functions to be minimised as follows:

$$\phi_1(x) = \sum_{i=1}^{n-1}(-10e^{-0.2\sqrt{x_i^2+x_{i+1}^2}}) \tag{3.13}$$

$$\phi_2(x) = \sum_{i=1}^{n}(|x_i|^{0.8} + 5sinx_i^3) \tag{3.14}$$

There are three variables (x_1, x_2, x_3) varying randomly in a search space between -5 and +5. The parameters assigned to the genetic algorithms are

listed in Table 3.1. Generally, to have a good mixing of genetic material the crossover probability has to be high ($p_c = 0.9$) and the mutation probability is $p_m = 1/n_r$ where n_r is the number of variables. For real-coded NSGA-II the distribution indexes for crossover and mutation operators as 20 and 20 respectively. The aforementioned parameters are used throughout this thesis for the simulations. For the KUR problem, the overall evolutionary

Table 3.1: NSGA-II parameters for KUR and CONSTR test functions

	KUR	CONSTR
Maximum generation	500	500
Population size	300	50
Crossover probability	0.9	0.9
Mutation probability	1/3	1/2
SBX parameter	20	20
Mutation parameter	20	20

procedure is depicted in Fig. 3.4. The maximum generation limit is set to 500 and the population to 300. Clearly, it can be seen that from the first 5 generations (Fig. 3.4(a)), the solutions are spread in the whole Pareto while on the 50^{th} (Fig. 3.4(b)) generation the optimum Pareto front is almost fully recovered showing that the convergence of the population is fast. Until the 100^{th} generation (Fig. 3.4(c)) the Pareto optimum is recovered and maintains its shape until the maximum generation is reached (Fig. 3.4(f)). This non-convex problem, has a disjoint Pareto optimum which is fully recovered from the selected algorithm. Running the code for a few trials, the results may slightly differ from each other but generally this is the final shape that appears.

The second case is the CONSTR problem, where two objective functions are to be minimised subject to the soft constraints $g_1(x) \geq 6$ and $g_2(x) \geq 1$.

The problem is formulated as follows

$$\phi_1(x) = x_1 \tag{3.15}$$
$$\phi_2(x) = (1 + x_2)/x_1 \tag{3.16}$$

subject to

$$g_1(x) = x_2 + 9x_1 \geq 6 \tag{3.17}$$
$$g_2(x) = -x_2 + 9x_1 \geq 1 \tag{3.18}$$

where, two variables are considered with a search space taken as $x_1 \in [0.1, 1]$ and $x_2 \in [0, 5]$ while the two constraints define the feasible and the infeasible areas. The static penalty approach is taken into account with penalty parameter values equal to $R_{f_1} = 1$ and $R_{f_2} = 10$ for the ϕ_1 and ϕ_2 respectively. The evolution is done within 500 generations and the population consists of 50 individuals (Table 3.1). The overall results are illustrated in Fig. 3.5. Clearly, the fast convergence algorithm, spread the solutions on the Pareto front the first 5 generations (Fig. 3.5(a)) while the optimum Pareto front is almost recovered in 20^{th} generation Fig. 3.5(b). Until the 50^{th} generation (Fig. 3.5(c)) the optimum Pareto front is fully recovered and retains the same shape until the maximum generation is reached (Fig. 3.5(f)). Clearly, the static penalty approach is simple and straight forward to use and it proves to be very successful if the penalty parameter is adjusted appropriately. In real applications (i.e control system optimisation) where the optimum Pareto front is not known a few trials may needed in order to assign the penalty parameters.

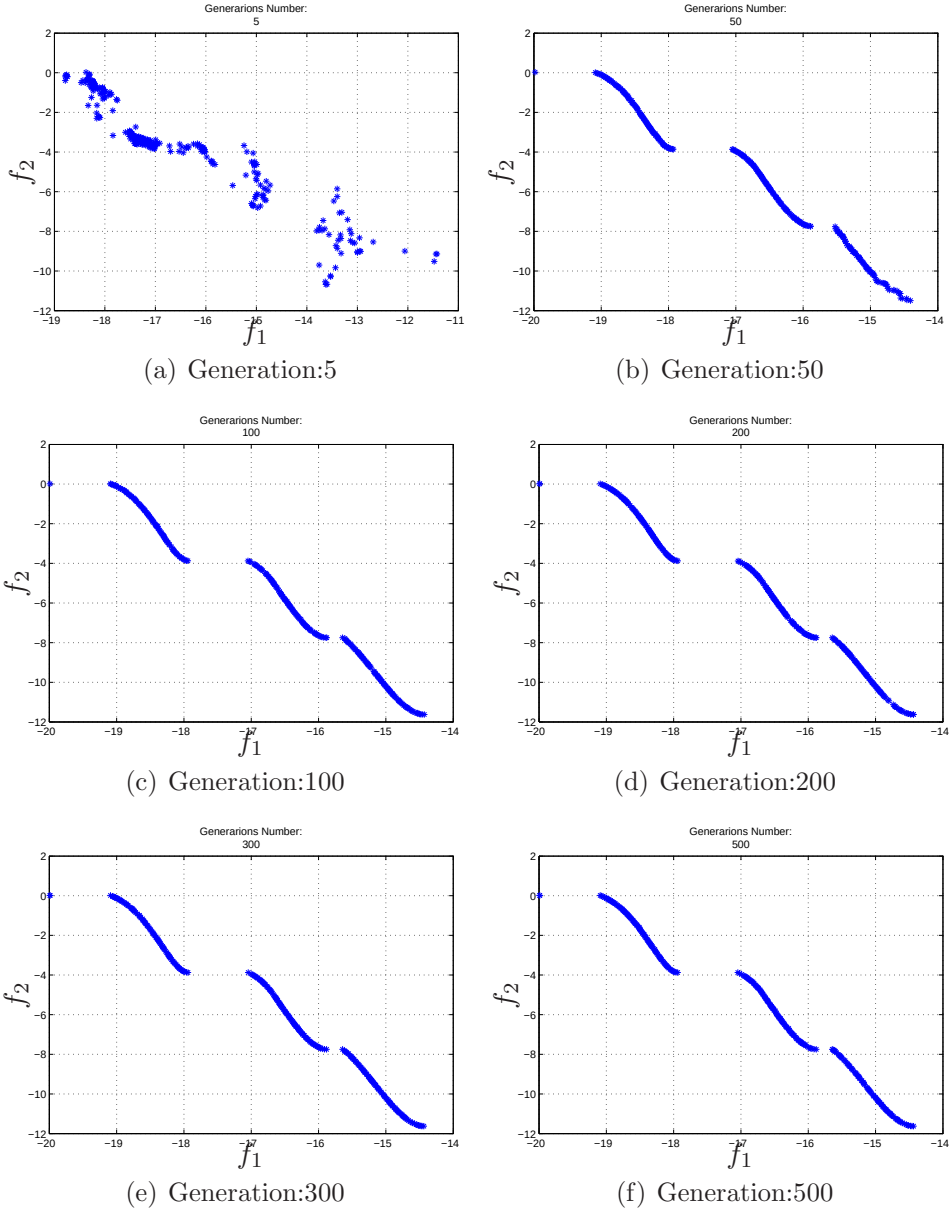

(a) Generation:5 (b) Generation:50

(c) Generation:100 (d) Generation:200

(e) Generation:300 (f) Generation:500

Figure 3.4: KUR problem generations evolution for 500 generations.

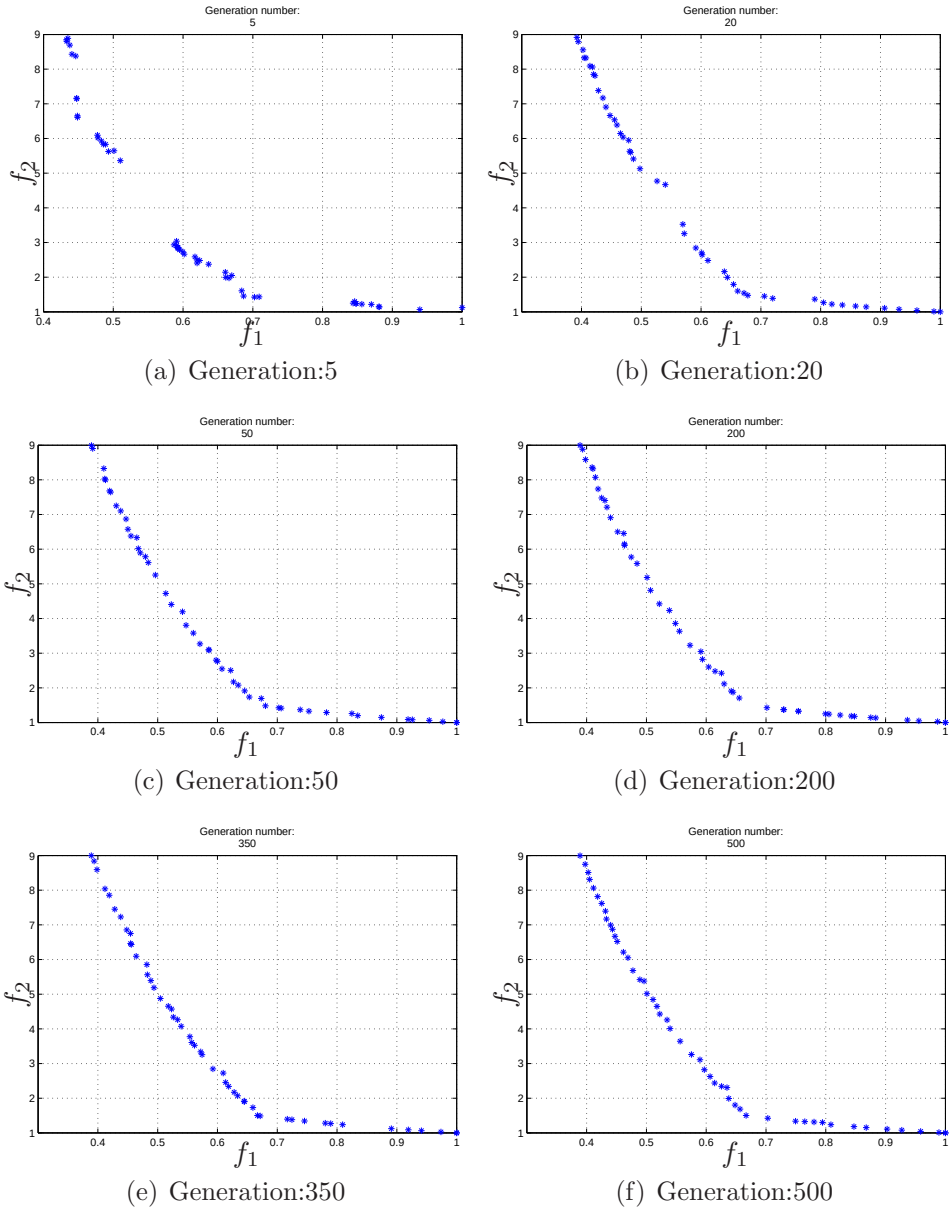

(a) Generation:5 (b) Generation:20

(c) Generation:50 (d) Generation:200

(e) Generation:350 (f) Generation:500

Figure 3.5: CONSTR problem generations evolution for 500 generations.

3.6 Summary

In this chapter, a survey on the different possible meta-heuristic approaches that are used within this thesis is given. Evolutionary algorithms are widely used in control system design and as Fleming and Purshouse [2002] says "*The evolutionary algorithm (EA) is a robust search and optimisation methodology that is able to cope with ill-behaved problem domains, exhibiting attributes such as multimodality, discontinuity, time-variance, randomness, and noise. It permits a remarkable level of flexibility with regard to performance assessment and design specification.*" In this thesis, the recently developed genetic algorithm NSGA-II that is a class of the Evolutionary Algorithms is used and proves to be very powerful optimisation tool for control systems design where multiple of objectives and constraints have to be considered.

The performance of the selected GA is illustrated in two examples where the elitism of the best population is retailed in both KUR and CONSTR examples during the evolution of the generations. In the KUR problem the disjoint optimum Pareto front between the two objective functions is successfully recovered. The second problem involves constraint-handling techniques. The minimisation of two objective functions subject to two constraints is considered. The optimum Pareto front is fully recovered using the static Penalty function approach that is used to reject the infeasible solutions and it proves to work effectively with the proposed NSGA-II. The proposed genetic algorithm performs well however, the efficacy of NSGA-II is shown in next chapter where two classical control strategies are used to present the baseline of the optimised sensor configurations concept.

Chapter 4

MAGnetic LEVitated (MAGLEV) suspension model

4.1 Introduction

The 1DOF (degree-of-freedom) model represents the quarter of a typical MAGLEV vehicle. In this chapter the single degree of freedom model of an Electromagnetic (EMS) suspension system is analysed. Track fundamentals as well as closed-loop response objectives and constraints are given. The model is non-linear therefore in order to design linear controllers, linearisation of the suspension model is required. The state space form of the linear model includes both control inputs and disturbance matrices.

4.2 Single degree of freedom model (quarter car model)

The basic quarter car model of the MAGLEV vehicle is shown in Fig. 4.1. As it can be seen from the front view in Fig. 4.1(a) the MAGLEV suspension consists of an electromagnet with a ferromagnetic core and a coil of N_c turns which is attracted to the rail that is made out of ferromagnetic material. The carriage mass (M_s) is attached on the electromagnet, with z_t the rail's position and z the electromagnet's position.

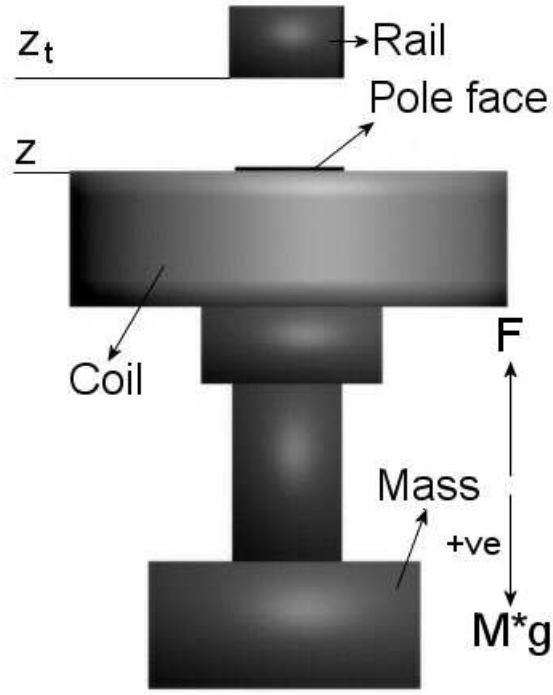

(a) Front view

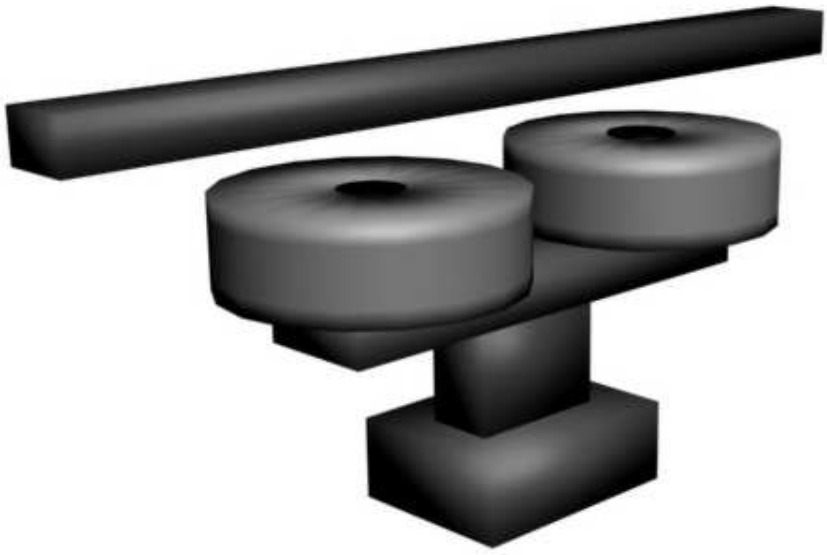

(b) Side View

Figure 4.1: Quarter car suspension diagram.

The air gap $(z_t - z)$ is to be maintained close to the operating condition required. Note that this is a single-stage electro-magnetic suspension that has been shown to be suitable for low speed vehicle (Goodall [2004]), where other MAGLEV systems, particularly those for high speed, have a separate conventional secondary suspension, for example using air spring to give good ride quality. The Tansrapid is the a high speed train that uses such technology as described in Abuzeid et al. [2006]. In the motion diagram vertically downwards is taken as positive. Four important variables in an electromagnet are force F, flux density B, air gap G and the coil current I.

Their relationships are given by Goodall [2008] and Goodall [1985] and they are presented in Fig. 4.2. As it can be seen from the graphs, the relationships between the variables show that the system is non-linear but the nonlinearities are considered as 'soft' because:

1. There are no hard nonlinearities present such as discontinuities.
2. The variations of the variables around the operating point of the air gap are relative small.

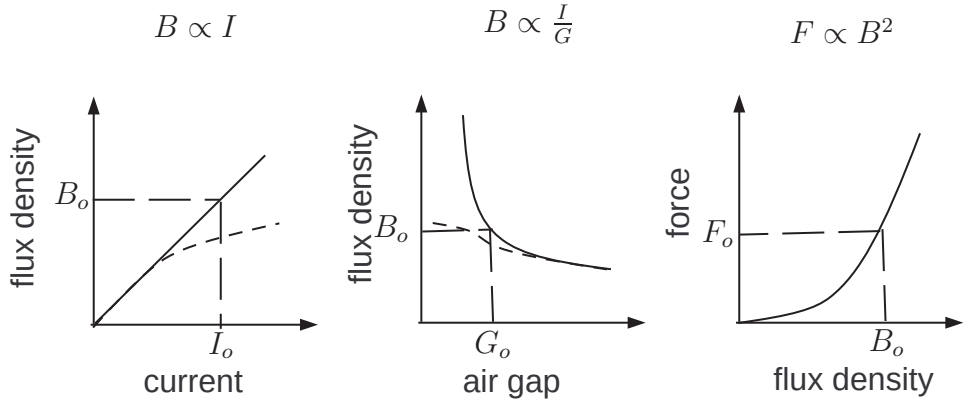

Figure 4.2: Relationship between the key variables describing the magnet. The straight lines show the theoretical relationships and the broken lines indicate the effects of magnetic saturation in the magnet core.

The assessment of the 'softness' of the nonlinearities is subjective, but the

experience of most magnetic suspension designers is that the system is soft enough to linearise and this allows the successful application of linear analysis and linear control strategies as it is implemented in this thesis. Nevertheless, to optimise the performance, the controllers are tuned for the non-linear model.

The flux density is given by

$$B = K_b \frac{I}{G} \tag{4.1}$$

and the Force is

$$F = K_f B^2 \Rightarrow F = K_f \left(\frac{I}{G}\right)^2 \tag{4.2}$$

The equation of motion from Newton's second law is

$$M_s \frac{d^2 Z}{dt^2} = M_s g - F \tag{4.3}$$

and the electrical circuit involved from the electromagnet's coil is

$$V_{coil} = I R_c + L_c \frac{dI}{dt} + N_c A_p \frac{dB}{dt} \tag{4.4}$$

From (4.3) and (4.4) the Simulink model is builded in Fig. 4.3. The non-linear model of the MAGLEV suspension includes the derivative term s which causes numerical errors resulting to false results. The derivative term s is removed and the modified non-linear model is discussed in the next section.

4.3 Modified non-linear model for the MAGLEV suspension

First substitute force equation (4.2) into motion equation (4.3)

$$\frac{d^2 Z}{dt} = g - \frac{K_f}{M_s} \frac{I^2}{G^2} \tag{4.5}$$

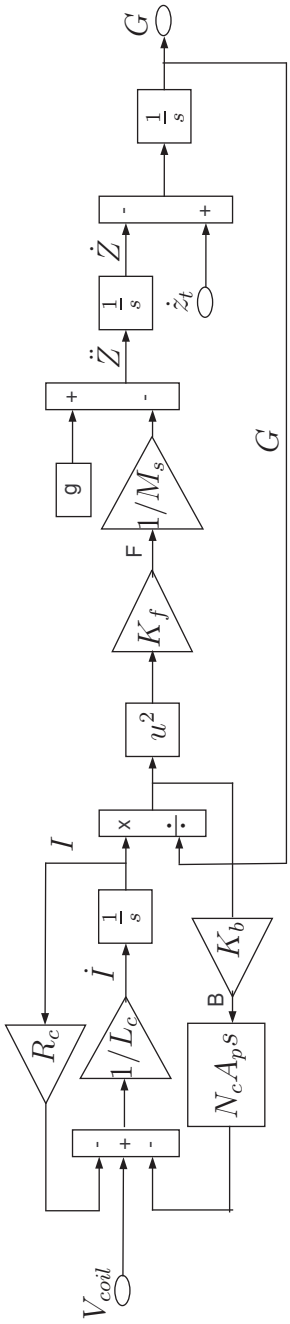

Figure 4.3: Non-linear model of the MAGLEV suspension.

Then, substitute the flux equation (4.1) into the input voltage equation (4.4) and rearrange as follows

$$L_c\frac{dI}{dt} = V_{coil} - IR_c - N_cA_pK_b\frac{d(\frac{I}{G})}{dt} \tag{4.6}$$

following the quotient rule

$$L_c\frac{dI}{dt} = V_{coil} - IR_c - N_cA_pK_b\left(\frac{G\frac{dI}{dt} - I\frac{dG}{dt}}{G^2}\right) \tag{4.7}$$

$\Rightarrow$

$$L_c\frac{dI}{dt} = V_{coil} - IR_c - \frac{N_cA_pK_b}{G}\frac{dI}{dt} + \frac{N_cA_pK_bI}{G^2}\frac{dG}{dt} \tag{4.8}$$

$\Rightarrow$

$$\frac{N_cA_pK_b}{G}\frac{dI}{dt} + L_c\frac{dI}{dt} = V_{coil} - IR_c + \frac{N_cA_pK_bI}{G^2}\frac{dG}{dt} \tag{4.9}$$

$\Rightarrow$

$$\frac{dI}{dt} = \frac{V_{coil} - IR_c + \frac{N_cA_pK_bI}{G^2}\frac{dG}{dt}}{\frac{N_cA_pK_b}{G} + L_c} \tag{4.10}$$

We also consider that

$$\frac{dG}{dt} = \frac{dz_t}{dt} - \frac{dZ}{dt} \tag{4.11}$$

from (4.1),(4.5), (4.10), and (4.11) the modified non-linear model of the MAGLEV suspension is illustrated in Fig. 4.4.

4.4 MAGLEV suspension linearisation

The linearisation of the MAGLEV suspension is based on the small perturbations of the variables around the operating points. The following definitions are used in which the lower case letters defines a small variation around the

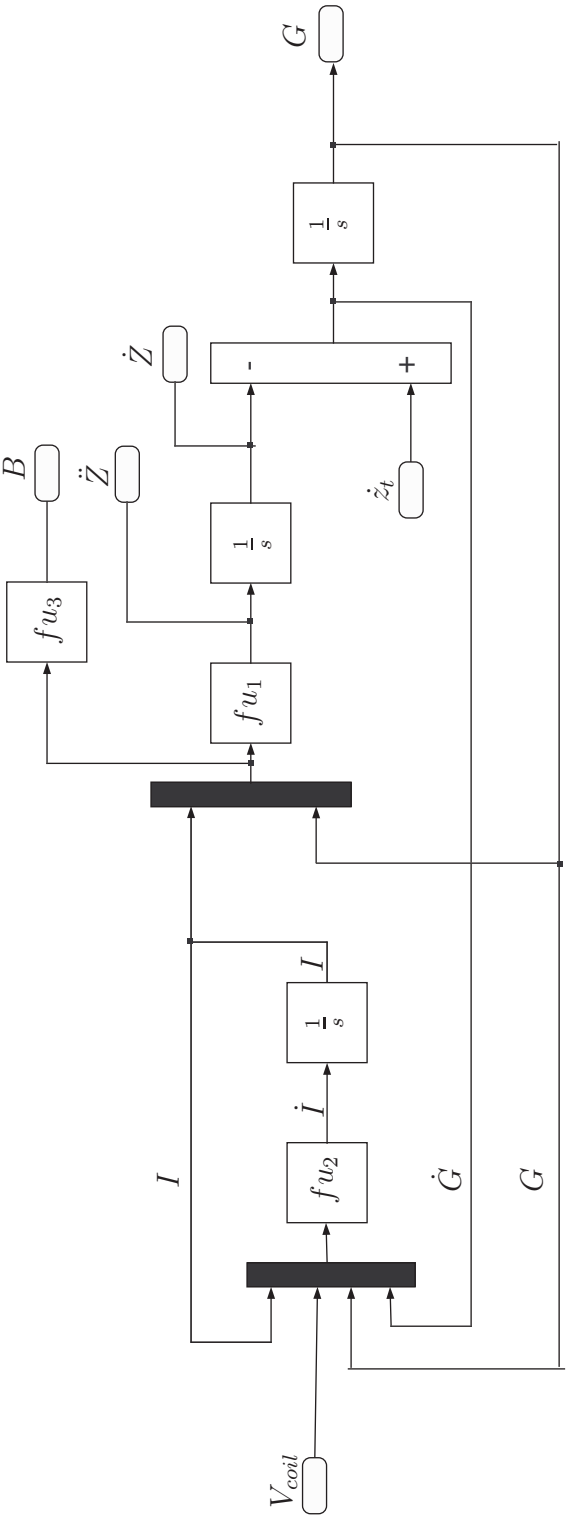

Figure 4.4: Modified Non-linear model of the MAGLEV suspension.

operating point and the subscript 'o' the refers the operating condition.

$$B = B_o + b \tag{4.12}$$

$$F = F_o + f \tag{4.13}$$

$$I = I_o + i \tag{4.14}$$

$$G = G_o + (z_t - z) \tag{4.15}$$

$$V_{coil} = V_o + u_{coil} \tag{4.16}$$

We also consider the variation around nominal value of the mass position Z

$$Z = Z_o + z \tag{4.17}$$

First substitute (4.2) into (4.3)

$$M_s \frac{d^2 Z}{dt^2} = M_s g - K_f \frac{I^2}{G^2} \tag{4.18}$$

and (4.14), (4.15) and (4.17) into (4.18)

$$M_s \frac{d^2 Z}{dt^2} = M_s g - K_f \frac{I^2}{G^2} \Rightarrow M_s \frac{d^2 (Z_o + z)}{dt^2} = M_s g - K_f \frac{(I_o + i)^2}{(G_o + (z_t - z))^2} \tag{4.19}$$

at the steady state (operating point) $\frac{d^2 Z_o}{dt^2} = 0$ hence,

$$M_s \frac{d^2 z}{dt^2} = M_s g - K_f \frac{(I_o + i)^2}{(G_o + (z_t - z))^2} \tag{4.20}$$

$\Rightarrow$

$$M_s \frac{d^2 z}{dt^2} = M_s g - K_f \frac{I_o^2}{G_o^2} \frac{\left(1 + \frac{i}{I_o}\right)^2}{\left(1 + \frac{(z_t - z)}{G_o}\right)^2} \tag{4.21}$$

Note:

$$\left(1 + \frac{i}{I_o}\right)^2 = \left(1 + 2\frac{i}{I_o} + \frac{i^2}{I_o^2}\right) \approx \left(1 + 2\frac{i}{I_o}\right)$$

and therefore, (4.21) is simplified to

$$M_s\frac{d^2z}{dt^2} = M_sg - K_f\frac{I_o^2}{G_o^2}\frac{\left(1+2\frac{i}{I_o}\right)}{\left(1+2\frac{(z_t-z)}{G_o}\right)} \tag{4.22}$$

the next step is to make denominator equal to 1

$$M_s\frac{d^2z}{dt^2} = M_sg - K_f\frac{I_o^2}{G_o^2}\frac{\left(1+2\frac{i}{I_o}\right)\left(1-2\frac{(z_t-z)}{G_o}\right)}{\left(1+2\frac{(z_t-z)}{G_o}\right)\left(1-2\frac{(z_t-z)}{G_o}\right)} \tag{4.23}$$

Note:

$$\left(1+2\frac{(z_t-z)}{G_o}\right)\left(1-2\frac{(z_t-z)}{G_o}\right) = 1-2\frac{(z_t-z)}{G_o}+2\frac{(z_t-z)}{G_o}-4\frac{(z_t-z)^2}{G_o^2} \approx 1$$

hence (4.23) is simplified

$$M_s\frac{d^2z}{dt^2} = M_sg - K_f\frac{I_o^2}{G_o^2}\left(1+2\frac{i}{I_o}-2\frac{(z_t-z)}{G_o}-4\frac{i(z_t-z)}{I_oG_o}\right) \tag{4.24}$$

$\Rightarrow$

$$M_s\frac{d^2z}{dt^2} = M_sg - K_f\frac{I_o^2}{G_o^2} - 2K_f\frac{I_o}{G_o^2}i + 2K_f\frac{I_o^2}{G_o^3}(z_t-z) \tag{4.25}$$

we also know that at operating point,$\frac{d^2Z}{dt^2} = 0$ and therefore from (4.3) the operating force is $F_o = M_sg$.
Substitute, (4.2) into (4.25)

$$M_s\frac{d^2z}{dt^2} = -2K_f\frac{I_o}{G_o^2}i + 2K_f\frac{I_o^2}{G_o^3}(z_t-z) \tag{4.26}$$

Next, the input voltage equation (4.4) is linearised. First the flux density term $\frac{dB}{dt}$ is linearised. Substitute (4.12), (4.14) and (4.15) into the flux density equation (4.1):

$$B_o + b = K_b\frac{I_o+i}{G_o+(z_t-z)} \tag{4.27}$$

$\Rightarrow$

$$B_o + b = K_b \frac{I_o}{G_o} \frac{\left(1 + \frac{i}{I_o}\right)}{\left(1 + \frac{(z_t - z)}{G_o}\right)} \tag{4.28}$$

$$B_o + b = K_b \frac{I_o}{G_o} \frac{\left(1 + \frac{i}{I_o}\right)\left(1 - \frac{(z_t - z)}{G_o}\right)}{\left(1 + \frac{(z_t - z)}{G_o}\right)\left(1 - \frac{(z_t - z)}{G_o}\right)} \tag{4.29}$$

Note:

$$\left(1 + \frac{(z_t - z)}{G_o}\right)\left(1 - \frac{(z_t - z)}{G_o}\right) \approx 1 \tag{4.30}$$

and the equation for the small variations around the nominal flux density is given as

$$b \approx \frac{K_b}{G_o} i - \frac{K_b I_o}{G_o^2}(z_t - z) \tag{4.31}$$

And the derivative term becomes

$$\frac{db}{dt} = \frac{K_b}{G_o}\frac{di}{dt} - \frac{K_b I_o}{G_o^2}\frac{d(z_t - z)}{dt} \tag{4.32}$$

Now, substitute (4.32) into (4.4) and the linearised voltage equation is

$$V_o + u_{coil} = I_o R_c + R_c i + \left(L_c + \frac{K_b N_c A_p}{G_o}\right)\frac{di}{dt} - \frac{K_b N_c A_p I_o}{G_o^2}\frac{d(z_t - z)}{dt} \tag{4.33}$$

$\Rightarrow$

$$u_{coil} = R_c i + \left(L + \frac{K_b N_c A_p}{G_o}\right)\frac{di}{dt} - \frac{K_b N_c A_p I_o}{G_o^2}\frac{d(z_t - z)}{dt} \tag{4.34}$$

$\Rightarrow$

$$u_{coil} = R_c i + \left(L_c + \frac{K_b N_c A_p}{G_o}\right)\frac{di}{dt} - \frac{K_b N_c A_p I_o}{G_o^2}\frac{dz_t}{dt} + \frac{K_b N_c A_p I_o}{G_o^2}\frac{dz}{dt} \tag{4.35}$$

$\Rightarrow$

$$\begin{aligned}\frac{di}{dt} = &-\frac{R_c i}{L_c + \frac{K_b N_c A_p}{G_o}} + \frac{K_b N_c A_p I_o}{G_o^2\left(L_c + \frac{K_b N_c A_p}{G_o}\right)}\frac{dz_t}{dt} - \\ &\frac{K_b N_c A_p I_o}{G_o^2(L_c + \frac{K_b N_c A_p}{G_o})}\frac{dz}{dt} + \frac{u_{coil}}{L_c + \frac{K_b N_c A_p}{G_o}}\end{aligned} \tag{4.36}$$

The derivative of the air gap is also given as

$$\frac{d(z_t - z)}{dt} = \frac{dz_t}{dt} - \frac{dz}{dt} \tag{4.37}$$

from the linearised equations (4.36), (4.37) and (4.26) the states are defined as $x = [i \;\; \dot{z} \;\; (z_t - z)]$ and the state space form of the linearised MAGLEV suspension is given as

$$\begin{bmatrix} \frac{di}{dt} \\ \frac{d^2z}{dt^2} \\ \frac{d(z_t - z)}{dt} \end{bmatrix} = \begin{bmatrix} -\frac{R_c}{L_c + \frac{K_b N_c A_p}{G_o}} & -\frac{K_b N_c A_p I_o}{G_o^2\left(L_c + \frac{K_b N_c A_p}{G_o}\right)} & 0 \\ -2K_f \frac{I_o}{M_s G_o^2} & 0 & 2K_f \frac{I_o^2}{M_s G_o^3} \\ 0 & -1 & 0 \end{bmatrix} \begin{bmatrix} i \\ \frac{dz}{dt} \\ (z_t - z) \end{bmatrix} + \begin{bmatrix} \frac{1}{L_c + \frac{K_b N_c A_p}{G_o}} \\ 0 \\ 0 \end{bmatrix} u + \begin{bmatrix} \frac{K_b N_c A_p I_o}{G_o^2\left(L_c + \frac{K_b N_c A_p}{G_o}\right)} \\ 0 \\ 1 \end{bmatrix} \frac{dz_t}{dt} \tag{4.38}$$

and the output equation is given as

$$\begin{bmatrix} i \\ b \\ (z_t - z) \\ \dot{z} \\ \ddot{z} \end{bmatrix} = \begin{bmatrix} 1 & 0 & 0 \\ \frac{K_b}{G_o} & 0 & -\frac{K_b I_o}{G_o^2} \\ 0 & 0 & 1 \\ 0 & 1 & 0 \\ -2K_f \frac{I_o}{M_s G_o^2} & 0 & 2K_f \frac{I_o^2}{M_s G_o^3} \end{bmatrix} \begin{bmatrix} i \\ \frac{dz}{dt} \\ (z_t - z) \end{bmatrix} + \begin{bmatrix} 0 & 0 \\ 0 & 0 \\ 0 & 0 \\ 0 & 0 \\ 0 & 0 \end{bmatrix} \begin{bmatrix} u_{coil} \\ \frac{dz_t}{dt} \end{bmatrix} \tag{4.39}$$

Where the output matrix C corresponds to the following 5 measurements

$$C = \begin{bmatrix} i \\ b \\ (z_t - z) \\ \dot{z} \\ \ddot{z} \end{bmatrix} \equiv \begin{bmatrix} \text{Coil's Current} \\ \text{Flux Density} \\ \text{Air gap} \\ \text{Vertical velocity} \\ \text{Vertical acceleration} \end{bmatrix}$$

4.5 Total number of feasible sensor sets

The sensor combinations available depends on the number of the output matrix C in (4.39). The total number of sensor combinations (or rows of sensor sets) is easily calculated from $N_s = 2^{n_s} - 1$ where, N_s is the total number of all feasible sensor sets and n_s the number of the total sensors that can be used. Table 4.1 tabulates the available sensor sets with 1,2,3,4 and 5 sensors that results to a total of 31 sensor sets.

Table 4.1: Total number of feasible sensor sets for the 1DOF MAGLEV suspension.

Number of measurements available	Number of feasible sensor sets
With 1 Sensor	5
With 2 Sensors	10
With 3 Sensors	10
With 4 Sensors	5
With 5 Sensors	1
Total	31

4.6 Track fundamentals and disturbances to the suspension

The intended variations in the position of the track have to be followed by the MAGLEV suspension while the unintentional irregularities in the track position have to be rejected. The first are taken as deterministic disturbance while the latter are considered as stochastic disturbance to the suspension. The weight of the vehicle is considered in the modelling while the load can be simulated as a force disturbance in the vertical direction.

4.6.1 Deterministic disturbances

The main deterministic inputs to a suspension for the vertical direction are the transitions onto track gradients. In this work, the deterministic input components utilised are shown in Fig. 4.5 and represent a gradient of 5% at a vehicle speed of $15m/s$ and an allowed acceleration of $0.5m/s^2$ while the jerk level is $1m/s^3$.

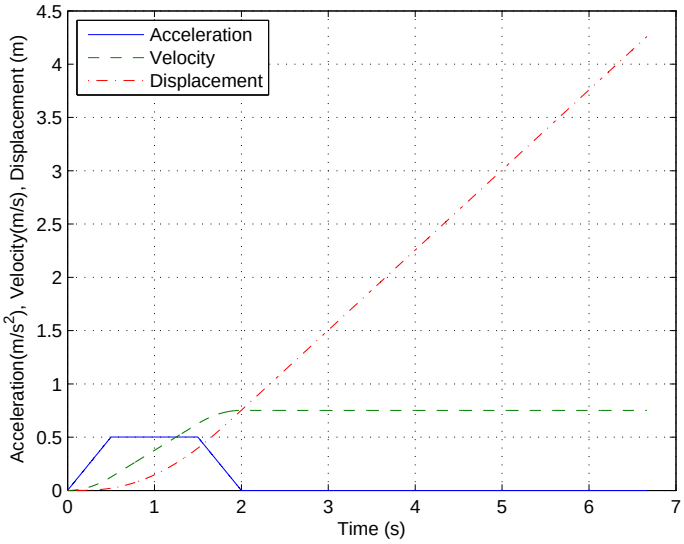

Figure 4.5: Deterministic input to the suspension with a vehicle speed of $15ms^{-1}$ and 5% gradient.

4.6.2 Stochastic disturbances

The random input to the MAGLEV suspension represents the inaccuracies of the laying track, the lack of straightness of the steel rail and the effects of fixtures. These effects are considered as stochastic disturbances to the MAGLEV suspension. Two stochastic models of the track behaviour are presented by Paddison [1995]. Considering the vertical direction, the velocity variations are quantified by a double-sided power spectrum density (PSD)

which in the frequency domain is expressed by

$$S_{\dot{z}_t} = \pi A_r V_v \tag{4.40}$$

where, V_v is the vehicle speed that in this work is taken as $15m/s$ and A_r represents the track roughness that for a typical high quality track is taken as $1 \times 10^{-7}m$. The corresponding (one-sided) autocorrelation function is given by

$$R(\tau) = 2\pi^2 A_r V_v \delta(\tau) \tag{4.41}$$

Stochastic closed-loop response calculations

Closed-loop response from the stochastic inputs are generally quantified by the Root Mean Square. The ride quality is generally quantified by the Root Mean Square (RMS) of the vertical acceleration experienced by the passengers when the vehicle is excited by the rail's random behaviour due to roughness and misalignments. For the ride quality assessment or the root mean square values of the MAGLEV outputs three methods are encountered:

- Frequency response analysis
- Covariance analysis
- Time history

All approaches can be used for linearised systems but only the last one can be used for non-linear systems. Since the simulations take into account the non-linear model only the time history method is presented here. The three methods are described by Zolotas [2002] but the time history method that is used in thesis is described next.

Calculating the RMS values of the desired outputs (vertical acceleration $\ddot{z}_{rms}$, driving signal ($u_{coil_{rms}}$), air gap $(z_t - z)_{rms}$, etc.) via time history data requires an extra simulation for each evaluation. This increases the time for the objective functions to be evaluated and consequently the overall evolution procedure computational time is increased. This cannot be avoided because

neither the frequency response nor covariance analysis can be used (that are much faster) since they work with the linear time invariant state space models only.

The stochastic track profile can be produced since the velocity variation of the track is known and simulate the stochastic closed-loop response of the MAGLEV suspension in MATLAB. The data from the outputs that can be saved represent the time history results. The results can be used to calculate the R.M.S values directly or a 'Fast Fourier Transform' can be performed to extract the frequency information of the signals (system resonances).

The root mean square value for a desired output is defined as

$$y_{rms} = \sqrt{E[y^2(t)]} = \sqrt{\bar{y^2}} = \sqrt{\lim_{T \longrightarrow \infty} \frac{1}{T} \int_0^T y^2 dt} \tag{4.42}$$

or it can be approximated as

$$y_{rms} \approx \sqrt{\frac{1}{n} \sum_{i=1}^{n} y_i^2} \tag{4.43}$$

where y_i is the time history data of the signal, y_{rms} is the rms value of the signal and n is the number of samples in the data collected. The accuracy of the result depends on the number of samples taken from the simulation. Theoretically to have the same result as in the continues time case, the number of samples should be infinite within the same execution time. The results are more precise as the time goes to infinity ($T \longrightarrow \infty$). Therefore, for accurate results a sufficiently long track should be selected together with an adequate number of sample points should be used to recover precise information of the signal frequency content (i.e improve resolution).

4.6.3 Force Inputs

The forces that can possibly act as disturbance on the suspension are the mass variation of the load and external disturbances such as braking and aerodynamic effects. For low speed vehicle the mass of a small vehicle can vary up to 40% from fully laden to unladen. Another factor is the speed of the mass variation. The load may change more rapidly as the passengers can disembark much faster than expected. The suspension should be robust enough to accommodate rapid mass variations. Throughout this thesis the mass is expected to change by 25% of the total mass of the vehicle within $10s$

4.7 MAGLEV suspension design requirements

The design requirements for an electromagnetic suspension (EMS) suspension depend on the type of the train and the speed. The dynamic characteristics of a MAGLEV suspension are described by Goodall [2004] as well as in Goodall [1994] that is focused upon the low speed Birmingham Airport Maglev vehicle EMS suspension requirements which operated successfully in the UK for more than 10 years.

The ride quality requirements for a transport system are quantified in terms of the RMS acceleration experienced by the passengers. For low speed systems with relative short journeys the acceptable level of RMS vertical acceleration can be taken as $5\%'g'$ which means $0.5m/s^2$.

For a MAGLEV vehicle in which the air gap size is around $15mm$ the RMS variations in air gap should be restricted to 4 or $5mm$. The air gap changes which occur at deterministic features must be restricted in either way and a practical limit is $7.5mm$ (half the air gap) such that there is clearance to accommodate random changes in the air gap.

Fundamentally there is a trade off between the deterministic response and

the stochastic response (ride quality) of the MAGLEV suspension. In this case, the deterministic characteristics are limited to the maximum standard values while stochastic characteristics have been set as objectives to be minimised i.e minimise the vertical acceleration (improve ride) quality and the RMS current variations. These objectives can the be formally written as

$$\phi_{s_1} = i_{rms}, \quad \phi_{s_2} = \ddot{z}_{rms} \tag{4.44}$$

Table 4.2 tabulates the design limitations for the deterministic as well as for the stochastic features. Note that the stochastic and deterministic inputs to the suspension are treated separately in the optimisation framework throughout this thesis. The steady state error for the deterministic response should return to zero within $3s$ and the input voltage to the magnet's coil is restricted to 300V ($3 \times R_c \times I_o$) for both deterministic and stochastic responses.

Table 4.2: Constraints for the Electro-magnetic suspension performance.

EMS limitations	Value
Stochastic response	
RMS acceleration($\simeq 5\%'g'$),($\ddot{z}_{rms}$)	$\leq 0.5ms^{-2}$
RMS air gap variation, $((z_t - z)_{rms})$	$\leq 5mm$
RMS control effort, $(u_{coil_{rms}})$	$\leq 300V$
Deterministic response	
Maximum air gap deviation,$((z_t - z)_p)$	$\leq 7.5mm$
Control effort,(u_{coil_p})	$\leq 300V(3I_0R_c)$
Settling time, (t_s)	$\leq 3s$
Air gap Steady state error, $((z_t - z)_{e_{ss}})$	$= 0$

The typical quarter car vehicle of 1000kg is considered and it requires a nominal force of $F_o = M_s \times g$ where M_s is the Mass of the vehicle and g is the gravity acceleration constant which is $9.81m/s^2$. The nominal air gap (G_o) is at $15mm$ to accommodate the track roughness while the operating flux density (B_o) in the air gap is 1T. The electromagnet design of MAGLEV vehicles is explained in more details by Goodall [1985]. Moreover, the coil

is of $N_s = 2000$ turns with coil resistance $R_c = 10\Omega$ and coil's inductance $L_c = 0.1H$. Furthermore, the nominal current (I_o) is at 10A and the pole face area (A_p) is $0.01m^2$. The parameters of the electromagnetic suspension are listed on Table 4.3

Table 4.3: Parameters of the Electro-magnetic suspension

Parameter	Value	Unit
M_s	1000	kg
G_o	0.015	m
B_o	1	T
I_o	10	A
F_o	9810	N
R_c	10	Ω
L_c	0.1	H
N_c	2000	turns
A_p	0.01	m^2

4.8 Summary

In this chapter the MAGLEV suspension non-linear model is presented. The MAGLEV suspension is a well known practical problem. In fact, the suspension is non-linear, unstable, safety-critical system with non-trivial requirements. There are 31 feasible sensor sets and therefore can serve as a good example for the optimised sensor configuration frameworks. The model is linearised and therefore linear controllers can be designed and optimally tuned via genetic algorithms in order to optimise the closed-loop performance with the non-linear model. Note that throughout this thesis the closed-loop time response results which are depicted on the graphs refer to the operating point of the suspension. i.e. for the air gap measurement, zero represents the operating air gap which is $15mm$.

Chapter 5

Optimised sensor configurations via classical control approaches

5.1 Introduction

Classical control strategies are used to achieve desired closed-loop optimum performance via the non-dominated sorting genetic algorithm (NSGA-II) presented in Chapter 3. The benefit of using inner loop control with classical control strategies is advantageous in controlling a MAGLEV suspension as indicated by Goodall [2000]. The problem is posed in a multi-objective constrained optimisation framework where the performance of the MAGLEV suspension is optimised subject to a number of constraints defined from maximum allowed working boundaries. Two cases are compared: (i) with the flux measurement for the inner loop and the air gap in the outer loop, (ii) current for inner loop and air gap for outer.

Although classical control structures for maglev suspensions have been studied previously, the purpose of this chapter is twofold. First is to illustrate the efficacy of using GA technique (namely NSGA-II) for tuning the controllers in a multiobjective framework for the aforementioned classical structures and secondly to use these as a baseline for further investigation via modern control and fault tolerant techniques.

5.2 Classical controller optimisation

The control strategies that are compared are illustrated in Fig. 5.2 and in Fig. 5.3. One is the air gap(outer)/flux(inner) and the other is air gap/current with the latter having poor robustness properties as it will be proved in the next sections. The configuration in Fig. 5.2 consists of an outer feedback loop with the air gap measurement and the inner loop with the flux density measurement. The same approach applies for the air gap(outer)/current(inner) case by replacing flux with current measurement as depicted in Fig. 5.3. The controller design is based upon the linearised model of the suspension while to achieve the required closed-loop time response from deterministic and stochastic disturbances the non-linear model of the MAGLEV suspension is used. The block diagram in Fig. 5.1 illustrates the concept of controlling a non-linear model via linearly designed controller based on the linearisation of the non-linear model around a operating point. The small perturbations δ_y around the operating point are derived from the nominal values and fed to the controller which gives the driving signal δ_u. In this way the linerised controller is able to control the non-linear MAGLEV suspension having in mind that the non-linearities have to be 'soft'. More details about controlling non-linear systems via linearised controllers are given by Friedland [1996].

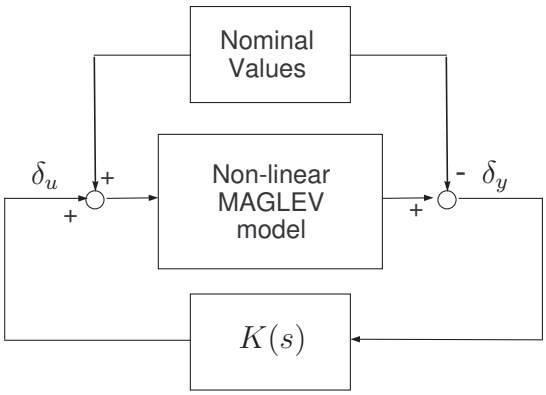

Figure 5.1: Control of the non-linear MAGLEV suspension using linear controller.

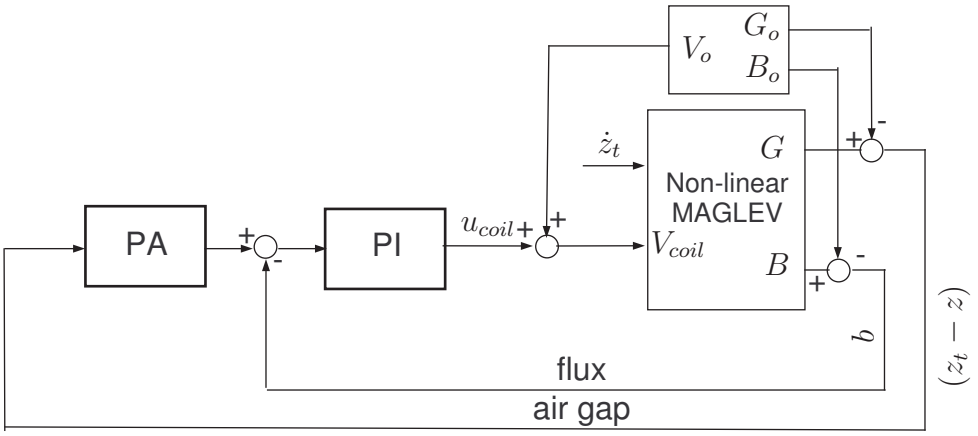

Figure 5.2: Classical controller implementation with flux inner loop feedback

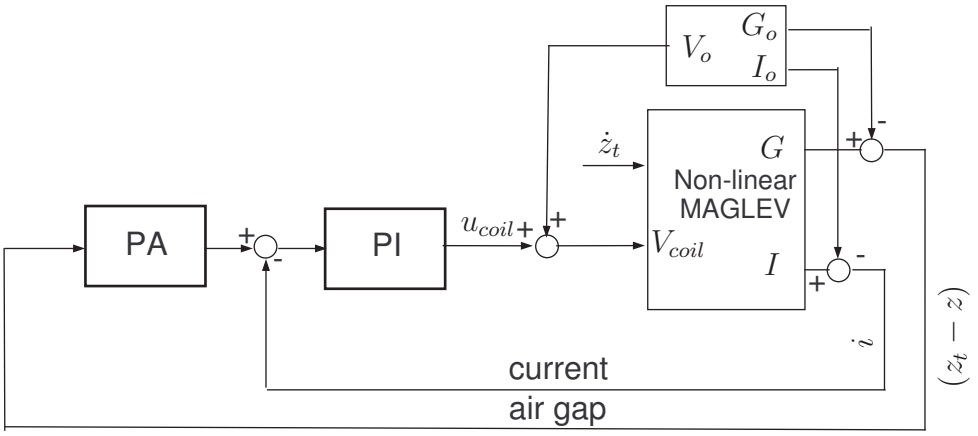

Figure 5.3: Classical controller implementation using the current inner loop feedback

To achieve sufficient robustness properties the inner loop bandwidth is required to be more than $50Hz$ (Goodall [2000]) and in this case its been set within $50Hz - 100Hz$. This may be achieved via a Proportional-Integral (PI) controller with a gain G_i and a time constant τ_i as given by (5.1).

$$PI = G_i \frac{\tau_i s + 1}{\tau_i s} \tag{5.1}$$

The outer loop with the air gap measurement is set to be less than $20Hz$. In fact, a lower outer loop bandwidth can be achieved with the flux measurement at the inner loop but this will be tuned from the genetic algorithm if necessary. The outer loop bandwidth is adjusted by tuning the Phase Advance (PA) controller in (5.2) with a gain of G_o, phase advance ratio k and time constant τ_o. The phase advance controller in (5.2) is used to provide adequate phase margin in the range of $35^o - 45^o$.

$$PA = G_o \frac{k\tau_o s + 1}{\tau_o s + 1} \tag{5.2}$$

Considering the performance requirements described in Section 4.7 as well as the robustness properties discussed here, clearly pose a multiobjective problem that aims to improve performance by minimising both objectives in (5.3) subject to the constraints listed in Table 5.1. The constraints combine design requirements from frequency method design and closed-loop time responses from both deterministic and stochastic track profiles.

$$\phi_{s_1} = i_{rms}, \quad \phi_{s_2} = \ddot{z}_{rms} \tag{5.3}$$

Firstly, the parameters tuning for the air gap-flux control configuration is performed. To achieve the required performance, the static penalty function approach is used here as described in Section 3.4.1. Figure 5.4 illustrates the overall evolution which is done within 500 generations with 70 chromosomes in the population. Note that each star $(*)$ on the graph

Table 5.1: Suspension system constraints for the optimisation of the classical strategies.

	Constrains	Value
g_1	RMS acceleration($\simeq 5\%'g'$),($\ddot{z}_{rms}$)	$\leq 0.5ms^{-2}$
g_2	RMS air-gap variation, $((z_t - z)_{rms})$	$\leq 5mm$
g_3	RMS input voltage,(u_{rms}),	$\leq 300V(3I_oR_o)$
g_4	Max air-gap deviation (det),$((z_t - z)_p)$	$\leq 7.5mm$
g_5	Max input voltage (det),(u_p)	$\leq 300V(3I_oR_o)$
g_6	Settling time, (t_s)	$\leq 3s$
g_7	Phase margin, (PM)	$\leq 45^o$
g_8	Phase margin, (PM)	$\geq 35^o$
g_9	Inner bandwidth ($f_{b_{in}}$)	$\leq 100Hz$
g_{10}	Inner bandwidth ($f_{b_{in}}$)	$\geq 50Hz$
g_{11}	Outer bandwidth ($f_{b_{out}}$)	$\leq 20Hz$
h_1	Steady state, (e_{ss})	$= 0$

represents a controller with the corresponding optimum parameters for the current generation. As it can be seen from Fig. 5.4(a), the first generations have scattered solutions within the search space but the convergence of the population to the solution area is obvious. As the generations evolve solutions start creating a Pareto front (Fig. 5.4(b)) from the 20^{th} generation while until the maximum generation (500^{th}) the optimum Pareto front is recovered (Fig. 5.4(f)). As it can be seen from Fig. 5.4(f) the final generation represents the optimum Pareto front of controllers that is evenly spread. The vertical acceleration (ride quality) ($\ddot{z}$) is limited to $0.5m/s^2$ while the current for the stochastic track profile remains at around $1A_{rms}$. Figure 5.5 shows the air-gap(outer)/current(inner) evolution process that is tuned using the same NSGA-II parameters. The evolution process is similar but as it can be seen from the 500^{th} generation, vertical acceleration constraint is violated.

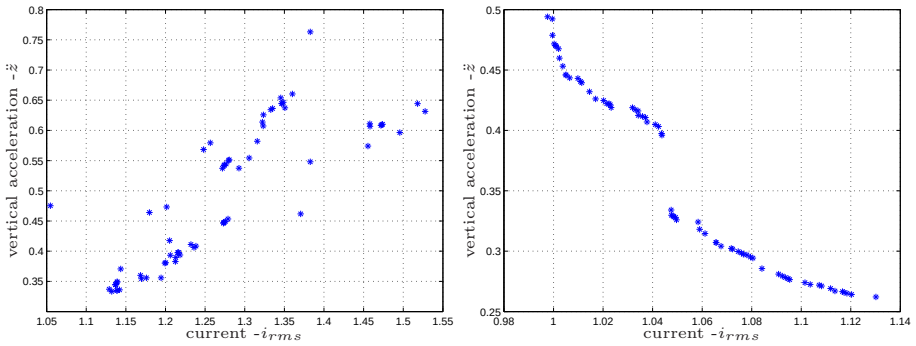

(a) Generation:5

(b) Generation:20

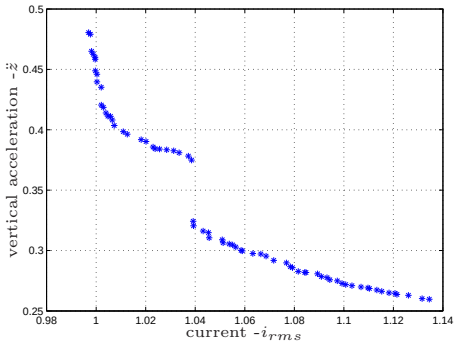

(c) Generation:50

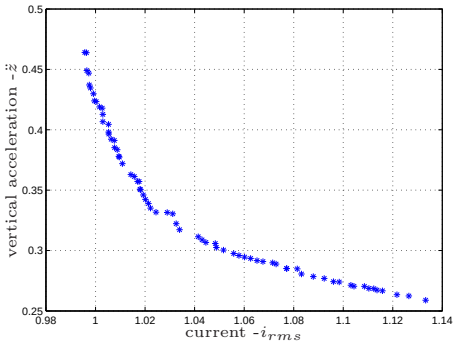

(d) Generation:100

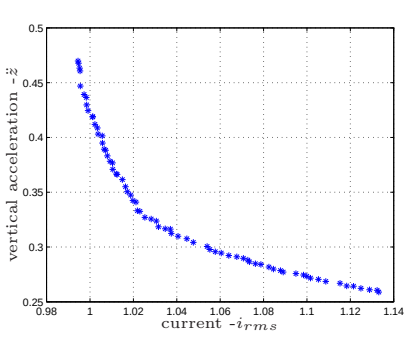

(e) Generation:200

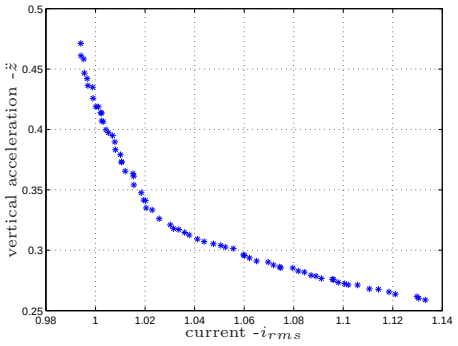

(f) Generation:500

Figure 5.4: Evolution process for the air-gap(outer)/flux(inner) strategy via NSGA-II.

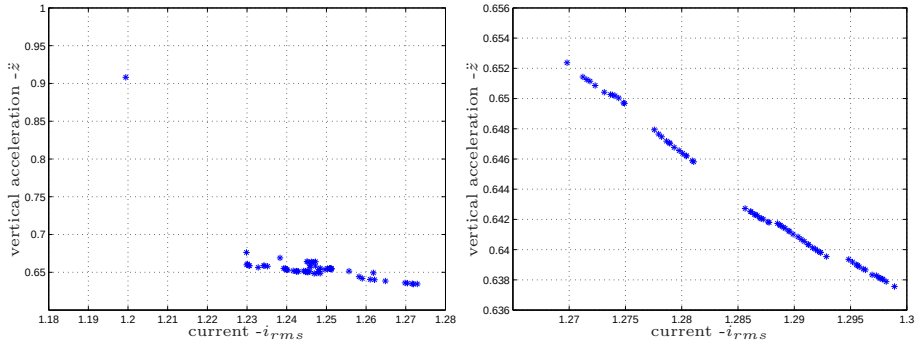

(a) Generation:20

(b) Generation:50

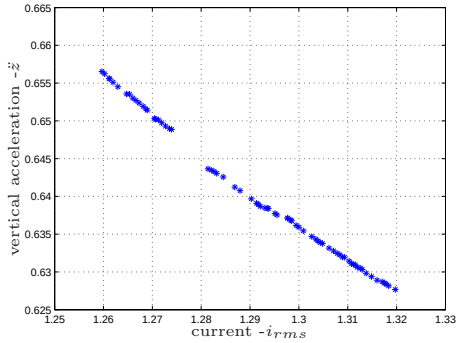

(c) Generation:100

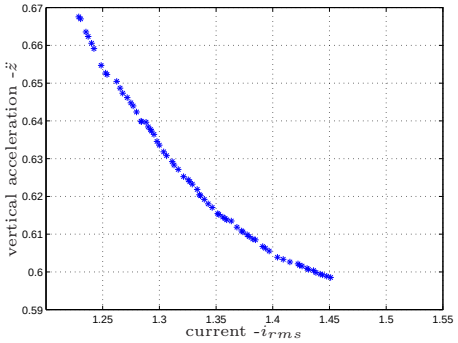

(d) Generation:200

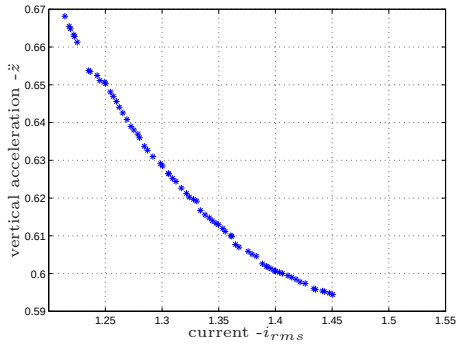

(e) Generation:300

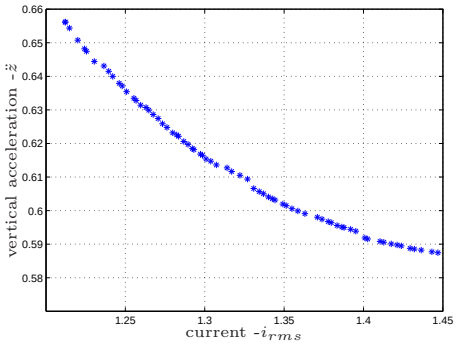

(f) Generation:500

Figure 5.5: Evolution process for the air-gap(outer)/current(inner) strategy via NSGA-II.

Comparing the two configurations the optimum Pareto front of the controllers for each configuration is depicted in Fig. 5.6 where the the Pareto-optimality is illustrated between the ride quality ($\ddot{z}_{rms}$) and the RMS coil current (i_{rms}) for the two controller configurations, i.e the air-gap(outer)/flux(inner) ($(z_t - z)/b$) and the air-gap(outer)/current(inner) ($(z_z - z)/i$) case. The dark dots correspond to the optimum Pareto front of controllers for air-gap(outer)/current(inner) ($(z_t - z)/i$) configuration while the white dots the air-gap(outer)/flux(inner) ($(z_t - z)/b$) configuration. Clearly, in both cases there is a trade-off between the ride quality and the input current which is successfully recovered from the NSGA-II. It can be

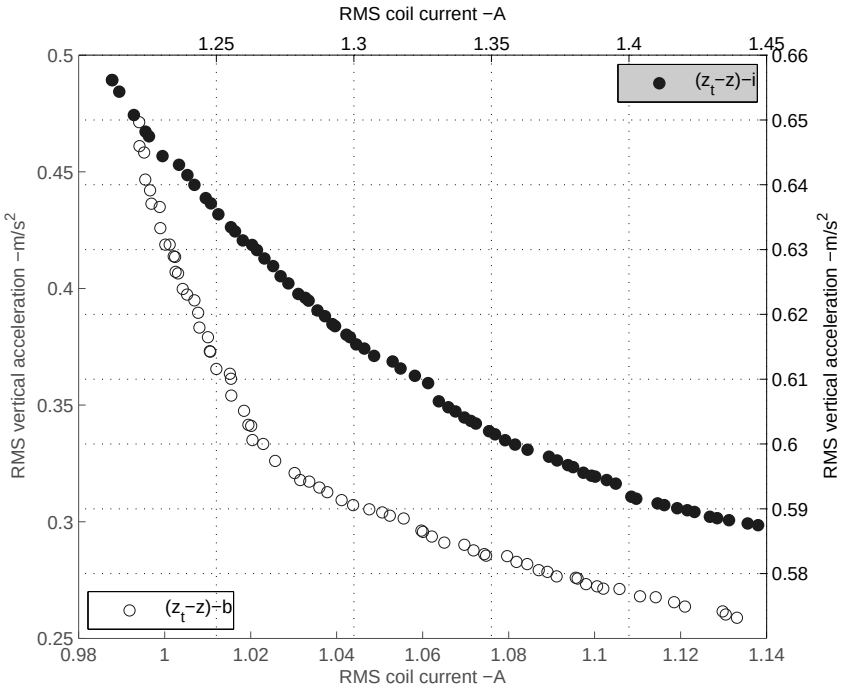

Figure 5.6: Optimum Pareto front of controllers for the two classical control strategies.

seen that a set of controllers can be selected that satisfy all constraints for the former case but not for the latter (more complex controllers are necessary for this case). Furthermore, the comparisons between the two sensor configurations is detailed on Table 5.2. As the results indicate for the

$(z_t - z)/i$ configuration the vertical acceleration limit is violated as well as the phase margin limitation. Clearly, with the air-gap/flux configuration an optimised performance has been achieved satisfying all closed-loop response requirements.

The resulted air-gap deflections and the input voltage for the deterministic profile response are depicted in Fig. 5.7. i.e from Fig. 5.7(a) the air gap deflection is limited to a maximum value of $7.5mm$, the settling time is below $3s$ and the steady state error is zero. Moreover, Fig. 5.7(b) shows the corresponding input voltage deflection which is constrained to a maximum value of about $55V$.

Table 5.2: Classical control - constraints values for each design.

Constraints	Assigned values	$(z_t - z)/b$	$(z_t - z)/i$	Units
RMS acceleration, $(\ddot{z}_{rms})$	≤ 0.5	0.26-0.47	**0.58-0.65**	ms^{-2}
RMS Air Gap,$((z_t - z)_{rms})$	≤ 5	1.26-1.53	1.4-1.7	mm
RMS input voltage, $(u_{coil_{rms}})$	≤ 300	32-108	63-80	V
Air gap peak,$(z_t - z)_p$	≤ 7.5	5-7.5	2.5-2.6	mm
Input voltage, (u_{coil_p})	$\leq 300V$	37-53	≈ 20	V
Settling time, (t_s)	≤ 3	$\surd$	$\surd$	s
Steady state error,(e_{ss})	$= 0$	$\surd$	$\surd$	mm
Phase margin, (PM)	$35^o - 45^o$	$35^o - 45^o$	**3.3-5.5**	
Outer bandwidth, $(f_{b_{out}})$	≤ 10	2.9-3.2	≈ 4	Hz
Inner bandwidth, $(f_{b_{in}})$	$50 - 100$	70-100	≈ 100	Hz

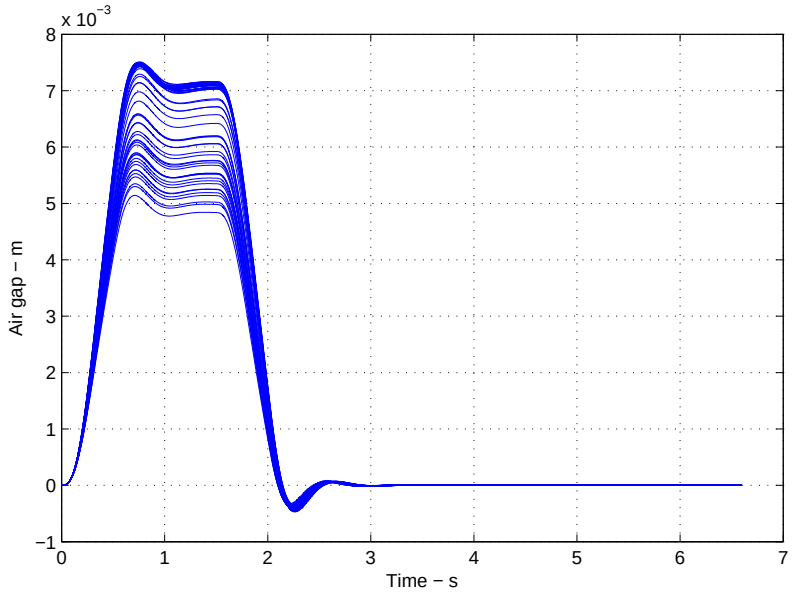

(a) Air gap deviation

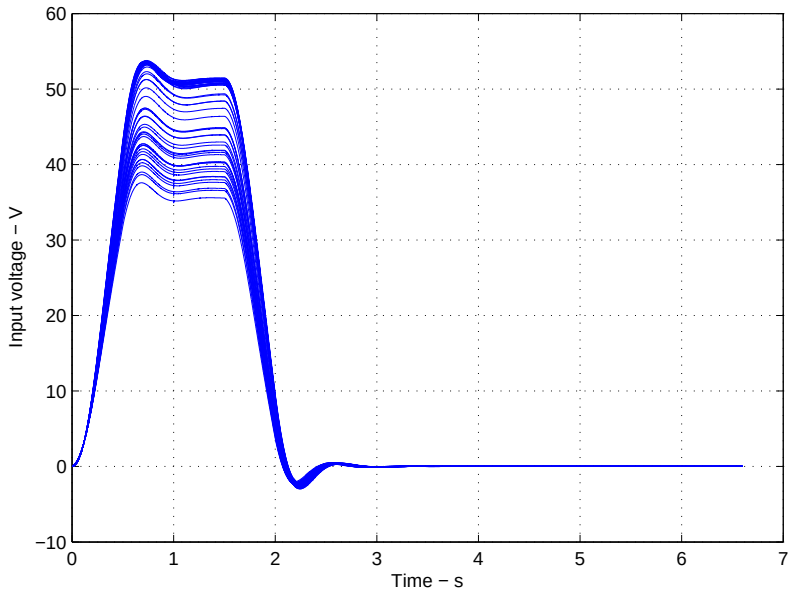

(b) Input voltage deviation

Figure 5.7: Air gap and input voltage deviations of the 70 controllers for air gap/flux measurements.

5.3 Controller selection criterion

The process of selecting a controller with desired closed-loop characteristics is rather simplified in this case where we have only two sensor configurations. From Table 5.2 it can be seen that the $(z_t - z)/i$ configuration violates two constraints therefore $(z_t - z)$/b sensor configuration is better to use. The problem becomes more complex when a large number of sensor sets have to be optimised using a specific modern control strategy. Particularly, if the feasible sensor sets number is large then a large number of controllers to choose from appears at the end of the sensor optimisation framework. In fact, this is a function of the number of chromosomes in the population and is given as

$$N_c = Pop_{num} \times N_s \tag{5.4}$$

where N_c is the total number of controllers for all sensor sets, N_s is the number of available sensor sets and Pop_{num} is the number of individuals in the population. For a system with a large number of sensors the number of controllers can be equally large and therefore the selection procedure is not trivial to perform manually (time consuming). The overall constraint violation function can be used to reject controllers that do not satisfy the preset constraints as described next.

The overall constraint violation function in (3.8), page 47 and (3.11), page 48 for the static and dynamic penalty functions respectively is very useful for controller selection because it reflects the amount or degree of the constraint violation/s. Particularly, using the last generation of each sensor set (which represents the Pareto-optimality) a vector can be produced (for the corresponding sensor set) that contains the overall constraint violation (Ω) for each sensor set. In fact, for the closed-loop response using a randomly produced controller Ω is zero if no constraint is violated or is up to a certain value if there is any constraint(s) violation(s). This can be illustrated with an example, as follows

Using the $(z_t - z)/b$ and $(z_t - z)/i$ configurations with the corresponding

closed-loop response with the optimum Pareto fronts of controllers as illustrated in Fig. 5.6, the controller that result to the best ride quality (i.e minimum vertical acceleration), can be selected for each sensor configuration. The parameters that form the controllers in (5.1) and (5.2) are then taken as:

Table 5.3: Selected controllers' parameters from $(z_t - z)/i$ and $(z_t - z)/b$.

	G_i	τ_i	G_o	τ_o	k
$(z_t - z)/b$	11949V/T	0.0181s	3.547T/m	0.038s	3.92
$(z_t - z)/i$	233V/A	0.023s	790.5A/m	0.0039s	2.781

The resulting constraint values for the suspension closed-loop response are shown on Table 5.4. For the $(z_t - z)/b$ configuration the penalty values are zero since all constraints are satisfied in contrast to $(z_t - z)/i$ that violates the ride quality as well as the phase margin (PM). Consequently, the overall constraint violation function (Ω) is zero for $(z_t - z)/b$ but 1.152 for $(z_t - z)/i$. Note that (3.5) and (3.7) in page 47 were used to obtain the penalty values.

The overall constraint violation function (Ω) can clearly serve as a controller selection criterion in case there is a large number of controllers exist to choose from.

5.4 The noisy measurements effect and filtering

In any real application sensors add noise to the measured quantities. It is also possible to increase the noise level on the measured quantity when there is interference from the surrounding components and therefore good shielding might be required. Since there is no exact information about the sensor noise elements, the noise covariance is taken as 1% of the maximum value of the deterministic response for the corresponding measured quantity. For the MAGLEV suspension, the noise coming from sensors can be amplified

Table 5.4: Constraint violations for the selected controllers that result to the best ride quality.

	$(z_t - z)/b$		$(z_t - z)/i$	
Quantity	Actual value	Penalty value	Actual value	Penalty value
$\ddot{z}_{rms}$	$0.26ms^{-2}$	0	$\mathbf{0.65ms^{-2}}$	0.312
$(z_t - z)_{rms}$	$1.5mm$	0	$1.4mm$	0
$u_{coil_{rms}}$	32.4V	0	80.1V	0
$(z_t - z)_p$	$7.48mm$	0	$2.5mm$	0
u_{coil_p}	53.6V	0	19.9V	0
t_s	2.37s	0	2.2s	0
e_{ss}	$10 \times 10^{-6}m$	0	$1 \times 10^{-6}m$	0
PM	35^o	0	$\mathbf{5.57^o}$	0.84
$f_{b_{out}}$	3.06Hz	0	3.91Hz	0
$f_{b_{in}}$	98Hz	0	98Hz	0
Ω		0		1.152

by the controllers and appear on the input voltage (at the driving signal of the suspension). Particularly, if the controllers have high gains then the amplitude of the noise can be large but the effect on the overall performance is rather limited if it is kept at a reasonable level. For example, the controller parameters in Table 5.3 for the $(z_t - z)/b$ configuration result to the input voltage and air gap signals in Fig. 5.8(a) and Fig. 5.8(b) respectively (for the deterministic response). Due to the fact that the controller is very fast noise components are shown amplified. However, because of the limited system bandwidth the effect on the air gap is very small (almost negligible). Note that the air gap measurement is shown prior to the injected sensor noise for better resolution.

The effect of the measured noise at the input voltage and the input current can be seen from Fig. 5.10 (page 90) where the frequency response from the control input (V_{coil}) to the air gap (G) and current (I) is depicted. As it can be seen the illustrated frequency response is similar to a low pass filter behaviour with very low cut-off frequency and therefore the noise is

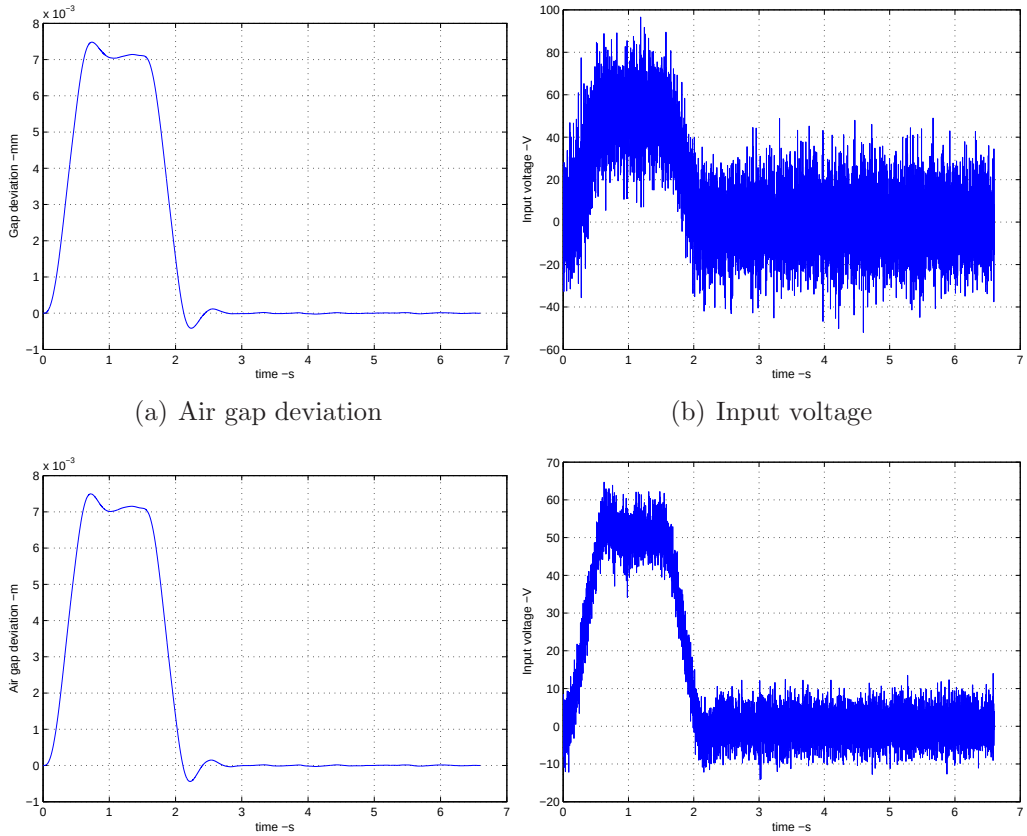

(a) Air gap deviation

(b) Input voltage

(c) Air gap deviation with LP filter

(d) Input voltage with LP filter

Figure 5.8: Air gap and input voltage deviations with and without LP filter.

filtered having very limited effect at the outputs (air gap and current) if the noise level is kept within reasonable amplitude. Nevertheless, in practical implementations the noise effect has to be taken into account (see Chapter 9). The solution to limit the noise amplitude at the input voltage for the classical control design is to insert a low pass filter at the output of the phase advance controller with a cut-off frequency of $30Hz$ as illustrated in Fig. 5.9. In Chapter 9 the LP filter inserted in the loop shows the filtering properties of the proposed method from the practical point of view although the optimisation procedure is different from this chapter (different performance requirements).

For the sensor optimisation frameworks via modern control techniques as studied in Chapter 6 and 7 there is no need to use a LP filter because the rms value of the noise is reduced by taking it into account either as a constraint i.e.($u_{coil_{noise}} \leq \alpha$) or as an extra objective function into the optimisation frameworks. Note that throughout this thesis and where $u_{coil_{noise}}$ is used an extra simulation is necessary to take the rms value of the noise on the input voltage with idle track profile. The input voltage depicted in Fig. 5.8(d)

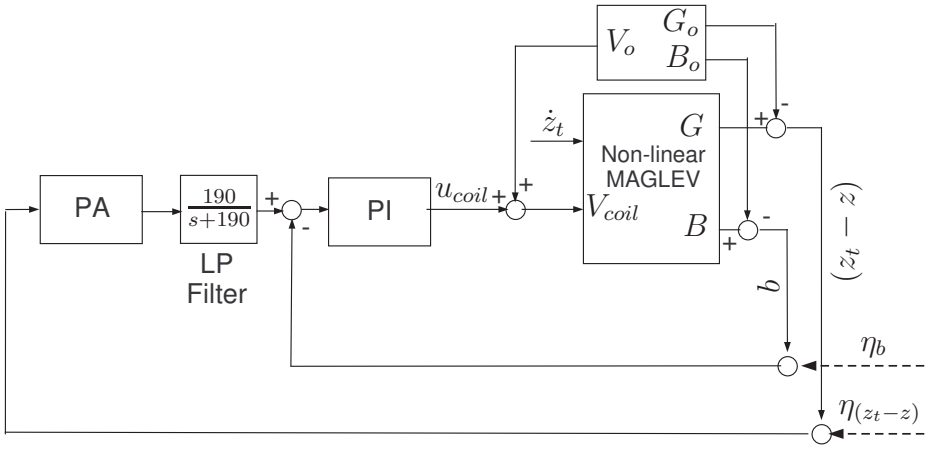

Figure 5.9: Flux inner loop feedback implementation with low pass filter.

shows that the noise amplitude is reduced significantly. The new dynamic system introduced in the closed-loop has affect the performance of the suspension with minor effects on the overall performance of the suspension system. There is no constraint violation and this can be verified from the overall constraint violation function (Ω) which has a very small value of 0.497×10^{-3}.

Testing for all controllers, the ride quality and the input current are also affected and the optimum Pareto front of controllers is given in Fig. 5.11 with white dots. The ride quality of the suspension is limited to $0.4m/s^2$ while the required current is increased. All performance constraints are satisfied with some of them having very small violation that can be neglected.

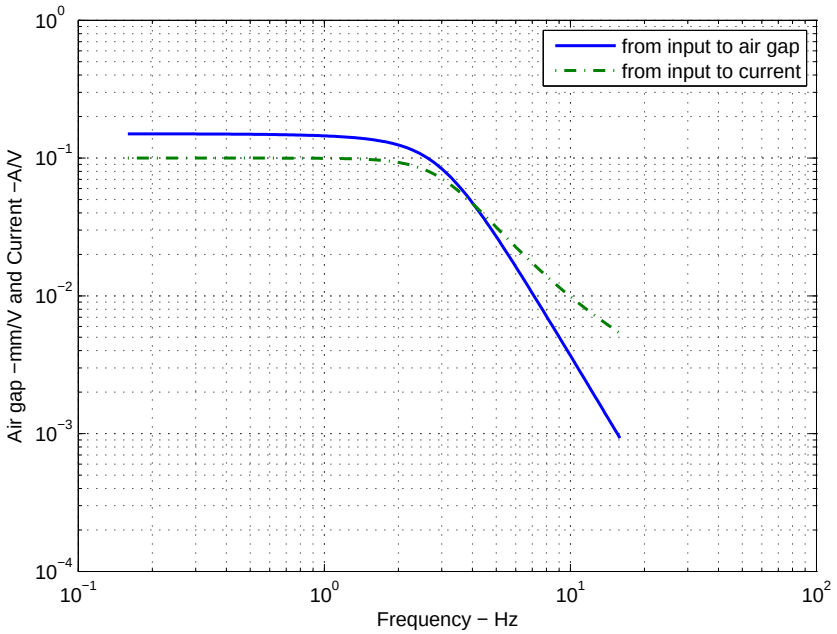

Figure 5.10: Frequency response from the control input to the air gap/current outputs.

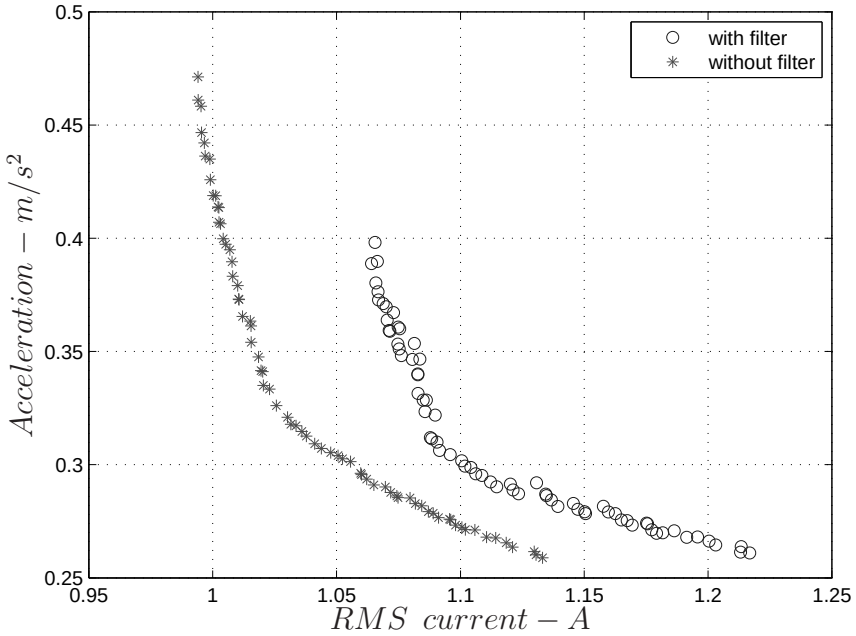

Figure 5.11: Pareto front of controllers for $(z_t - z)/b$ with and without LP filter.

5.5 Robustness to load variations

In this section the load variation of the MAGLEV suspension is considered. The maglev suspension has to support the large mass of the vehicle as well as the passengers' weight (load) which can vary up to 40% of the total mass of vehicle. This is a significant variation of the total mass and the robustness of the closed-loop response has to be taken into account to ensure performance and stability for a fully laden or unladen vehicle. For this test assume that the load variation is up to 25% of the total vehicle mass which means that the load can varied from $1000kg$ to $1250kg$ for a fully unladen and laden vehicle respectively.

The load variation can be simulated as input disturbance force (F_d) onto the MAGLEV suspension at the vertical direction and therefore the Newton's motion of equation is modified as follows

$$M_s \frac{d^2 Z}{dt^2} = M_s g - F + F_d \tag{5.5}$$

where $F_d = m_s g$ and m_s is the passengers' mass. In this way, the closed-loop response is tested for robustness to a mass variation of $250kg$. The assumption is that m_s varies from $0 - 250kg$ $(0 - 2452N)$ within $10sec$ with a ramp form. This simulates the passengers that could move into the vehicle during the stop in a typical train station as depicted in Fig. 5.12. Initially the force disturbance is zero and gradually reaches the maximum load of $250kg$ at $10sec$. After the passengers boarding the MAGLEV suspension is tested for both deterministic and stochastic responses. Note that the inputs to the track are injected after $10sec$ when the load is at maximum and the total mass is $1250kg$.

The closed-loop response of the MAGLEV suspension for the load variation profile from zero to ten seconds is depicted in Fig. 5.13. Clearly, the response of the air gap is unacceptable because there is large constraint violation for the air gap maximum deflection, steady state error as well as for the settling time.

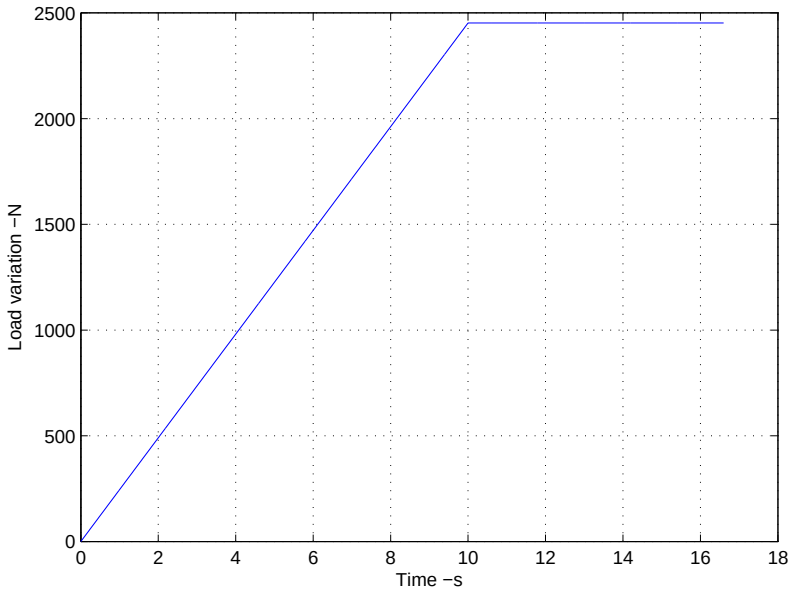

Figure 5.12: Load disturbance profile to the MAGLEV suspension.

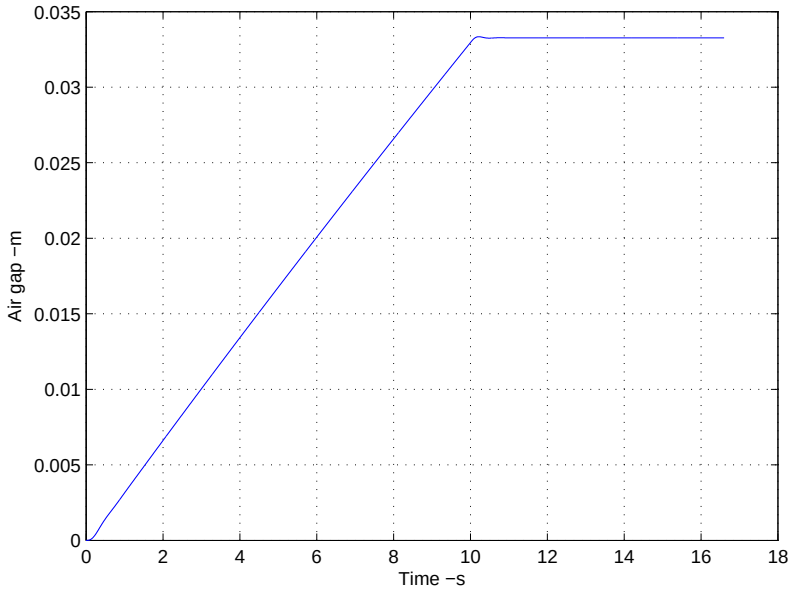

Figure 5.13: Closed-loop response of the MAGLEV suspension for 25% load variation of the total mass of the vehicle without the self-zero integrator.

Taking into account the low frequency of the load variation a self-zero integrator can be used on the flux measurement as illustrated in Fig. 5.14 in order to accommodate the load variations.

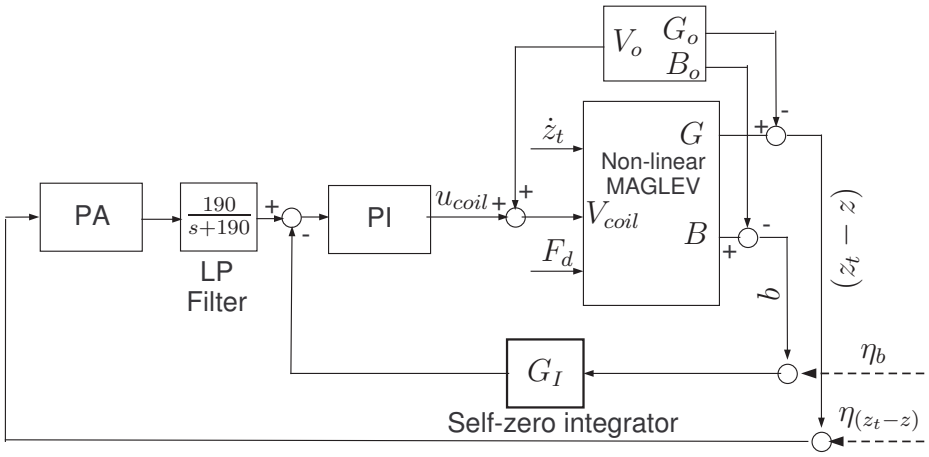

Figure 5.14: Air gap/flux configuration with self-zero integrator.

The self zero integrator (G_I) is a second order butterworth filter as described by Goodall [2000] and is given as follows

$$G_I = \frac{2.209s}{2.284s^2 + 4.7s + 4.7} \tag{5.6}$$

The Bode plot of the self-zero integrator is depicted in Fig. 5.15. The cut-off frequency is at $1.2rad/s$ with 0^o phase shift. A comparison of the frequency response from the the air gap ($z_t - z$) to the force input (F_d) is depicted in Fig. 5.16. As it can be seen the frequency response without the self-zero integrator (with dotted line) is flat at low frequencies while it starts dropping at around $10rad/s$ which explains the closed-loop response in Fig. 5.13. The straight line is the frequency response using the self-zero integrator. Although there is amplification at $10rad/s$ the low frequencies magnitude becomes very low. This means that the low frequency load variation should be rejected and this is verified from the closed-loop responses in Fig. 5.17 and Fig. 5.18.

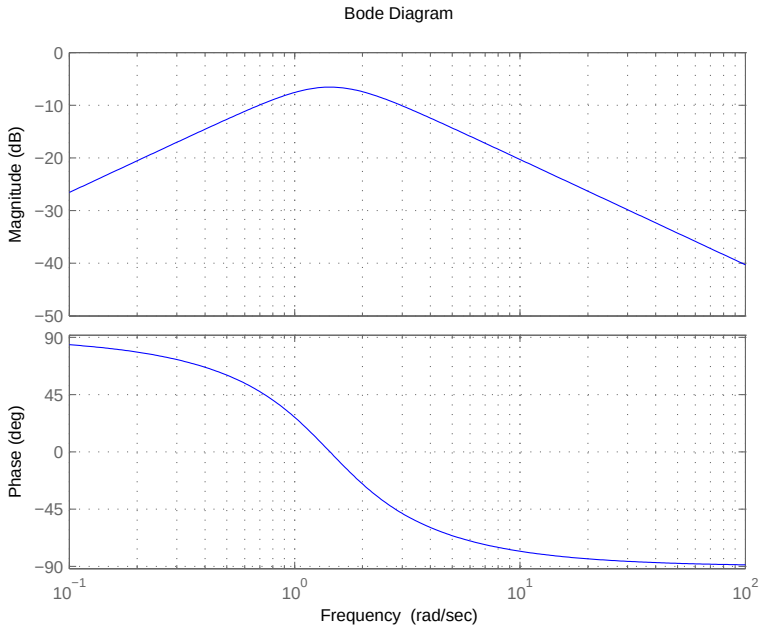

Figure 5.15: Bode plot of the self-zero integrator.

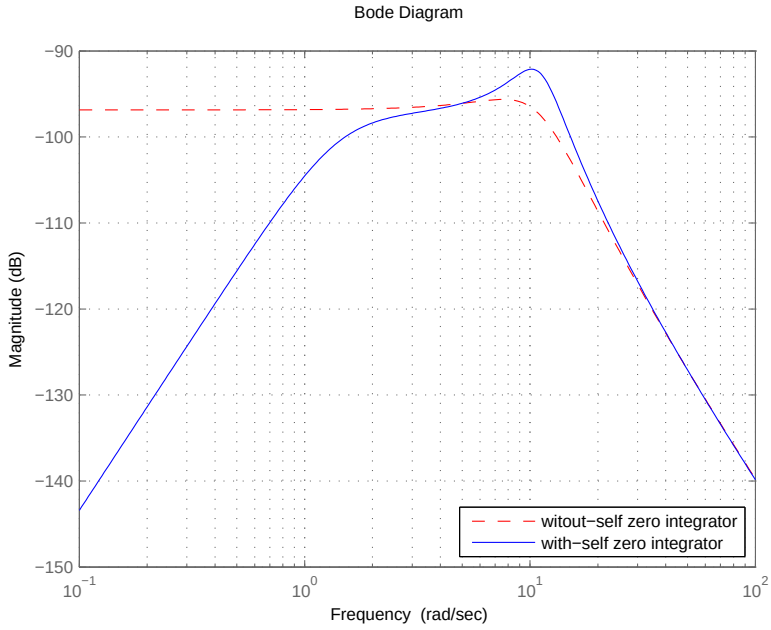

Figure 5.16: Frequency response from $(z_t - z)$ to F_d with and without self-zero integrator.

In Fig5.17(a) and 5.17(b) the closed-loop responses with deterministic input are depicted for the air gap $(z_t - z)$ and the control voltage u_{coil} respectively. As it can be seen from Fig. 5.17(a) the load variation from 1000kg to 1250kg is successfully rejected within about $2sec$ while the deterministic response is acceptable as well. The same test is done for the stochastic response and is illustrated in Fig. 5.18(a) and Fig. 5.18(b). Again the response is within limits but there is some increment to the current and the vertical acceleration $(i_{rms} = 2.27A, \ddot{z}_{rms} = 0.41m/s^2)$. Finally it can be said that the self-zero integrator can be used in order to accommodate the low frequency changes of the load therefore ensure robustness to low frequency load variations.

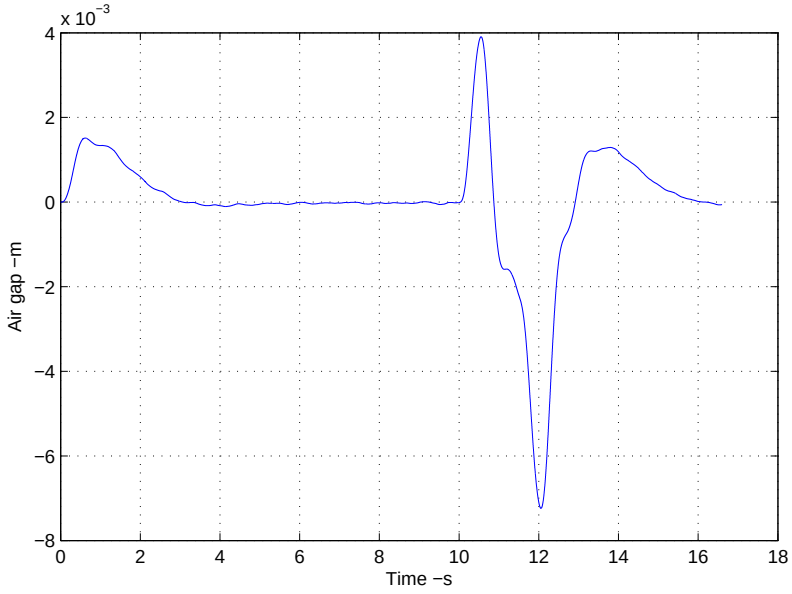

(a) Air gap ($z_t - z$) response with deterministic input.

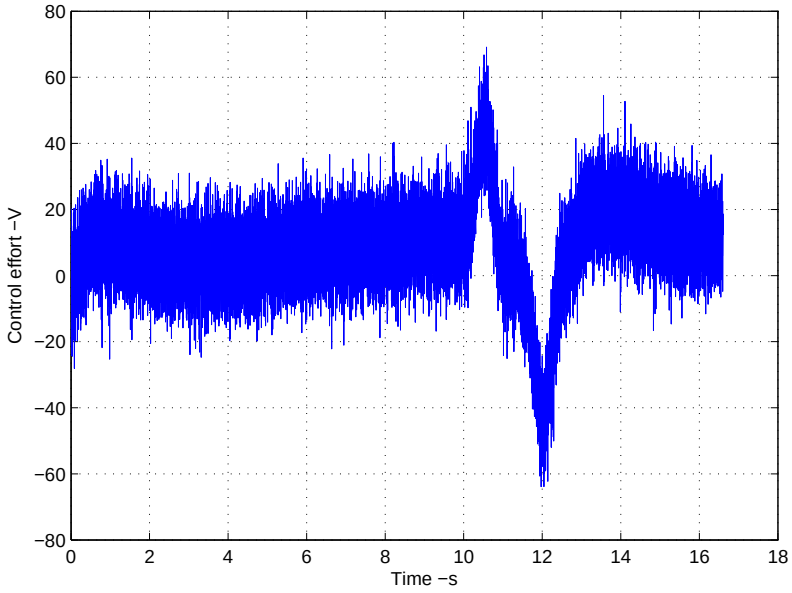

(b) Input voltage u_{coil} response with deterministic track profile.

Figure 5.17: Closed-loop response of the MAGLEV suspension using the self-zero integrator (Deterministic track profile).

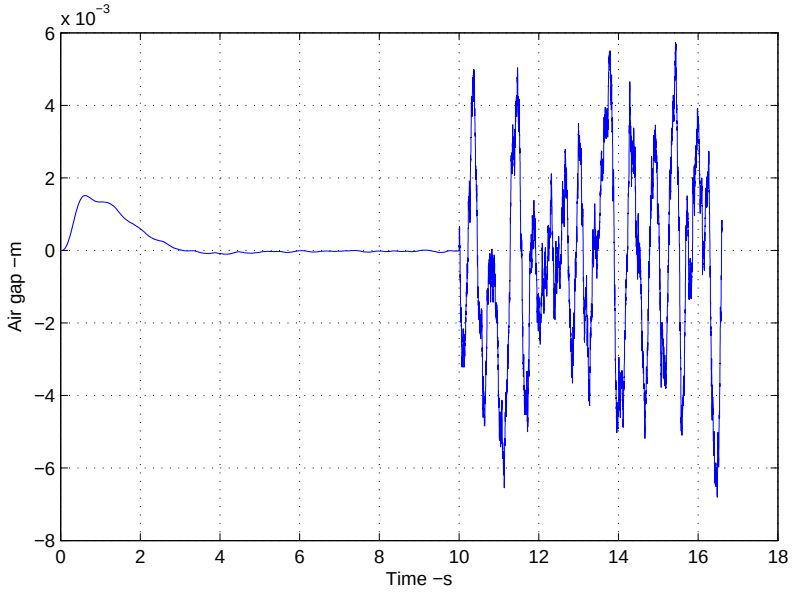

(a) Air gap ($z_t - z$) response with with stochastic input.

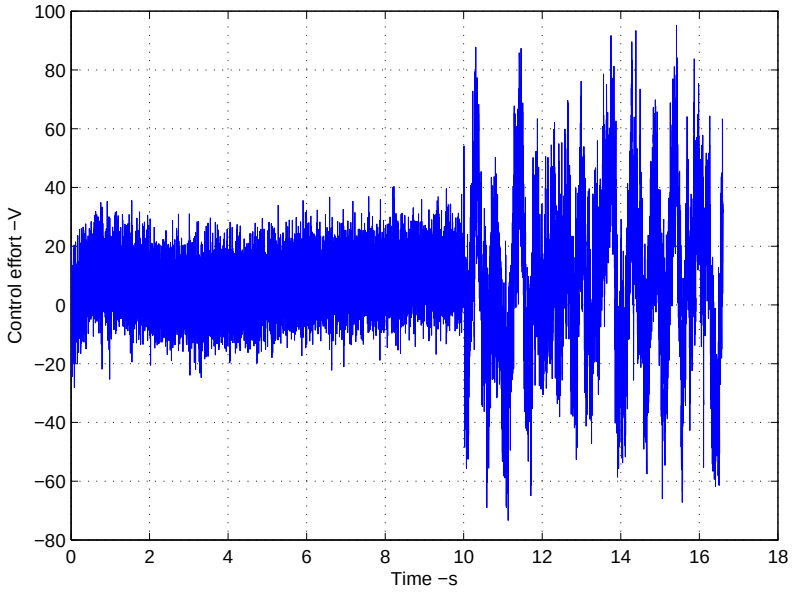

(b) Coil's voltage u_{coil} response with stochastic input.

Figure 5.18: Closed-loop response of the MAGLEV suspension using the self-zero integrator (Stochastic track profile).

5.6 Robustness to operating point perturbations

In this section the parametric variations are taken into account for the MAGLEV suspension. According to the model description in Chapter 4 a typical MAGLEV suspension has parameter values as listed in Table 5.5. The electromagnets are designed based on the operating point of the suspension. Details for design and construction of electromagnets is found in Mansfield [2007]. Equations (5.7) and (5.8) assist to define the parameters of the electromagnets according to the nominal mass to be supported. Assuming that the electromagnet characteristics do not change (i.e R_c, L_c, N_c and A_p) the perturbation of the operating air gap is considered.

Table 5.5: Perturbed and nominal parameters for the EMS system

Parameter	Value	Perturbed value	Unit
M_s	1000	0	kg
G_o	0.015	$\pm 25\%$	m
B_o	1	0	T
I_o	10	$\pm 25\%$	A
F_o	9810	0	N
R_c	10	0	Ω
L_c	0.1	0	H
N_c	2000	0	turns
A_p	0.01	0	m^2

Although for a safety-critical system the control system design has to be accurate such that perturbations of the operating point do not happens but the stability and performance can be tested under such conditions. Assuming that the mass of the vehicle (M_s) remains the same, nominal flux (B_o) has to remain the same as well according to (5.7). Therefore, in order to balance (5.8) the nominal current I_o varies as well in a linear way. In this section $\pm 25\%$ perturbation of the operating air gap is tested under closed-

loop response to disturbances.

$$F_o = \frac{B_o^2 A_{ptotal}}{2\mu_o}(N) \tag{5.7}$$

$$G_o = \frac{N_c I_o \mu_o}{2B_o} \tag{5.8}$$

The air gap variation is assumed to be varied by $\pm 25\%$ around the operating point which means from $0.0113m$ to $0.0187m$ that will cause the operating current to change from $7.5A$ to $12.5A$. The response of the suspension to the operating air gap variations are shown in Fig. 5.19 and Fig. 5.20 for the deterministic and stochastic responses respectively. The stability is maintained for both disturbance inputs while robust performance is maintained.

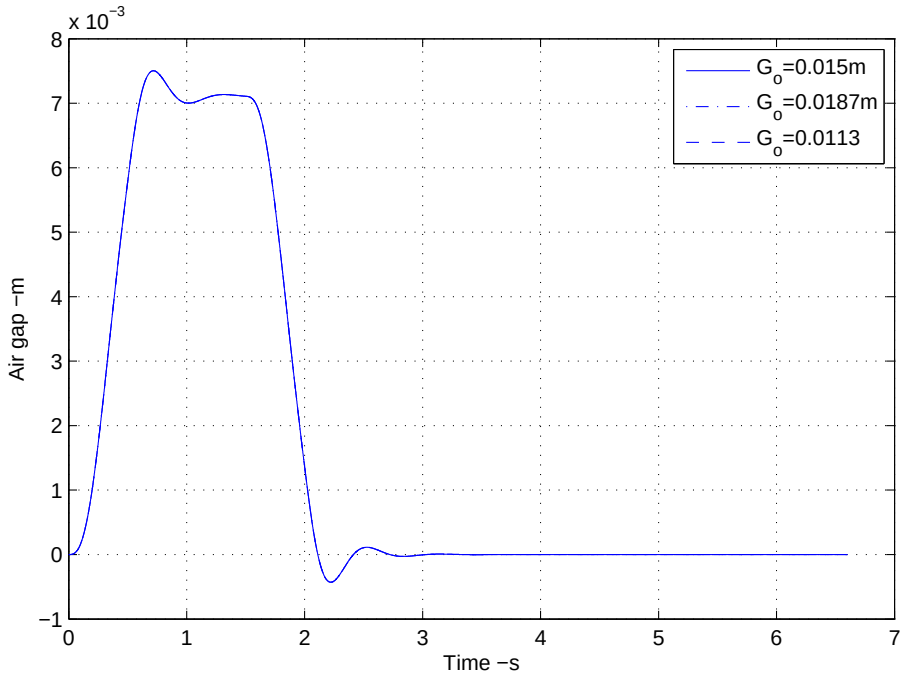

(a) Air gap responses ($z_t - z$).

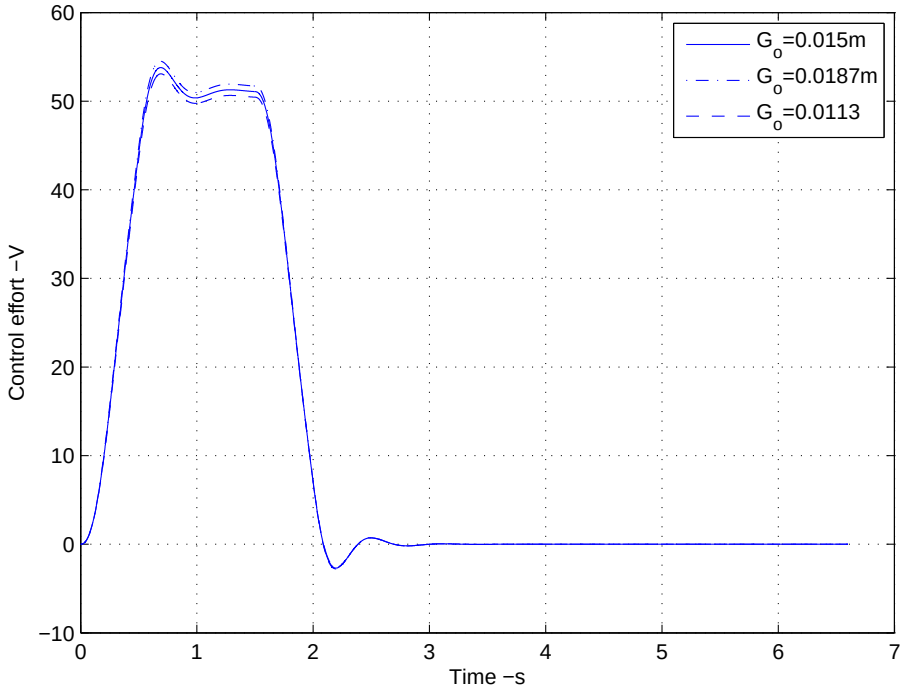

(b) Input voltage responses (u_{coil}).

Figure 5.19: Deterministic response of the suspension for ±25% perturbation of operating air gap.

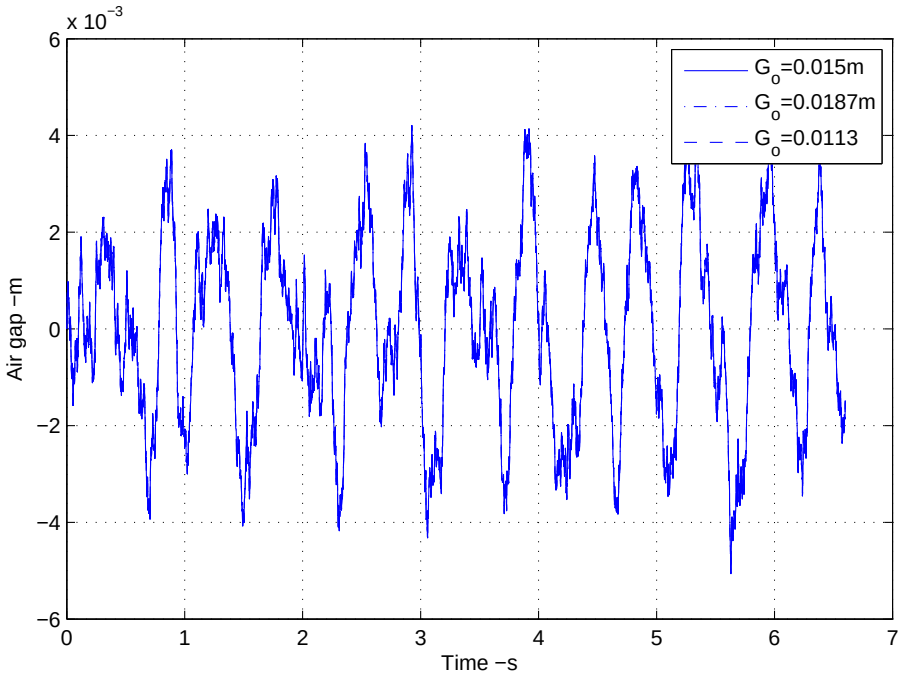

(a) Air gap responses ($z_t - z$).

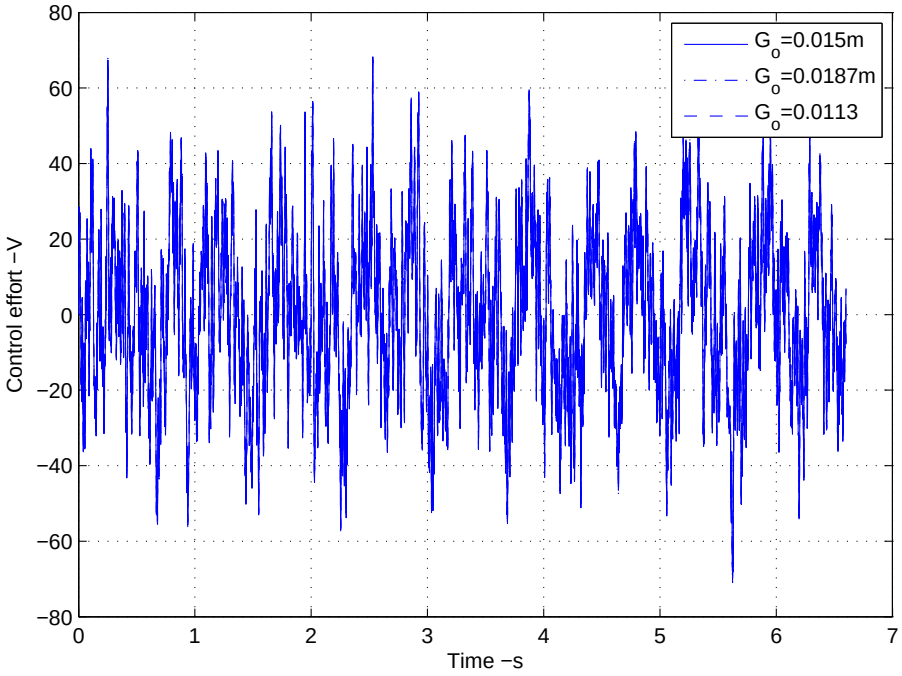

(b) Input voltage responses (u_{coil}).

Figure 5.20: Stochastic response of the suspension for ±25% perturbation of operating air gap.

5.7 Summary

Two classical control strategies were studied from a localised sensor optimisation point of view using the non-linear model of the MAGLEV suspension. The two control configurations are based on inner loop strategies that take into account not only performance requirements but robustness and optimisation of the two strategies. Both approaches require that the air gap measurement is used for the outer loop and for the inner loop either the flux density (b) or the current (i) is used. The Non-dominated Genetic Algorithm II successfully recover the optimum Pareto fronts of controllers for both cases and the results show that using the $(z_t - z)/b$ configuration all the requirements can be satisfied something which is reflected onto the overall constraint violation. In fact, the penalty function approaches are used in the NSGA-II in order to achieve the best possible performance subject to a number of constraints but they can also be used as controller selection criterion. In the next chapters modern control strategies are implemented within a systematic frameworks for optimising all possible sensor sets for the MAGLEV suspension which means that the need to select controllers that satisfy specific requirements among large number of controller arises. This is where the overall constraint violation function is useful as well.

The sensor measurements are noisy and this noise appears on the input voltage of the suspension. In order to reduce the noise level a low pass filter is used at the output of the phase advance controller. In the next chapters it will be taken into account within the optimisation process.

The air gap/flux configuration is tested under large load variations. As the closed-loop response is very sensitive to load variations a self-zero integrator is used to accommodate the load changes. The particular sensor configuration has been tested under closed-loop system uncertainties. Particularly, the optimised controller was tested under $\pm 25\%$ operating air gap variation and it proves to be robust as both stability and performance are maintained.

Chapter 6

Optimised sensor configurations via LQG control

6.1 Introduction

In this chapter, the optimised sensor configurations systematic framework using modern control strategies is presented. The systematic framework combines the **L**inear **Q**uadratic **G**aussian (LQG) control strategies and the genetic algorithm in order to optimally tune the closed-loop performance for each feasible sensor set of the MAGLEV suspension. The overall optimisation process is done in two steps: (i) the state feedback regulator is tuned to recover the optimum Pareto front of controllers between the multiple objectives from where the controller which results to the desired closed-loop response is selected as the 'ideal' or reference response for the second part. (ii) The Kalman estimator is optimally tuned for every feasible sensor set in order to achieve the 'ideal' closed-loop response from the selected state feedback gains. At the end of the second part a table with optimised sensor configurations is given where the selection of the best sensor set is done.

6.2 Liner Quadratic Gaussian control preliminaries

In this chapter the optimised sensor configurations via the very well documented LQG method is considered. In fact, such controller design is based upon the combination of a **L**inear **Q**uadratic **R**egulator (LQR) and a Kalman state estimator. The LQG controller design is performed according to the separation principle, as described in Skogestad and Postlethwaite [2005], and depicted in Fig. 6.1. u is the plant control inputs, y is the plant outputs, w is the process noise and η is the measurement noise. The state feedback gains (LQR design), $-K_r$, are appropriately selected in order to achieve the desirable control properties while the Kalman state estimator is merged into the loop at the second stage, to provide appropriate state estimation.

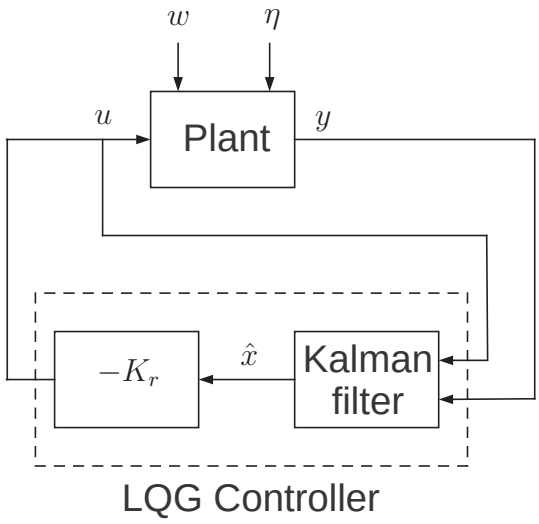

Figure 6.1: LQG design based on the separation theorem (Skogestad and Postlethwaite [2005]).

The LQG control problem is to find the optimal control $u(t)$ which minimises the following performance index

$$J = E\left\{\lim_{T\to\infty}\int_0^T [x^T Q x + u^T R u]dt\right\} \tag{6.1}$$

6.2.1 Liner Quadratic Regulator basics

Linear **O**ptimal **C**ontrol is a type of optimal control, using quadratic performance index, in terms of the control, regulation and/or tracking error variables.

The majority of the plants that exist are non-linear but they can be linearised around operating point conditions. Provided that non-linearities are 'soft' linear controllers can be used to achieve the desired performance. LQR control is well documented in the available literature i.e Maciejowski [1990], Anderson and Moore [1990] and Friedland [1986] but in this thesis a brief summary is given for completeness.

The standard description of a **L**inear **T**ime **I**nvariant (LTI) plant is given by the state space equations (external disturbances or references inputs are not included)

$$\dot{x} = Ax + Bu \tag{6.2}$$

$$y = Cx + Du \tag{6.3}$$

where x is $(n \times 1)$, u is $(m \times 1)$ and y is $(q \times 1)$. The aim is to find a control law

$$u = -K_r x \tag{6.4}$$

where K_r is a gain vector, which minimises the following general form quadratic index

$$J = \int_0^T [x^T Q x + u^T R u]d\tau \tag{6.5}$$

The weighting matrices Q (state weighting matrix) and R (control input

weighting matrix) must be symmetric (because J is scalar), i.e $Q^T = Q$ and $R^T = R$. There is no specific restriction about the form which Q and R should appear, but in most cases are presented in diagonal form. In case that the output y is to be regulated (Output regulation which is very popular in practical engineering applications) then the quadratic performance index is rearranged as

$$J = \int_0^T [y^T Q_o y + u^T R u] d\tau \tag{6.6}$$

where Q_o is the output weighting matrix. It is straightforward show that $Q = C^T Q_o C$ by setting $y = Cx$ for a strictly proper system.

The gain matrix K_r is the solution of the following general form matrix Riccati differential equation

$$A^T P_c + P_c A + \dot{P}_c + Q = P_c B R^{-1} B^T P_c \tag{6.7}$$

subject to given A, B, C, Q and R. Restricting ourselves to the time-invariant case, P_c is constant i.e $\dot{P}_c = 0$. The Riccati equation is then simplified to the following algebraic equation

$$A^T P_c + P_c A + Q - P_c B R^{-1} B^T P_c = 0 \tag{6.8}$$

and the solution of the gain matrix is then given by

$$K_r = R^{-1} B^T P_c \tag{6.9}$$

subject to (A, B) being stabilisable, $R > 0$ (positive definite, for finite control energy), $Q \geq 0$ (positive semi-definite), and that (Q, A) has no unobservable modes on the imaginary axis.

6.2.2 P+I control with output regulation for the EMS system

This section extends the conventional LQR to that of including extra integral states for disturbance rejection/reference following. This is important for appropriate air gap regulation in the EMS system application.

The linearised model of the vehicle is described by the state-space expressions in (6.2) and (6.3) assuming that $D = 0$. The state vector x consists of the vehicle states $[i \;\; (z_t - z) \;\; (\dot{z}_t - \dot{z})]^T$ and $u = [u_{coil}]$. The plant is subject to constant and known external disturbances at the input (deterministic and stochastic track behaviour) and also the constant reference input r which is zero in this case ($r = 0$).

For disturbance rejection and reference tracking ($r = 0$), a new state is introduced that is the integral of the air gap ($\int (z_t - z)$). Note that the air gap is critical to regulate. This approach will produce an optimal P+I controller (Anderson and Moore [1990]) rather than a proportional state feedback controller. Therefore, the system is augmented to include $\int (z_t - z)$ as a state.

$$\begin{pmatrix} \dot{x} \\ \dot{x}' \end{pmatrix} = \begin{pmatrix} A & 0 \\ C' & 0 \end{pmatrix} \begin{pmatrix} x \\ x' \end{pmatrix} + \begin{pmatrix} B \\ 0 \end{pmatrix} u \tag{6.10}$$

where $x' = \int (z_t - z)$ and C' is the selection matrix for integral action and is found from $(z_t - z) = C'x$. The control law is of the form

$$u = \begin{pmatrix} K_p & K_i \end{pmatrix} \begin{pmatrix} x \\ x' \end{pmatrix} \tag{6.11}$$

and including output regulation the quadratic performance index is given as

$$J = \int_0^T [y^T Q_o y + u^T R u] dt \tag{6.12}$$

where $y = [\ddot{z} \;\; (z_t - z) \;\; \int (z_t - z)]^T$ and $u = [u_{coil}]$. $Q_o(3,3)$ regulates the

speed of response $\int (z_t - z)$ while $Q_o(1,1)$ and $Q_o(2,2)$ regulates the vertical acceleration and the air gap respectively. The block diagram is depicted in Fig. 6.2.

The optimal gain is $K_r = R^{-1}B^T P_c$ with $K_r = [K_p \;\; K_i]$, where P_c is the solution of the following algebraic Riccati equation

$$A^T P_c + P_c A + C^T Q_o C - P_c B R^{-1} B^T P_c = 0 \tag{6.13}$$

and C matrix is the regulated outputs $[\ddot{z} \;\; (z_t - z) \;\; \int (z_t - z)]^T$.

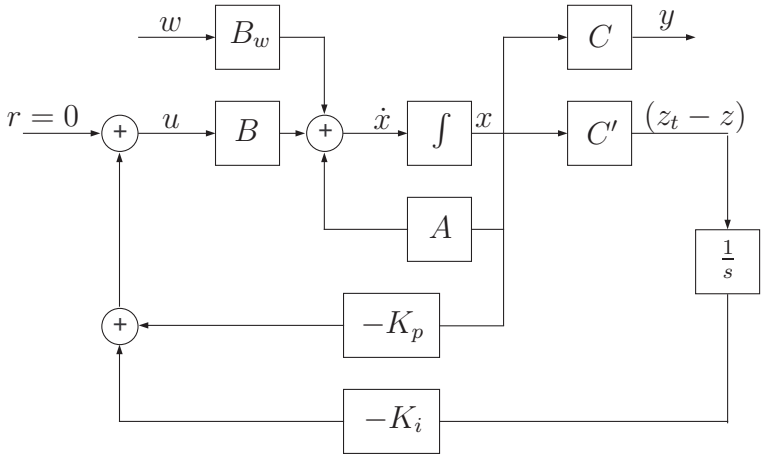

Figure 6.2: Optimal P+I with output regulation.

6.2.3 Kalman State Estimator basics

A typical linearised process of state space form is given by

$$\dot{x} = Ax + Bu + B_w w \tag{6.14}$$

with input and outputs measurements given as

$$y = Cx + \eta \tag{6.15}$$

where the process noise (w) and the measurement noise (η) are assumed to be uncorrelated white noise processes with known constant spectral density W and V respectively. Their covariances are given by

$$\begin{aligned} E\{w(t)w(\tau)^T\} &= W\delta(t-\tau) \\ E\{\eta(t)\eta(\tau)^T\} &= V\delta(t-\tau) \\ E\{w(t)\eta(\tau)^T\} &= 0 \\ E\{\eta(t)w(\tau)^T\} &= 0 \end{aligned} \tag{6.16}$$

where E defines the expectation operator and $\delta(t-\tau)$ is the delta function.

The state space form of the linear Kalman estimator is expressed as

$$\dot{\hat{x}} = A\hat{x} + Bu + K_{LQG}(y-\hat{y}) \overset{(\hat{y}=C\hat{x})}{=} A\hat{x} + Bu + K_{LQG}(y - C\hat{x}) \tag{6.17}$$

$$\hat{y} = C\hat{x} \tag{6.18}$$

where K_{LQG} is the optimally chosen observer gain matrix, minimising $E\{[x-\hat{x}]^T[x-\hat{x}]\}$ and is given by

$$K_{LQG} = P_f C^T V^{-1} \tag{6.19}$$

P_f is a unique positive semi-definite matrix, $P_f = P_f^T \geq 0$ of the algebraic Riccati equation

$$P_f A^T + AP_f - P_f C^T V^{-1} C P_f + B_w W B_w^T = 0 \tag{6.20}$$

subject to (C,A) being detectable, $V > 0$, $W \geq 0$ and $(A, B_w W B_w^T)$ has no uncontrollable modes on the imaginary axis. Thus the V and W matrices tune the Kalman filter so that $E\{[x-\hat{x}]^T[x-\hat{x}]\}$ is minimised.

6.3 Sensor optimisation systematic framework via LQG control

The theoretical framework developed for the sensor optimisation via LQG is shown in Fig. 6.3. The flowchart illustrates the sensor optimisation framework for the MAGLEV suspension. Note that in the LQG framework, the sensor selection relates to the sensor information fed to the Kalman filter part. The LQR part relates to the control objectives ('ideal' closed-loop response).

The initialisation of the algorithm starts with the GA parameter assignment, where in this case are listed on Table 6.1 for the LQR and Kalman estimator tuning respectively. The objective functions as well as the constraints are assigned along with the user's controller selection criteria that defines the desired closed-loop response of the MAGLEV suspension.

Table 6.1: NSGA-II parameters for the LQG sensor optimisation framework

Parameter	LQR	LQG
Maximum generation	500	50
Population size	50	20
Crossover probability	0.9	0.9
Mutation probability	$1/n_r$	$1/n_r$

Next, the state feedback controller is optimally tuned in order to recover the optimum Pareto front of controllers between the objective functions as given in (4.44), page 73. Moreover, the desired LQR gains are selected for the required MAGLEV performance that will be used as the 'ideal' closed-loop response for the Kalman estimator tuning. The controller selection is based on the user's controller selection criteria f_{c_i}, f_u. After that, the first sensor set is selected for the optimisation and check the system's observability. If the system is not observable the algorithm proceeds to the next sensor set ignoring the current one. When observability of states is achieved, the NSGA-II tunes the Kalman state estimator with the aim of estimating the states in

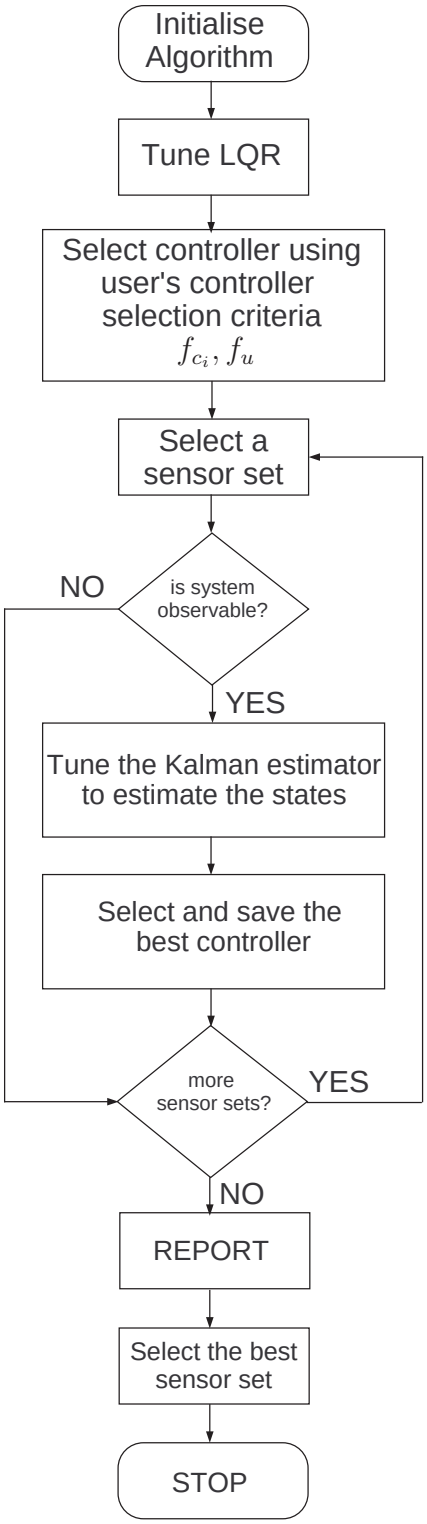

Figure 6.3: Flowchart of the sensor optimisation systematic framework via LQG control.

the best possible way and select and save the best controller. The process is repeated for all feasible sensor sets and at the end of the optimisation process the best sensor set can be selected. As it can be seen the optimisation process is done in two parts. One is the LQR tuning and the second where the sensor information becomes critical is the Kalman estimator tuning. This work is published by Michail et al. [2008a] and Michail et al. [2008c] but the controller tuning is done with the linearised model of the MAGLEV suspension rather than the non-linear model like in this Chapter. More details for the overall systematic framework are given in the next sections and the MATLAB code is given in AppendixA.

6.3.1 LQR tuning

Tuning via Q (or Q_o) and R, for the LQR controller, is not a trivial task to perform. Manual tuning is usually time-consuming especially in the case of more complex engineering problems (as in the case of the MAGLEV suspension). Note that one seeks to pose the problem of control tuning and sensor selection in a multiobjective optimisation framework as shown on Fig. 6.4.

The output weighting regulation matrix is in diagonal form as shown in (6.21) while the input weighting matrix (single control input) is given as $R = 1/r^2$.

$$Q_o = diag\left(\frac{1}{Q_{\ddot{z}}^2}, \frac{1}{Q_{(z_t-z)}^2}, \frac{1}{Q_{\int(z_t-z)}^2}\right) \tag{6.21}$$

The objective functions and the suspension's constrains mentioned in Section 4.7 are included for completeness. The objective functions are formally written as

$$\phi_{s_1} = i_{rms}, \quad \phi_{s_2} = \ddot{z}_{rms} \tag{6.22}$$

Note that, the level of the noise on the input voltage has to be taken into

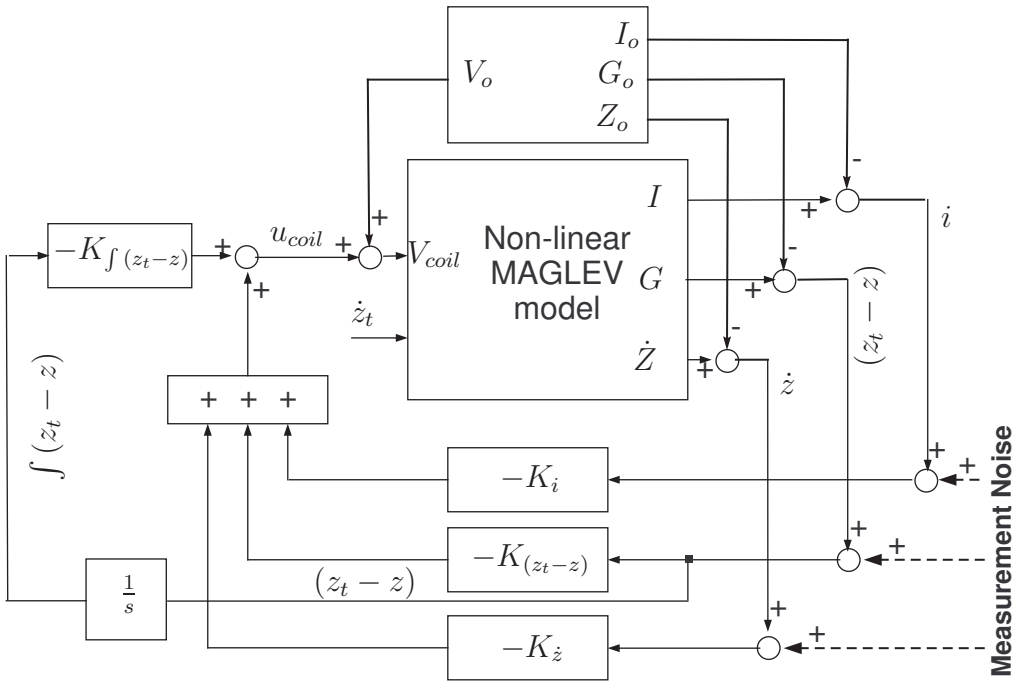

Figure 6.4: Tuning LQR weights for the MAGLEV nonlinear model.

account and thus limited. In particular, to comply with practical limitations and to avoid large amplification by the Kalman filter, extra constraint of $50Vrms$ RMS is added in the framework ($u_{coil_{noise}} \leq 50Vrms$). Refereing to Section 5.4, it is worth noting that the MAGLEV suspension has Low Pass Filter characteristics and thus a large amount of noise is expected to be reduced at the output. The constraints are summarised in Table 6.2. The constraint handling in this framework is done using the static penalty method as described in Section 3.4.1, page 45.

The selection of parameters Q_o is to minimise the system responses on straight track irregularities while enhancing the performance onto gradient track move. In this content, NSGA-II is implemented in an attempt to find the best possible parameters in the case of state feedback. Five variables ($n_r = 5$) with real-coded values were used to represent the output weight factors. The rest of the parameters are listed in Table 6.1.

Table 6.2: Constraints of the magnetic suspension for LQR tuning.

EMS limitations	Value
Stochastic track profile	
RMS acceleration($\simeq 5\%'g'$),($\ddot{z}_{rms}$)	$\leq 0.5ms^{-2}$
RMS air gap variation, $((z_t - z)_{rms})$	$\leq 5mm$
RMS control effort, $(u_{coil_{rms}})$	$\leq 300V$
Deterministic track profile	
Maximum airgap deviation,$((z_t - z)_p)$	$\leq 7.5mm$
Input voltage,(u_{coil_p})	$\leq 300V(3I_0R_c)$
Settling time, (t_s)	$\leq 3s$
Air gap Steady state error, $((z_t - z)_{e_{ss}})$	$= 0$
Idle track profile	
RMS of the noise on u_{coil} $(u_{coil_{noise}})$	$\leq 50V_{rms}$

Figure 6.5 illustrate the overall evolution for the LQR state feedback (note this step does not consider any sensor selection i.e. Kalman filter tuning) tuning is depicted (including screenshots of generations). Until the first 20 generations the solutions are concentrated to around $0.5m/s^2$ (Fig. 6.5(a)) while in the 200^{th} generation NSGA-II starts spreading the solutions onto the optimum Pareto front until the 500^{th} generation. Figure 6.5(f) clearly shows that NSGA-II successfully spread the optimally tuned controllers onto the optimum Pareto front.

Moreover, the selection of the solutions should be compromised between the deterministic and stochastic performance. Figure 6.6 shows the air gap $(z_t - z)$ deviations for the deterministic response and input voltage (u_{coil}) for the 50 controllers at the 500^{th} generation. At it can be seen from the figure the deterministic responses are restricted to the limitations as listed on Table 6.2. The maximum air gap deviation is less than $7.5mm$, the steady state error is zero within less than $3s$ while the maximum input voltage is restricted to around $50V$. Note that for good resolution the input voltage does not contains the measurements noise amplification. At this point, the

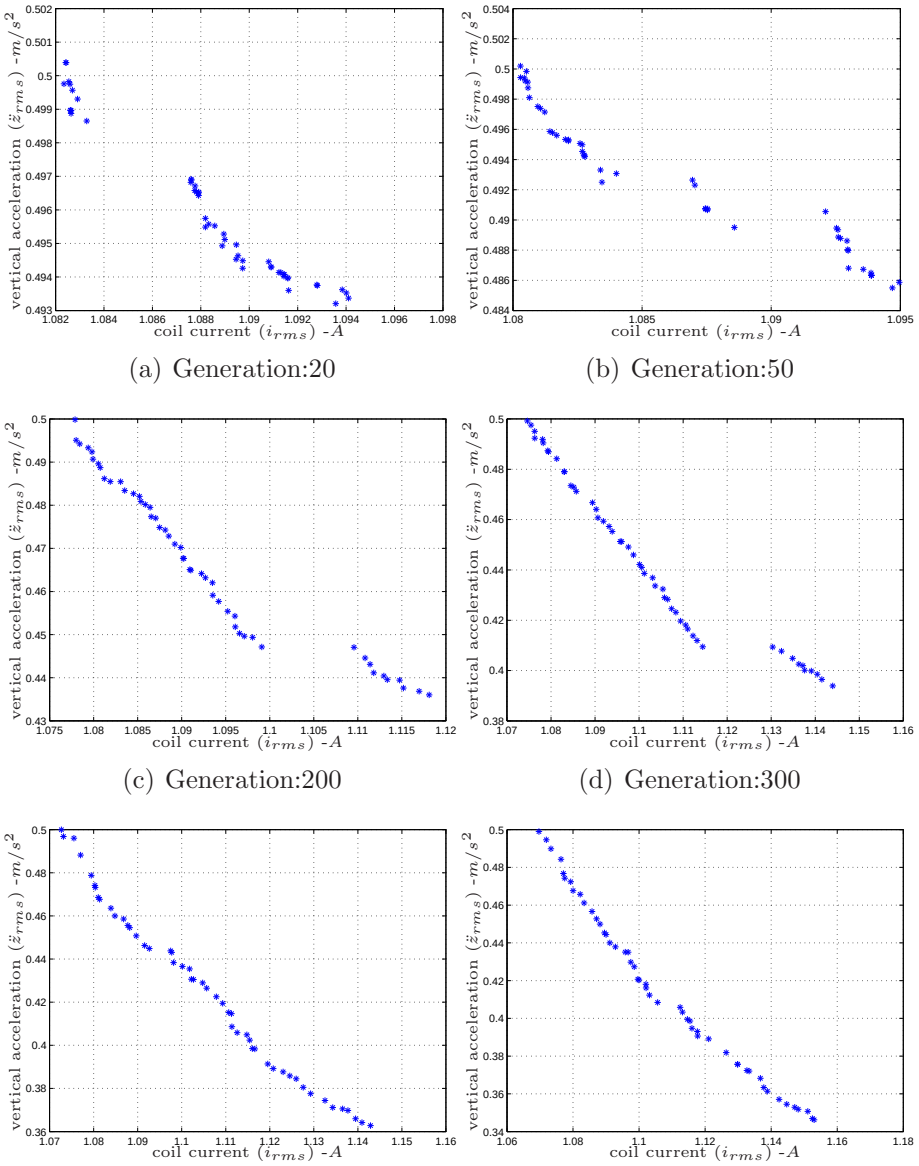

(a) Generation:20 (b) Generation:50

(c) Generation:200 (d) Generation:300

(e) Generation:400 (f) Generation:500

Figure 6.5: Generations evolution process for the state feedback tuning via NSGA-II.

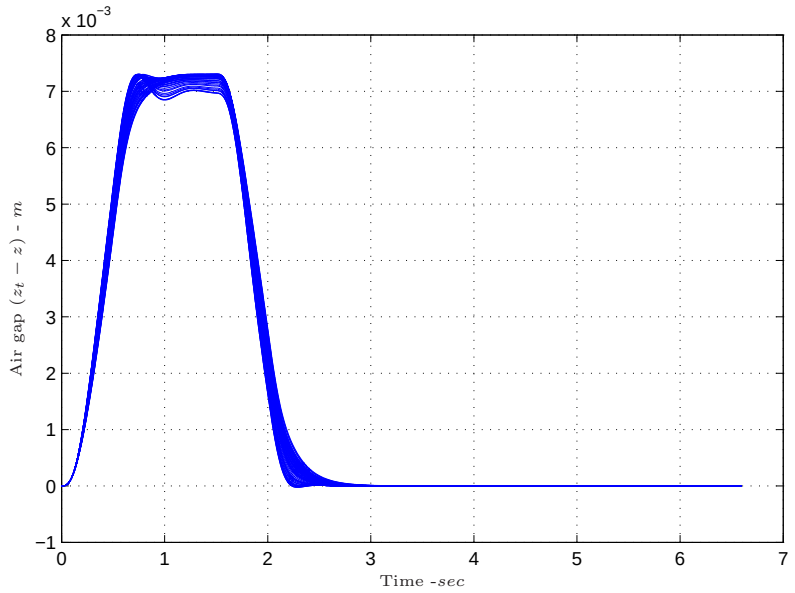

(a) Air gap deviations

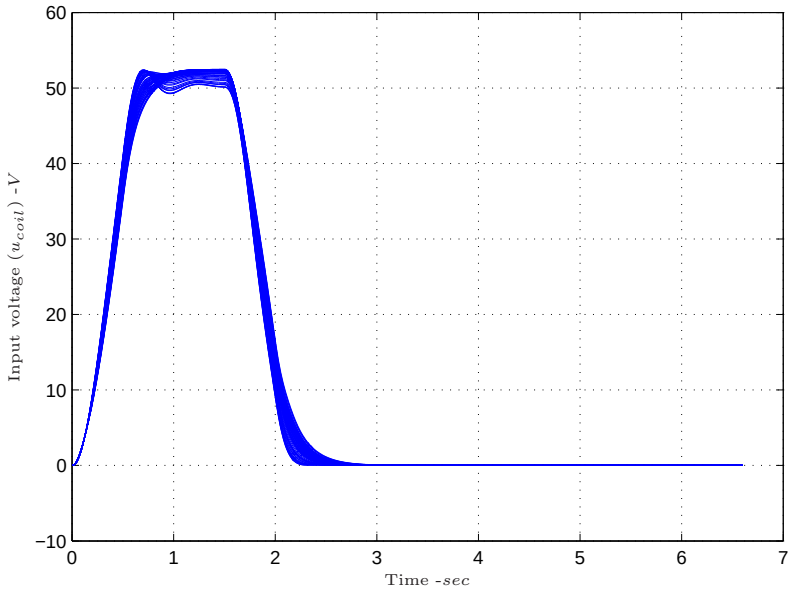

(b) Input voltage deviations

Figure 6.6: Deterministic closed-loop responses for the LQR optimisation for 50 controllers at 500^{th} generation.

controller that results to a desired performance has to be selected which will represent the 'ideal' performance response. The choice of the desired closed-loop response is based on the user's controller selection criteria (f_{c_i}, f_u) that are given as follows

1. Guarantee that the selected controller results to the closed-loop response with vertical acceleration of less than $0.5m/s^2$.($f_{c_1} \equiv \ddot{z}_{rms} < 0.5m/s^2$).

2. Ensure that the excitation coil's current from the closed-loop response of less than 2A ($f_{c_2} \equiv i_{rms} < 2A$).

3. Ensure that the closed-loop response results to the best ride quality ($f_u \equiv min(\ddot{z}_{rms})$.

The controller selection criteria are summarised as follows

$$f_{c_1} \equiv \ddot{z}_{rms} < 0.5m/s^2, \quad f_{c_2} \equiv i_{rms} < 2A, \quad f_u \equiv min(\ddot{z}_{rms}) \tag{6.23}$$

The closed-loop response with the best ride quality results to the vertical acceleration of $0.31m/s^2$. The corresponding state gains are given as

$$\begin{aligned} K_r &= [K_i \;\; K_{\dot{z}} \;\; K_{(z_t - z)} \;\; K_{\int (z_t - z)}] \\ &= [-246.85, \; -3.366 \times 10^3, \; 2.145 \times 10^5, \; 2.417 \times 10^5] \end{aligned} \tag{6.24}$$

The resulting performance with these gains is depicted in Fig. 6.7 and it will be used as the 'ideal' response for the sensor optimisation via LQG control i.e. in the next step the Kalman filter has to be tuned aiming to achieve performance close to the 'ideal' response for every feasible sensor set.

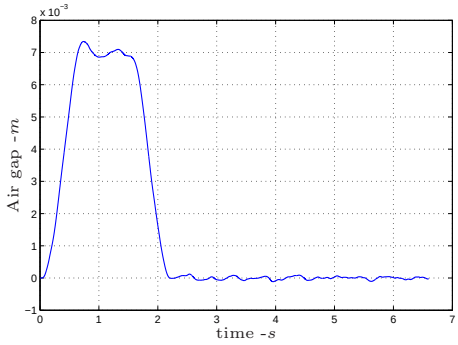

(a) Air gap response for deterministic behaviour of the track.

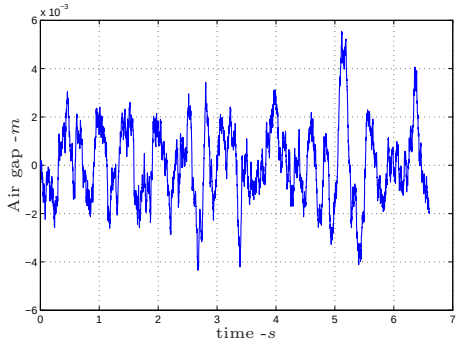

(b) Air gap response for stochastic behaviour of the track.

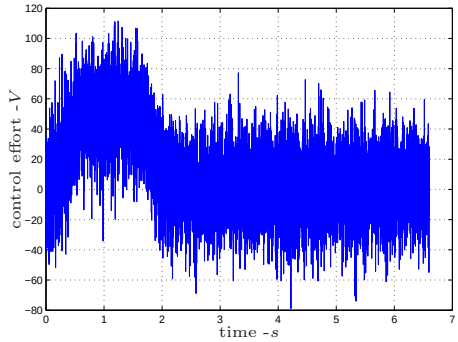

(c) Input voltage for deterministic behaviour of the track.

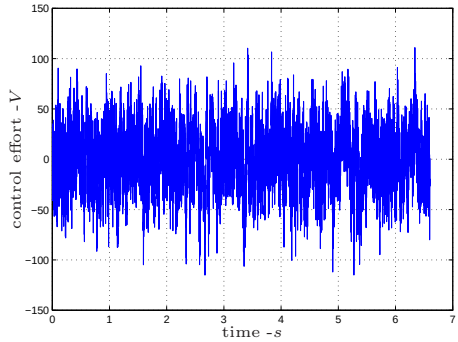

(d) Input voltage for stochastic behaviour of the track.

Figure 6.7: MAGLEV suspension closed-loop response using the selected state feedback gain matrix.

6.3.2 Kalman estimator tuning

The next stage is to tune the Kalman estimator for every possible sensor set, with the overall diagram of the concept illustrated on Fig. 6.8. In this step, i.e Kalman filter introduction in the loop, the sensor information becomes critical. In particular, in order to achieve the same response as in the state feedback response the Kalman filter should provide the best possible set of estimated states (close to the actual state information). This can be achieved by appropriately select the matrix V and W in order to minimise $E\{[x-\hat{x}]^T[x-\hat{x}]\}$ as explained in Section 6.2.3, page 108. The measurement noise weighting (V) is constant and given in (6.25) for all available measurements. In a practical situation, this can be found from sensor equipment data sheets or prior simulation of baseline controller designs (note that in practical systems sensors are very sensitive to external interference and therefore shielding them is a very important issue and sometimes difficult in case that no shielding can be used i.e the air gap measurement). For the simulations, it is assumed that the noise covariance for each corresponding measurement is equal to 1% of the peak value for each variable from the deterministic track profile response of the closed-loop MAGLEV suspension control system (this is something usual in the area of railway).

$$V = diag(V_i, V_b, V_{(z_t-z)}, V_{\dot{z}}, V_{\ddot{z}}) \tag{6.25}$$

In this design the process noise matrix $B_w = B_{\dot{z}_t}$ and the process noise covariance refers to the track velocity input and is tuned for each sensor set (this is a realistic process noise input to the system).

In order to achieve the best possible performance onto track gradient and with the straight track stochastic behaviour with the Kalman-bucy filter in the loop, the minimised objective functions are the comparison between the LQR response (which is the desired performance) and the response with the Kalman-bucy filter in the loop.

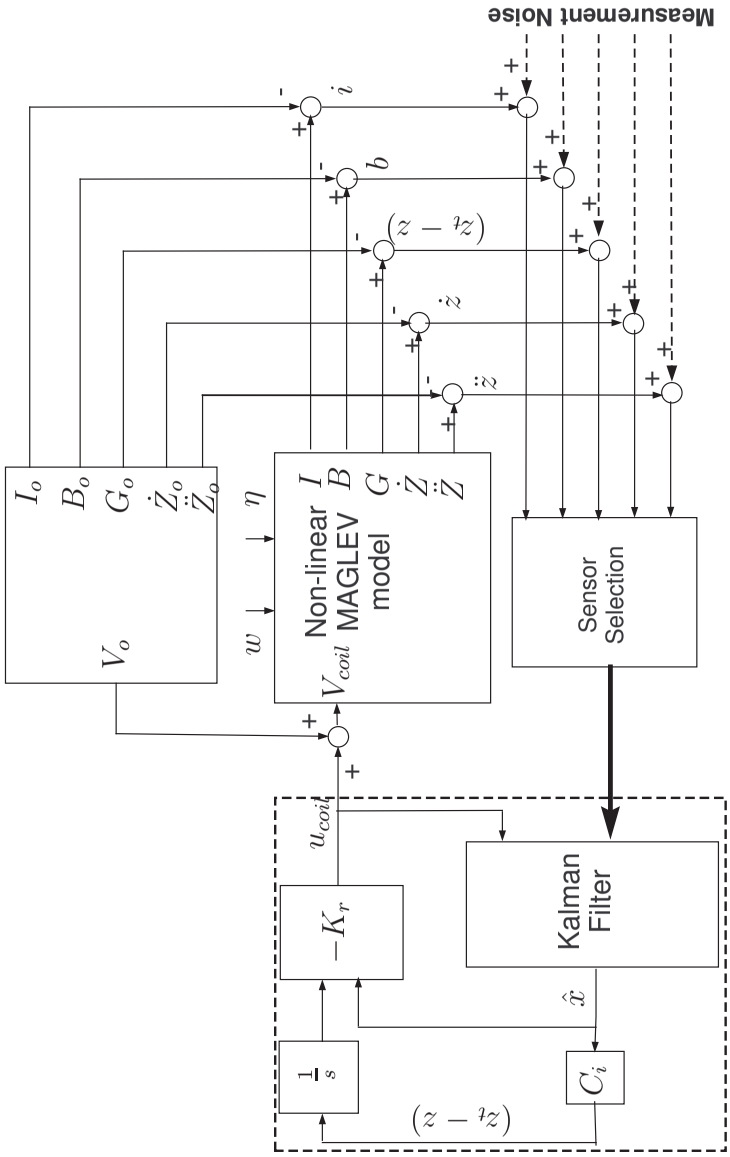

Figure 6.8: Sensor optimisation via LQG for the MAGLEV suspension

For this purpose, three time domain metrics can be used described by the following generic equation (Ingimundarson et al. [2003] and Panagopoulos et al. [2002])

$$I_a = \int_0^\infty t^n |e(t)^m| dt \tag{6.26}$$

where, t is the time, $e(t)$ is the error between the desired and the actual elements and I_a determines the area under $e(t)$ that can take the following specific forms:

- if $n = 0$ and $m = 1$ is the Integral Absolute Error (IAE) of $e(t)$,
- if $n = 0$ and $m = 2$ is the Integral Square Error (ISE) of $e(t)$, and
- if $n = 1$ and $m = 2$ is the Integral Time-Square Error (ITSE) of $e(t)$

The IAE approach is used in order to achieve the same performance for the response onto gradient track and the objective functions to be minimised are expressed in (6.27). For the stochastic response onto straight track of the MAGLEV suspension the RMS is used, see (6.28). An extra objective function is considered (6.29) which is the root mean square value of the noise that appears on the input voltage (u_{coil}) from noisy measurements of the MAGLEV suspension without any track input. This limits the gains of the Kalman filter so that are limited without amplifying the measured noise from the sensors. The final objective functions to be minimised are formally written as

$$\phi_{d_{1,2,3}} = \int_0^t |x_o - x_a| dt \tag{6.27}$$

$$\phi_{s_{4,5,6}} = RMS(x_o - x_a) \tag{6.28}$$

$$\phi_7 = u_{noise_{rms}} \tag{6.29}$$

where, x_o is the vector of the monitored states of interest of the closed-loop with the LQR state feedback (e.g. 'ideal' closed-loop response) and x_a the monitored states of interest of the closed-loop with the overall LQG controller, e.g. actual closed-loop (prior to adding sensor noise). Note that the MAGLEV system is open-loop unstable and this assessment in tuning is

quite attractive i.e taking directly in account the domain differences. This makes a total of 7 individual objective functions. Note that the sensor information entering the Kalman filter are affected by sensor noise.

At the end of the optimisation process, since there is no sensor set that is unobservable there are 620 tuned Kalman filters according to (5.4), in Section 5.3, page 85. There is a large number of controllers, hence in order to avoid manual selection of the controller for each sensor set the overall penalty parameter Ω in (3.8), is used. Particularly, if Ω is zero this means that all assigned constraints are satisfied and close to zero if the constraints are almost satisfied (see (3.5), page 46). The overall penalty function can be very large if there is large constraint violation. Since for a sensor set there could be (which is the usual case) more that one controllers that satisfy all constraints another criterion is needed to select the best controller among them. This criterion describes the sum of the objective functions in (6.27) and (6.28) (states for deterministic and stochastic response) as shown below,

$$S_f = \sum_{i=1}^{3} \phi_{d_i} + \sum_{j=1}^{3} \phi_{s_j} \tag{6.30}$$

From every optimised sensor set, each final population is checked and the individual(s) that give(s) the smallest overall penalty function is (are) selected. If there is more than one, the Kalman filter that gives the smallest S_f is selected as the best Kalman estimator. When the optimisation procedure is completed the end result gives a Kalman estimator for each sensor set, with 24 out of 31 sensor sets found to satisfy the 'ideal' performance (the performance with the state feedback gains only).

On Table 6.3 the results listed include some of the optimised sensor configurations randomly selected. The third row corresponds to the state feedback response while columns 3-9 are the constraint values taken from the response with the best Kalman filter for each sensor set. The sensor sets that satisfy all constraints are marked (✓). An initial comparison between

the LQR performance and the rest of the results it can be seen that although, there is a small variation of the performance using Kalman estimators in the loop most of sensor sets can be used to control the MAGLEV suspension with acceptable performance. Secondly, since at this stage appropriate control of the suspension is the main aim, one may conclude that instead of using 5 measurements (id:13), only one can be used (sensor set id:2 or id:4).

The flux density (id:2) as well as vertical acceleration (id:4) measurements are good choices ensuring that the MAGLEV suspension is working within constraints. Another observation is that Kalman estimator gains are different for each sensor set. With id:4 the Kalman gains are given as $K_{LQG_{\hat{z}}} = [-108025 \quad 2 \quad -170]^T$ and for the id:2 $K_{LQG_b} = [-2150737 \quad 39 \quad -3388]^T$. This issue could serve as an additional criterion in the choice of sensor selection i.e possible one might choose the sensor sets. Offering reduced Kalman gains (attenuation of Kalman gains). However, this is something that could be considered for future work.

At this point, it is worth noting the importance of the results from the LQG tuning to the issue of sensor fault tolerance. In particular, a longer set of sensor provides more information to the controller, and monitors more signals. Thus provides the means of switching to different controllers (with subsets of sensors), if necessary, subject to fault conditions and controller banks ready from the off line framework for maintaining performance (or almost desired performance). However, larger set of sensors imply increased number of sensor fault possibility. On the contrary, a single sensor provides simplicity straight forward hardware redundancy (by using duplicates of the sensor in a voting selection scheme) but limited costs (in the case of hardware redundancy). Albeit, a single sensor is a good first choice to provide an insight into performance issues and simplified solutions.

Table 6.3: Optimised sensor configurations via LQG control.

Sensor set id		$(z_t - z)_{rms}$	$u_{coil_{rms}}$	$\ddot{z}_{rms}$	$(z_t - z)_p$	u_{coil_p}	t_s	e_{ss}	
		mm	V	ms^{-2}	mm	V	s	mm	
	LQR response →	1.5	21.83	0.31	7.3	52.4	2.16	0.019	✓
1	i	1.78	29.16	0.50	2.09	22.93	**6.18**	**0.18**	x
2	b	1.46	22.47	0.32	6.74	63.82	2.18	0.019	✓
3	$(z_t - z)$	1.49	22.41	0.31	**10.69**	84.83	2.56	**0.77**	x
4	$\ddot{z}$	1.46	22.44	0.32	6.82	63.04	2.19	0.013	✓
5	$i, \dot{z}$	1.47	22.48	0.32	7.08	65.21	**4.70**	**0.16**	x
6	$i, \ddot{z}$	1.46	22.18	0.32	6.82	58.91	2.18	0.03	✓
7	$i, b, (z_t - z)$	1.46	22.06	0.32	6.79	55.99	2.18	0.02	✓
8	$i, b, \ddot{z}$	1.42	22.11	0.31	6.77	56.59	2.18	0.01	✓
9	$i, b, \dot{z}$	1.46	22.21	0.32	6.79	59.55	2.20	0.06	✓
10	$i, (z_t - z), \dot{z}$	1.48	22.18	0.32	**7.69**	63.04	2.35	**0.10**	x
11	$i, b, (z_t - z), \dot{z}$	1.46	22.06	0.32	6.84	56.38	2.19	0.05	✓
12	$i, b, (z_t - z), \ddot{z}$	1.46	22.03	0.32	6.81	55.72	2.18	0.02	✓
13	$i, b, (z_t - z), \dot{z}, \ddot{z}$	1.46	22.02	0.32	6.84	55.98	2.19	0.03	✓

In this content, Fig. 6.9 and Fig. 6.10 illustrates the choice of a single sensor i.e vertical acceleration. This choice provides a rather appropriate set of state estimates, with a small drift in the care of the velocity estimate. Thus drift is improved by higher Kalman gains but in the expense of more noise into the system. However, more sensor information improve the situation as shown in Fig. 6.11 where sensor set id:8 is used that includes two extra measurements, the current and the acceleration measurements. As it can be seen in this case using more sensor information the states estimation is precise. The corresponding deterministic air gap and input voltage are depicted in Fig. 6.12(a) and Fig. 6.12(b) respectively.

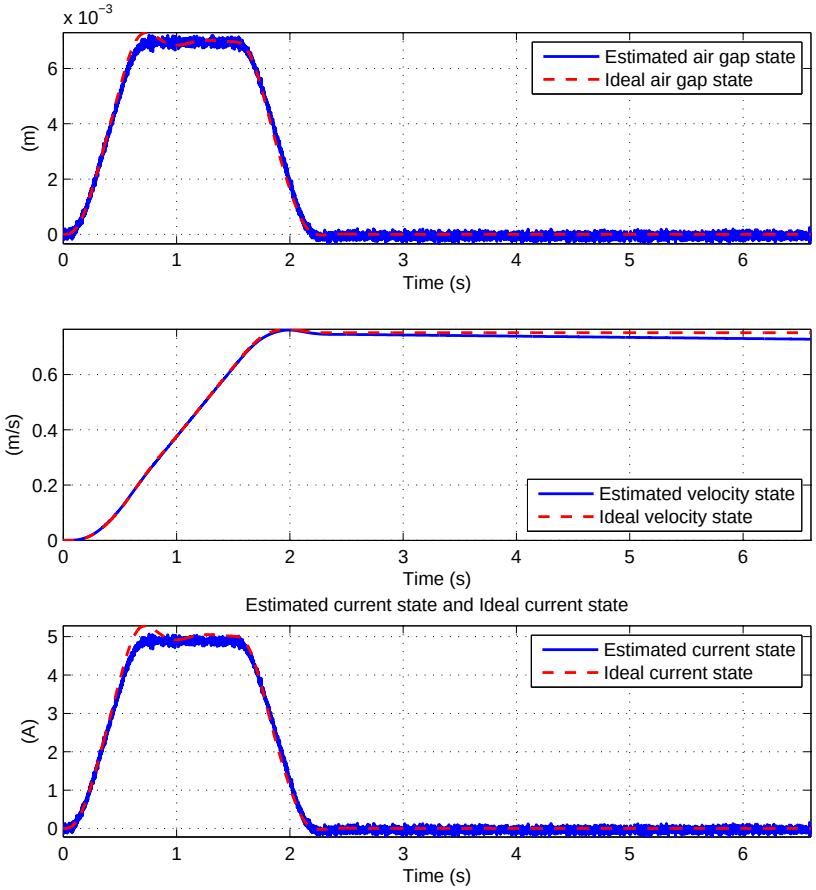

Figure 6.9: The estimated and 'ideal' states using id:4.

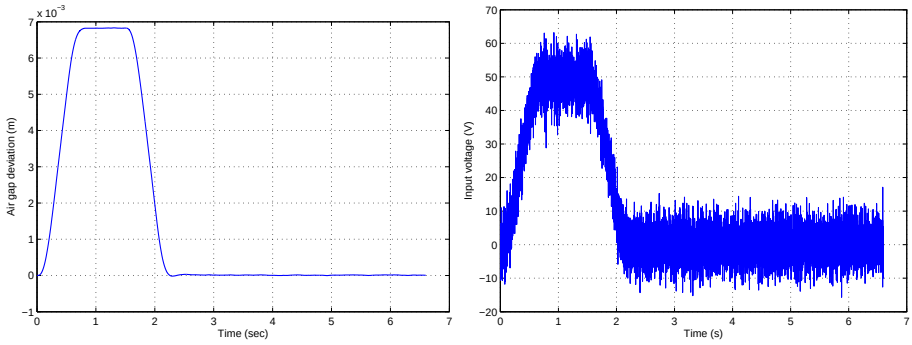

(a) Air gap deviation ($z_t - z$). (b) Input voltage (u_{coil}).

Figure 6.10: MAGLEV suspension response to deterministic track profile using id:4 (single measurement).

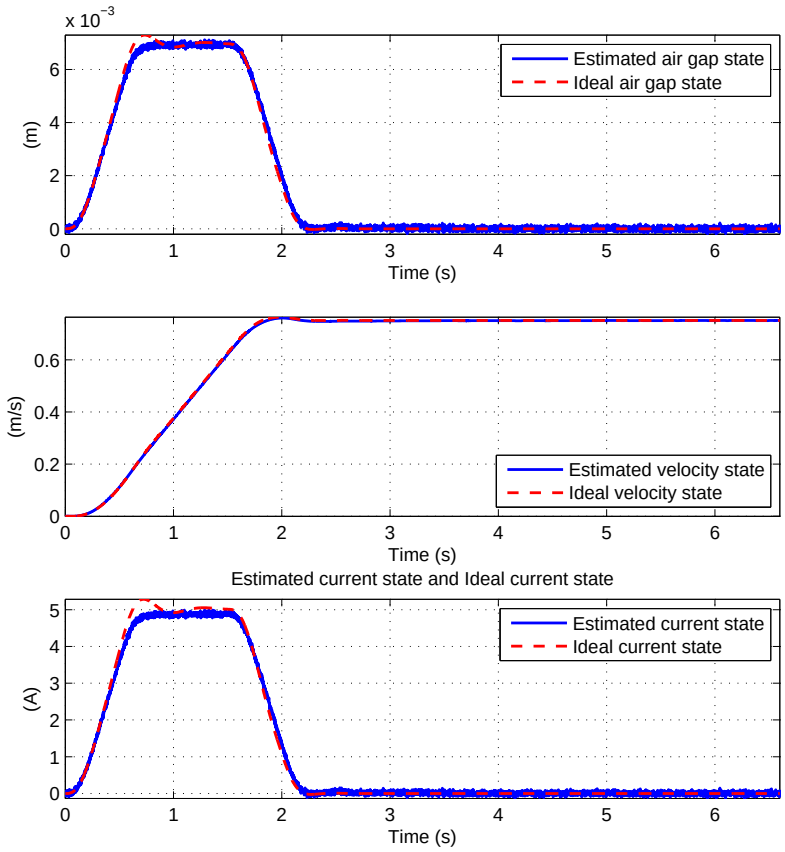

Figure 6.11: The estimated and 'ideal' states using id:8.

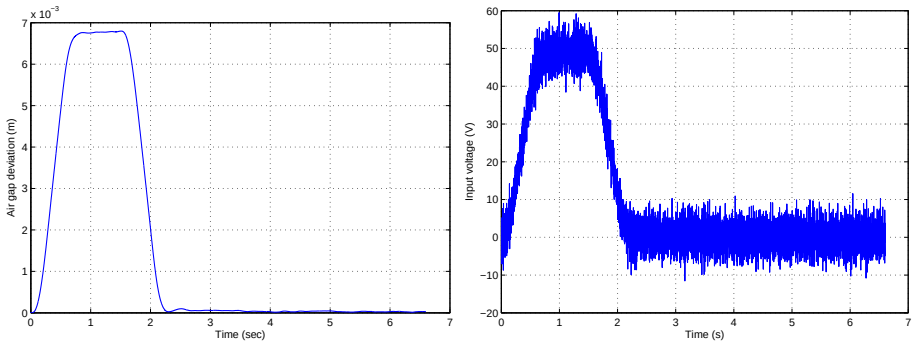

(a) Air gap deviation ($z_t - z$). (b) Input voltage (u_{coil}).

Figure 6.12: MAGLEV suspension response to deterministic track profile using id:8 (three measurements).

6.3.3 Robustness load variation

In this section the robustness to load variation is assessed for two sensor sets. The single measurement id:4 is tested as well as the sensor set id:8 with three measurements. The profile for the load variation is discussed in Section 5.5, page 91. The operating mass gradually increases from $1000kg$ to $1250kg$ within 10 seconds and after that the MAGLEV suspension is tested under the deterministic and stochastic responses. The load variation is treated as a force disturbance (F_d) to the vertical direction of the MAGLEV suspension as described in Section 5.5 and included in the motion equation as follows:

$$M_s \frac{d^2 Z}{dt^2} = M_s g - F + F_d \tag{6.31}$$

Although the mass variation hasn't been taken into account in the sensor optimisation framework the closed-loop response can be sufficient and the stability is quarantined under these circumstances. The closed-loop response to the load variation is shown in Fig. 6.13 and Fig. 6.14 for Id:4 and id:8 respectively. The closed-loop response using the acceleration measurement illustrated in Fig. 6.13 shows both air gap ($z_t - z$) and input voltage u_{coil} for deterministic and stochastic inputs. In both Fig. 6.13(a) and 6.13(c) the effect of the low frequency load increment results to a steady state error of about $1.5mm$ the rest of the constraints remains within normal boundaries. The closed-loop response to the mass variation for the id:8 is depicted in Fig. 6.14. Note that this disturbance may be included into the sensor optimisation framework in order to make sure that the disturbance is rejected for all sensor sets. However, by including the force disturbance rejection into the proposed systematic framework extra simulations are required resulting to more computational power.

6.3.4 Robustness to perturbed operation point

Although the operating point characteristics should be designed in order to remain unchangeable, robustness to perturbed operating point is tested in this section to make sure that stability and performance are maintained under

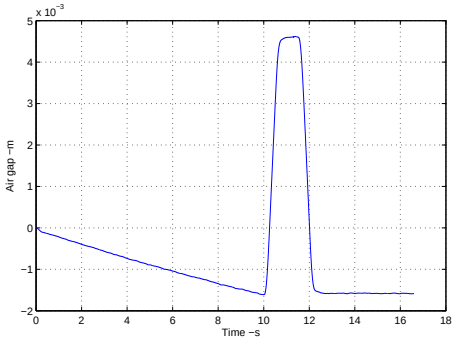

(a) Deterministic air gap response.

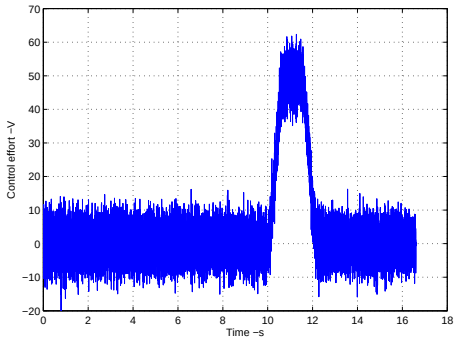

(b) Deterministic input voltage response.

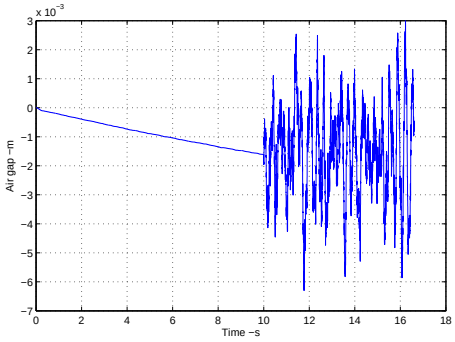

(c) Stochastic air gap response.

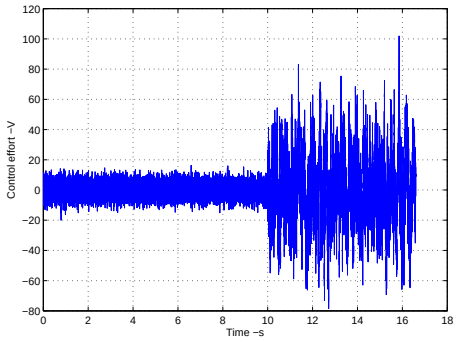

(d) Stochastic input voltage response.

Figure 6.13: Closed-loop response to mass variation with id:4

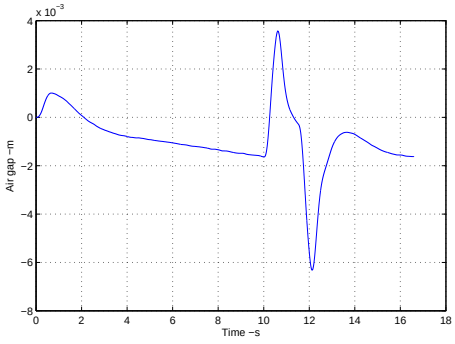

(a) Deterministic air gap response.

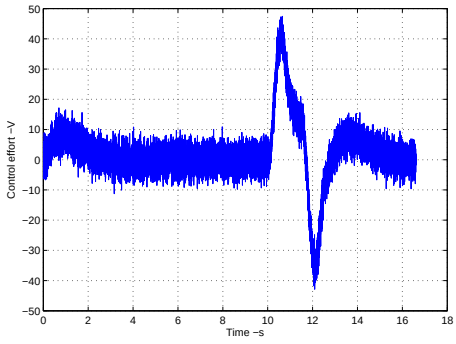

(b) Deterministic input voltage response.

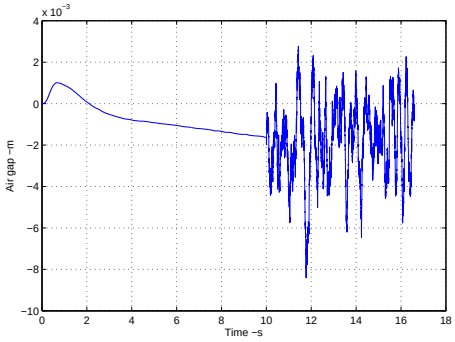

(c) Stochastic air gap response.

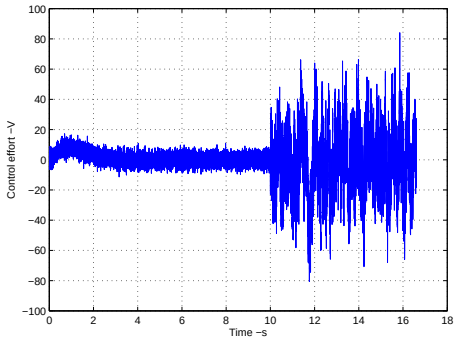

(d) Stochastic input voltage response.

Figure 6.14: Closed-loop response to mass variation with id:8

certain parametric variations. The closed-loop response is tested under the same conditions as in Section 5.6, page 98. Assuming that the mass of the vehicle remains constant at $1000kg$ the operating air gap changes by $\pm 25\%$ which cause $\pm 25\%$ changes in the operating current. Note that since the mass remains constant the operating force remains constant as well.

Figure 6.15 shows the deterministic closed-loop responses under the perturbed operating point using the id:4 and id:8. It can be seen that for those sensor sets the nominal performance slightly changes. This ensures stability and performance under these parametric variations. Tests for parametric variations with each available sensor set are not described here but larger parametric variations with many parameters can be tested within the systematic framework. In fact, the overall constraint violation function Ω can be used to test the stability and performance for parametric variations. This concept is briefly described by the author in Michail et al. [2008d]. However, if it is merged in the systematic framework increases the overall computational effort and time because extra simulations are required to test the closed-loop response using a set of perturbed operating points.

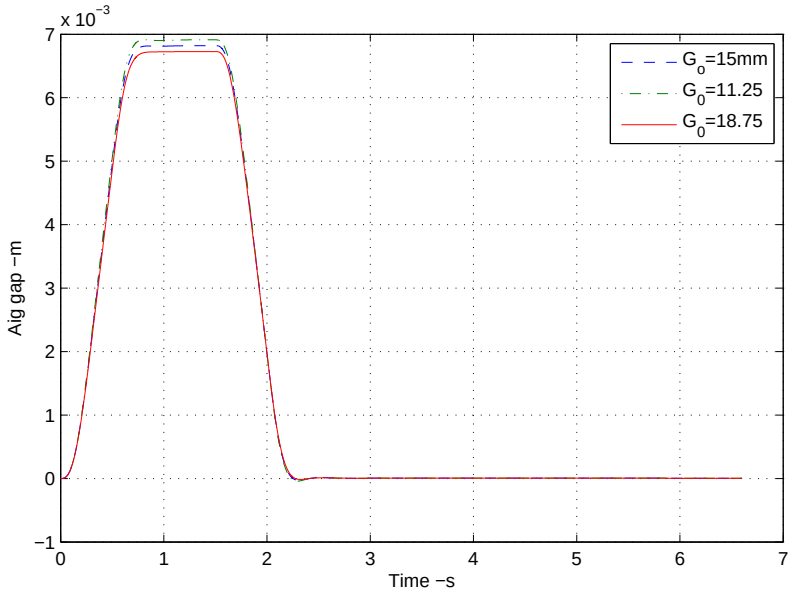

(a) Deterministic air gap responses with id:4.

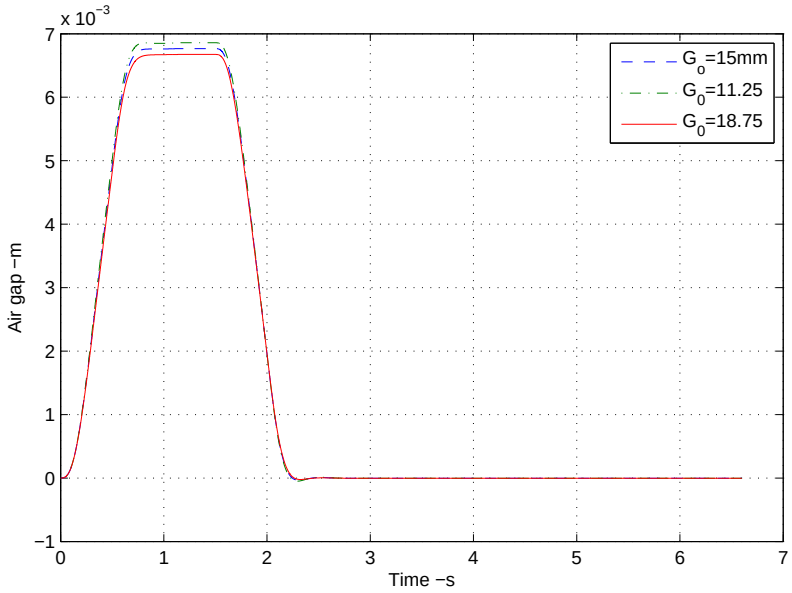

(b) Deterministic air gap responses with id:8.

Figure 6.15: Closed-loop responses to air gap operating point perturbation with id:4 and id:8

6.4 Summary

In this chapter, the optimised sensor configurations systematic frameworks via LQG control design is presented. From the results it can be seen that the proposed systematic framework successfully recovers an optimally tuned controller for each sensor set using the NSGA-II. The two criteria (overall constraint violation function, Ω and sum of the objective functions, S_f) assist with the best controller selection within a population of controllers simplifying the process of selecting the best controller for each sensor set. At the end of the optimisation process 24/31 sensor sets found to satisfy the required performance with two single sensor sets among them. From the control point of view either of them sufficiently satisfy the MAGLEV performance as well as other sensor sets with 2 or more sensors. Moreover, two sensor sets id:4 and id:8 were tested under 25% load variations of the total vehicle mass. Results shows that although the performance is slightly affected the suspension closed-loop response remains within the predefined constraints and the stability is maintained. Furthermore, the operating point perturbation is considered. The operating air gap is perturbed by $\pm 25\%$ around the nominal air gap but stability and performance are maintained in both id:4 and id:8. Finally, the systematic framework is extended towards robust control design strategies as presented in the next chapter.

Chapter 7

Optimised sensor configurations via $\mathcal{H}_\infty$ robust control

7.1 Introduction

This chapter extends the concept of sensor optimisation towards more robust schemes, related to $\mathcal{H}_\infty$ robust control. The chapter introduces preliminary information for $\mathcal{H}_\infty$ control, basic notation and discusses on the multiobjective $\mathcal{H}_\infty/\mathcal{H}_2$ robust control design. In addition, the selection approach via **L**oop **S**haping **D**esign **P**rocedure (LSDP) control system design is also discussed. In particular, this chapter exploits two issues: (i) the performance of NSGA-II in tuning the general weighting functions for the $\mathcal{H}_\infty$ schemes and (ii) the usefulness of the $\mathcal{H}_\infty$ methodologies within the framework of sensor selection for the MAGLEV application.

7.2 Overview of $\mathcal{H}_\infty$ control

The need for the $\mathcal{H}_\infty$ for robust control arises because of the weakness of LQG control to deal with good robustness properties as well as its interpretation of uncertain disturbances based upon white noise (which is often unrealistic). The $\mathcal{H}_\infty$ robust control is largely considered by Zames [1981] while a number of extensive discussions implementations exist in literature (Zhou et al.

[1996], Skogestad and Postlethwaite [2005], Gu et al. [2005]). Due to the frequency-domain nature and the systematic incorporation of uncertainty, H_∞ optimisation has become famous robust control design method since the $1990s$.

Applications on $\mathcal{H}_\infty$ optimisation have been considered for both Single Input Single Output (SISO) and Multiple Input Multiple Output (MIMO) (Skogestad and Postlethwaite [2005], Gu et al. [2005]). However, the $\mathcal{H}_\infty$ optimisation design suffers from complexity of selecting the frequency-dependent weights. There is no general approach to select the weighting factors for the H_∞ optimisation design because it is application dependant. A number of authors have attempted to propose ways of selecting the aforementioned weights. These can be found in Postlethwaite et al. [1990], Beaven et al. [1996], Ortega and Rubio [2004], Hu et al. [2000] and Yang et al. [1994] but these do not strictly offer a generalised approach and they mainly refer to the mixed sensitivity optimisation problem. Particular applications include control of vertical aircraft by Hu et al. [2000] and DC servo control by Yang et al. [1994].

The work in this thesis concentrates on studying the sensor selection problem via (i) M.O. $\mathcal{H}_\infty/\mathcal{H}_2$ design approach and (ii) a $\mathcal{H}_\infty$ loop-shaping (LSDP) via coprime factorisation by (McFarlane and Glover [1990]). The particular issue is to investigate and thus drawn conclusions on the way the aforementioned methodologies deal with the problem studied in hand. Note that especially in the loop-shaping approach a number of classical control issues is introduced (by the nature of the design method). However, the issue of weight selection is very important because is directly related to the complexity of the controller design. Hence, the work addressed here proposes the utilisation of NSGA-II or a mean of tuning the weighting filter in an optimal fashion subject to given performance indices.

Dakev et al. [1997] proposed the main idea of using GAs in tuning weighting filters for the LSDP method however, different type of genetic algorithm have been used (Multi-Objective Genetic Algorithm) and the

sensor optimisation for the MAGLEV suspension system has not been considered.

Recent developments incorporated the use of Linear Matrix Inequalities (LMI) in the $\mathcal{H}_\infty$ optimisation. Work published by Chilali and Gahinet [1996] is using an LMI approach for the $\mathcal{H}_\infty$ design with pole placement constraints, and this relates mainly to the $\mathcal{H}_\infty/\mathcal{H}_2$ methodology considered in here.

7.2.1 Basic notations

Before proceeding to the main part of this chapter, some basic notations necessary for implementing the $\mathcal{H}_\infty$ controllers is introduced for completeness (while the interested reader can refer to the references included in this chapter and information within, for more details on the techniques).

A Linear Time Invariant (LTI) continues time control system in state space form is given as

$$\dot{x}(t) = Ax(t) + Bu(t) \tag{7.1}$$

$$y(t) = Cx(t) + Du(t) \tag{7.2}$$

where $A \in \Re^{n\times n}$, $B \in \Re^{n\times m}$, $C \in \Re^{p\times n}$ and $D \in \Re^{p\times m}$. The above state space system is characterised by the following transfer function with dimension $p \times m$

$$G(s) = C(sI - A)^{-1}B + D \tag{7.3}$$

which can be then rewritten in a packed form as

$$G(s) \stackrel{s}{=} \left[\begin{array}{c|c} A & B \\ \hline C & D \end{array}\right] \tag{7.4}$$

and the complex conjugate of $G(s)$ is given by

$$G^*(s) = G^T(-s) \stackrel{s}{=} \left[\begin{array}{c|c} -A^T & -B^T \\ \hline C^T & D^T \end{array}\right] \tag{7.5}$$

7.2.2 Frequency domain spaces and norms

The meaning of frequency domain spaces and norms of real rational, matrix valued, transfer functions are given. For detailed descriptions refer to Chilali and Gahinet [1996] and Zhou and Doyle [1998]. Let $\mathcal{R}$ denote the space of all real rational transfer function matrices. The $\mathcal{L}_2/\mathcal{H}_2$ norm of $G(s)$ is given by

$$||G||_2 \stackrel{\Delta}{=} \sqrt{\frac{1}{2\pi}\int_{-\infty}^{\infty} tr(G^*(j\omega)G(j\omega))d\omega} \tag{7.6}$$

which is used to define the following spaces

1. $\mathcal{RL}_2$ refers to the space of all real rational strictly proper transfer function matrices with no poles on the imaginary axis and is characterised by a finite $\mathcal{L}_2$ norm.

2. $\mathcal{RH}_2$ defines the space of all transfer function matrices in $\mathcal{RL}_2$ with no poles in $Re(s) > 0$.

The $\mathcal{L}_\infty/\mathcal{H}_\infty$ norm of $G(s)$ is given by

$$||G||_\infty \stackrel{\Delta}{=} \sup_{\omega\in\Re} \overline{\sigma}[G(j\omega)] \tag{7.7}$$

and

1. $\mathcal{RL}_\infty$ refers to the space of all real rational proper transfer function matrices with no poles on the imaginary axis (with finite $\mathcal{L}_\infty$ norm)

2. $\mathcal{RH}_\infty$ defines the space of all transfer function matrices in $\mathcal{RL}_\infty$ with no poles in $Re(s) > 0$.

Also, the $\mathcal{H}_\infty$ norm of a stable transfer function $G(s)$ is its largest input/output RMS gain of

$$||G||_\infty \triangleq \underset{\substack{u\in\mathcal{L}_2 \\ u\neq 0}}{sup} \frac{||y||_{\mathcal{L}_2}}{||u||_{\mathcal{L}_2}} \tag{7.8}$$

where $\mathcal{L}_2$ is the space of signals having finite energy and y is the output of the system G for a given input u. Thus, for any input u of unit energy, the output energy in y is bounded by the $\mathcal{H}_\infty$ norm of $G(s)$.

7.2.3 Linear Fractional Transformations

The basic concept of **L**inear **F**ractional **T**ransformations (LFT) is presented here. LFTs are frequently used in the area of $\mathcal{H}_\infty$ optimisation. In fact, the LFTs can be used to take the closed-loop system, include any structural uncertainties (i.e parametric uncertainties) as well as in other areas of control theory. In fact they can be used to represent ways of standardising a wide variety of feedback problems (Zhou and Doyle [1998] or McFarlane and Glover [1990]).

Let the generalised plant $P(s)$ be given in packed form as

$$G(s) \overset{s}{=} \left[\begin{array}{c|cc} A & B_1 & B_2 \\ \hline C_1 & D_{11} & D_{12} \\ C_2 & D_{21} & D_{22} \end{array}\right] \tag{7.9}$$

which is partitioned in the following way

$$G(s) \overset{s}{=} \left[\begin{array}{c|c} P_{11} & P_{12} \\ \hline P_{21} & P_{22} \end{array}\right] \tag{7.10}$$

where $P_{ij}(s) = C_i(sI - A)^{-1}B_j + D_{ij}$. The block diagram of the generalised regulator configuration is depicted in Fig. 7.1. Where, u is the control input (driving signal), w the exogenous inputs (i.e disturbances w_d and commands r), y the measurements and z are the desired regulated variables,

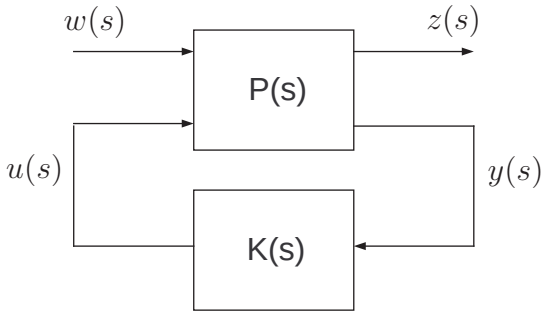

Figure 7.1: The Generalised Regulator Configuration.

i.e the signals need to be minimised so that the desired design objectives are achieved.

The lower linear fractional transformation of the generalised plant $P(s)$ and the controller $K(s)$ is described by (note that subscript s is omitted for simplicity)

$$\mathcal{F}_L(P,K) \stackrel{s}{=} P_{11} + P_{12}K(I - P_{22}K)^{-1}P_{21} \tag{7.11}$$

for $det(I - P_{22}K) \neq 0$. $P(s)$ represents the generalised plant which forms the nominal model $G(s)$ combined with all frequency weighting appropriately chosen to shift the emphasis with frequency between different design objectives. In fact, from Fig. 7.1, the $\mathcal{F}_L(P,K)$ represents the transfer function from w and z given as

$$z(s) = [P_{11} + P_{12}K(I - P_{22}K)^{-1}P_{21}]w(s) \tag{7.12}$$

$\mathcal{H}_\infty$ and $\mathcal{H}_2$ optimal control methods perform minimisation of the $\mathcal{H}_\infty$-norm and the $\mathcal{H}_2$-norm of $\mathcal{F}_L(P,K)$ respectively.

7.2.4 Multi-objective $\mathcal{H}_\infty/\mathcal{H}_2$ robust control

Recall that the $\mathcal{H}_\infty$ norm of a system is the worst-case energy transfer (bounded energy) between regulated outputs and disturbances. As a result can be conservative when disturbances are naturally modelled as persistent

or white noise signals. In such cases, provided that the interests falls upon minimising the RMS value of a regulated output, the $\mathcal{H}_2$ norm of the corresponding closed-loop transfer function is a more appropriate measure of stochastic performance. Nevertheless, the $\mathcal{H}_2$ found not to be necessary for the given situation but the description of the multi-objective $\mathcal{H}_\infty/\mathcal{H}_2$ robust control design follows.

The general multi-objective $\mathcal{H}_\infty/\mathcal{H}_2$ optimisation problem, defined in the generalised-regulator setting is shown in Fig. 7.2. The $P(s)$ is the generalised plant while $K(s)$ is the designed controller. The vector of external disturbances are defined as $w = [w_1, w_2, ...w_n]^T$ (for the MAGLEV suspension only one, the track input) and the corresponding scaling factors are $W_i = [W_{i_1}, W_{i_2}, ...W_{i_n}]$ emphasise the relative weight between the disturbances for the design (In this thesis are considered as one). The Output vector y is the vector of measured variables and the input vector u is the control input to the generalised plant. The z_∞ defines the regulated outputs for the $\mathcal{H}_\infty$ performance index with the corresponding diagonal weights W_1 and z_2 which is the regulated outputs for the $\mathcal{H}_2$ performance index with the diagonal weights W_2. The overall multi-objective optimisation problem is formulated as

$$\underset{K\in\mathbb{S}}{min}\ \alpha\|W_1 T_{z_\infty w}\|_\infty^2 + \beta\|W_2 T_{z_2 w}\|_2^2 \tag{7.13}$$

in which $\mathbb{S}$ denotes the set of all internally stabilising controllers. Scalars α and β are positive definite design parameters which may be used to shift the emphasis of the optimisation problem between the $\mathcal{H}_\infty$-norm and the $\mathcal{H}_2$-norm. Multi-objective optimisation typically refers to the joint optimisation of a vector consisting of two or more functions, typically representing conflicting objectives [1].

Typical examples of multi-objective problems in our context include:

[1]Note that the term "multi-objective" in the $\mathcal{H}_\infty$ robust control design framework is different from the term used in the evolutionary algorithm (Chapter 3) and in fact here, it refers to the cost function of the optimisation problem involving two different types of norms ($\mathcal{H}_\infty$ and $\mathcal{H}_2$).

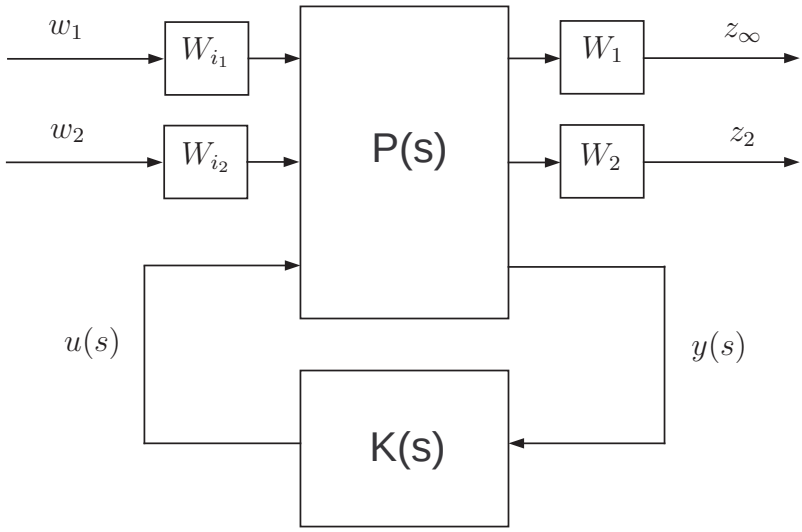

Figure 7.2: The Generalised Regulator Configuration for M.O. $\mathcal{H}_\infty/\mathcal{H}_2$ control.

1. Constraint minimisation:
   Minimise $\|W_2 T_{z_2 w_2}\|_2$ subject to $\|W_1 T_{z_\infty w_1}\|_\infty < \gamma$

2. Unconstraint minimisation:
   Minimise $\beta\|W_2 T_{z_2 w_2}\|_2 + \alpha\|W_1 T_{z_\infty w_1}\|_\infty$,and

3. Feasibility problem: Find a stabilising $K(s)$ (if exist) such that
   $\|W_2 T_{z_2 w_2}\| \leq \gamma_1$ and $\|W_1 T_{z_\infty w_1}\|_\infty \leq \gamma_2$

Note that $T_{z_2 w_2}$ and $T_{z_\infty w_1}$ are the corresponding closed-loop transfer functions from the corresponding disturbance to the regulated variables. This is a generally formulated multi-objective optimisation problem but for the MAGLEV suspension, the $\mathcal{H}_2$ performance index wasn't necessary as the deterministic and stochastic performances were found to be satisfied using only the $\mathcal{H}_\infty$ norm solved via LMI approaches. However, note that the procedure can be naturally extended in a $\mathcal{H}_2$-norm sense by addition of $\mathcal{H}_2$-norm regulated signals. This can be implemented in a straightforward way by using the MATLAB Robust Control Toolbox (Balas et al. [2005]).

7.3 Sensor Optimisation Systematic Framework via multiobjective $\mathcal{H}_\infty$ robust control

In this section the sensor optimisation systematic framework via $\mathcal{H}_\infty$ robust control for the MAGLEV suspension is described. Two regulated variables are considered (i.e air gap and control input) while the W_p and W_u are the weighting filters to tune for best performance. The problem set up is depicted on the diagram of Fig. 7.3. The aim is to tune the weights (W_p, W_u) so that a Pareto optimum front of controllers $\mathbf{K(s)}$ is recovered between the objective functions that satisfy all of the constraints listed in Section 4.7 for each feasible sensor set y_i. The sensor sets for the MAGLEV suspension are given in Section 4.5 and repeated in Table 7.1 for completeness. The sensor sets used for feedback control are selected using the output matrix (C_y). There are totally 5 measurements available as it has been mentioned in Section 4.5 which result to 31 feasible sensor sets.

Table 7.1: Total number of feasible sensor sets for the 1DOF MAGLEV suspension used in multiobjective $\mathcal{H}_\infty$ robust control.

Number of measurements available	Number of feasible sensor sets
with 1 Sensor	5
with 2 Sensors	10
with 3 Sensors	10
with 4 Sensors	5
with 5 Sensors	1
Total	31

The linearised MAGLEV suspension state space in (4.38) is imposed into

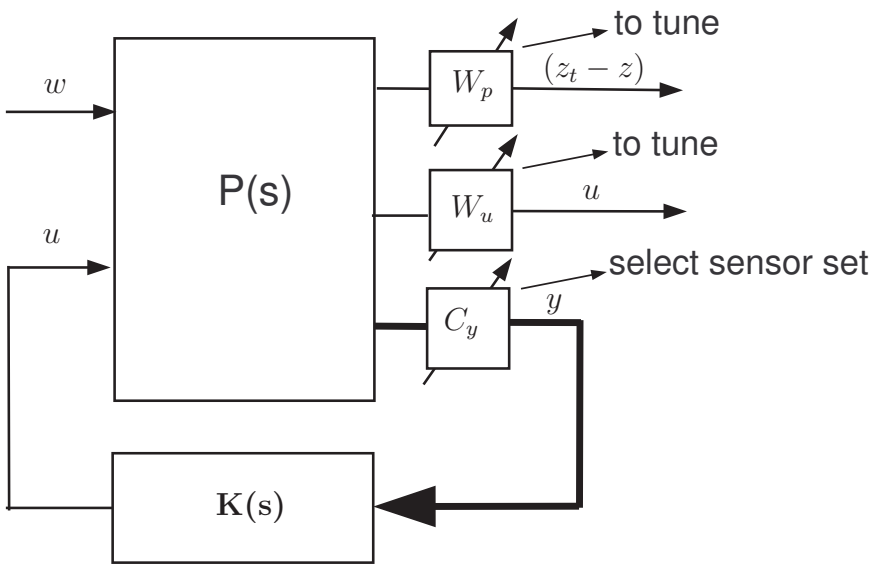

Figure 7.3: Generalised plant configuration for sensor optimisation.

the generalised form of (7.14).

$$\begin{aligned} \dot{x} &= Ax + B_w w + B_u u \\ z_\infty &= C_\infty x + D_{\infty 1} w + D_{\infty 2} u \\ y &= C_y x + D_{y1} w + D_{y2} u \end{aligned} \tag{7.14}$$

w is exogenous input (track disturbance $(\dot{z}_t)$), u the controller output and z_∞ is the regulated outputs related to $\mathcal{H}_\infty$ norm, i.e control effort u_{coil} and air gap $(z_t - z)$. y is the corresponding sensor set that is selected using C_y. The $\mathcal{H}_\infty$ norm of the closed loop transfer function from the exogenous inputs to the regulated outputs is minimised subject to performance requirements described in Section 4.7.

$$\| T_{zw} \|_\infty < \gamma \tag{7.15}$$

The weighting filters W_p and W_u are appropriate low pass and high pass filters respectively as indicated in (7.16), to adjust the performance of the controller by varying their parameters. As it was mentioned there is no

general approach to select the weighting functions as this depends on the application but some guidelines on selecting the weights for the $\mathcal{H}_\infty$ design of a plant are suggested in Skogestad and Postlethwaite [2005].

$$W_p = \left(\frac{\frac{s}{M_p^{1/n_p}} + \omega_p}{s + \omega_p A_w^{1/n_p}} \right)^{n_p} \qquad W_u = \left(\frac{\tau s + A_u^{1/n_u}}{\frac{\tau}{M_u^{1/n_u}} s + 1} \right)^{n_u} \tag{7.16}$$

In particular, for the performance weighting (W_p), M_p is the high frequency gain, A_w the low frequency gain and ω_p the crossover frequency. For the control input weighting filter, (W_u) τ determines the crossover frequency, A_u is the low frequency gain and M_u is the high frequency gain. Both n_p and n_u control the roll-off rates of the filters taken as 1 in this case (i.e $20dB/dec$). Note, that if higher order weights are necessary n_p and n_u can be used both as extra variable and extra minimisation objective in order to find the controllers with the minimum possible order. The weighting filters structures used for the $\mathcal{H}_\infty$ optimisation are illustrated in Fig. 7.4. Note that the controller's output is fixed, as this is only the applied voltage (u_{coil}) to the MAGLEV system, however the controllers' inputs vary based upon the sensors utilised i.e. SISO controller for 1 sensor, MISO controller for more sensor sets. In fact, the order of the controller is fixed to the order of the plant and the order of the filters (currently $3 + 2 = 5^{th}$ order in a state space description - note that further controller reduction could be followed if necessary) via balanced truncation and for closed-loop reduction (Obinata and Anderson [2001]).

The proposed systematic framework is presented with the flow chart shown in Fig. 7.5. The flow chart shows how the NSGA-II is merged to the sensor optimisation framework efficiently, producing the optimum Pareto front of controllers for each possible sensor set. Initially, the NSGA-II parameters, the objective functions (ϕ_i), design constraints (ω_i, ψ_j) and controller selection criteria (f_{c_i}, f_u) are given. Then the first sensor set is selected and the algorithms tests for detectability of the system and if either

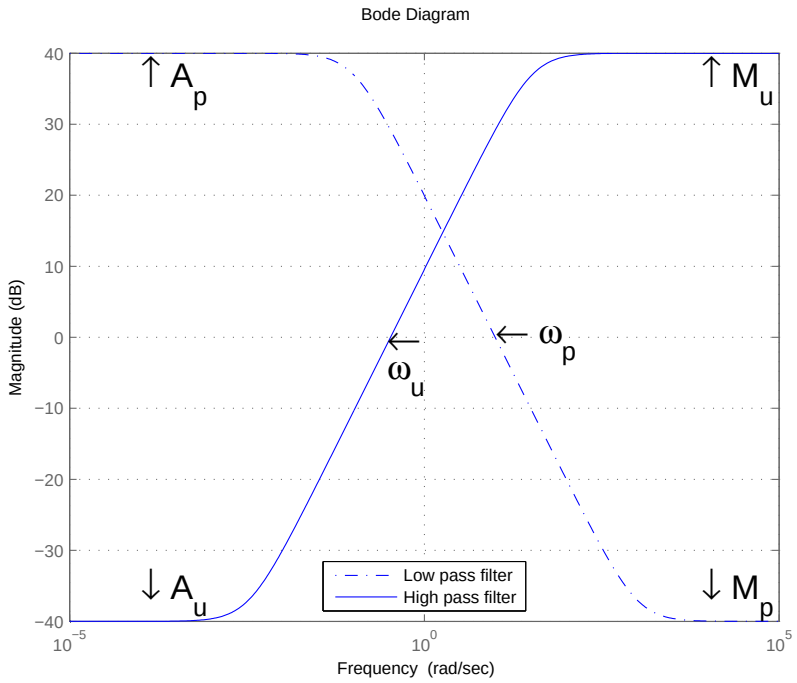

Figure 7.4: Performance weights structure for multiobjective $\mathcal{H}_\infty$ controller design.

of them is not satisfied the next sensor set is selected otherwise the next step is taken where the evolutionary algorithm tunes the weights to recover the optimum Pareto front of controllers. Note that the number of controllers forming the optimum Pareto front is equal to the number of population ($Pop_{num} = 50$). Then, the controllers satisfying all constraints are selected based on the overall constraint violation function in (3.8). Recall that the overall constraint violation function is zero if no constraint is violated or it has a certain value if one or more constraints are violated as explained in Section 5.3. The controllers that do not satisfy the preset constraints are rejected and thereafter the controller which satisfy the user's controller selection criteria (f_c, f_u) is chosen. In case there is no available controller to satisfy the design requirements then the selection is performed by selecting the controller which results in the minimum constraint violation $(min(\Omega)_{k_i})$.

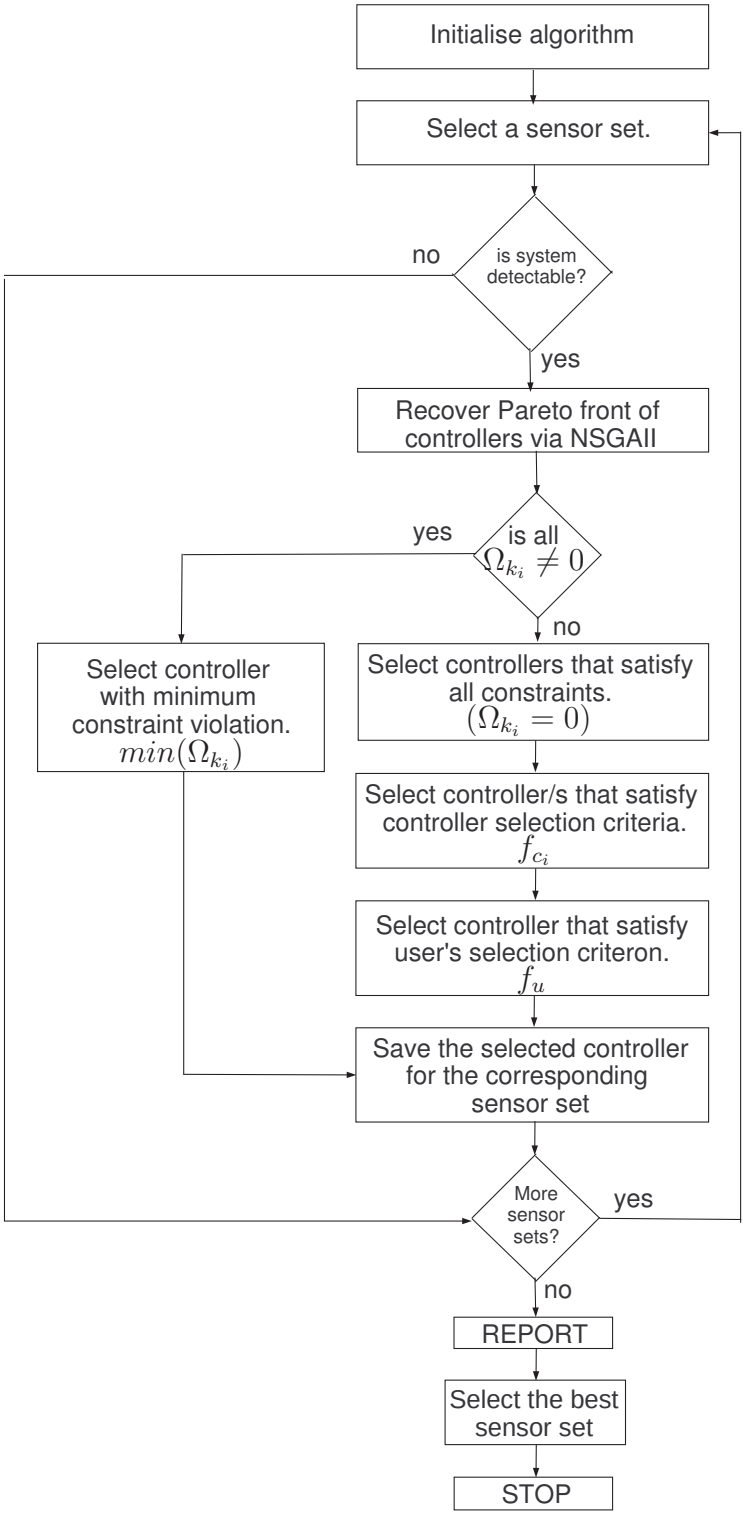

Figure 7.5: Flowchart of the proposed systematic framework proposed via M.O. $\mathcal{H}_\infty$ robust control.

The selected controller is saved and the next sensor set is optimised until the algorithm optimise all sensor sets. The proposed systematic framework is presented by Michail et al. [2008b] and reprinted as a journal in Michail et al. [2009a] but the non-linear model of the MAGLEV suspension wasn't consider. The MATLAB code for this systematic framework is given in AppendixA.

For the sensor optimisation framework via $\mathcal{H}_\infty$ norm, except the mimin-isation of the current and vertical acceleration from the stochastic response, the robustness margin (γ) has been also assigned to be minimised as well as the RMS value of the level of the noise that appears onto the driving signal ($u_{coil_{noise}}$) which comes from the noisy measurements with track input. These objective functions can be can be formally summarised as

$$\begin{aligned} \phi_1 = \gamma, \quad \phi_{s_2} = i_{rms}, \\ \phi_{s_3} = \ddot{z}_{rms}, \quad \phi_4 = u_{coil_{noise}} \end{aligned} \tag{7.17}$$

where, the objective functions are:

1. the $\mathcal{H}_\infty$ robustness margin ($\phi_1 = \gamma$),
2. the RMS value of the input current to the coil from the stochastic behaviour on a straight track ($\phi_{s_2} = i_{rms}$),
3. the RMS value of the vertical acceleration from the stochastic behaviour on a straight track ($\phi_{s_3} = \ddot{z}_{rms}$) and
4. the RMS value of the noise that appears at the input of the driving signal from noisy measurements with idle track profile ($\phi_4 = u_{coil_{noise}}$)

Note that ϕ_{s_2}, ϕ_{s_3} and ϕ_4 are taken from the time history results via simulations with the non-linear model of the MAGLEV suspension. The minimisation of the objective functions mainly refers to the stochastic response of the MAGLEV suspension and the deterministic response is constrained within specific working boundaries as described in Section 4.7. It was found that for the $\mathcal{H}_\infty$ related controller tuning dynamically updated penalty functions was necessary to handle the constraints and avoid infeasible

solution areas.

The controller selection for each sensor set optimisation [1] is simpler in LQG sensor optimisation framework because the controller that results to a response closer to the LQR (that represents the 'ideal' response is selected as the best controller using one criterion which is precision of the state estimation via S_f in (6.30). For the $\mathcal{H}_\infty$ sensor optimisation there is an optimum Pareto front of controllers for each sensor set therefore some criteria have to be used in order to select the best controller that will result to the desired closed-loop response of the MAGLEV suspension. It is possible to assign such criteria depending on the stochastic and/or deterministic response of the suspension. There is a variety of measurements available including the input voltage (u_{coil}), the input current (i), the robustness margin (γ) and the ride quality ($\ddot{z}_{rms}$). In this case the controller selection criteria have been assigned to ensure that the selected controller results to a closed loop response that has the following properties

- ensure that the vertical acceleration (ride quality) is less that $0.5m/s^2$ ($f_{c_1} \equiv \ddot{z}_{rms} < 0.5m/s^2$)
- ensure that the robustness margin is less than one ($f_{c_2} \equiv \gamma < 1$)
- and make sure that the minimum noise on the control effort is selected ($f_u \equiv min(u_{coil_{noise}})$).

The first two criteria define the selection criteria for a group of controllers and the last is the final controller selection criterion. As it has been mentioned previously, if the aforementioned controller selection criteria cannot be met the selection of the best controller is performed by using the overall constraint violation Ω.

The $\mathcal{H}_\infty$ control of the non-linear MAGLEV suspension model is depicted in Fig. 7.6. The overall evolution process is done within 200 generations

[1] Note that at the end of the optimisation for each sensor set there are 50 optimally tuned controllers

with a population of 50 individuals that guarantee a definite solution within the predefined search space. The genetic algorithm parameters are listed in Table 7.2.

Table 7.2: NSGA-II parameters for the M.O H_∞ sensor optimisation framework.

Parameter	Value
Maximum generation	200
Population size	50
Crossover probability	0.9
Mutation probability	1/5

At the end of the evolutionary process, the final result is about 1550 optimally tuned controllers assuming none of them violates the constraints with all sensor sets. However, the proposed systematic framework is able to find controllers that satisfy the constraints for 29 out of 31 sensor sets and about 1440 optimally tuned controllers that satisfy the constraints.

Table 7.3: Sensor optimisation via M.O $\mathcal{H}_\infty$ robust control design results.

id	sensor set	$n[K(s)]_{\Omega_{k_i}=0}$	$n[K(s)]_{\Omega_{k_i}=0,f_{c_1},f_{c_2}}$
1	i	0	0
2	b	50	13
3	$(z_t - z)$	0	0
4	$\dot{z}$	22	18
5	$\ddot{z}$	49	0
6	i,$\ddot{z}$	47	0
7	b,$(z_t - z)$	50	10
8	i,$\dot{z}$,$\ddot{z}$	50	12
9	i,b,$\dot{z}$	50	24
10	i,b,$\ddot{z}$	50	18
11	b,$(z_t - z)$,$\ddot{z}$	49	23
12	i,b,$(z_t - z)$,$\dot{z}$,$\ddot{z}$	50	5

In Table 7.3 some randomly selected sensor sets are listed. In the

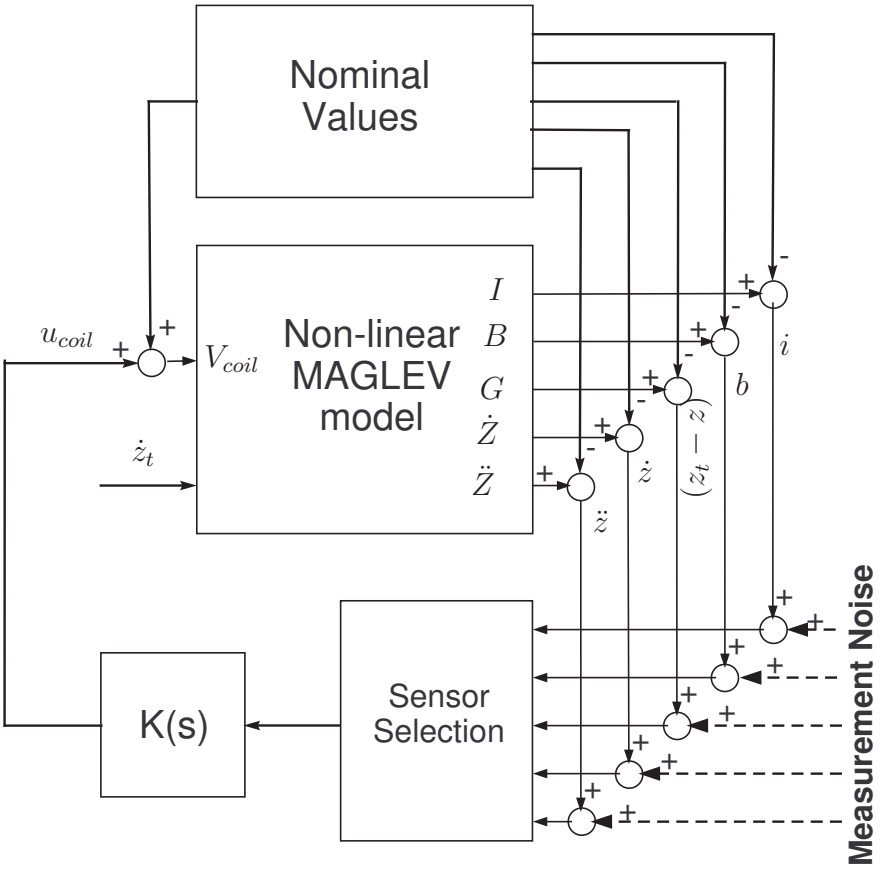

Figure 7.6: $\mathcal{H}_\infty$ control for the non-linear MAGLEV suspension

first column the number of controllers that satisfy the required constraints ($n[K(s)]_{\Omega_{k_i}=0}$) are shown while in the next column the number of controllers that satisfy the two criteria f_{c_1} and f_{c_2} are listed ($n[K(s)]_{\Omega_{k_i}=0,f_{c_1},f_{c_2}}$). No controllers were found to meet some of the constraints ((t_s, $(z_t-z)_{e_{ss}}$)) for two single sensor sets id:1 (current) and id:3 (air gap). From the 29 sensor sets there exist 11 sets that do not satisfy the user's controller selection criteria f_{c_1} and f_{c_2}. It is interesting to note that there are 2 single measurements (id:2 and id:4) which have controllers that satisfy the user's controller selection criteria just like the full sensor set (id:12). Particularly, there exist 13 controllers for the id:2 and 18 for the id:4 while 5 controllers exist for the id:12 (full sensor set).

In the cases where the objectives are more than three the parallel cord graph is used to present the trade off between them. For the id:2 the trade-off of the objectives is illustrated in Fig. 7.7. The x-axis has the four objectives while on the y-axis the values of the objectives are normalised around 1. The same approach is used for the full sensor set (id:12) and the trade off is depicted in Fig. 7.8.

The corresponding deterministic response of the closed-loop with controllers that satisfy the constraints $(n[K(s)]_{\Omega_{k_i}=0})$ for sensor sets with id:2 and id:12 are depicted in Fig. 7.9(a) and Fig. 7.9(b) respectively. It can be seen that the maximum air gap deviation is less that $7.5mm$ while the settling time is less than $3s$. Comparing the two figurens, it can be seen that the responses with id:12 are affected by the noisy control input but in the id:2 the responses are clear. Although the effect is not very serious it shows that the level of the noise on the control effort should be kept as low as possible especially when a large number of sensors is used. This emphasises the fact that there is a possibility that the number and the locations of sensors to be used is vital for the final closed-loop response.

The final step is to show the results from the overall sensor optimisation framework via the multiobjective $\mathcal{H}_\infty$ robust control. Taking into account the user's controller selelction criterion $f_u \equiv min(u_{coil_{noise}})$ one controller for each sensor set is selected. Some sensor sets selected with the corresponding results are listed in Table 7.4. Columns 3-6 are measurements from the stochastic response and the next four are measurements from the deterministic response. Column 11 is the robustness margin (γ), 12^{th} column is the RMS value of the noise that appears on the driving signal with idle track profile $(u_{coil_{noise}})$. The thirteenth column shows the constraint violation Ω with the last two columns showing if the two criteria (f_{c_1}, f_{c_2}) are satisfied (✓) or not (x).

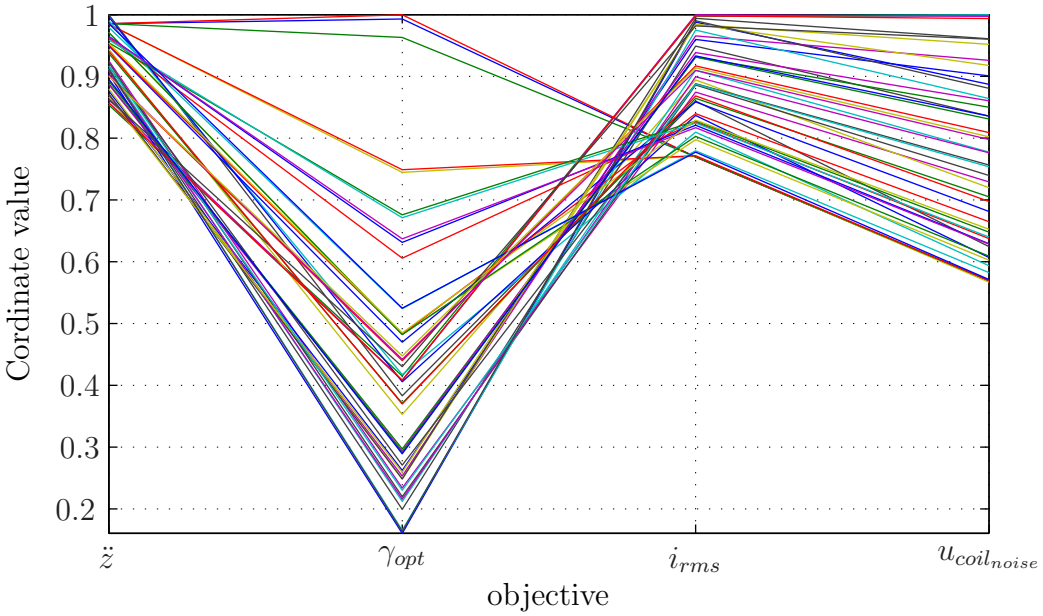

Figure 7.7: Parallel cord shows the trade-off between the objectives for sensor set with id:2

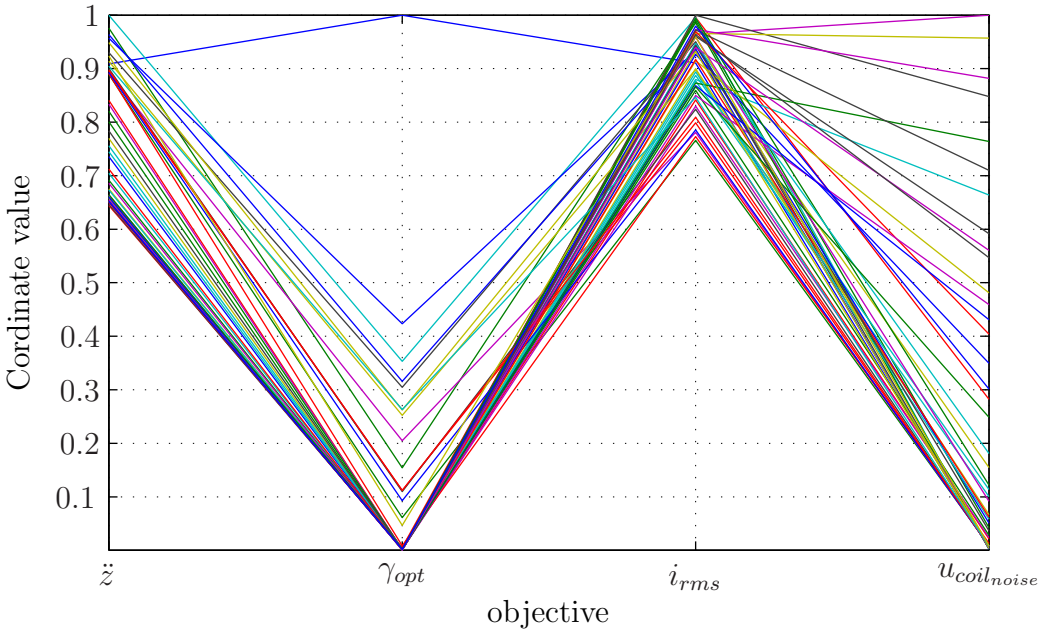

Figure 7.8: Parallel cord shows the trade-off between the objectives for sensor set with id:12

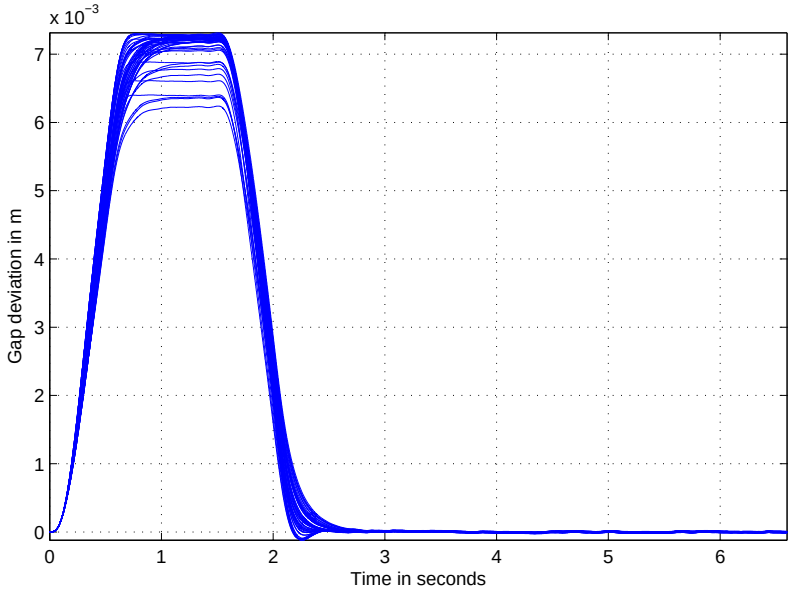

(a) Air gap deviation of the optimally tuned controllers with id:2

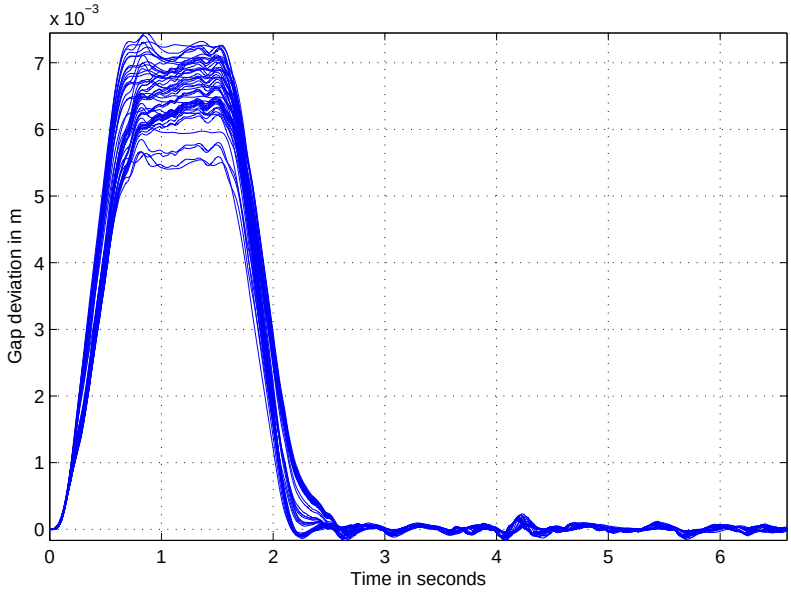

(b) Air gap deviation of the optimally tuned controllers with id:12

Figure 7.9: Air gap deviation of controllers with id:2 and id:12 at 200^{th} generation

Table 7.4: Optimised sensor configurations via multiobjective $\mathcal{H}_\infty$ robust control.

		Stochastic				Deterministic								
		g_{rms}	$u_{coil_{rms}}$	$\ddot{z}_{rms}$	i_{rms}	g_p	u_{coil_p}	t_s	e_{ss}	γ	$u_{noise_{rms}}$	Ω	f_{c_1}	f_{c_2}
id	Sensor set	mm	V	ms^{-2}	A	mm	V	s			V			
1	i	1.7	33.7	**0.71**	1.50	2.66	18.87	2.69	x	*645*	0.47	x	x	x
2	b	1.6	21.4	0.43	1.29	7.25	52.0	2.28	✓	0.89	2.07	✓	✓	✓
3	$(z_t - z)$	1.9	23.7	0.50	1.51	4.36	33.20	2.82	✓	*219*	0.51	✓	✓	x
4	$\ddot{z}$	1.3	77.8	0.44	1.06	5.42	39.5	2.35	✓	*1.44*	16.18	✓	✓	x
5	$i, \dot{z}$	1.8	19.9	0.39	1.38	6.98	49.97	2.14	✓	*1.24*	122.5	✓	✓	x
6	$i, \ddot{z}$	1.8	22.6	0.48	1.43	5.41	39.3	2.12	✓	*2.93*	1.4	✓	✓	x
7	$i, b, (z_t - z)$	1.8	20.3	0.41	1.39	6.53	47.1	2.14	✓	0.66	1.4	✓	✓	✓
8	$i, b, \ddot{z}$	1.6	23.6	0.48	1.29	6.93	49.4	2.30	✓	0.99	0.90	✓	✓	✓
9	$i, b, \dot{z}$	1.2	123.2	0.49	1.00	5.77	41.4	2.46	✓	0.10	10.67	✓	✓	✓
10	$i, (z_t - z), \dot{z}$	1.8	22.3	0.47	1.41	5.79	42.15	2.11	✓	0.95	34.3	✓	✓	✓
11	$i, b, (z_t - z), \dot{z}$	1.3	41.2	0.49	1.07	5.72	41.62	2.40	✓	*1.82*	21.9	✓	✓	x
12	$i, b, (z_t - z), \ddot{z}$	1.8	22.0	0.46	1.41	5.69	41.2	2.1	✓	0.44	1.4	✓	✓	✓
13	$i, b, (z_t - z), \dot{z}, \ddot{z}$	1.3	37.7	0.47	1.06	7.05	50.7	2.5	✓	0.40	19.0	✓	✓	✓

$g_p \equiv (z_t - z)_p$,$g_{rms} \equiv (z_t - z)_{rms}$

As it can be seen from the Ω column, only the current measurement (id:1) violates constraints. In fact, the ride quality is violated while none of f_{c_1} or f_{c_2} are satisfied. Actually, the γ value of id:1 is much higher than the others along with id:3. The remaining values are close to one. Moreover, the flux measurement (id:2) does satisfy all requirements like the id:7, id:8, id:9, id:10 and the full sensor set id:13. Sensor sets id:1, id:3, id:4, id:5, id:6 and id:11 do not satisfy the robustness margin but id:4, id:5, id:6, id:10 and id:11 can be used because γ is close to the required value ($\gamma < 1$).

In Id:9 there are three sensors that result to 123V driving signal for the stochastic response which means it requires more power with worse ride quality than the full id:13. Still, the id:4 (single measurement) can be used in order to achieve a better ride quality but with more input power and a slightly larger robustness margin ($\gamma = 1.44$).

7.3.1 Robustness to load variations and perturbed air gap

Robustness to load variations has been considered before in Section 5.5, page 91. The profile of the load variation is kept the same. It is considered that the operating mass of the vehicle increases by 25% of the total mass of the vehicle within $10s$. Two sensor sets are tested under such conditions. One is the closed-loop response with accelerometer (id:4) and the other includes more sensors i.e. current, flux density and acceleration (id:8). Figure 7.10 and Fig. 7.11 illustrate the closed-loop response to the deterministic and stochastic inputs to the suspension with id:4 and id:8 respectively. It can be seen that stability of the suspension (note that the non-linear model is used for the tests) is maintained in both cases while the performance is maintained within the required constraints except from the steady state error where in both cases is around $1mm$ but is not a problem for the suspension as it is working within the critical predefined constraints. Note here that the sensitivity to load variations with the flux density measurement is high. One can choose not to include the flux density in the selected sensor set like in this

section. However, the load variation could be accommodated by taking into account the disturbance in the design of the controller. Extra simulations should be included for load variation which may solve or at least limit the sensitivity to acceptable level while tuning for optimum performance with the expense of increasing computational complexity and overall time.

Robustness to perturbed operating point is considered next. Again this concept is described in Section 5.6 (page 98) therefore details are omitted here. The mass remains constant at $1000kg$ while the operating air gap is perturbed by $\pm 25\%$. As illustrated if Fig. 7.12 the stability as well as performance of the closed-loop response are maintained for both sensor sets id:4 and id:8. Stability and performance is maintained with stochastic input but not shown here.

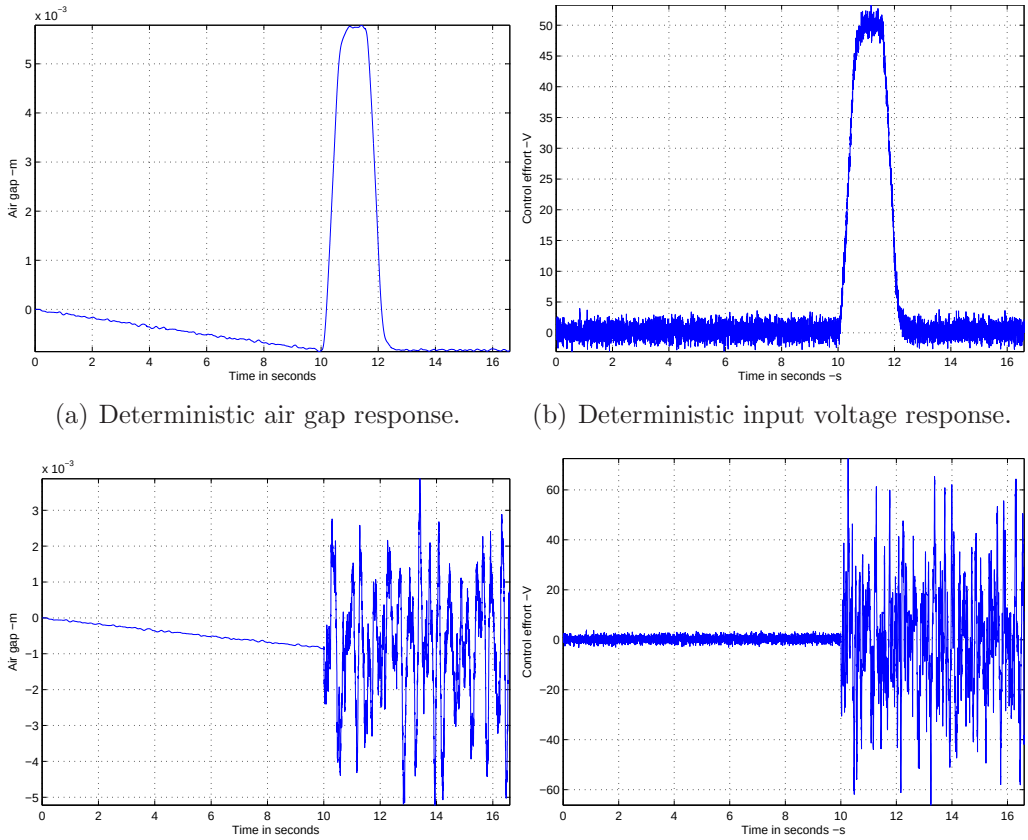

(a) Deterministic air gap response.

(b) Deterministic input voltage response.

(c) Stochastic air gap response.

(d) Stochastic input voltage response.

Figure 7.10: Closed-loop response to mass variation with id:4

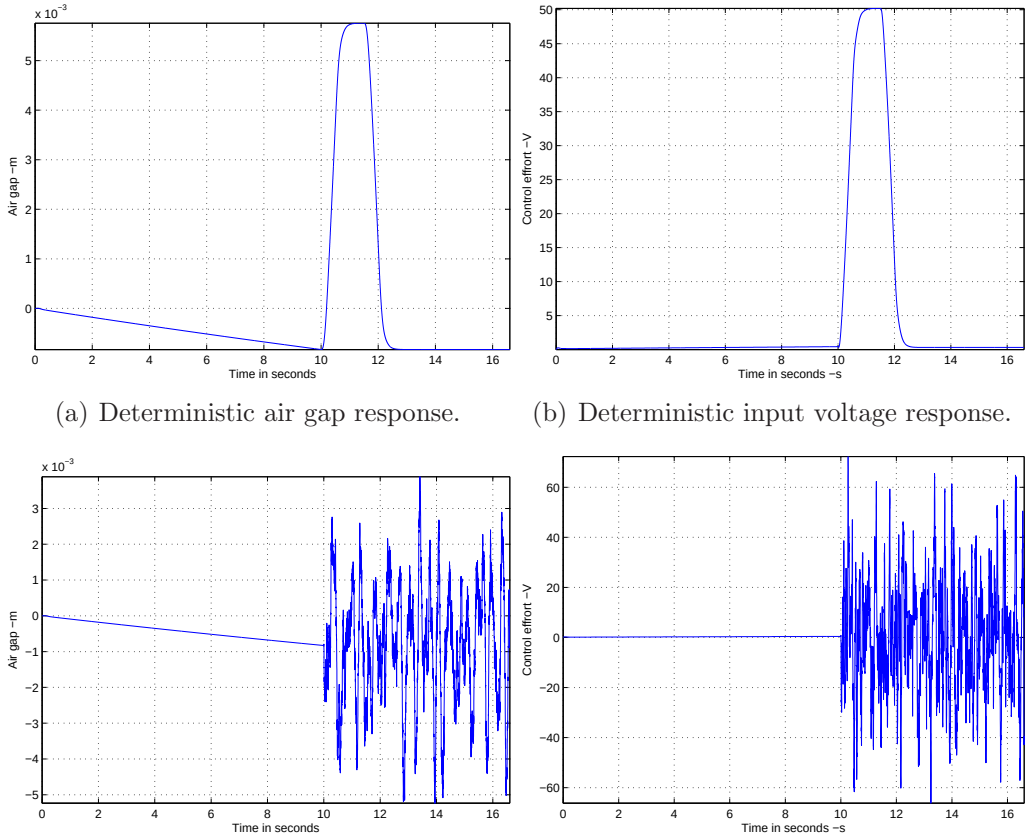

(a) Deterministic air gap response.

(b) Deterministic input voltage response.

(c) Stochastic air gap response.

(d) Stochastic input voltage response.

Figure 7.11: Closed-loop response to mass variation with id:8

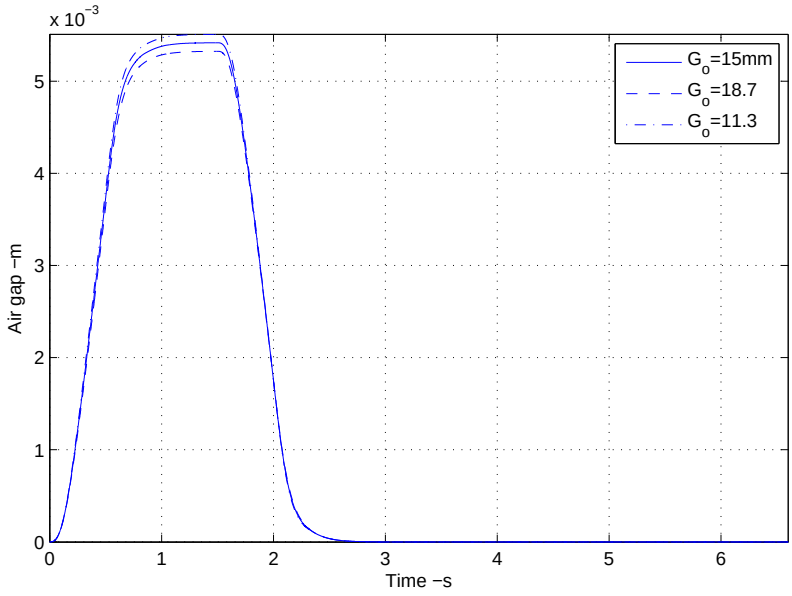

(a) Deterministic air gap responses with id:4.

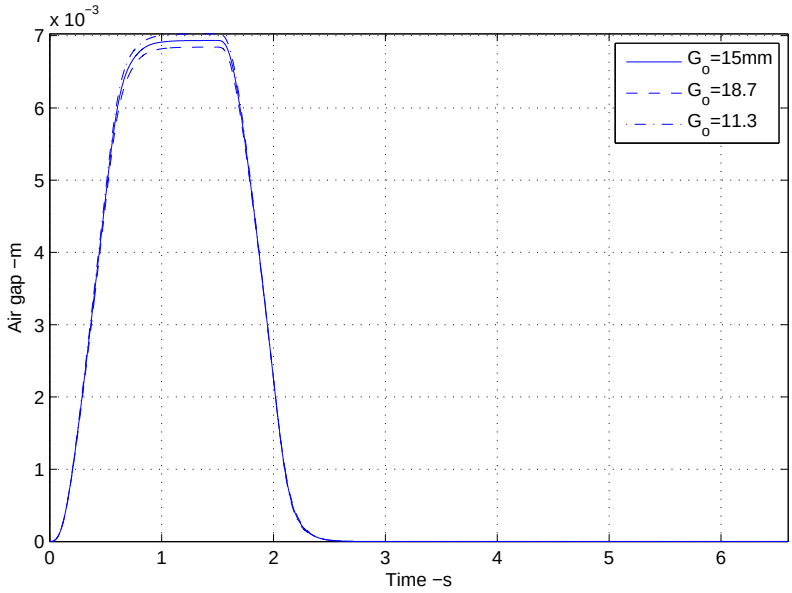

(b) Deterministic air gap responses with id:8.

Figure 7.12: Closed-loop responses to air gap operating point perturbation with id:4 and id:8

7.4 LSDP in the context of sensor optimisation

In this section, the sensor optimisation incorporates the robust controller design approach based on coprime-factor plant description introduced by McFarlane and Glover [1992] (LSDP). This approach also known as $\mathcal{H}_\infty$ loop-shaping, utilises $\mathcal{H}_\infty$ methods to provide robust stability in an open loop shaping design approach and achieve certain specifications for the closed loop system (in a similar fashion as in classical loop shaping problems). This section is published by Michail et al. [2008d] but without taking into account the non-linearities of the MAGLEV suspension during the optimal tuning. The detail MATLAB code is given in Appendix A.

7.4.1 $\mathcal{H}_\infty$ Loop shaping robust Control via Coprime factorisation method

In this section the preliminaries for the controller design via $\mathcal{H}_\infty$ Loop Shaping Robust-Control Design via Coprime factorisation method is described. The design of the controller is based on the normalised coprime-factor plant description developed by McFarlane and Glover [1992]. The nominal plant is factored as

$$G = M^{-1}(s)N(s), \tag{7.18}$$

where $M(s)$ and $N(s)$ are stable transfer functions representing the **L**eft **C**oprime **F**actorisation (LCF) of the nominal plant $G(s)$ (for more details the reader is suggested to refer to the book of Skogestad and Postlethwaite [2005]).

Typically, the LCF of the following is given as example.

$$G(s) = \frac{(s-a_1)(s+a_2)}{(s-b_1)(s+b_2)} \tag{7.19}$$

Note that $a_1, a_2, b_1, b_2 > 0$. To obtain a coprime factorisation make the

RHP-poles of $G(s)$ zeros of M and all the RHP-zeros of $G(s)$ zeros of N. Then allocate the poles of N and M so that are both proper and identify $G = M^{-1}(s)N(s)$ holds. Thus

$$N(s) = \frac{s - a_1}{s + b_2}, M(s) = \frac{s - b_1}{s + a_2} \tag{7.20}$$

is a coprime factorisation of $G(s)$.

Coprime factorisations are not unique but it is possible to make the factors $M(s)$ and $N(s)$ unique (i.e unique up to left multiplication by a unitary matrix), by forcing them to satisfy the normalisation equation

$$NN^* + MM^* = I \tag{7.21}$$

In this setting, the uncertain plant is described by the set:

$$G_\Delta = \{(M + \Delta_M)^{-1}(N + \Delta_N) : \|\Delta_M \ \Delta_N\|_\infty < \epsilon\} \tag{7.22}$$

where ϵ quantifies the 'size' of model uncertainty. The left and right coprime factorisations for the robust stability concept were first introduced by Vidyasagar [1985]. The robust-stabilisation problem associated with (7.22) is given as follows: *For a fixed ϵ, does there exist a feedback controller K(s) which internally stabilises the closed-loop system of Fig. 7.13 for all $G \in G_\Delta$?*. The corresponding maximum robust stabilisation problem is to *Find the largest $\epsilon = \epsilon_o$ so that the feedback loop of Fig. 7.13 is internally stable for all $G \in G_\Delta$, and the corresponding set of optimal controllers $K(s)$.*

Actually, when the normalisation condition is imposed on the coprime factors, the two aforementioned problems have rather simple solutions. In particular, the maximum stability radius (or stability margin) ϵ_o and the set of all optimal controllers can be obtained in closed form, i.e the iterative procedure (γ-iteration), which is used for the typical $\mathcal{H}_\infty$ is avoided. For the sensor optimisation, thousands of simulations may be required and therefore, for the time consumption point of view is very important that $\gamma - iterations$

is no longer required. In fact, the computational effort is much less than the sensor optimisation framework via the M.O. $\mathcal{H}_\infty$ robust control presented in the previous section.

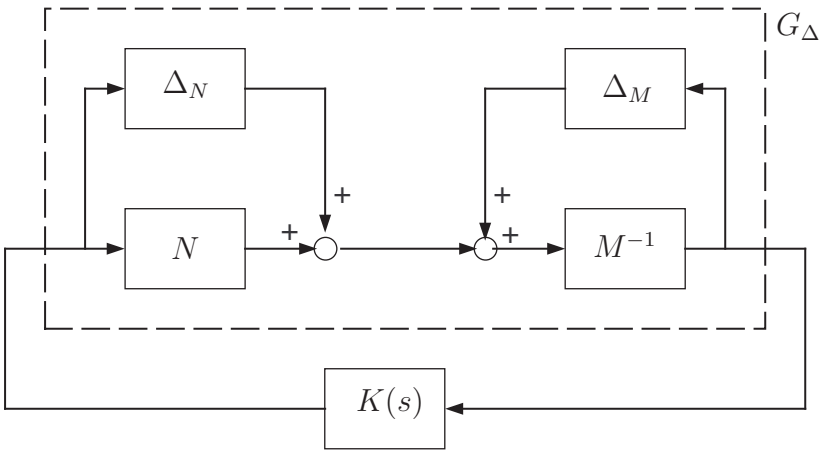

Figure 7.13: Coprime factor robust stabilisation problem (McFarlane and Glover [1992]).

The solution to the normalised coprime-factor robust stabilisation problem as described by McFarlane and Glover [1992] is summarised as follows

Theorem 7.4.1. (McFarlane & Glover [1992]): *Let $G(s)$ have a minimal state-space realisation (A,B,C,D) and let X and Y be the unique stabilising solutions to the generalised control and filtering algebraic Riccati equations,*

$$(A - BS^{-1}D^TC)^TX + X(A - BS^{-1}D^TC) - XBS^{-1}B^TX + C^TR^{-1}C = 0 \tag{7.23}$$

and

$$(A - BD^TR^{-1}C)Y + Y(A_BD^TR^{-1}C)^T - YC^TR^{-1}CY + BS^{-1}B^T = 0 \tag{7.24}$$

where $R = I + DD^T$ and $S = I + D^TD$. Define further the control gain matrix $F = -S^{-1}(D^TC + B^TX)$. Then:

1. *The maximum robust stability radius is given by $\epsilon_o = (1+\lambda_{max}(YX))^{-\frac{1}{2}}$;*

2. *For each $\epsilon < \epsilon_o$ the ϵ-suboptimal central controller has a state-space realisation:*

$$\left[\begin{array}{c|c} A_k & B_k \\ \hline C_k & D_k \end{array}\right] = \left[\begin{array}{c|c} A + BF + \epsilon^{-2} W_1^{-T} Y C^T (C + DF) & \epsilon^{-2} W_1^{-T} Y C^T \\ \hline B^T F & -D^T \end{array}\right]$$

where, $W_1 = I + (XY - \epsilon^{-2} I)$

The LSDP proceeds by shaping the open-loop characteristics of the plant by means of weight functions $W1(s)$ and $W2(s)$ (also known as pre- and post- compensators, respectively) as depicted in Fig. 7.14(a). The plant is temporarily redefined as $G_s(s) = W2(s) \times G(s) \times W1(s)$ and the controller $K(s)$ is designed via Theorem 7.4.1. Finally the weighting functions are absorbed into the finalised controller by defining $\hat{K}(s) = W1(s) \times K(s) \times W2(s)$, as illustrated in Fig. 7.14(b).

7.4.2 Sensor optimisation systematic framework via LSDP

The loop-shaping design procedure is integrated to the sensor optimisation process as depicted in Fig. 7.15. In order to shape the open-loop response weighting filters are used for every input/output. For the MAGLEV suspension model, one weighting filter is used for the input W_u and a weighting filter per sensor (up to five in total) for the outputs. In each randomly produced weights, a controller $K(s)$ is designed. After that, the weights and the controller are integrated forming the $\hat{K}_s$. This controller is used in combination with the non-linear model of the MAGLEV suspension to tune the closed-loop response using time history data from simulations. This is repeated for every randomly produced weighting filters from the NSGA-II in an attempt to optimise the performance.

For every feasible sensor set, the weighting filters are optimally tuned to achieve the optimum Pareto front between the objectives as illustrated in the flowchart in Fig. 7.5, page146. The sensor optimisation flow chart is the same as in sensor optimisation via the M.O. $\mathcal{H}_\infty$ robust control but in this

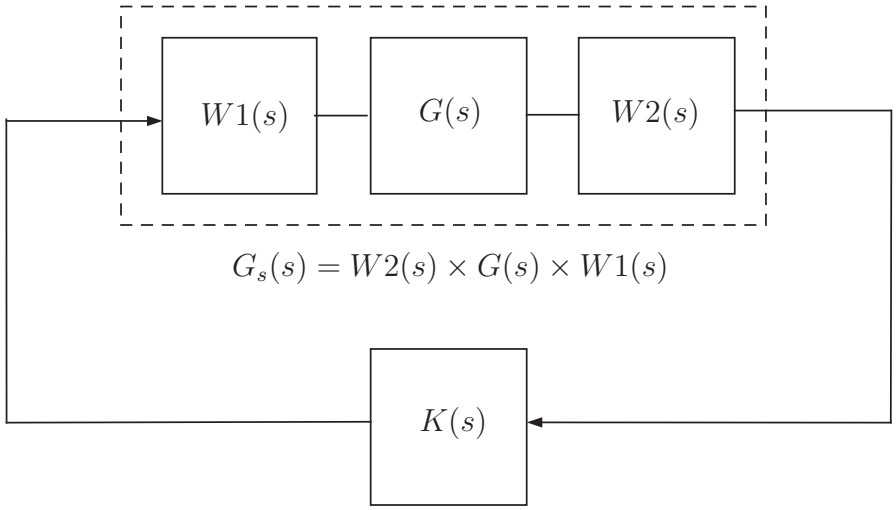

(a) Shape plant $G(s)$ using weighting filters.

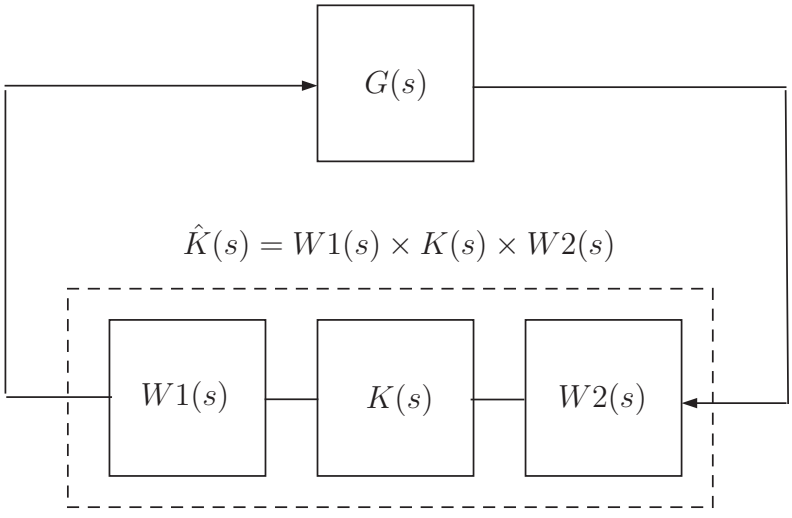

(b) Augment filters into $K(s)$.

Figure 7.14: Loop Shaping Design Procedure.

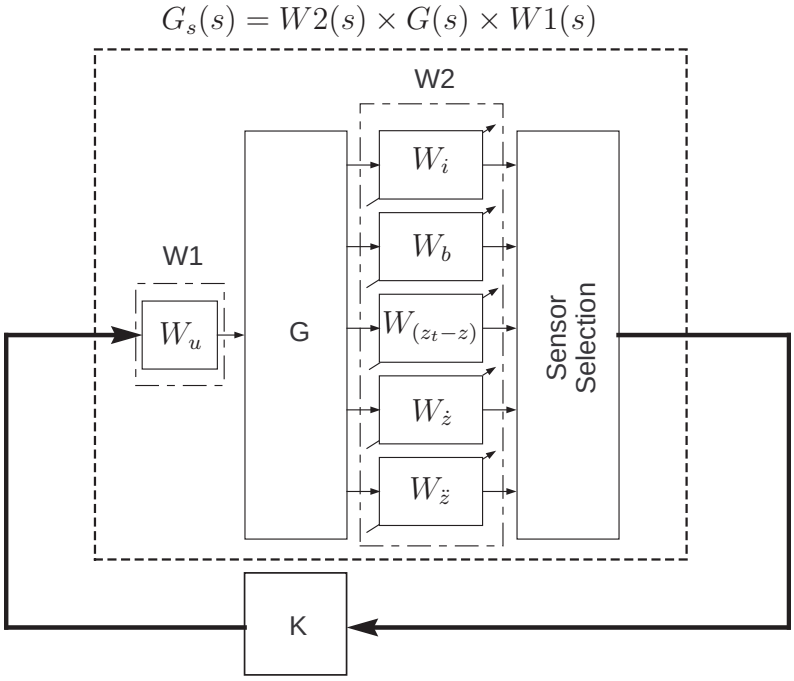

(a) Loop-Shaping of the plant.

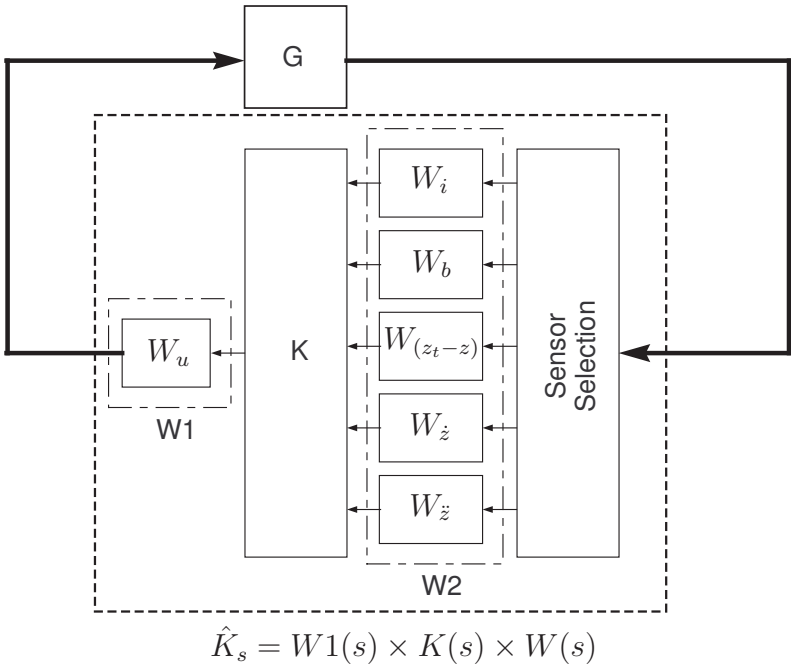

(b) Integrate weighting into controller $\hat{K}(s)$

Figure 7.15: Loop-shaping controller design into sensor optimisation framework.

case less sensor sets are feasible because the air gap measurement has to be a standard measurement. Table 7.5 tabulates all the feasible sensor sets that can be optimised via LSDP approach.

Table 7.5: Feasible sensor sets for the MAGLEV suspension with the sensor optimisation via loop-shaping controller design.

Number of measurements available	Number of feasible sensor sets
with 1 Sensor	1
with 2 Sensors	4
with 3 Sensors	6
with 4 Sensors	4
with 5 Sensors	1
Total	16

The post and pre compensators used for the MAGLEV are given as follows

$$W1 = W_u, \quad W2 = diag(W_i, W_b, W_{(z_t - z)}, W_{\dot{z}}, W_{\ddot{z}}) \tag{7.25}$$

For the pre-compensator (W1) a fixed unity gain is chosen (for simplicity). The weighting filters for the post-compensator(W2), $W_i, W_b, W_{\dot{z}}, W_{\ddot{z}}$ are assigned to variable scalar values as a first choice and in order to avoid weight complexity. However, for the air-gap $(z_t - z)$ a LP type filter is chosen of the form,

$$W_{(z_t - z)} = \left(\frac{\frac{s}{M_p^{1/n_p}} + \omega_p}{s + \omega_p A_w^{1/n_p}} \right)^{n_p} \tag{7.26}$$

This is a low pass filter (stable and linear transfer function) with the same structure and parameters defined in Section 7.3. There is no systematic approach to select the structure of the weighting functions. In this case, the problem may become very complicated if the weights are complex especially during the full sensor set optimum tuning. In this case, assuming a full sensor set for feedback with these simple structure of weights there are a maximum

of seven variables ($n_r = 7$). Since the number of variables change during the sensor optimisation process, some of the NSGA-II parameters change as well. In fact, the maximum generations are dynamically updated between 150-200 depending on the number of sensors used. With 1, 2 and 3 sensors the maximum generation is set to 150 ($Gen_{num} = 150$) while for 4 and 5 sensor sets, $Gen_{num} = 200$. Also, the population is set to $Pop_{num} = 50$ and the rest of the NSGA-II parameters remains unchanged (see Table 7.2). Although the LSDP does not require a $\gamma - iterative$ process, for more complex control systems this approach can become very complicated and time consuming depending on the number of feasible sensor sets and the weighting function structures. In order to improve efficiency of the algorithm dynamical updated of the maximum generations and population number are used. These depends on the type and the structure of the weighting functions as well as the number of feasible sensor sets.

The objective functions to be minimised are described in Section 7.2.4 and summarised as follows

$$\begin{aligned} \phi_1 = \gamma, \quad \phi_{s_2} = i_{rms}, \\ \phi_{s_3} = \ddot{z}_{rms}, \quad \phi_4 = u_{coil_{noise}} \end{aligned} \tag{7.27}$$

The design constraints of the MAGLEV suspension are described in Section 4.7 with the only difference that the vertical acceleration (from the stochastic response) constraint is relaxed to $1m/s^2$. The stability margin (ϵ) of 0.25 allows 25% coprime factor uncertainty see Skogestad and Postlethwaite [2005]. In this case an extra constraint is used which limits the stability margin to at least 0.15 or 15% coprime factor uncertainty ($\epsilon > 0.15$), note that $\gamma = \frac{1}{\epsilon}$. These limitations do not affect the final controller selection for the corresponding sensor set but they can allow controllers to 'survive' as the generations evolve so that they can be used in a sensor Fault Tolerant Control scheme. The design constraints are summarised on Table 7.6.

The final controller selection when the optimum Pareto front of controllers

Table 7.6: Suspension system constraints for the sensor optimisation via LSDP controller design.

	Constrains	Value
g_1	RMS acceleration, $(\ddot{z}_{rms})$	$\leq 1ms^{-2}$
g_2	RMS air-gap variation, $((z_t - z)_{rms})$	$\leq 5mm$
g_3	RMS input voltage,$u_{coil_{rms}}$,	$\leq 300V(3I_oR_o)$
g_4	Max air-gap deviation (det),$((z_t - z)_p)$	$\leq 7.5mm$
g_5	Max Input voltage (det),(u_p)	$\leq 300V(3I_oR_o)$
g_6	Settling time, (t_s)	$\leq 3s$
g_7	Stability margin, (ϵ)	≥ 0.15
h_1	Steady state, (e_{ss})	$= 0$

is recovered is selected via the user's controller selection criteria given as follows

1. Guarantee that the selected controller results to the restricted ride quality ($f_{c_1} \equiv \ddot{z}_{rms} < 0.5m/s^2$).

2. In this case, the LSDP shapes the open loop response of the suspension that results to a low bandwidth therefore the measurement noise is limited to low level but an extra criterion is introduced to limit the noise level to 10Vrms (RMS) ($f_{c_2} \equiv u_{coil_{noise}} < 10V$).

3. The third criterion is to select the controller that results to the highest robust stability margin. This allows the highest possible coprime uncertainties to be accommodated. i.e better robustness ($f_u \equiv max(\epsilon)$).

The controller selection criteria are summarised as follows

$$f_{c_1} \equiv \ddot{z}_{rms} < 0.5m/s^2, \quad f_{c_2} \equiv u_{coil_{noise}} < 10V, \quad f_u \equiv max(\epsilon) \quad (7.28)$$

The actual deterministic response as well as the stochastic response measurements are taken from time history of simulations using the non-linear model as explained in the previous chapter and depicted in Fig. 7.6, page 150. Of course the controller $K(s)$ is replaced by $\hat{K}(s)$ as explained in this section

(see Fig. 7.15).

When the sensor optimisation framework with LSDP is finished, 800 controllers are optimally tuned which is less than in the previous section since in this case 16 feasible sensors sets are available instead of 31 (The controller selection for each sensor set is described in Section 7.3). In this case the air gap measurement is standard there exist controllers for 11 out of 16 sensor sets that satisfy the performance requirements of the suspension. There are no controllers found to satisfy the constraints with single measurements and from the two measurement cases only one sensor set found to satisfy the constraints (id:4 on Table 7.7). Table 7.7 presents some randomly selected sensor sets after the sensor optimisation is completed. In the first column ($n[K(s)]_{\Omega_{k_i}=0}$) the number of controllers that satisfy all design constraint are given while in the second one ($n[K(s)]_{\Omega_{k_i}=0,f_{c_1},f_{c_2}}$) the number of controllers that satisfy the first two controller selection criteria (f_{c_1}, f_{c_2}) are given. It can be seen that id:4 has 49 controllers that satisfy all constraints while for the id:12 (full sensor set) 50 controllers have been found to satisfy the criteria. Moreover, 24 and 44 controllers found to satisfy the two aforementioned criteria for the id:4 and id:12 respectively.

The closed-loop air gap deviations for the deterministic inputs with id:4 and id:12 are presented in Fig. 7.16. All responses in both sensor sets id:4 (Fig. 7.16(a)) and id:12 (Fig. 7.16(b)), are within the required constraints. Particularly, it can be seen that the maximum air gap deviation is less than the predefined $7.5mm$ while the steady state error is zero and the settling time is less than $3s$. In general there is a number of controllers that are successfully tuned for optimum MAGLEV suspension performance using a variety of sensor sets.

In Fig. 7.17 the Pareto-optimality for two sensor sets is illustrated. The two cases where, the minimum number of sensors and the full sensor set is compared from the control point of view. Figure 7.17(a) shows the trade-off parallel cord between the objectives for id:4 while Fig. 7.17(b) shows the

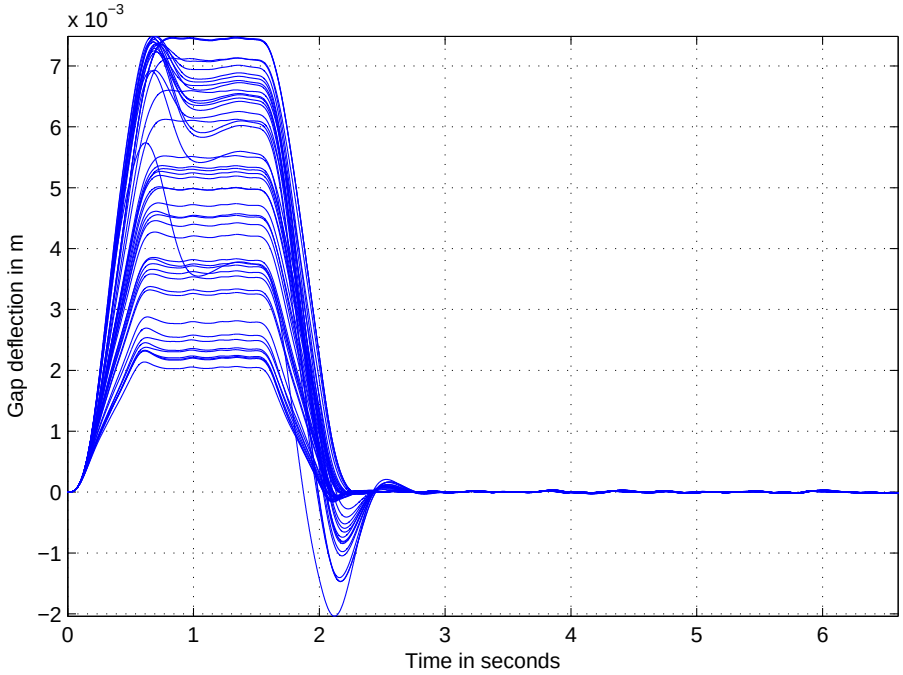

(a) Air gap deviation for id:4

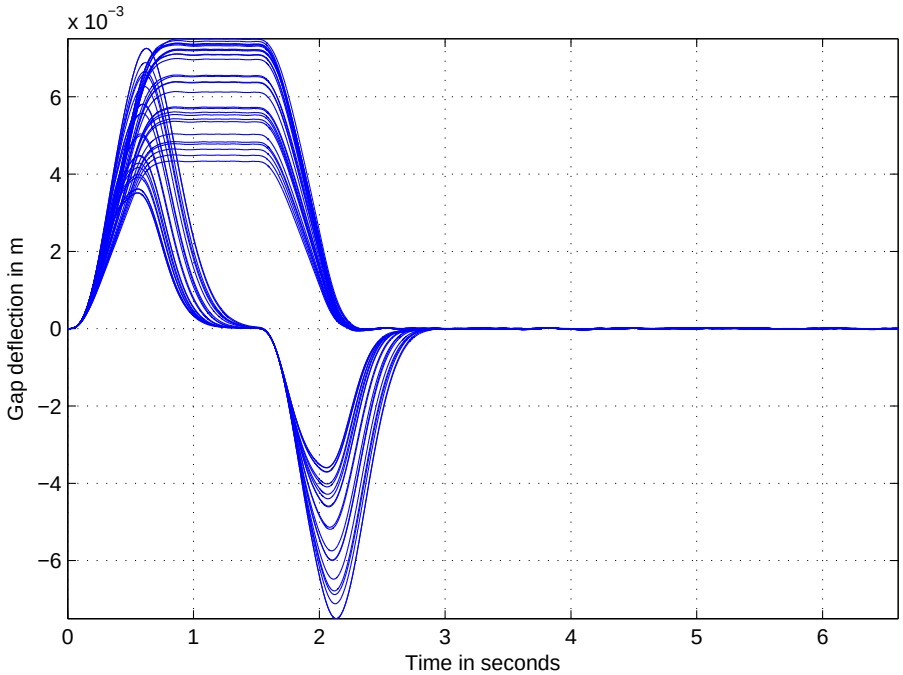

(b) Air gap deviation for id:12

Figure 7.16: Air gap deviation of controllers with id:4 and id:12

Table 7.7: Results for the sensor optimisation via LSDP controller design.

id	sensor set	$n[K(s)]_{\Omega_{k_j}=0}$	$n[K(s)]_{\Omega_{k_j}=0,f_{c1},f_{c2}}$
1	$(z_t - z)$	0	0
2	$i, (z_t - z)$	0	0
3	$b, (z_t - z)$	0	0
4	$(z_t - z), \ddot{z}$	49	25
5	$i, b, (z_t - z)$	44	24
6	$i, (z_t - z), \dot{z}$	0	0
7	$i, (z_t - z), \ddot{z}$	48	17
8	$b, (z_t - z), \ddot{z}$	48	19
9	$i, b, (z_t - z), \dot{z}$	50	26
10	$i, (z_t - z), \dot{z}, \ddot{z}$	49	17
11	$b, (z_t - z), \dot{z}, \ddot{z}$	48	20
12	i,b,$(z_t - z)$,$\dot{z}$,$\ddot{z}$	50	44

trade-off for the id:12. Note that the objective functions are normalised around 1.

The overall results from the sensor optimisation scheme are listed in Table 7.8. The results presents both deterministic and stochastic measurements for the corresponding desired closed-loop response with each sensor set where the air gap measurement is obligatory as mentioned before. Note that if for a sensor set all controllers violate the constraints then the controller that results to the smallest constraint violation is selected (see the flowchart depicted in Fig. 7.5), i.e. see sensor sets id:1, id:2, id:3 and id:6. Moreover, for these sensor sets there are either robustness and ride quality constraint violation or user's controller selection criterion is not satisfied. Nevertheless, these sensor sets can be used within a fault tolerant control scheme for sensor failures but towards the acceptance of graceful performance degradation rather than total cost of operation. Also, note that with id:7 the maximum noise level is 7.25Vrms which is fairly low and does not affect the MAGLEV suspension performance. The stability margin (ϵ) values shows that the robustness does not increase with more sensors in a set.

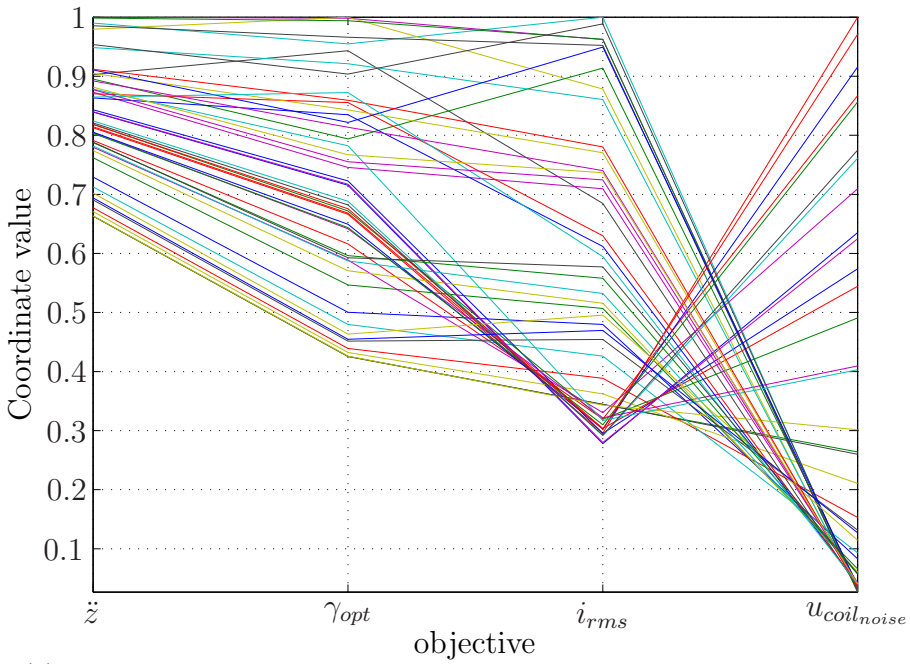

(a) Parallel cord shows the trade-off between the objectives for sensor set with id:4

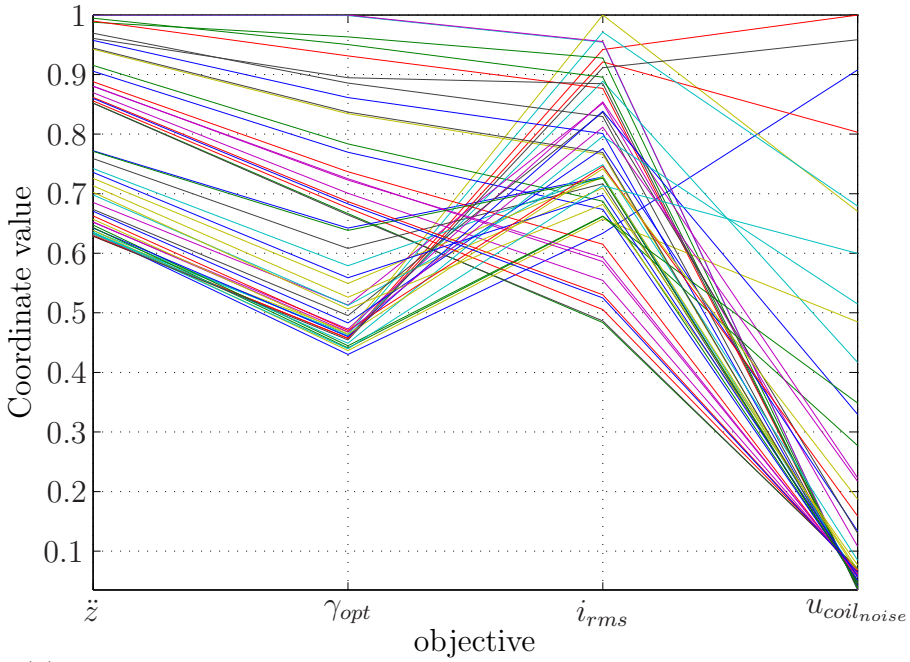

(b) Parallel cord shows the trade-off between the objectives for sensor set with id:12

Figure 7.17: Parallel cord shows the trade-off between the objectives for sensor set with id:4 and id:12

Table 7.8: Optimised sensor configurations via LSDP controller design.

		Stochastic				Deterministic								
		g_{rms}	$u_{coil_{rms}}$	$\ddot{z}_{rms}$	i_{rms}	g_p	u_{coil_p}	t_s	e_{ss}	ϵ	$u_{noise_{rms}}$	Ω	f_{c_1}	f_{c_2}
id	Sensor set	mm	V	ms^{-2}	A	mm	V	s			V			
1	$(z_t - z)$	1.83	48.6	*1.00*	1.69	1.32	12.4	2.2	✓	**0.14**	0.26	x	x	✓
2	$i, (z_t - z)$	1.95	61.3	**1.19**	1.86	0.81	5.2	2.3	✓	**0.09**	0.28	x	x	✓
3	$b, (z_t - z)$	1.82	48.7	*1.00*	1.69	1.32	12.4	2.2	✓	**0.14**	0.26	x	x	✓
4	$(z_t - z), \ddot{z}$	1.46	24.7	0.34	1.11	7.47	53.4	2.2	✓	0.35	1.70	✓	✓	✓
5	$i, b, (z_t - z)$	1.63	19.7	0.36	1.24	7.50	53.7	2.1	✓	0.25	0.66	✓	✓	✓
6	$i, (z_t - z), \dot{z}$	1.90	49.8	**1.06**	1.90	0.97	6.3	2.3	✓	**0.08**	0.26	x	x	✓
7	$i, (z_t - z), \ddot{z}$	1.36	42.6	0.33	1.04	7.29	52.3	2.2	✓	0.34	7.25	✓	✓	✓
8	$b, (z_t - z), \ddot{z}$	1.49	23.0	0.35	1.14	7.46	53.3	2.1	✓	0.33	0.86	✓	✓	✓
9	$i, b, (z_t - z), \dot{z}$	1.63	19.7	0.36	1.24	7.50	53.7	2.1	✓	0.25	0.66	✓	✓	✓
10	$i, (z_t - z), \dot{z}, \ddot{z}$	1.38	36.2	0.33	1.05	7.35	52.7	2.2	✓	0.33	4.73	✓	✓	✓
11	$b, (z_t - z), \dot{z}, \ddot{z}$	1.47	24.2	0.34	1.12	7.47	53.4	2.2	✓	0.34	1.11	✓	✓	✓
12	$i, b, (z_t - z), \dot{z}, \ddot{z}$	1.36	40.9	0.34	1.04	7.22	51.8	2.2	✓	0.34	6.28	✓	✓	✓

$g_p \equiv (z_t - z)_p$,$g_{rms} \equiv (z_t - z)_{rms}$

In fact, id:4 (2 sensors) results to similar robustness with id:12 (full sensor set). Also, the level of the noise on the control effort from the measurements is much less with id:4 while the ride quality as well as the input power is similar for both sensor id:4 and id:12 sets.

It is worth mentioning that although the weighting filters have very simple structure there exist many sensor sets that can satisfy all the design requirements. Using complex weighting structure may improve performance or recover more sensor sets that satisfy the performance requirements. However, complicated weight structures may increase computational time.

7.4.3 Robustness to load variations and perturbed operating point

Robustness to load variations has been considered before in Section 5.5 page 91. The profile of the load variation is kept the same. It is considered that the operating mass of the vehicle increases by 25% within $10s$ and then the suspension it tested under the disturbance track inputs for two sensor sets. One is the closed-loop response with air gap and acceleration (id:4) and the other includes more sensors i.e. current, air gap and acceleration (id:7). Figure 7.18 and Fig. 7.19 illustrate the closed-loop response to the deterministic and stochastic inputs to the suspension. It can be seen that stability of the suspension is maintained in both cases. The performance is maintained as well but in both cases a steady state error occurs. Particularly, with id:4 the steady state error is around $0.2mm$ while with id:7 the steady state error is around $2mm$, much higher than with id:4. Although, the load variation cannot be used as a disturbance to the design of the controller the concept may included in the sensor optimisation framework in an attempt to optimise the performance under the fully laden conditions. However, this increases computational time because extra simulations are necessary to optimally tune the time domain responses for the load variation conditions.

Robustness to perturbed operating point is considered next. Again this

concept is described in details in Section 5.6, page 98 therefore are omitted here. The mass remains constant while the operating air gap is perturbed by ±25%. As illustrated in Fig. 7.20 the stability as well as performance of the closed-loop response is maintained for both sensor sets id:4 and id:7. Stability and performance is maintained with stochastic input but not shown here.

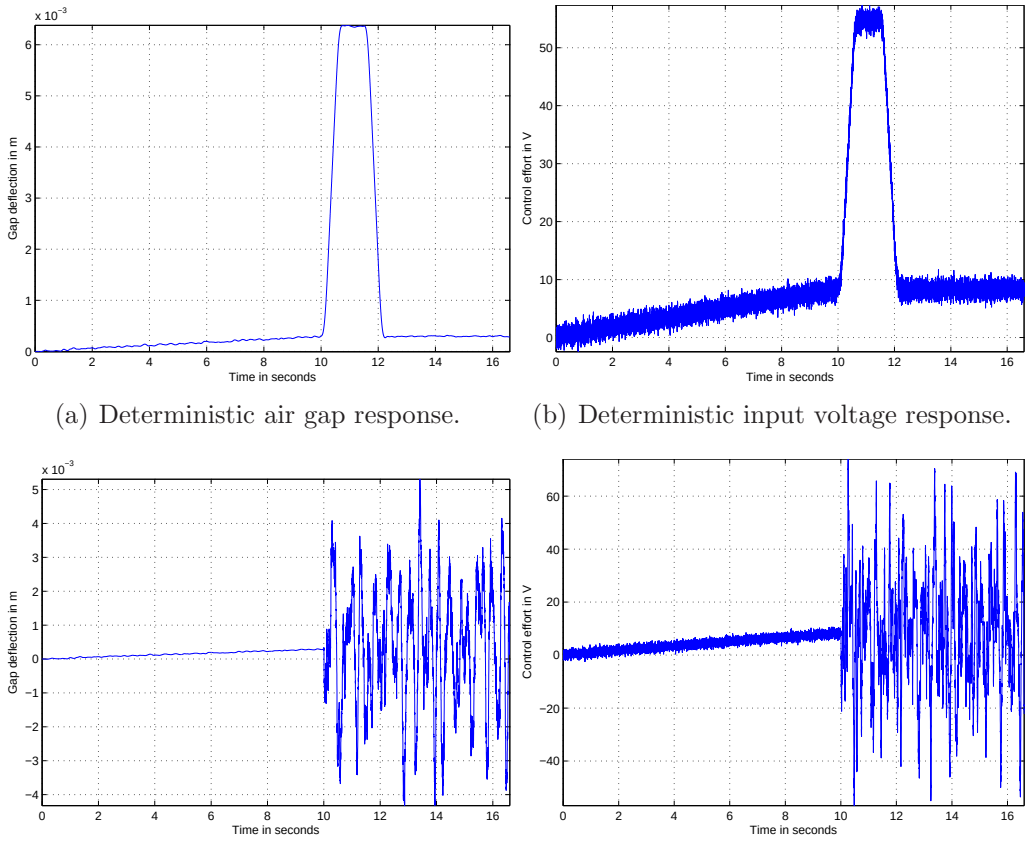

(a) Deterministic air gap response.

(b) Deterministic input voltage response.

(c) Stochastic air gap response.

(d) Stochastic input voltage response.

Figure 7.18: Closed-loop response to mass variation with id:4

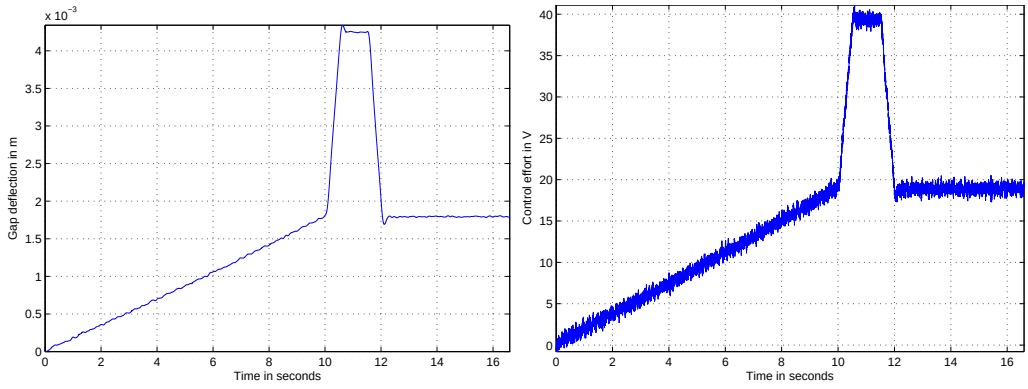

(a) Deterministic air gap response.

(b) Deterministic input voltage response.

(c) Stochastic air gap response.

(d) Stochastic input voltage response.

Figure 7.19: Closed-loop response to mass variation with id:7

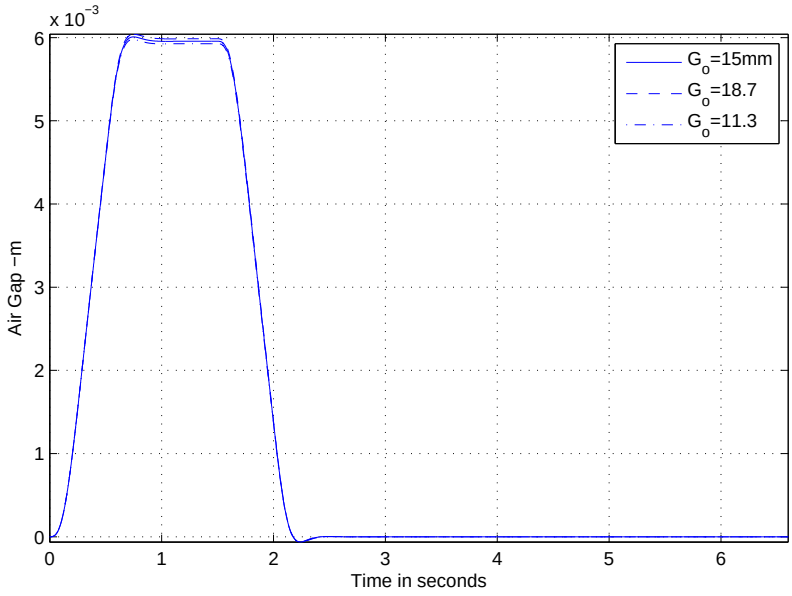

(a) Deterministic air gap responses with id:4.

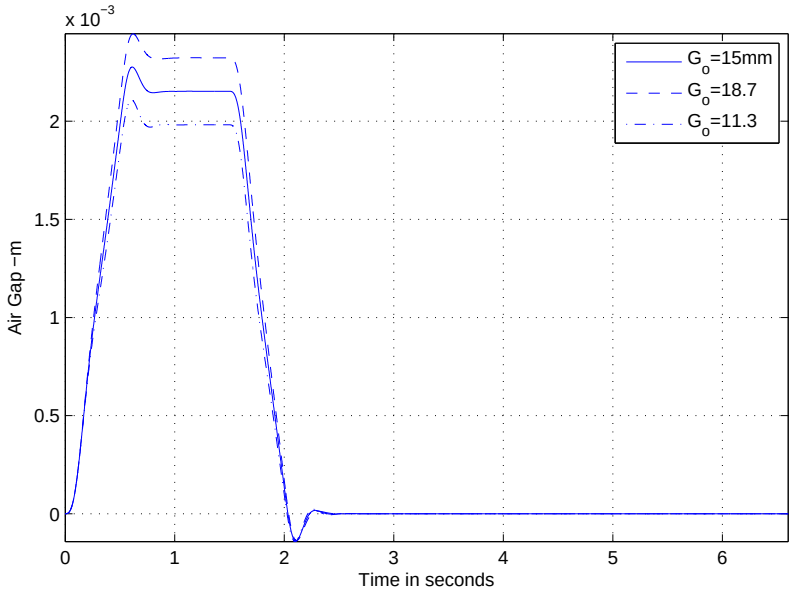

(b) Deterministic air gap responses with id:7.

Figure 7.20: Closed-loop responses to air gap operating point perturbation with id:4 and id:7

7.5 Remarks on the sensor optimisation systematic framework

The time consumption and computational complexity is an important issue in multiobjective constraint optimisation using genetic algorithms since a large number of simulations are required for a sensor optimisation framework to be completed. For example, if 500 generations and 50 chromosomes and assuming that 3 simulations have to run for every randomly designed controller a sensor set may require 75000 simulations to complete the optimisation. To complete a sensor optimisation framework with 31 sensor sets about 2,3 million simulations are required. The completion time for a sensor optimisation framework is a function of a lot of parameters including the type of the genetic algorithm to be used, the maximum number of generations, the population number, the number of feasible sensor sets the control strategy used and the available computational power. For the simulation in this thesis an ordinary personal computer is used with MATLAB v7.4 but without the java tool facilities (i.e the task is completed much faster if neither JAVA or display outputs are used). The computer characteristics are: $2.13GHz$ dual intel processor with 4GB DDR memory.

The overall time for each optimisation framework is given in Table 7.9. The sensor optimisation framework using multiobjective $\mathcal{H}_\infty$ control requires 175 hours to be completed which is triple the time than the other two control strategies (LQG,LSDP). The sensor optimisation via LSDP and LQG requires 42 and 54 hours respectively but in the first case only 16 feasible sensor sets are available. From this point of view it can be said that for the specific problem, the sensor optimisation via LQG requires less computational effort than the other two methods. Nevertheless, these results change for different dynamic models that may require different problem formulation (i.e different weighting filters, NSGA-II parameters etc).

Moreover, the number of sensor sets that satisfy all performance requirements (i.e satisfy the overall constraint violation) using each approach is

shown in the fourth column. Although using the LQG approach requires the least computational effort it was found that 24/31 sensor sets satisfy the constraints while the multiobjective $\mathcal{H}_\infty$ robust control approach has 29/31 sensor sets that were found to satisfy the constraints. The LSDP approach requires the air gap measurement as a standard measurement and therefore 16 sensor sets are feasible while among them 11 sensor sets found to satisfy all the constraints.

Furthermore, if the control of the MAGLEV suspension is done with the minimum number of sensors then single measurements can be used (in a fault-free environment). From the sensor optimisation framework using LQG single measurements are enough. In fact, the flux density or the vertical acceleration shows that are able to achieve the constraint requirements. Similarly, using $\mathcal{H}_\infty$-multiobjective control either flux density or acceleration or air gap are able to satisfy the design constraints. For the sensor optimisation framework using the LSDP approach 2 sensors are the minimum that can be used for control. Actually, the air gap and vertical acceleration measurements can be used in order to satisfactorily control the MAGLEV suspension within constraints.

Table 7.9: Remarks on the systematic framework via modern control strategies.

Sensor Optimisation approach	Number of Feasible sensor sets	Required time (hrs)	Sensor sets that satisfy Ω
LQG	31	54	24
M.O $\mathcal{H}_\infty$	31	175	29
LSDP	16	42	11

7.6 Summary

The optimised sensor configurations for control systematic frameworks via $\mathcal{H}_\infty$ robust control methods have been presented. Two approaches have been studied. One is the $\mathcal{H}_\infty$-multiobjective controller deign and the other is the $\mathcal{H}_\infty$ loop shaping design. Although two different approaches were studied the sensor optimisation algorithms have the same flow chart as depicted in Fig. 7.5 with some modifications in the MATLAB code. Both approaches found sensor sets satisfying the required performance using different sensor sets. From the comparison it was found that although the $\mathcal{H}_\infty$-multiobjective approach had 29 sensor sets that satisfy the required performance, computational effort (175 hours) is required. The LSDP requires 42 hours but less feasible sensor sets are available and only 11 sensor sets were found to satisfy the required performance. Compared with the LSDP, the LQG approach requires 54 hours but 24 sensor sets have found to satisfy the performance requirements (out of 31 feasible sensor sets). Moreover, from the control point of view if the minimum number of sensors is to be used, the LQG and $\mathcal{H}_\infty$-multiobjective approaches are acceptable with single measurements, the flux density and vertical acceleration for LQG and the flux density for the $\mathcal{H}_\infty$-multiobjective approach. In the latter case the vertical acceleration does not satisfy the user's controller selection criteria but the overall constraint violation is satisfied and therefore it could be used for different controller selection criteria or within a FTC scheme. The sensor optimisation via M.O. $\mathcal{H}_\infty$ robust control is found to be simpler because standard regulated variables are to be tuned in contrast with the LSDP which can become very complex since one weight function is necessary for each measurement for the open loop shaping. Nevertheless, it was found that most of feasible sensor sets found to satisfy the required performance even with simple weighting functions. In the next chapter the optimised sensor configurations concept is extended towards the fault tolerant control area aiming to reduce the sensor hardware redundancy while ensuring optimum performance under all possible sensor fault conditions.

Chapter 8

Optimised Sensor Configurations for Fault Tolerant Control

8.1 Introduction

This chapter introduces sensor selection for fault tolerant control aiming to minimise the sensor hardware redundancy. Active fault tolerant control is often used for safety-critical systems. Active FTC involves controller reconfiguration by detecting and isolating possible faults (see Blanke et al. [2003]). The methodology mainly concentrates on the utilisation of classical control, and analytical redundancy (see Patton [1997a]). Particularly, the measured air gap signal in combination with the estimated and the calculated air gap signals provide air gap sensor fault tolerance by masking the air gap sensor fault. This method is for single sensor fault while for multiple sensor faults the optimised sensor configurations are taken into account. Particularly, the optimised sensor configurations via LQG are considered for multiple sensor faults. For safety-critical system a number of sensors is usually required and assessing the scheme under such failures is important. In the context of this thesis aims to minimise the number of required sensor with controller reconfiguration subject to possible sensor faults.

8.2 Fault Tolerant Control for air gap sensor failure

In this section a method to recover the performance of the MAGLEV suspension in case of a faulty air gap measurement (being a critical measurement) is presented. The technique uses a combination of the measured, estimated and analytically calculated air gap signals in order to recover the performance in case of an air gap sensor failure. When the air gap sensor fails the air gap signal is recovered using the estimated and the calculated air gap signals. This concept is referred to as *sensor fault masking* (see Wu et al. [2006]) and the diagram on Fig. 8.1 illustrates the process. The main part of this work has been published in Michail et al. [2009c] (see Appendix E). Three outputs are necessary for the sensor fault tolerance: the air gap (G), the flux (B) and the current (I). Note that the scheme is implemented on the nonlinear model, with appropriate variations around the operating point (i.e i,b,$(z_t - z)$) included for proper simulation (because of the linear nature of the controller).

In order to detect a fault at the air gap measurement three air gap signals are compared: the measured air gap $(z_t - z)_{mea}$, the estimated air gap $(z_t - z)_{est}$ and the calculated air gap $(z_t - z)_{calc}$. The latter is calculated from 8.1 (as firstly noted by Goodall [1989]).

$$(z_t - z)_{calc} = K_b \frac{I}{B} - G_o \tag{8.1}$$

Fault detection and isolation is very important where active fault tolerance is implemented (Patton [1997b]). The Fault Detection and Isolation mechanism illustrated in Fig. 8.2 assesses the residuals (i.e $r_{(z_t-z)_{mea,est}}$, $r_{(z_t-z)_{mea,cal}}$ and $r_{(z_t-z)_{est,cal}}$) derived from the comparison between the three measurements (see Blanke et al. [2003]). The residuals indicate if the actual air gap measurement is either healthy or faulty by comparison to the corresponding thresholds.

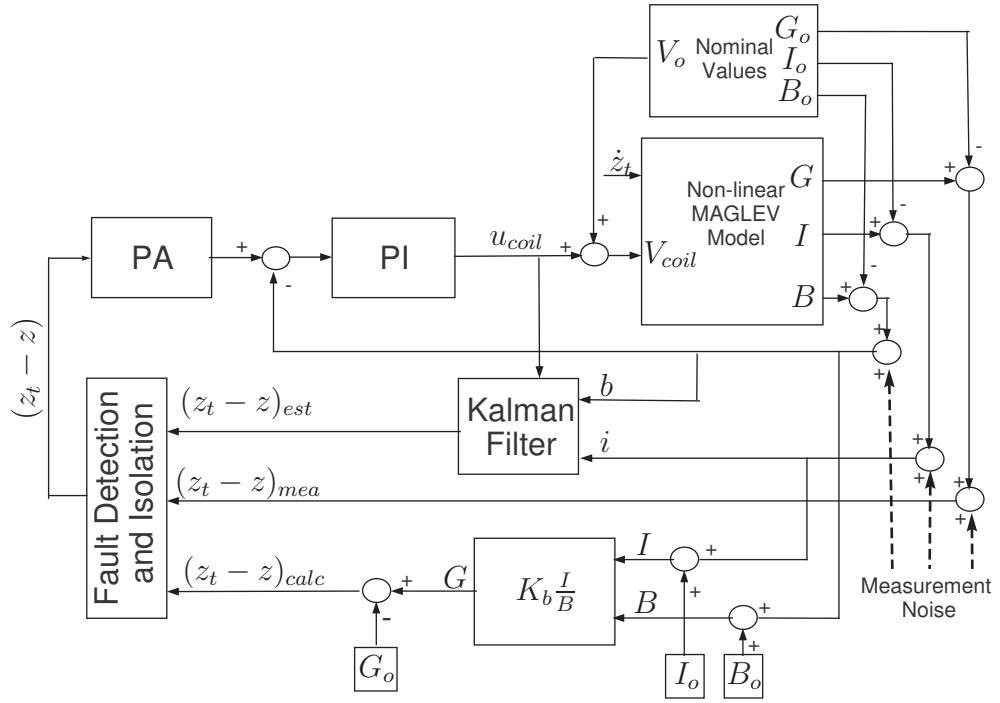

Figure 8.1: Fault tolerant control scheme for the accommodation of the suspension's air gap sensor failure.

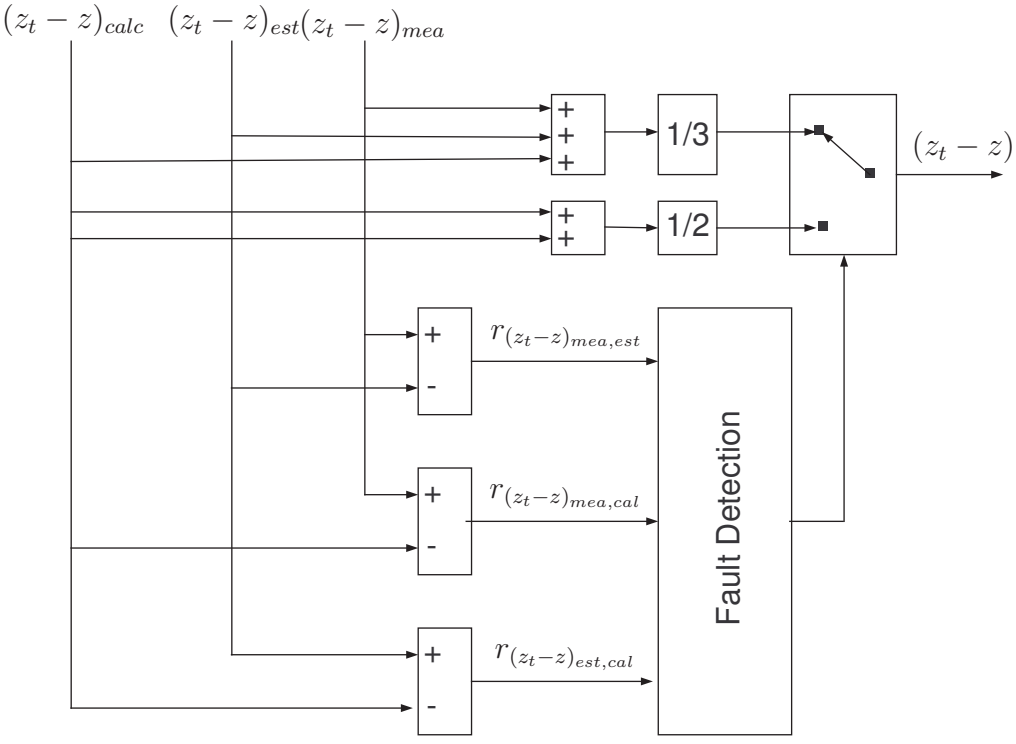

Figure 8.2: Diagram of the Fault Detection and Isolation mechanism.

In a healthy situation the air gap signal $(z_t - z)$ that is fed to the PA controller is given by

$$(z_t - z) = \left[(z_t - z)_{mea} + (z_t - z)_{est} + (z_t - z)_{calc}\right]/3 \tag{8.2}$$

When the air gap measurement is faulty, the FDI mechanism detects and isolates the faulty sensor and the air gap signal $(z_t - z)$ is given by

$$(z_t - z) = \left[(z_t - z)_{calc} + (z_t - z)_{est}\right]/2 \tag{8.3}$$

In this way the faulty air gap measurement is masked. In fact, the method is partitioned in two stages. The first stage relates to optimising the classical control strategy via NSGA-II, while the second stage concerns the tuning of the Kalman filter to estimate the air gap signal using current and flux information. The MATLAB code is given in AppendixA.

8.2.1 Classical controller with inner loop design

In order to achieve fault-free performance a similar scheme to the one illustrated in Fig. 8.1 is used. Particularly, only the measured air gap $((z_t - z)_{mea})$ and flux (b) are fed to the controllers. The classical controller optimisation approach using the air gap/flux sensors is described in details in Section 5.2. The optimisation with the given objective functions and constraints in the same section results to the optimum Pareto front of controllers depicted in Fig. 8.3.

From the Pareto optimum front of controllers the controller pair which results to the best ride quality $(0.26m/s^2)$ is selected as described in Chapter 5 and repeated here

$$PA = 3.92\frac{0.1519s+1}{0.0387s+1} \quad PI = 1.0949e4\frac{0.018s+1}{0.018s} \tag{8.4}$$

The corresponding closed-loop response for the deterministic and the stochastic track profiles are illustrated in Fig. 8.4 and Fig. 8.5 respectively.

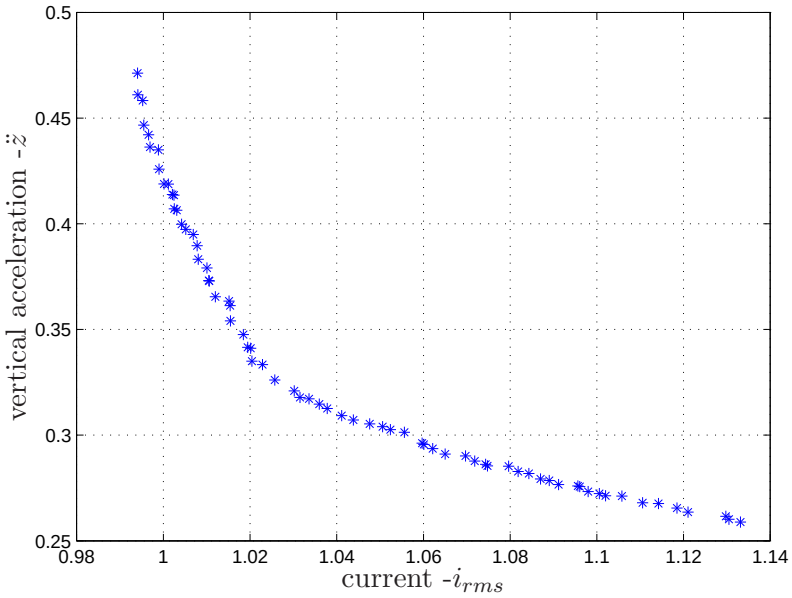

Figure 8.3: Pareto front of controllers using NSGA-II.

The actual response measurements for the air gap signal and the input voltage are successfully working within working boundaries for both deterministic and stochastic track profiles (Again this has been investigated in Section 5.2).

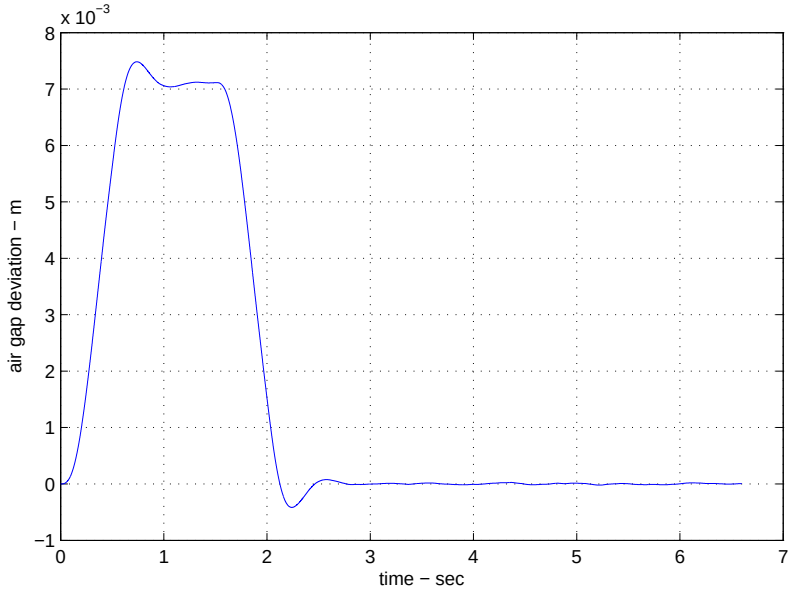

(a) Air gap deviation $(z_t - z)_{mea}$.

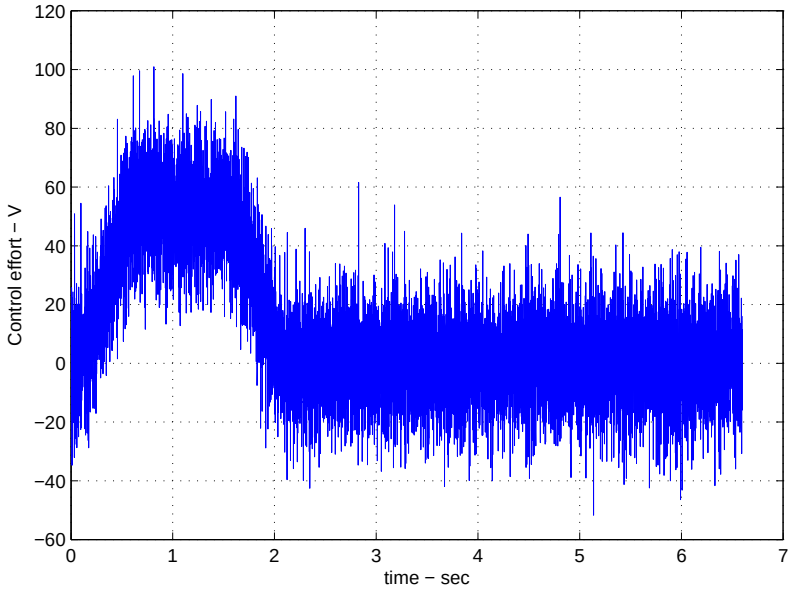

(b) Input voltage (u_{coil}).

Figure 8.4: Air gap and input voltage responses to deterministic track profile.

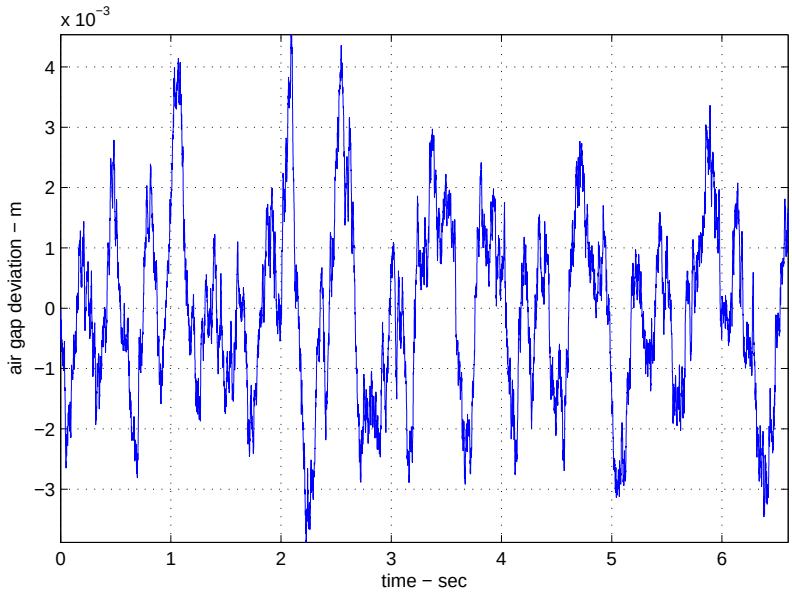

(a) Air gap $(z_t - z)_{mea}$.

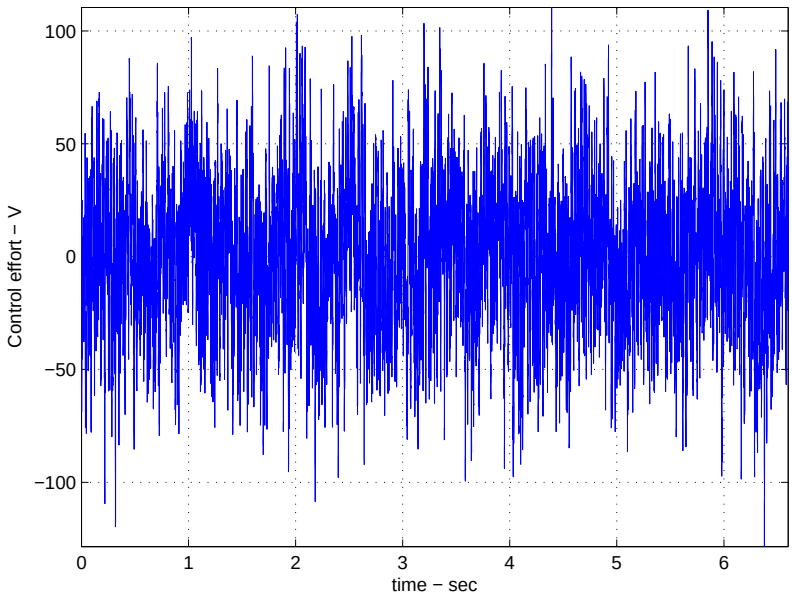

(b) Input voltage (u_{coil})

Figure 8.5: Air gap and input voltage responses to stochastic track profile.

8.2.2 Kalman estimator tuning

The air gap measurement is merged as a state in the linearised model of the MAGLEV suspension thus the Kalman estimator may be used to estimate it. Preliminary information for Kalman filters are described in Section 6.2.3.

The Kalman filter has the structure of an ordinary state-estimator with the state equation being

$$\dot{\hat{x}} = A\hat{x} + Bu + K_{LQG}(y - C\hat{x}) \tag{8.5}$$

where the state space matrices are given from (8.6) and (8.7) as described in Section 4.4 and repeated here for completeness.

$$\begin{bmatrix} \frac{di}{dt} \\ \frac{d^2z}{dt^2} \\ \frac{d(z_t-z)}{dt} \end{bmatrix} = \begin{bmatrix} -\frac{R_c}{L_c+\frac{K_bN_cA_p}{G_o}} & -\frac{K_bN_cA_pI_o}{G_o^2\left(L_c+\frac{K_bN_cA_p}{G_o}\right)} & 0 \\ -2K_f\frac{I_o}{M_sG_o^2} & 0 & 2K_f\frac{I_o^2}{M_sG_o^3} \\ 0 & -1 & 0 \end{bmatrix} \begin{bmatrix} i \\ \frac{dz}{dt} \\ (z_t - z) \end{bmatrix} + \begin{bmatrix} \frac{1}{L_c+\frac{K_bN_cA_p}{G_o}} \\ 0 \\ 0 \end{bmatrix} u + \begin{bmatrix} \frac{K_bN_cA_pI_o}{G_o^2\left(L_c+\frac{K_bN_cA_p}{G_o}\right)} \\ 0 \\ 1 \end{bmatrix} \frac{dz_t}{dt} \tag{8.6}$$

$$\begin{bmatrix} i \\ b \\ (z_t - z) \\ \dot{z} \\ \ddot{z} \end{bmatrix} = \begin{bmatrix} 1 & 0 & 0 \\ \frac{K_b}{G_o} & 0 & -\frac{K_bI_o}{G_o^2} \\ 0 & 0 & 1 \\ 0 & 1 & 0 \\ -2K_f\frac{I_o}{M_sG_o^2} & 0 & 2K_f\frac{I_o^2}{M_sG_o^3} \end{bmatrix} \begin{bmatrix} i \\ \frac{dz}{dt} \\ (z_t - z) \end{bmatrix} + \begin{bmatrix} 0 & 0 \\ 0 & 0 \\ 0 & 0 \\ 0 & 0 \\ 0 & 0 \end{bmatrix} \begin{bmatrix} u_{coil} \\ \frac{dz_t}{dt} \end{bmatrix} \tag{8.7}$$

The optimal choice of K_{LQG} via W and V minimises $E\{[x - \hat{x}]^T[x - \hat{x}]\}$ (Skogestad and Postlethwaite [2005]). The optimum choice of W and V eventually controls the precision of the state estimation and therefore the

evolutionary algorithm is used to tune the Kalman filter in order to give the same estimated air-gap as the actual measurement for both deterministic and stochastic responses.

The noise covariance matrix V is selected to be, diagonal 2×2 matrix with values of the noise covariance for the current and flux measurements, i.e $V = diag(V_i, V_b)$ (V_i and V_b are taken as the square of 1% of the maximum value for the deterministic response). The W matrix is given as $W = diag(W_i, W_{\dot{z}}, W_{(z_t - z)})$ where W is a 3×3 process noise matrix directly affect each state ($B_w = 3 \times 3$).

Two objectives are selected for the Kalman tuning i.e to tune the Kalman filter presented in (8.5) the Integral Absolute Error between the actual and the estimated ar gaps signals for both deterministic and stochastic responses is used as shown in (8.8). Although the Kalman filter is stable by default it was important to take the appropriate time domain signal comparison for the performance test.

$$\begin{aligned} \phi_d &= \int_0^t |(z_t - z)_{mea} - (z_t - z)_{est}| dt \\ \phi_s &= \int_0^t |(z_t - z)_{mea} - (z_t - z)_{est}| dt \end{aligned} \tag{8.8}$$

Recall that ϕ_d and ϕ_s are the objective functions from deterministic and stochastic responses respectively. In this case, it is important to have a good precision for the estimated air-gap therefore two constraints are assigned so that the precision is better than 5% ($\leq 5\%$). One for the deterministic (g_d) and the one for the stochastic responses (g_s).

$$\begin{aligned} g_d &= \int |(z_t - z)_{mea} - (z_t - z)_{est}| dt \leq 0.05 \\ g_s &= \int |(z_t - z)_{mea} - (z_t - z)_{est}| dt \leq 0.05 \end{aligned} \tag{8.9}$$

The parameters for the NSGA-II are listed on Table 8.1. In order to reduce the computational effort, the chromosome population is set to $Pop_{num} = 50$ and the maximum generations to $Gen_{num} = 100$. Using the proposed optimisation method, the controllers are successfully tuned and the next stage is to illustrate that the Kalman filter is also able to estimate the

air gap signal using only the current (i) and the flux (b) measurement(Both in the deterministic and stochastic approach).

Table 8.1: NSGA-II parameters for Kalman estimator tuning

NSGA-II Parameter	Value
Maximum generation	100
Population size	50
Crossover probability	1/3
Mutation probability	0.2

In Fig. 8.6 the residuals from the deterministic response are illustrated. Figure 8.6(b) shows the residual between the measured and the estimated ($r_{(z_t-z)_{mea,est}}$), Fig. 8.6(a) shows the residual from the measured and calculated ($r_{(z_t-z)_{mea,calc}}$) and Fig. 8.6(c) shows the residual from the estimated and calculated air gap signals ($r_{(z_t-z)_{est,calc}}$) under the deterministic response test. The residuals obtained using stochastic track inputs have low amplitude as well but they are not illustrated here. In both cases the errors are small and therefore they can be used for the fault detection and isolation mechanism.

The next step is to inject a fault in the actual air gap measurement and observe the results. The fault scenario is that the actual air gap measurement sensor suddenly develops fault at $t = 1s$ and the output varies around zero in the form of a undesired coloured noise disturbance. The three air gap signals with the measured air gap signal which fails at $t = 1s$ are depicted in Fig. 8.7. Figure 8.8 shows the difference between the actual air gap with no fault and with faulty air gap measurement for the deterministic input to the MAGLEV suspension. It can be seen, the performance of the suspension is successfully recovered with the actual air gap been fully recovered. The same test has been performed with stochastic inputs as illustrated in Fig. 8.9 and the performance of the suspension has been recovered as seen from Fig. 8.10.

A few remarks on this approach are given next. Although the methodol-

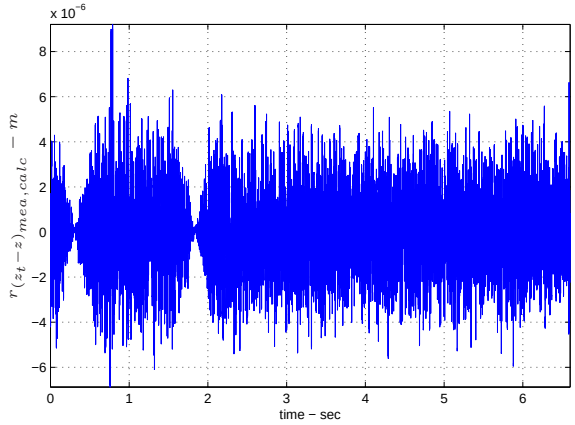

(a) Residual from measured and calculated air gap signals ($r_{(z_t-z)_{mea,calc}}$).

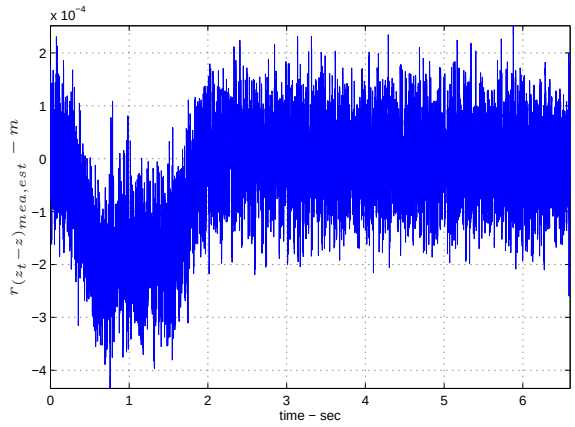

(b) Residual from the measured and the estimated air gap signals ($r_{(z_t-z)_{mea,est}}$).

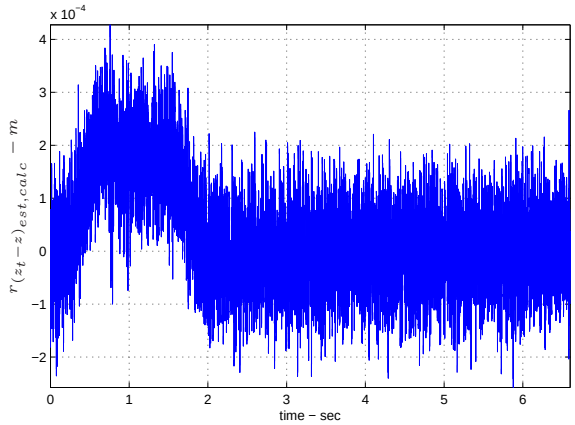

(c) Residual from the estimated and calculated air gap signals ($r_{(z_t-z)_{est,calc}}$).

Figure 8.6: Residual signals produced from the deterministic response for the FDI mechanism.

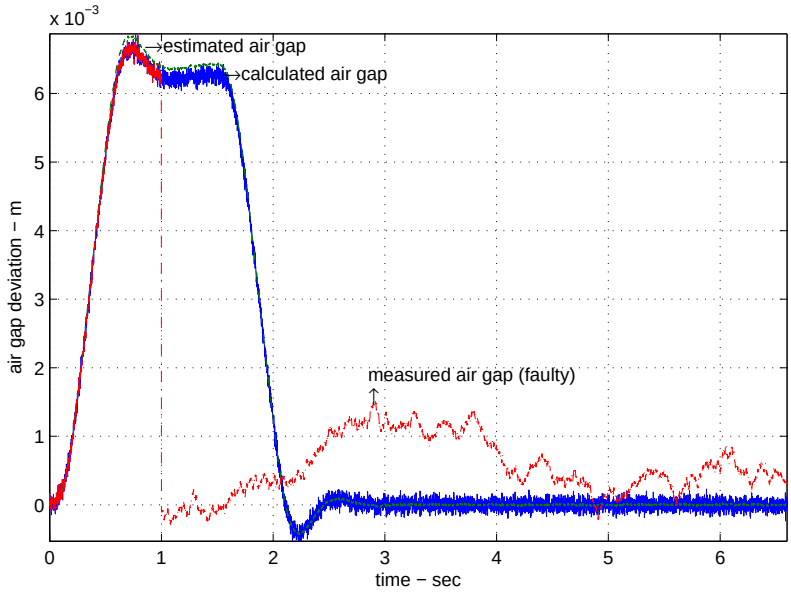

Figure 8.7: The two air gap signals, and the faulty air gap measurement for deterministic response.

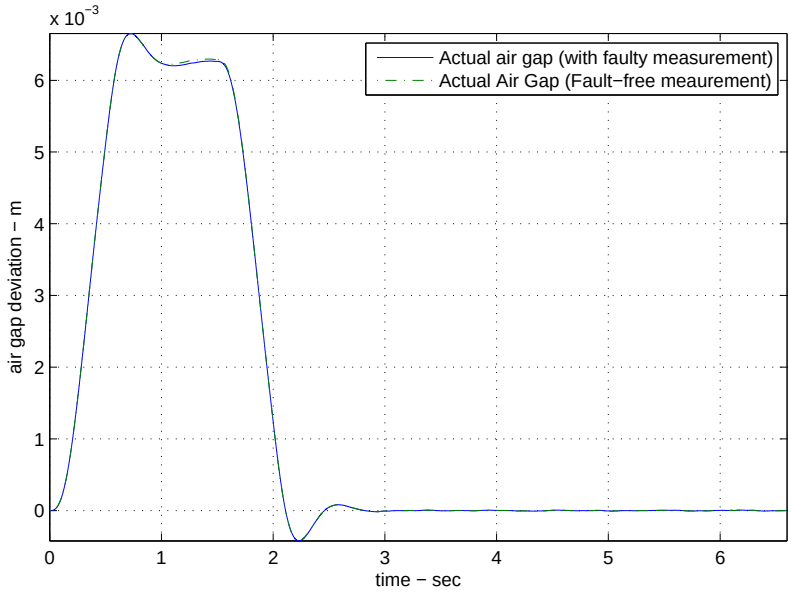

Figure 8.8: Actual air gap signal for fault and fault-free air gap measurement for deterministic response.

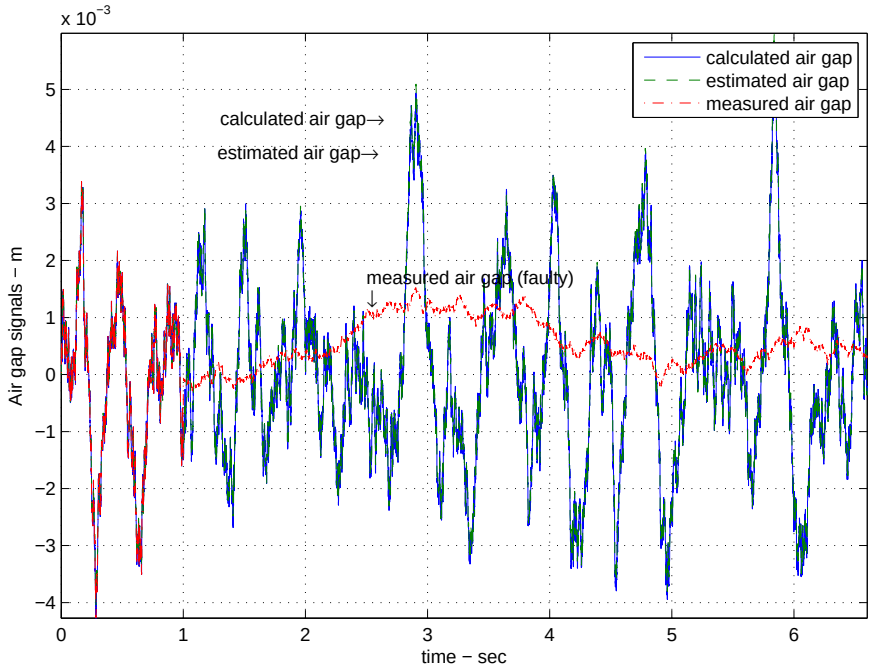

Figure 8.9: The two air gap signals, and the faulty air gap measurement for stochastic response.

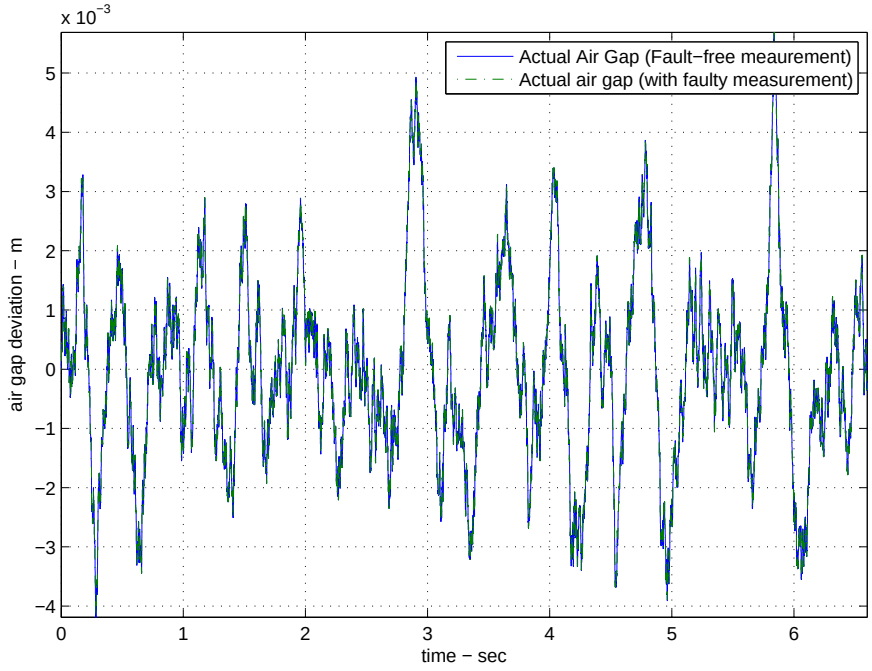

Figure 8.10: Actual air gap signal for fault and fault-free air gap measurement for stochastic response.

ogy is rather simple, it has the disadvantage of employing two extra sensors i.e current and flux (necessary to produce the air gap signal). However, both the current and flux sensors are cheaper compare to the air gap sensor and also subject to less hazardous environment. At this stage, the scheme offers no fault tolerance in the case of current or flux sensor failure (although hardware redundancy could be used in multiple current and flux sensor via voting schemes but with increasing financial cost). Moreover, multiple sensor faults cannot be afforded which is taken into account within the next section. The next scheme discussed in this thesis, addresses the fact of multiple sensor faults and an alternative way of fault tolerance in such cases.

8.3 Sensor selection for sensor fault tolerance

The information from sensor optimisation frameworks can be used in order to apply FTC for multiple sensor failures, with an attempt to minimise the sensor hardware redundancy and maintain optimum performance for every possible sensor set under relevant sensor fault conditions (with the given Kalman filters tuned for optimum performance via NSGA-II). This section has been published by Michail et al. [2009b] (see Appendix E).

It is possible to recover the performance of the MAGLEV suspension when a sensor fails using an active fault tolerant control method. This can be done via controller reconfiguration as illustrated in Fig. 8.11 (see Blanke et al. [2003] for general details.). Any sensor information from the three systematic frameworks can be used but in this chapter the data from the sensor optimisation via LQG is considered for illustration.

All necessary data from the optimised sensor configurations framework via LQG approach is listed on Table 8.2 and 8.3. As it can be seen from the tables there exist a number of sensor sets that can be used to control the suspension satisfactorily (i.e 24 out of 31 sensor sets found to satisfy the performance requirements). Ideally, the sensor set that results to the same performance as in the LQR case is selected. There are a lot of sensor sets that result to very similar performance. If the minimum number of sensors is to be selected for control, Id:2 and Id:5 can be used (single measurements). The problem is that in neither cases there is no sensor fault tolerance, since only one measurement is used in each sensor set (i.e if the sensor fails instability of the suspension is unavoidable).

The MAGLEV suspension is a critical safety-critical and open-loop unstable system. Sensor fault tolerance is thus important issue and should be carefully considered. In the following, one considers sensor fault scenarios and discusses on the possibility of using the proposed sensor optimisation schemes for controller reconfiguration, in the case of multiple sensor failures.

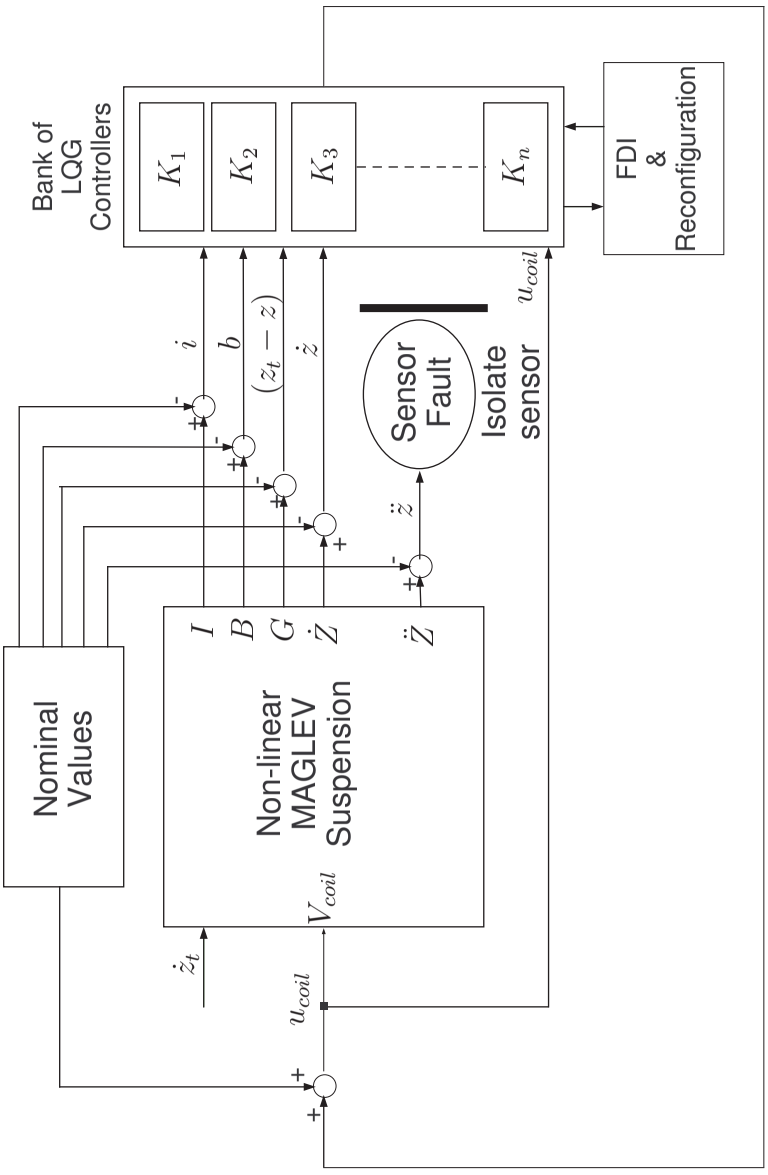

Figure 8.11: FTC diagram for multiple sensor failures using a bank of LQG controllers.

Table 8.2: Optimised sensor configurations via LQG control - Part A.

Sensor set id		$(z_t - z)_{rms}$	$u_{coil_{rms}}$	$\ddot{z}_{rms}$	$(z_t - z)_p$	u_{coil_p}	t_s	e_{ss}	
		mm	V	ms^{-2}	mm	V	s	mm	
	LQR response →	1.5	21.83	0.31	7.3	52.4	2.16	0.019	✓
1	i	1.78	29.16	0.50	2.09	22.93	**6.18**	**0.18**	x
2	b	1.46	22.47	0.32	6.74	63.82	2.18	0.019	✓
3	$(z_t - z)$	1.49	22.41	0.31	**10.69**	84.83	2.56	**0.77**	x
4	$\dot{z}$	1.57	171	**6.83**	**14.6**	**709**	**6.58**	**8.78**	✓
5	$\ddot{z}$	1.46	22.44	0.32	6.82	63.04	2.19	0.013	✓
6	i, b	1.42	22.24	0.31	6.73	59.13	2.18	0.024	✓
7	$i, (z_t - z)$	1.45	22.25	0.31	**10.81**	85.21	2.77	**0.76**	x
8	$i, \dot{z}$	1.47	22.48	0.32	7.08	65.21	**4.70**	**0.16**	x
9	$i, \ddot{z}$	1.46	22.18	0.32	6.82	58.91	2.18	0.03	✓
10	$b, (z_t - z)$	1.43	22.17	0.32	6.81	57.41	2.18	0.027	✓
11	$b, \dot{z}$	1.43	22.29	0.32	**7.73**	64.27	**6.14**	**0.14**	x
12	$b, \ddot{z}$	1.43	22.20	0.32	6.78	59.64	2.18	0.011	✓
13	$(z_t - z), \dot{z}$	1.43	22.29	0.32	**7.73**	64.27	**6.14**	**0.14**	x
14	$(z_t - z), \ddot{z}$	1.43	22.12	0.32	6.91	58.76	2.18	0.028	✓
15	$\dot{z}, \ddot{z}$	1.43	22.42	0.32	6.85	63.16	2.99	0.049	✓
16	$i, b, (z_t - z)$	1.46	22.06	0.32	6.79	55.99	2.18	0.02	✓
17	$i, b, \dot{z}$	1.46	22.21	0.32	6.79	59.55	2.20	0.06	✓
18	$i, b, \ddot{z}$	1.42	22.24	0.31	6.80	59.55	2.20	0.06	✓
19	$i, (z_t - z), \dot{z}$	1.48	22.18	0.32	**7.69**	63.04	2.35	**0.10**	x
20	$i, (z_t - z), \ddot{z}$	1.43	22.06	0.32	6.88	58.31	2.18	0.03	✓

Table 8.3: Optimised sensor configurations via LQG control - Part B.

Sensor set id		$(z_t - z)_{rms}$	$u_{coil_{rms}}$	$\ddot{z}_{rms}$	$(z_t - z)_p$	u_{coil_p}	t_s	e_{ss}	
		mm	V	ms^{-2}	mm	V	s	mm	
21	$i, \dot{z}, \ddot{z}$	1.43	22.16	0.32	6.84	58.98	2.18	0.04	✓
22	$b, (z_t - z), \dot{z}$	1.43	22.17	0.32	6.87	57.85	2.19	0.057	✓
23	$b, (z_t - z), \ddot{z}$	1.43	22.08	0.32	6.83	56.56	2.15	0.015	✓
24	$b, \dot{z}, \ddot{z}$	1.42	22.19	0.32	6.81	59.67	2.19	0.045	✓
25	$b, \dot{z}, \ddot{z}$	1.42	22.19	0.32	6.81	59.67	2.19	0.05	✓
26	$i, b, (z_t - z), \dot{z}$	1.46	22.06	0.32	6.84	56.38	2.19	0.05	✓
27	$i, b, (z_t - z), \ddot{z}$	1.46	22.03	0.32	6.81	55.72	2.18	0.02	✓
28	$i, b, \dot{z}, \ddot{z}$	1.42	22.11	0.32	6.81	56.82	2.19	0.03	✓
29	$i, (z_t - z), \dot{z}, \ddot{z}$	1.43	22.05	0.32	6.90	58.55	2.18	0.03	✓
30	$b, (z_t - z), \dot{z}, \ddot{z}$	1.43	22.08	0.31	6.86	56.75	2.19	0.03	✓
31	$i, b, (z_t - z), \dot{z}, \ddot{z}$	1.46	22.02	0.32	6.84	55.98	2.19	0.03	✓

Aiming to cover multiple sensor faults and assuming that control is achieved with id:31, i.e the full sensor set. Using the information extracted from Tables 8.2 and 8.3, a bank of Kalman filters can be used in order to restore performance following one or multiple sensor faults. In fact, the suspension performance after reconfiguration when a sensor fault happens, is easily predicted from the data listed. For example when four measurements fail and the air gap remains it is possible to lead to catastrophic failure since there is a serious air gap constraint violation (see Id:3). Although it is unlikely for four sensors to simultaneously fail, this shows that a safety-critical system might require some form of hardware redundancy for the air gap signal (that is probably expensive solution). The alternative approach is to avoid using the air gap measurement. Particularly, assume that the worst sensor fault case condition is to remain with one measurement (i.e Id:1, Id:2 and Id:5). According to the given data, if a sensor remains after some sensor failures the performance is satisfactory. From this point of view, the Id:18 can be used instead of the full sensor set that includes Id:1, Id:2 and Id:5. Note that Id:18 and Id:31 have very similar performance, therefore if Id:18 is used, the worst resulting performance when both b and $\ddot{z}$ fail is the response with Id:1 which has steady state violation but it can be safely used until the vehicle decelerates and proceeds to maintenance. In order to achieve sensor fault tolerance, fault detection and isolation and reconfiguration of the controller is required. When Kalman estimators are used, a common approach for the fault detection is to use the residual r_{y_i} (where y_i is the corresponding measurement). After a sensor fault occurs, the fault is detected, isolated and the controller is reconfigured in order to recover performance using the healthy sensors. For this purpose, a bank of Kalman filters is used (one for each possible remaining sensor set following one or more faults).

An alternative sensor set is Id:16 with current, flux and air gap measurements. The problem with this sensor set is that four sensor fault conditions can be covered via controller reconfiguration (i.e Id:1, Id:2, Id:6 and Id:10) the remaining two i.e Id:3 and Id:7, result to critical constraint violation (air gap) during gradients onto track. Also a drawback is that

the air gap measurement to be used is generally expensive and vulnerable to external hazards. An alternative option is Id:17 with current, flux and velocity measurements. Again the selected sensor set can cover only three out of six fault conditions with Id:1, Id:2 and Id:6. One can say, selecting a sensor set with four measurements or the full sensor set but in such case more sensor fault probabilities are introduced with increasing number of sensors. With the sensor set Id:18, there are 6 possible fault conditions that could occur. The first three are individual faults on current, flux and acceleration and the remaining three are combined current/flux, current/acceleration and acceleration/flux faults. Note that here simultaneous faults are taken into account that is the worst fault case for two sensor faults. In order to accommodate the 6 possible fault conditions via controller reconfiguration a bank of 6 Kalman estimators can be used as explained previously.

8.3.1 Sensor fault scenarios

In order to test the proposed sensor fault tolerance scheme some fault scenarios are taken into account. The fault scenario used for the sensors is that at time=1s the sensor is impaired giving wrong readings with random low frequency characteristics. This is illustrated in Fig. 8.12 for current, acceleration and flux density measurements while for the combined sensor fault combinations, the fault scenarios in Fig. 8.12 are combined accordingly. For example if current and flux fail simultaneously (for the deterministic response test), the test signals in Fig. 8.12(c) and Fig. 8.12(e) are selected. All the tests are performed for both deterministic and stochastic responses.

After the fault(s), illustrated in Fig. 8.12, is(are) injected the proposed FTC scheme detects and isolates the faulty measurement. After that immediate remedial action via controller reconfiguration is followed by switching to the controller that works with the remaining healthy measurement(s). The assumption here is that not all three measurements can fail. In such case the closed-loop system becomes unstable and there is nothing that can be done to accommodate such fault condition unless sensor hardware redundancy is

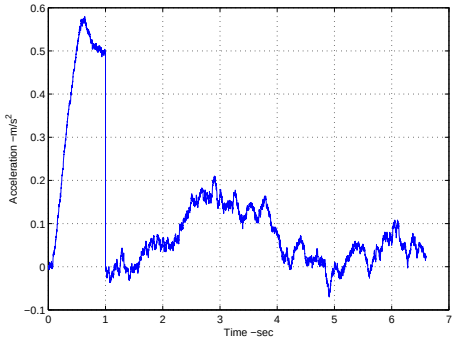

(a) Faulty acceleration measurement for deterministic response.

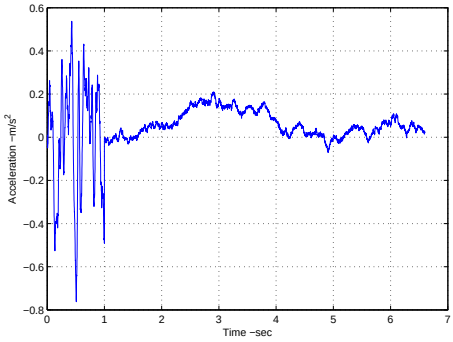

(b) Faulty acceleration measurement for stochastic response.

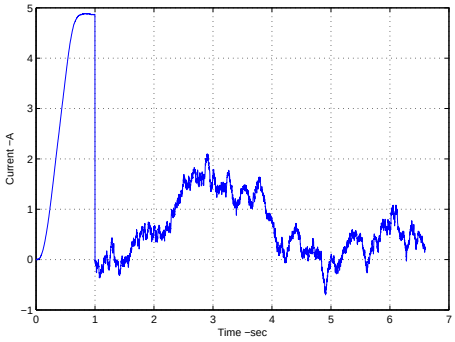

(c) Faulty current measurement for deterministic response.

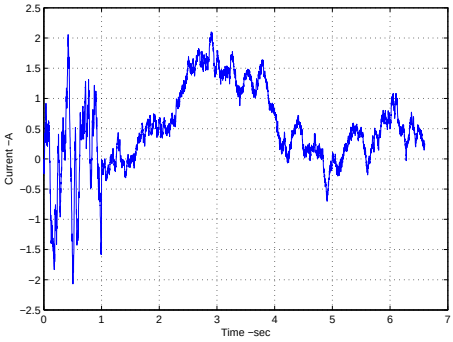

(d) Faulty current measurement for stochastic response.

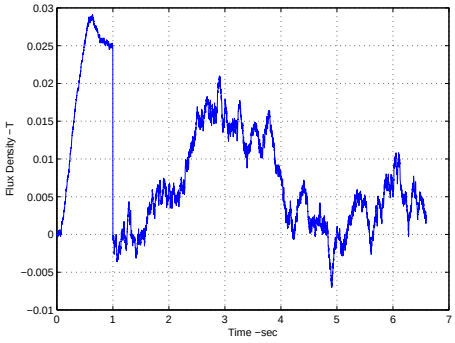

(e) Faulty flux measurement for deterministic response.

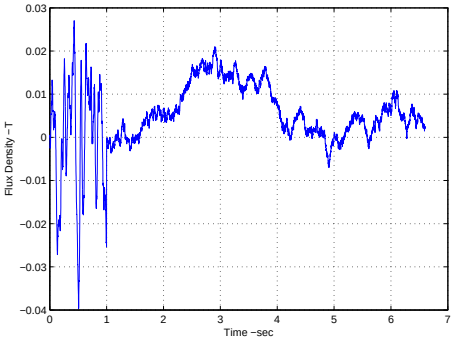

(f) Faulty flux measurement for stochastic response.

Figure 8.12: Faulty measurements scenarios.

used (i.e use triple measurements for each sensor and reconfigure when three of them fail).

8.3.2 FDI and reconfiguration

The fault detection is achieved using a binary sense vector that is residual dependent and indicates which and if a measurement is healthy or faulty (see Blanke et al. [2003]). Faulty measurements, indicated by '1' and healthy by '0'. For example, if $i, b, \ddot{z}$ results to the binary vector [0 0 0] means that all measurements are healthy and the corresponding Kalman filter is used (i.e $K_{i,b,\ddot{z}}$). If one or more faults are detected the Fault Detection and Isolation mechanism detects and isolates the faulty sensor(s) while the reconfiguration mechanism introduces the new Kalman estimator for the remaining healthy sensor(s). As it was mentioned before, the fault detection is performed using the residual of the corresponding measurement. For example if the residual of the current measurement is larger than a predefined threshold ($r_i > V_{th_i}$) then the binary vector indicates the fault in a binary sense ([1 0 0]) and reconfiguration takes place by switching to the relevant Kalman estimator $K_{b,\ddot{z}}$. The possible sensor fault conditions with the resulting binary vector and the corresponding Kalman estimators are listed in Table 8.4.

Table 8.4: Possible sensor fault conditions with Id:18.

Sensor set	Healthy Sensors	Faulty Sensor(s)	Binary Vector	Kalman estimator
			$[i \;\; b \;\; \ddot{z}]$	
$i, b, \ddot{z}$	$i, b, \ddot{z}$	-	[0 0 0]	$K_{i,b,\ddot{z}}$
	i, b	$\ddot{z}$	[0 0 1]	$K_{i,b}$
	$b, \ddot{z}$	i	[1 0 0]	$K_{b,\ddot{z}}$
	$i, \ddot{z}$	b	[0 1 0]	$K_{i,\ddot{z}}$
	i	$b, \ddot{z}$	[0 1 1]	K_i
	b	$i, \ddot{z}$	[1 0 1]	K_b
	$\ddot{z}$	i, b	[0 0 1]	$K_{\ddot{z}}$

8.3.3 Simulation results

The next step is to test the sensor fault tolerance under different fault conditions (stability is tested and negligible switching time is assumed). The results under all possible conditions are illustrated in Fig. 8.13, Fig. 8.14, Fig. 8.15, Fig. 8.16, Fig. 8.16 for both the deterministic and stochastic responses. The figures show the error between the air gap with fault-free conditions $(z_t - z)$ and the air gap under the sensor fault conditions $(z_t - z)_f$. The errors in all figures are very small and it is clear that under 5 fault conditions the reconfiguration is successful for both deterministic and stochastic responses except where simultaneous fault happens at 1 second for flux and acceleration measurements. In such case, when switching to the Kalman estimator with current measurement (K_i) the performance recovery is not possible and instability of the closed-loop response follows for both deterministic and stochastic responses. In such case, the performance is not possible to recover under those specific fault conditions but extra hardware redundancy can be used for b and $\ddot{z}$ in order to avoid having the current, information on its own (if both b and $\ddot{z}$ fail) (However it is a scenario that really stretches the limits of the reconfiguration scheme, i.e only the current measurement remains).

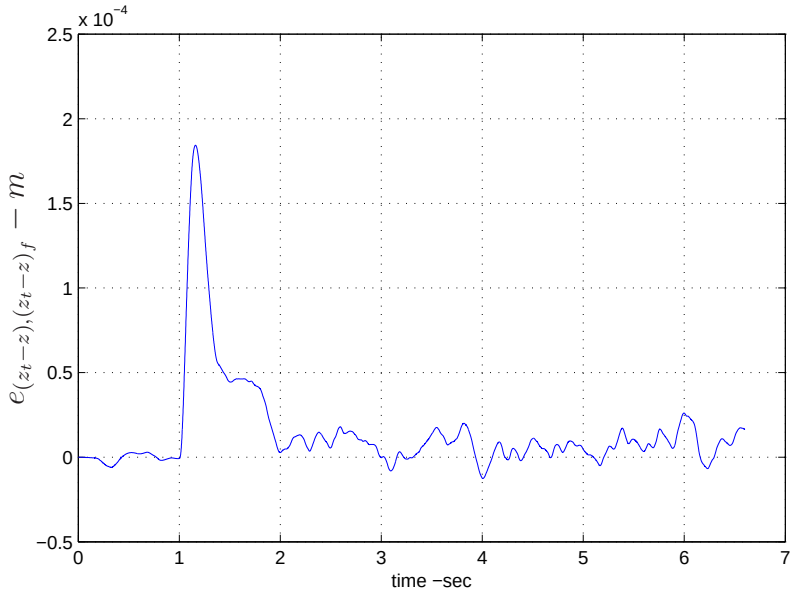

(a) Error between air gap with fault-free and faulty acceleration measurement ($e_{(z_t-z),(z_t-z)_f}$) during deterministic response.

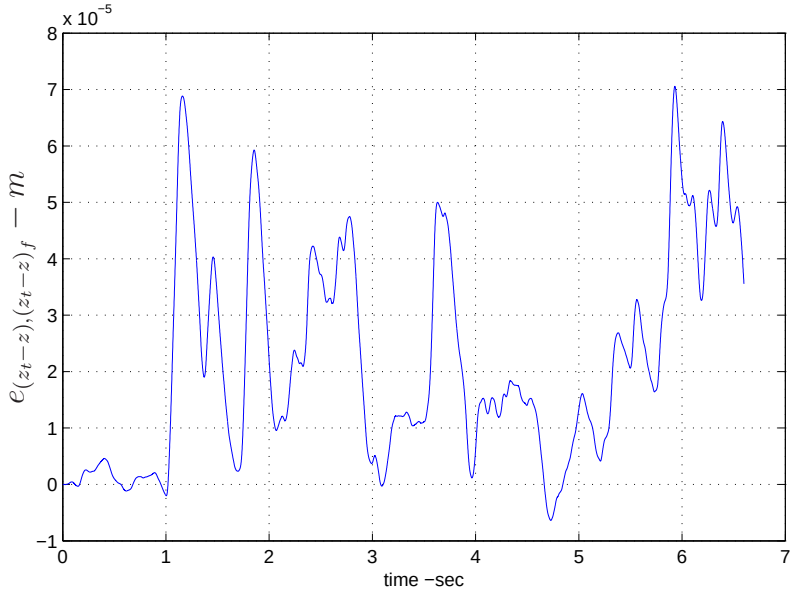

(b) Error between air gap with fault-free and faulty acceleration measurement ($e_{(z_t-z),(z_t-z)_f}$) during stochastic response.

Figure 8.13: Error between air gap with fault-free and faulty acceleration measurement.

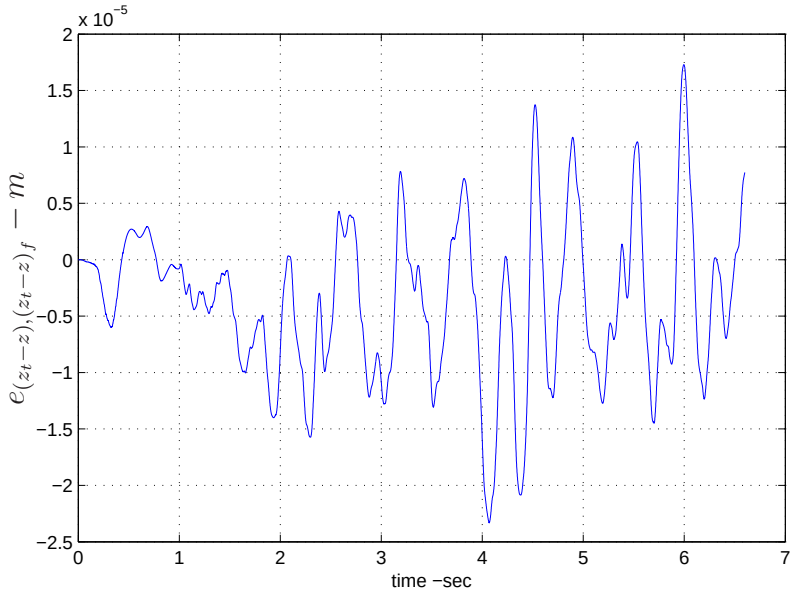

(a) Error between air gap with fault-free and faulty current measurement ($e_{(z_t-z),(z_t-z)_f}$) for deterministic response.

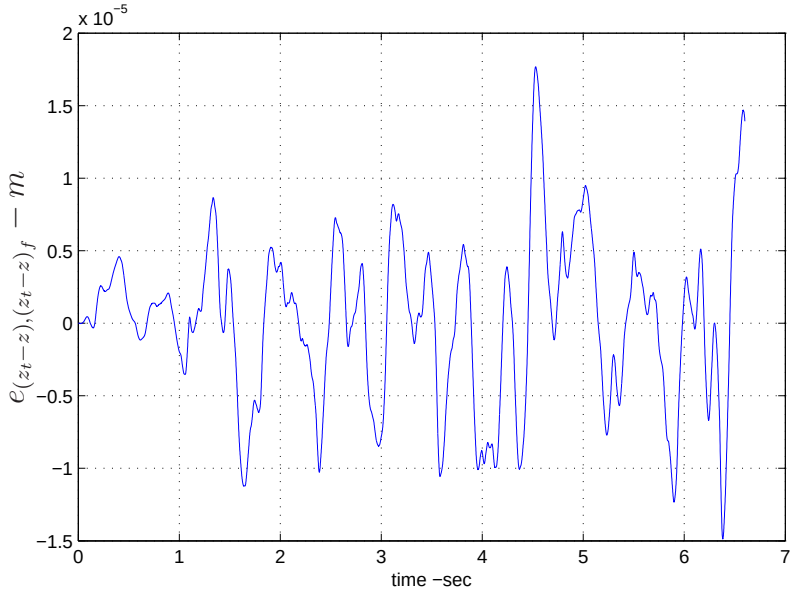

(b) Error between air gap with fault-free and faulty current measurement ($e_{(z_t-z),(z_t-z)_f}$) during stochastic response.

Figure 8.14: Error between air gap with fault-free and faulty current measurements.

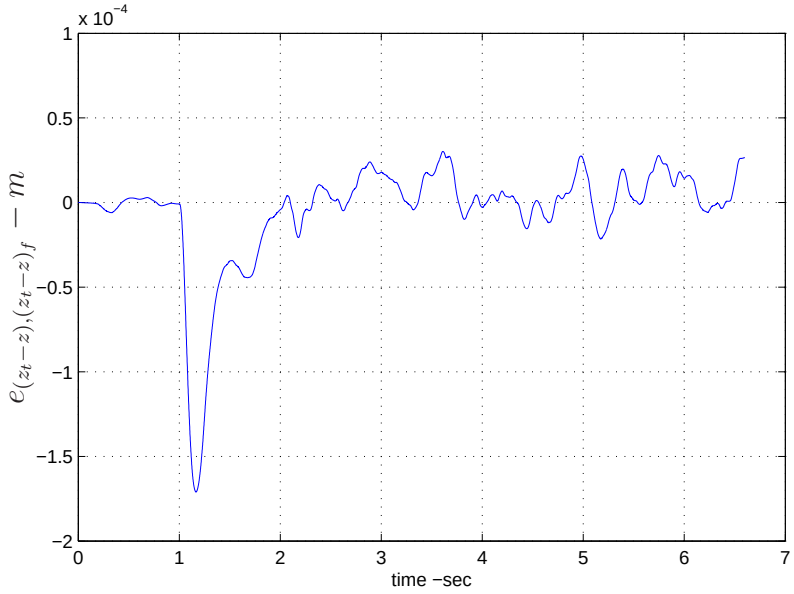

(a) Error between air gap with fault-free and faulty flux measurement ($e_{(z_t-z),(z_t-z)_f}$) during deterministic response.

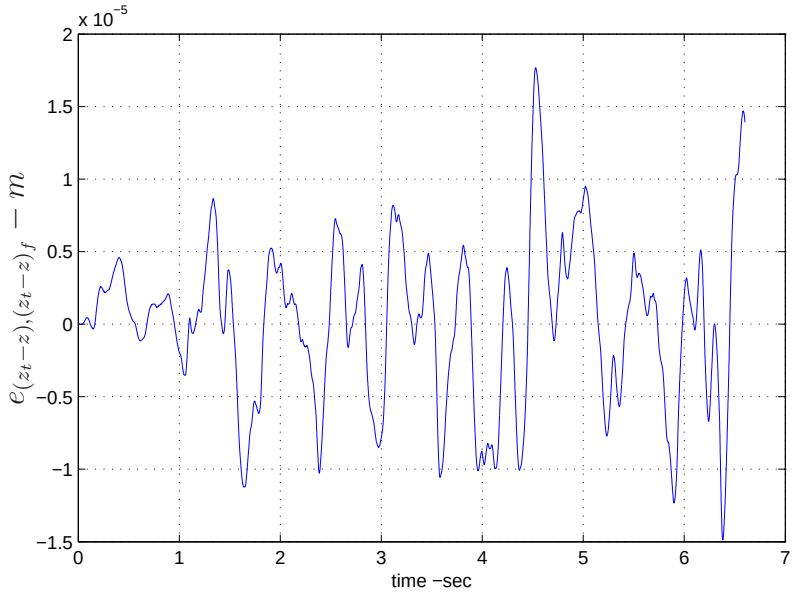

(b) Error between air gap with fault-free and faulty flux measurement ($e_{(z_t-z),(z_t-z)_f}$) during stochastic response.

Figure 8.15: Error between air gap with fault-free and faulty flux measurement ($e_{(z_t-z),(z_t-z)_f}$).

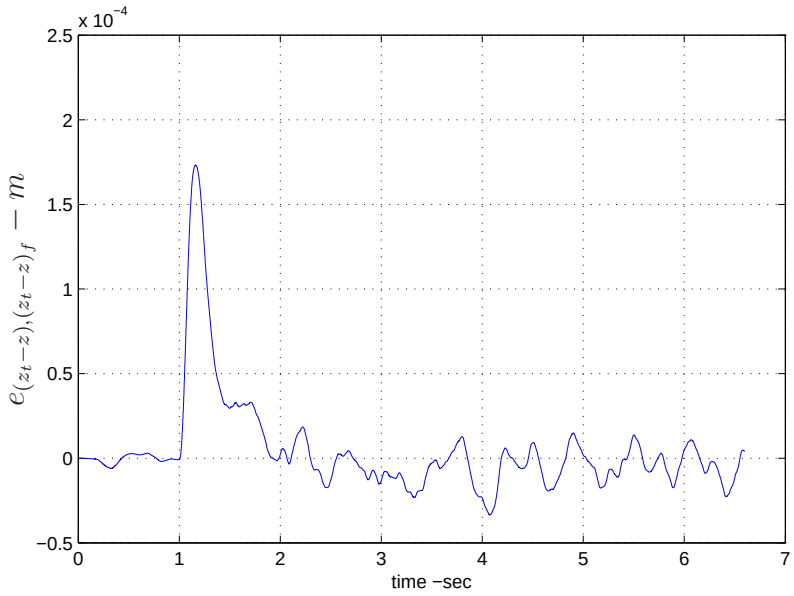

(a) Error between air gap with fault-free and faulty current/acceleration measurement ($e_{(z_t-z),(z_t-z)_f}$) during deterministic response.

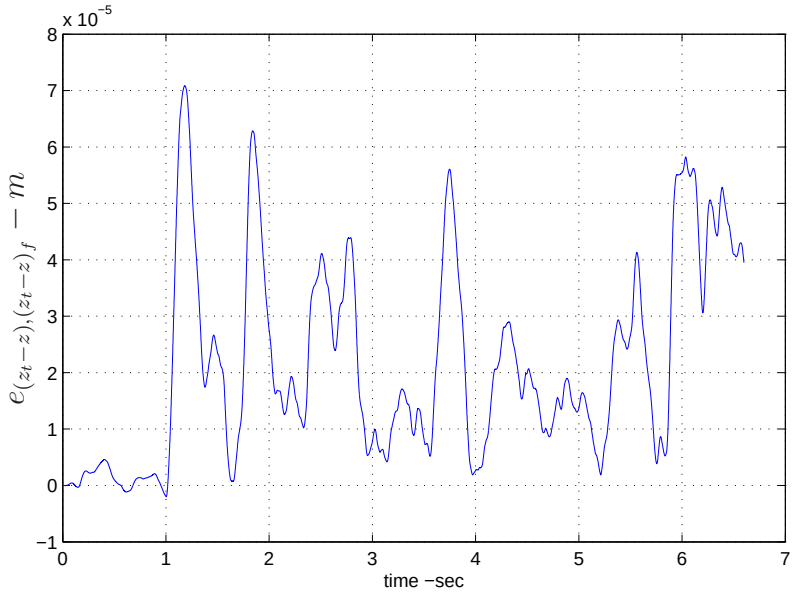

(b) Error between air gap with fault-free and faulty current/acceleration measurement ($e_{(z_t-z),(z_t-z)_f}$) during stochastic response.

Figure 8.16: Error between air gap with fault-free and faulty current/acceleration measurement.

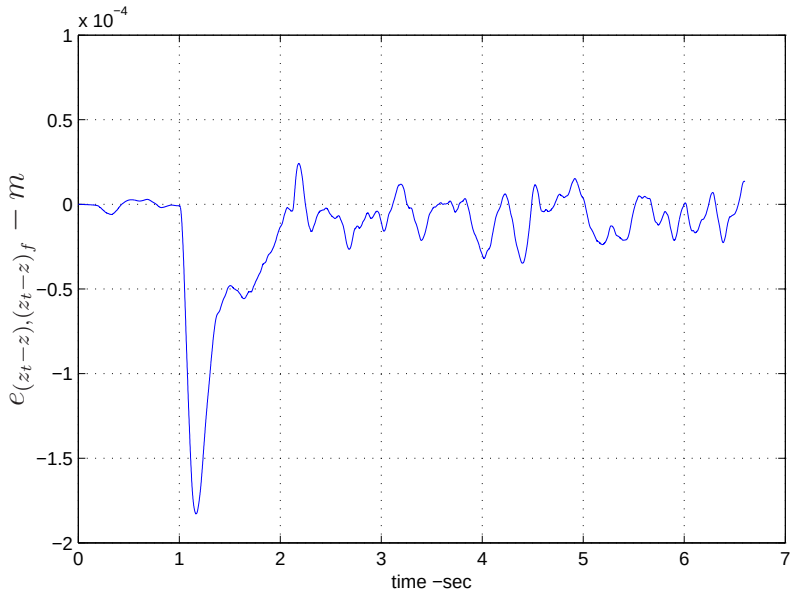

(a) Error between air gap with fault-free and faulty current/flux measurement ($e_{(z_t-z),(z_t-z)_f}$) during deterministic response.

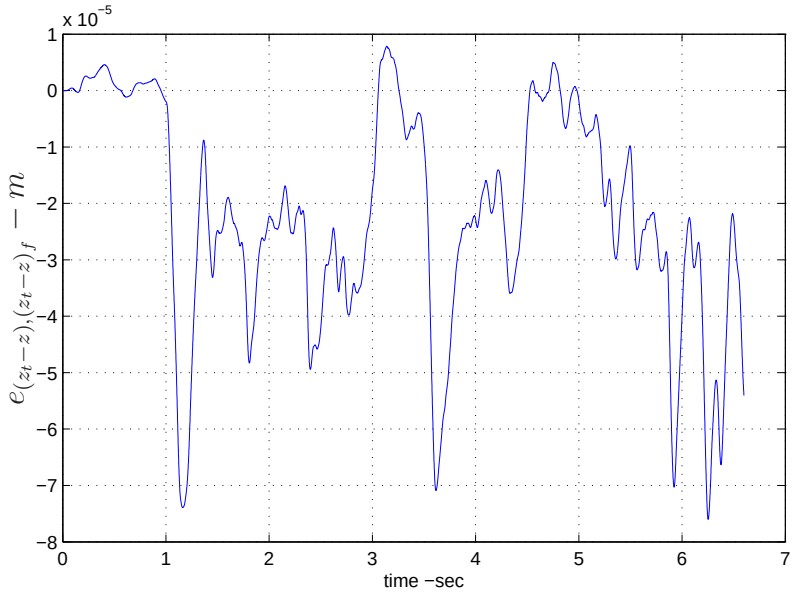

(b) Error between air gap with fault-free and faulty current/flux measurement ($e_{(z_t-z),(z_t-z)_f}$) during stochastic response.

Figure 8.17: Error between air gap with fault-free and faulty current/flux measurement.

8.4 Summary

In this chapter two sensor fault tolerance approaches have been studied. One is the combination of the classical control strategy with Kalman estimator and analytical redundancy and the second is using the optimised sensor configurations via modern control approaches.

In the former case the fault tolerance against air gap failure was considered. The method is using three air gap signals to achieve sensor fault tolerance. One is the measured $(z_t - z)_{mea}$, the other is the estimated $(z_t - z)_{est}$ and the calculated $(z_t - z)_{calc}$ air gaps. The last two signals are generated using the current and flux measurements. The proposed method is verified via simulations using the non-linear model for both deterministic and stochastic responses. Although the method covers only single sensor failure (i.e air gap sensor) it avoids having air gap sensor redundancy.

The problem of selecting the number of sensors to be used for control as well as for sensor fault tolerance is the next issue considered in this chapter. In particular, the MAGLEV suspension is a safety-critical system where the performance and stability have to be ensured under any sensor faults. Depending on the desired MAGLEV suspension performance any of the three (previously in this thesis) developed systematic frameworks can be used for the sensor fault tolerance but in this chapter LQG is considered for illustration. From the analysis of the presented results it seams that the best sensor set to be used (at least on a first step) is the current, flux and acceleration (in terms of control and fault tolerance). The air gap sensor does not appear although this might be desired from a financial point of view (note that this signal can be estimated).

Chapter 9

Design and construction of a MAGLEV rig and experimental results

9.1 Introduction

The design and construction of a $25kg$ MAGLEV suspension is described. Details for the Mechanical construction, electromagnets, power amplifier design and the measurement sensors are given. The aim of the experimental MAGLEV rig is to verify the proposed sensor optimisation frameworks via classical and modern control techniques. As the stochastic and deterministic track profiles are not possible to test under the available equipment, the control is taken into account for the operating point of the suspension as well as the tracking for a reference air gap signal. The model of the suspension is simple and described in Chapter 4 as it is based on Newton's motion law and the sum of the induced voltages across the coil. In this chapter, the model verification is done and experimental results of the classical as well as modern control strategies are presented.

9.2 Design and construction of an electromagnetic suspension

In this section a detailed description of the $25kg$ rig is given along with all necessary information for the mechanical construction as well as the power amplifier design and the measurements practical implementation. The control system implementation is done via XPC target that is provided by MATLAB v7.2 and the 12Bit DAQ card PCI6070E from National Instruments card with 8 digital input/output channels, 2 analogue outputs and 16 analogue inputs. For this application, one analogue output is used for the driving signal and 5 analogue inputs for the measurements (i.e current, flux density, air gap, vertical velocity and vertical acceleration).

9.2.1 Mechanical construction

The mechanical construction consists of the two electromagnets that are fitted onto a metal lever made of mild steel. The lever is supported on a pivot and is freely moving in the vertical direction while the track is fixed above the electromagnets. This is depicted in Fig. 9.1 where a simple diagram is given in order to demonstrate the concept. More detailed description on the design and construction of the mechanical parts of the MAGLEV suspension can be found in Appendix C while a photo of the side view showing the electromagnets that are supported onto the lever below the track is depicted in Fig. 9.2.

9.2.2 Electromagnets and amplifier design

Electromagnets characteristics

The electromagnets have been designed to lift $50kg$ extra weight at an operating air gap of $10mm$ each. Thus they can easily lift their weight and the metal lever that they are fixed on. The characteristics of the electromagnets are listed on Table 9.1.

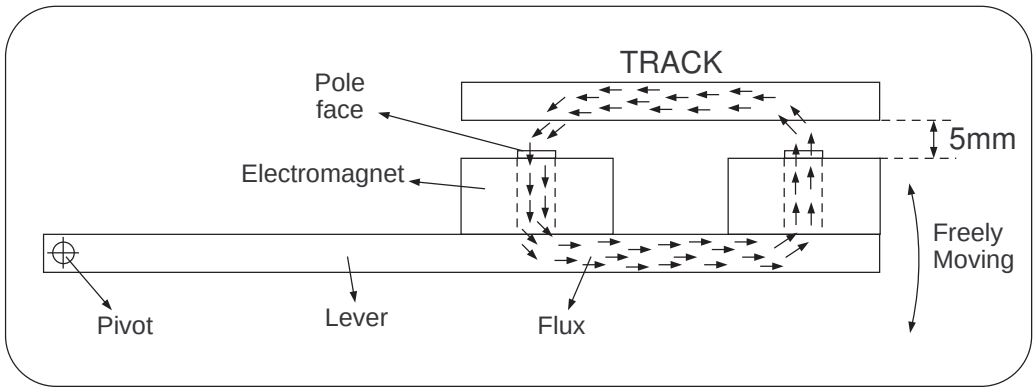

Figure 9.1: Simple diagram of the MAGLEV suspension rig.

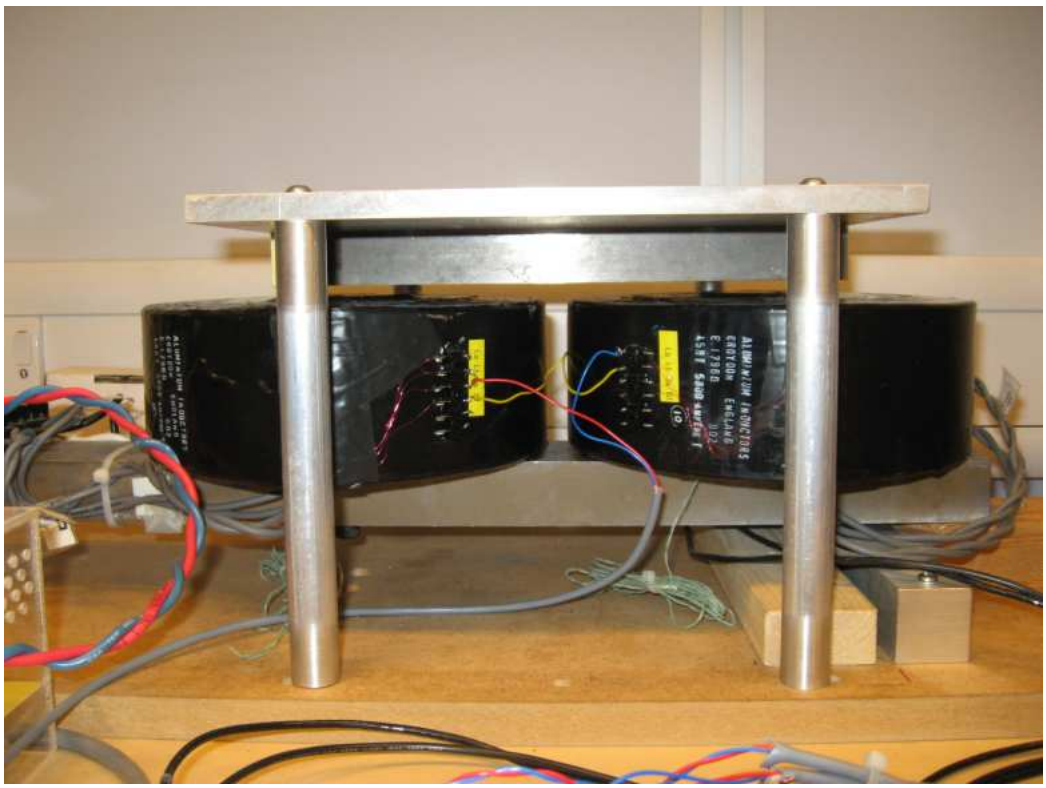

Figure 9.2: Photo of the MAGLEV suspension (side view).

Table 9.1: Parameters for one coil.

Parameter	Value	Unit
Coil's resistance (R_{coil})	0.674 @40^oC	Ω
Pole face area (A_p)	0.005	m^2
Pole diameter (D_c)	56	mm
Weight (M_c)	7	kg
Number of turns (N_c)	228	turn

The operating point is calculated according to the nominal air gap and the total mass to be supported. Assuming that the operating air gap is $5mm$ and the total mass is $25kg$, the current and flux density operating points are calculated from the force and flux in (9.1) and (9.2) respectively (see Mansfield [2007]).

$$F_o = \frac{B_o^2 A_{ptotal}}{2\mu_o}(N) \tag{9.1}$$

Where, F_o the operating force and A_{ptotal} is the total pole face area.

$$B_o = \frac{N_c I_o \mu_o}{2G_o}(T) \tag{9.2}$$

Where, N_c is the number of turns, I_o the operating current, G_o the operating air gap and μ_o is the permeability of air given as $4\pi \times 10^{-7}$.

The operation point values can be calculated now very easily. The force for $25kg$ is about $245N$ ($F_o = 250N$) and therefore the operating flux density is calculated as $B_o = 0.33T$ and the current $I_o = 5.7A$.

Electro-Magnets power amplifier design

The power amplifier is one of the most critical parts of the MAGLEV rig. The simple electrical diagram in Fig. 9.3 shows the basic electrical connections of the MAGLEV Rig. A fast response as well as linear characteristics power amplifier is required to achieve the high bandwidth flux control of

the suspension (in the classical control). Most suspensions use a pulse-width modulated DC-DC converters where the switching devices are switched ON and OFF at high frequency ($20kHz$). The power amplifier is able to supply the electromagnets with a maximum of $10A$ which is the current limit. A protection circuit is included under overload situation and therefore a second current sensor is used (see Appendix D). Note that the power amplifier is designed in such a way that the final state is totally isolated from the DAQ card. The reason is to avoid damage from large voltage spikes coming from the switching power converter during a possible MOSFET or DIODE failure. Also, it is important to twist the cables in order to miminise electro-magnetic compatibility problems regarding the transducers.

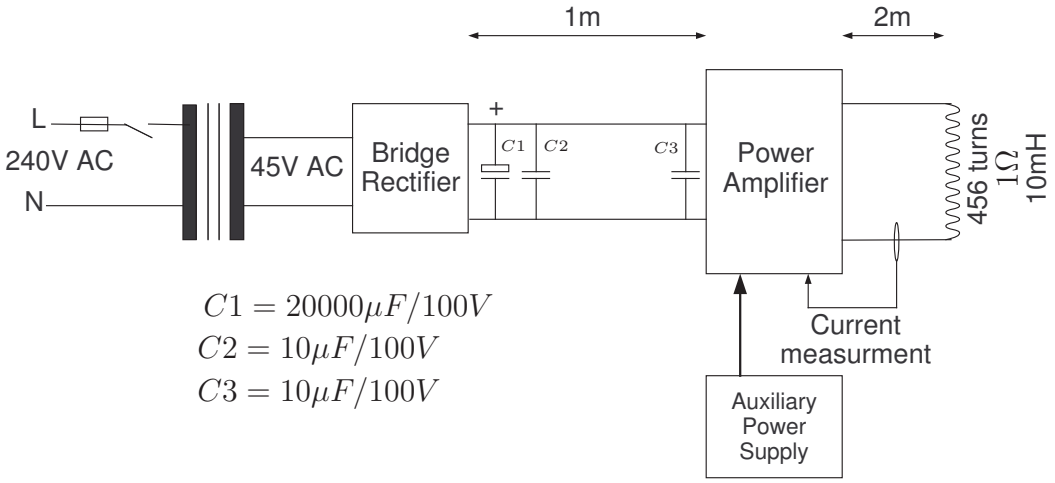

Figure 9.3: Electrical diagram for the electromagnet supply.

The power amplifier is designed based on dual forward DC-DC converter using MOSFET devices and the PWM pulses are produced using the MAXIM function generator MAX038. A photo of the power amplifier is given in Fig. 9.4 while a detailed description of the power amplifier electronic circuits are given in Appendix D.

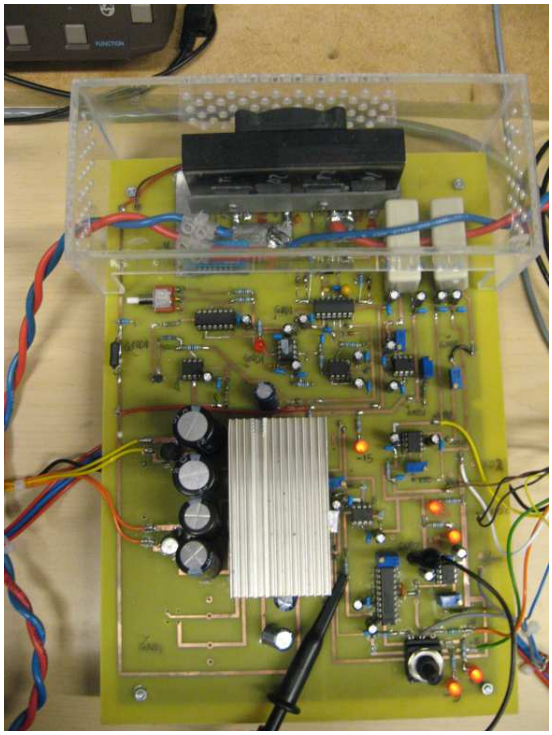

Figure 9.4: Photo of the power amplifier.

9.2.3 Transducers and signal conditioning

Air gap position sensor

Non-contacting Sensagap displacement transducers from RDP Electronics were used on the rig. These are capacitive devices which operate over a range of $20mm$ when both the target and the sensor's packing case are grounded. For the particular application the SG10 model is used which is able to measure a distance between $0.5 - 10.5mm$ with a sensitivity of $300mV/mm$.

The sensor is intended to measure the distance between the magnet pole face and the track. The target is made of aluminium and is fixed on the side of the metal lever where the electromagnets are supported. As it is illustrated in Fig. 9.5, the air gap sensor is fitted below the target on a wooden base

and both the target and air gap sensor are grounded. Note that for complete isolation from the electromagnetic field a magnetic isolation material is placed between the target and the metal lever. The accelerometer is placed on the target next to the front electromagnet (the detailed position on the MAGLEV rig is shown in Appendix C). More details about the vertical acceleration and velocity measurements are given in the next section.

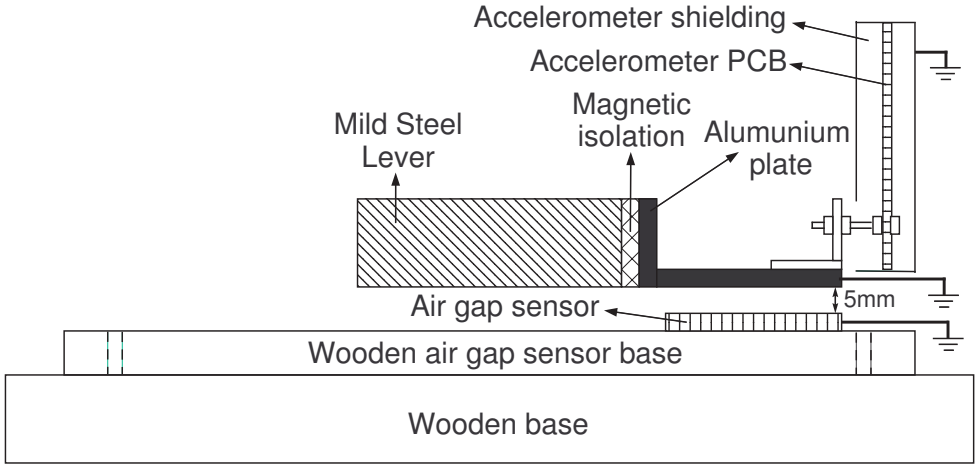

Figure 9.5: Air gap and accelerometer sensors installation (front view).

Accelerometer and velocity measurements

The acceleration measurement which have good linear response down to low frequencies, is compact and robust. The accelerometer used in this case is the MXA6500G/M by MEMSIC. The maximum acceleration that can be measured is $\pm 1g$ with a sensitivity of 500mV/g at 3V in an ambient temperature of 25^oC. The accelerometer is placed onto the PCB board that is supported on the air gap's target (aluminium plate) as shown in Fig. 9.5. The accelerometer is placed next to the pole face of the electromagnet so that the electromagnetic interference from the electromagnetic field is strong. Thus PCB is shielded and the shielding is grounded in order to reduce the output noise.

The output of the accelerometer is used to derive the velocity. The velocity can be derive by integrating the acceleration but a pure integrator is not practical and therefore a self-zeroing integrator. A second order Butterworth high-pass filter as proposed by Goodall [2004] is used as self-zeroing integrator and given as follows

$$G_I = \frac{s}{s^2 + 1.4\omega_I + \omega_I^2} \tag{9.3}$$

The cut off frequency is $\omega_I = 1.5rad/s$ and the actual implementation of the self-zero integrator is depicted in Fig. 9.6 with $\tau_{i_1} = 1.034s$, $\tau_{i_2} = 0.454s$, $G_{\ddot{z}} = 3$ and $\rho = 2.052$. The corresponding integrator is implemented in practice using an operational amplifier configurations (Goodall [2000]). The corresponding practical and simulated Bode magnitude plot of the integrator are shown in Fig. 9.7.

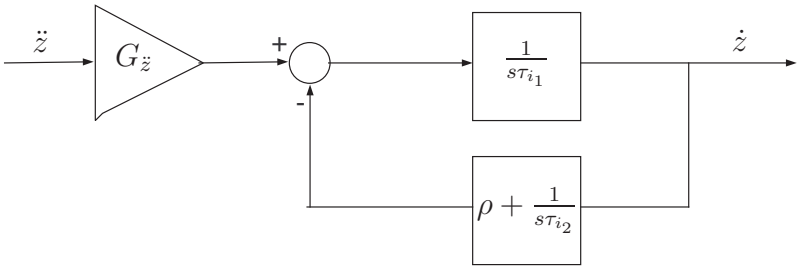

Figure 9.6: Diagram of the self zeroing integrator.

Flux sensor

The flux sensor consists of a search coil and an analogue self-zeroing integrator. The electromagnets have two circular grooves for each pole face, the inner and the outer. On the current configuration one inner and an outer search coils are used with 130 turns each. The diagram of the pole face is shown in Fig. 9.9(a). The search coils are embedded in the groove in order to make it robust with the magnet pole face impacting on the track (this condition happens a lot during tests). A photo of the pole face showing the two search coils is illustrated in Fig. 9.9(b). As the flux density changes a

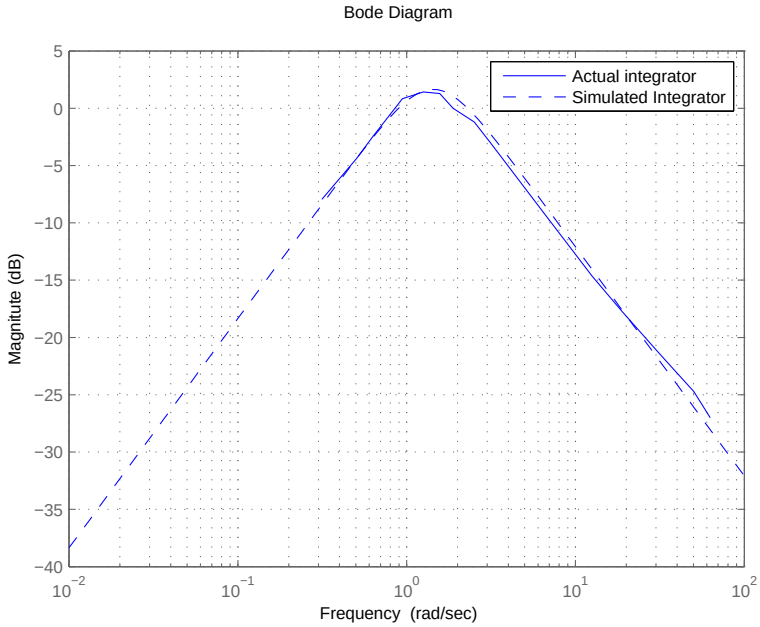

Figure 9.7: Bode magnitude of the velocity integrator.

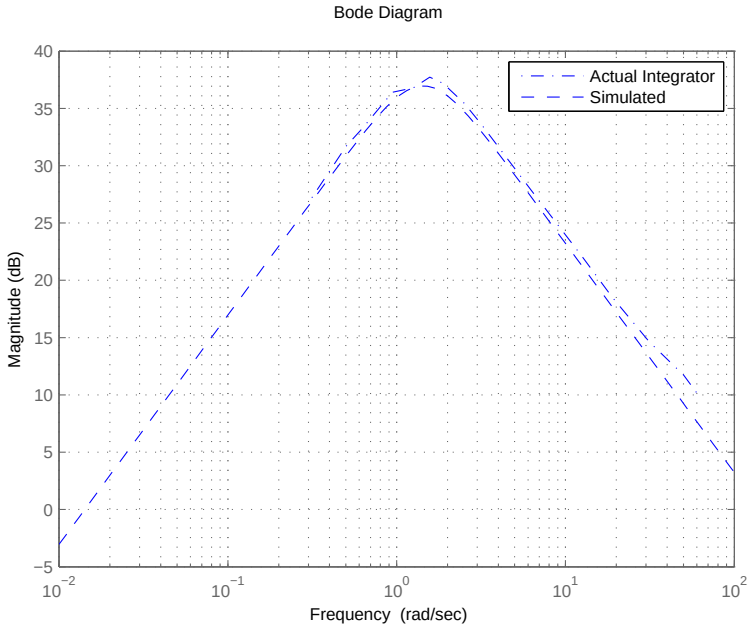

Figure 9.8: Bode magnitude of the flux integrator.

voltage is induced in the search coil. The area of the search coil is known, so by integrating and scaling the resulting voltage the change in flux density can be determined. Again to avoid drifting the circuit requires a self zeroing integrator as described previous section. The resulting Bode magnitude of the flux integrator with $\tau_{i_1} = 1.034s$, $\tau_{i_2} = 0.454s$, $G_b = 150$ and $\rho = 2.052$ is depicted in Fig. 9.8.

Current sensor

Two current sensors are used in the circuit. One is used for the current limiter to protect the power amplifier from overload (explained in Section 9.2.2) and the second current sensor is used to give a measurement for the control purposes. There are a PCB mounting Hall effect current transformer by TELCON (HTP25) that can measure to the range of $\pm 25A$ each.

9.2.4 Rig commissioning

The rig as a whole was assembled as initially envisaged. Although the MAGLEV rig is simple to construct, extra care has to be taken for the scaling, polarity and the shielding of the sensors have to be considered. The mechanical assembly proved to be particularly successful with the pole face being at $5mm$ from the track on horizontal position. The overall diagram of the complete control system is depicted in Fig. 9.10. Two computers are required for the control system. One is the host PC where the MATLAB is installed with the XPC target that is required to build the necessary control system using simulink blocks and the second that is used as a target PC where the compiled code is uploaded and the real controllers are running. The 5 measurements are fed into the analogue inputs of the 12bit resolution DAQ card from national instruments while one analogue output is selected to supply the driving signal at the input of the amplifier.

The current measurement is relatively easy to be obtained with very limited noise interference as well as the air gap measurement (of course extra care must be taken during installation to void interference from surrounding

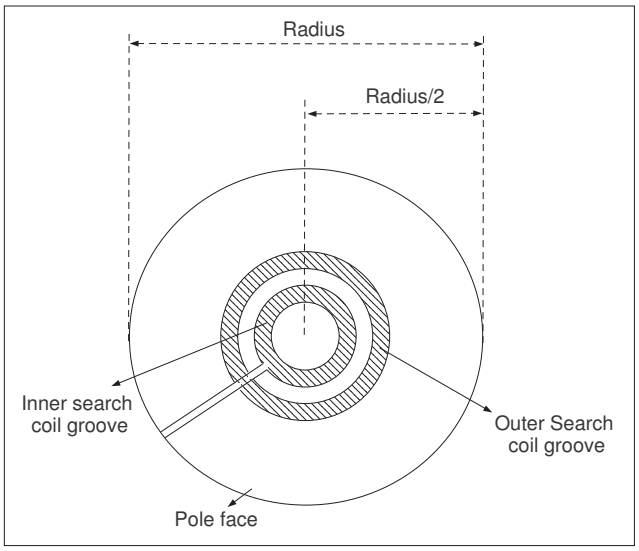

(a) Pole face diagram showing the two grooves for the search coils.

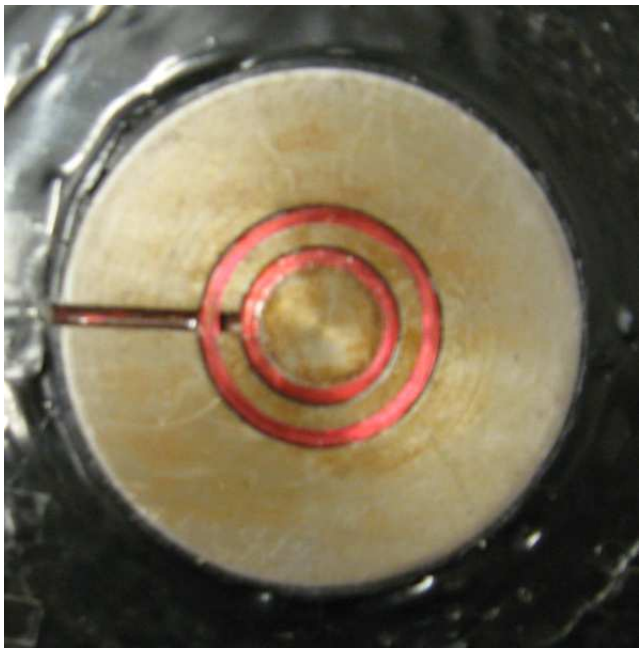

(b) Electromagnet's pole face photo.

Figure 9.9: Diagram and the photo of the pole face.

components). Although the accelerometer is shielded, the noise interference is relatively high but for the velocity measurement is reduced because of the filtering properties of the integrator G_I. The flux density measurement consists of two search coils (one on each magnet) that pick up the flux circulation and a self zero integrator to transform to flux density. A photo of the experimental setup is depicted in Fig. 9.11 while a demo to show the different parts of the experimental rig is uploaded on Youtube by Michail [2008c] (The link is given with the reference).

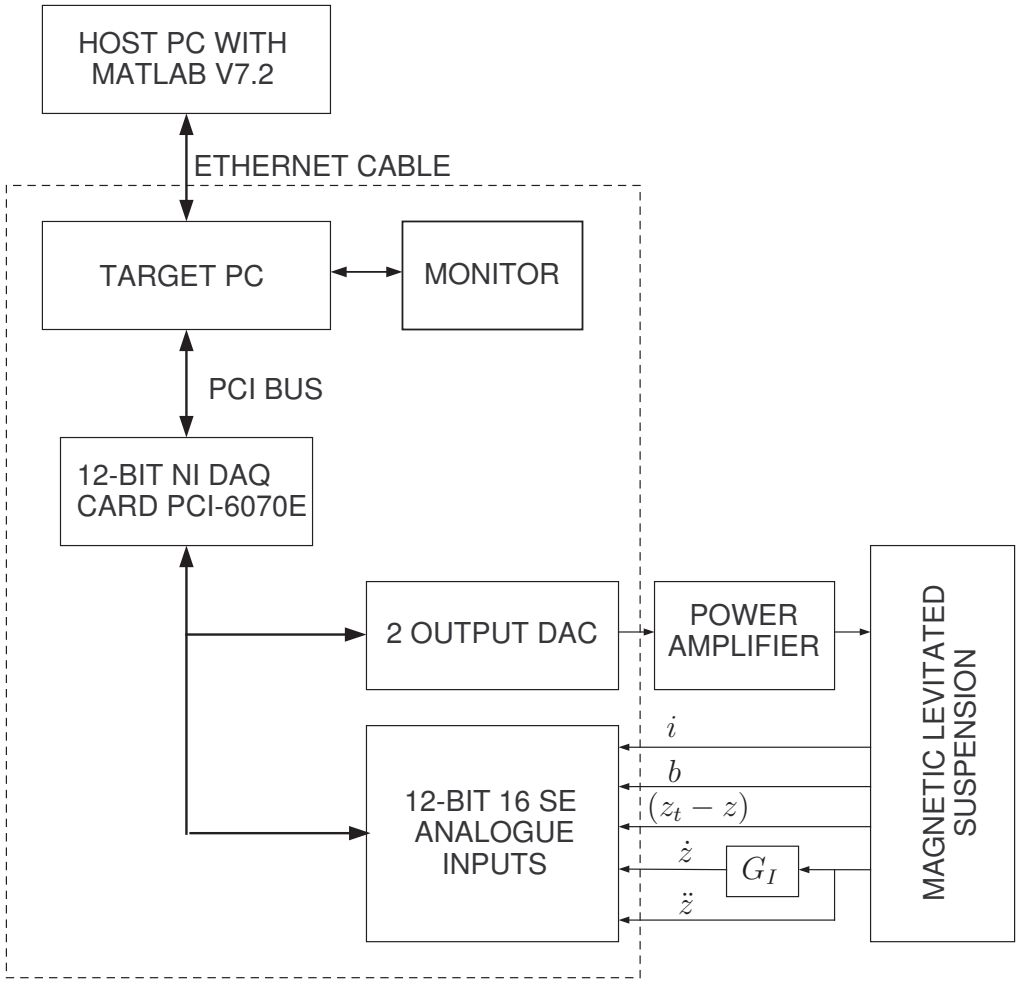

Figure 9.10: Diagram of the MAGLEV Rig commissioning.

Figure 9.11: Photo of the 25kg MAGLEV suspension rig.

9.2.5 Model verification

In order to have good control over the real plant, the model validation is necessary in order to ensure that the model's parameter are correct. Although the state space model of the MAGLEV suspension is derived using the fundamental equations from Newton's and Kirchhoff's Law the model validation is necessary in order to verify not only the dynamics but to ensure that non-linearities in the system are fairly low. The model verification is done using the Bode plot of the state space model from the input (u_{coil}) to the air gap ($z_t - z$) and this is compared with practical measurements within a frequency range between 0.2Hz to 5Hz. Because the MAGLEV suspension is open loop unstable, the stabilization using closed-loop configuration is necessary. The control approach used is the classical air-gap/flux configuration using a PI controller for the inner loop and a PA for the outer loop as discussed in Chapter 5. The diagram depicted in Fig. 9.12 illustrates the concept.

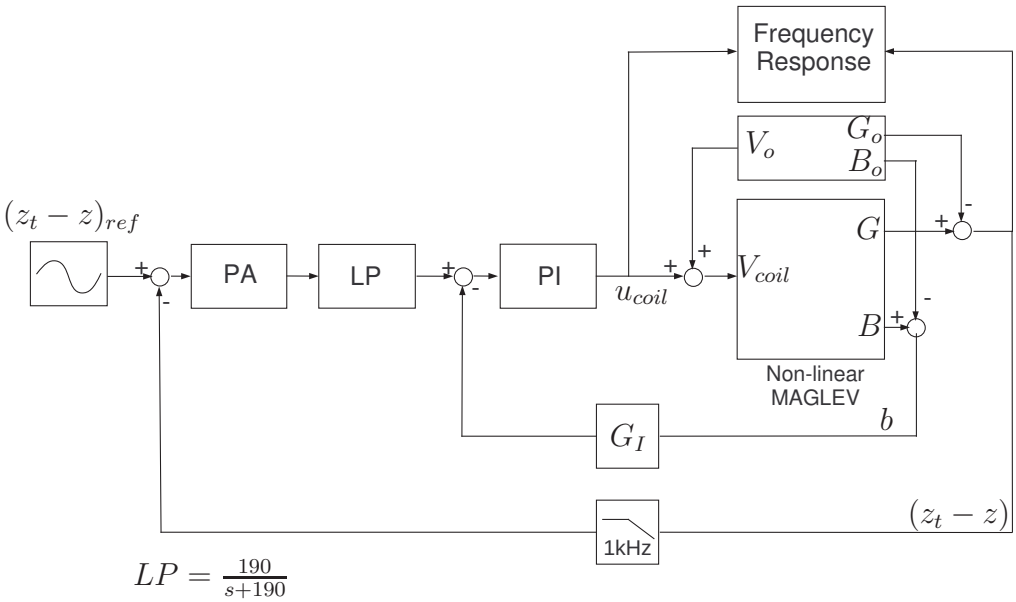

Figure 9.12: Block diagram for plotting the frequency response of the 25kg MAGLEV rig.

The controllers' parameters are tuned via NSGA-II for optimum tracking

of an input sinusoidal signal of while measurements of the input voltage (u_{coil}) and output air gap ($z_t - z$) are taken in order to plot the frequency response of the suspension. The selected controllers are taken as

$$PI = 535\frac{0.023s + 1}{0.023s} \tag{9.4}$$

$$PA = 24.7\frac{0.0354s + 1}{0.0038s + 1} \tag{9.5}$$

Note that according to input frequency the input amplitude is adjusted i.e the higher the frequency the lower the input amplitude. This maintains the stability of the closed-loop response. The linear controllers are tuned for the non-linear model in simulink and implemented onto the real system using the XPCtarget. The real parameter values of the MAGLEV rig are listed on Table 9.2. The overall weight is $25kg$ while the operating air gap is $5mm$. From those two requirements the other parameters are calculated as shown before (Note that the coils are ready made and therefore R_c,L_c,A_p and N_c are given).

Table 9.2: MAGLEV Rig parameters.

Parameter	Value	Unit
M_s	25	kg
G_o	0.005	m
B_o	0.33	T
I_o	5.5	A
F_o	245.25	N
R_c	0.67	Ω
L_c	10	mH
N_c	456	turns
A_p	0.0062	m^2

The Bode plot of the MAGLEV rig is depicted in Fig. 9.13. The measurements taken show that the linearised state space model is very close to the actual (non-linear) MAGLEV rig up to around $30rad/s$. The state space model is very close to the real MAGLEV with some difference that is probably due to some small parametric uncertainties and non-linearities in

the system.

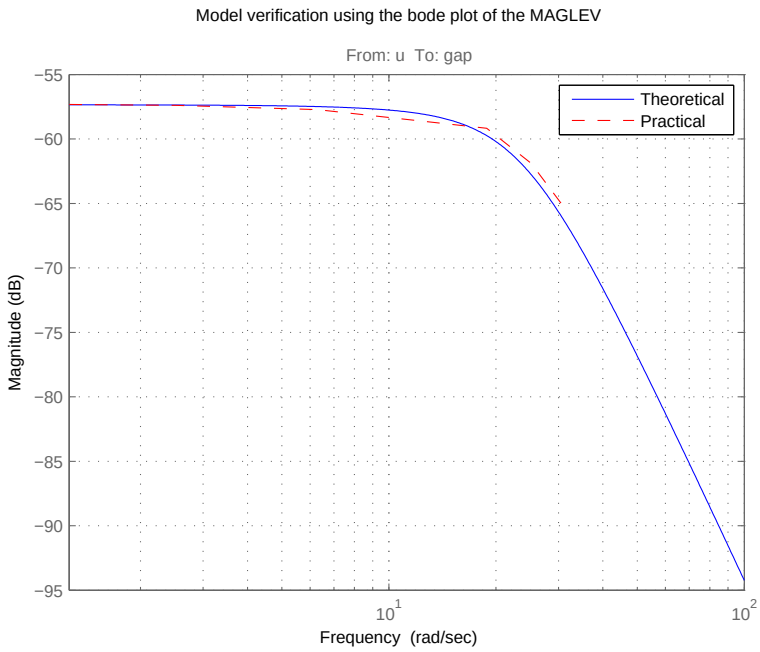

Figure 9.13: Theoretical and practical Bode plot for the MAGLEV rig.

9.3 Experimental results

In this section practical results for the real application are presented via classical and modern control strategies under fault-free conditions. Since a shaker is not available to inject disturbances to the track the problem will be formulated as tracking (i.e inject a sinusoidal changes around the operating point). For further studies on the disturbance rejection can be done as future work.

9.3.1 Classical control implementation

In this case, the same configuration is taken into account as in the model validation section (see Fig. 9.12). PA and PI controllers are used for the outer

and inner loops respectively while a low pass filter is used at the output of the PA with $\omega_c = 190 rad/s$ in order to reduce the noise level on the driving signal. Figure 9.12 illustrates the concept while the objective functions used for the optimisation algorithm are given as

$$\phi_1 = \int_0^t |(z_t - z)_{ref} - (z_t - z)_{act}| dt \tag{9.6}$$

$$\phi_2 = \int_0^t |u_{coil}| dt \tag{9.7}$$

where ϕ_1 is the integral absolute error between the reference and the actual air gap and ϕ_2 is the integral absolute error of the driving signal (u_{coil}). The corresponding design limitations are listed on Table 9.3. Sufficient robustness is achieved using a phase margin between $35^o - 45^o$ and the inner loop bandwidth is allowed to be within $50 - 70Hz$. The outer loop bandwidth is allowed from $5 - 15Hz$ and the maximum air gap deflection is no more than $3mm$.

Table 9.3: MAGLEV Suspension rig constraints using the classical control.

	Constrains	Value
g_1	Max air-gap deviation (det),$((z_t - z)_p)$	$\leq 3mm$
g_2	Phase margin, (PM)	$\leq 45^o$
g_3	Phase margin, (PM)	$\geq 35^o$
g_4	Inner bandwidth ($f_{b_{in}}$)	$\leq 70Hz$
g_5	Inner bandwidth ($f_{b_{in}}$)	$\geq 50Hz$
g_6	Outer bandwidth ($f_{b_{out}}$)	$\leq 15Hz$
g_7	Outer bandwidth ($f_{b_{out}}$)	$\geq 5Hz$

The controllers parameters are selected with a closed-loop response which results to the minimum IAE between the reference and the measured air gap, (i.e $min[\phi_1]$). The controllers are shown in (9.4) and (9.5). The injected sinusoidal signal instructs the electromagnets to vary by $\pm 2mm$ around the operating ($5mm$) air gap. The response to the reference air gap signal is depicted in Fig. 9.14. Figure 9.14(a) shows the actual $(z_t - z)_{act}$ and the reference $(z_t - z)_{ref}$ air gap signals. As it can be seen the actual air gap cannot

follow the reference signal precisely but it is fairly close. The corresponding driving signal is depicted in Fig. 9.14(b). The amplitude is limited to a maximum of about $1.5V$ while the level of the noise is low without having any serious effect on the actual air gap. A demo of the current control strategy is uploaded on Youtube by Michail [2008a] (The link is with the reference).

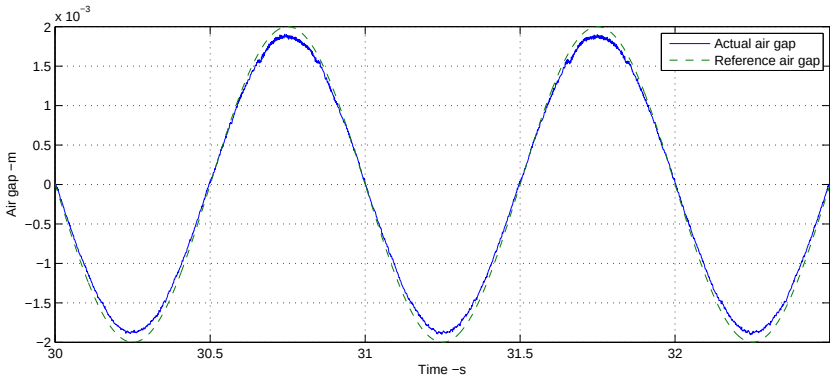

(a) Actual and reference air gap signals.

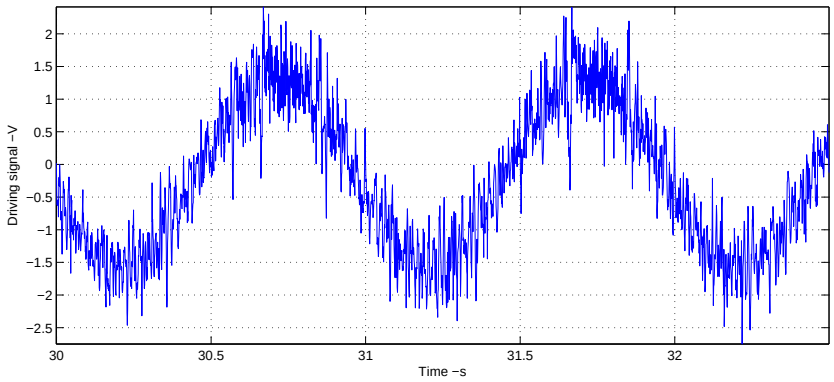

(b) Coil's driving signal.

Figure 9.14: Closed-loop response using the air gap/flux measurements.

Another important point in this design is the scaling and polarity of the signals that have to be adjusted in order for the controllers to respond with proper signal levels to changes. In order to make sure that signal scaling is correct the practical results are compared with the corresponding simulations during the execution of this experiment.

9.3.2 Sensor optimisation via LQG

In this section, the sensor optimisation via LQG control is presented. Detailed description of this is given in Chapter 6 with the process summarised below:

(i) During the first part, LQR weights are optimally tuned using the NSGA-II in order to achieve an optimum Pareto front of controllers which shows the trade-off between the objective functions. From the optimum Pareto front of the resulting controllers the one that results to the desired closed-loop response is selected using the user's controller selection criteria. The selected closed-loop response serves as the reference or 'ideal' response for the Kalman optimum tuning in the second part described next.

(ii) The second part is the Kalman estimator tuning where the sensor information becomes critical. Particularly, the Kalman estimator is optimally tuned to achieve the 'ideal' closed-loop response for every feasible sensor set. As described in Chapter 6 the V and W matrices have to be tuned to precisely estimate the states. In this problem the V is constructed from the noise covariance of the measurements while W is the tunable process noise quantity.

State feedback control tuning and implementation

The state feedback control is taken into account in this section under fault free conditions. The block diagram in Fig. 9.15 illustrates the state feedback control of the non-linear MAGLEV rig using the current, air gap, velocity and the integral of the error between the measured and the reference air gap signals ($e_{(z_t-z)_{ref},(z_t-z)}$). Note that the velocity signal is derived by integrating the acceleration measurement as explained in Section 9.2.3. The closed-loop response should be able to follow the air gap reference signal of sinusoidal form with $\pm 3mm$ changes around the operating air gap point. The tuning process takes into account the state regulation instead of output regulation as in Chapter 6. The Q and R matrices are given as follows

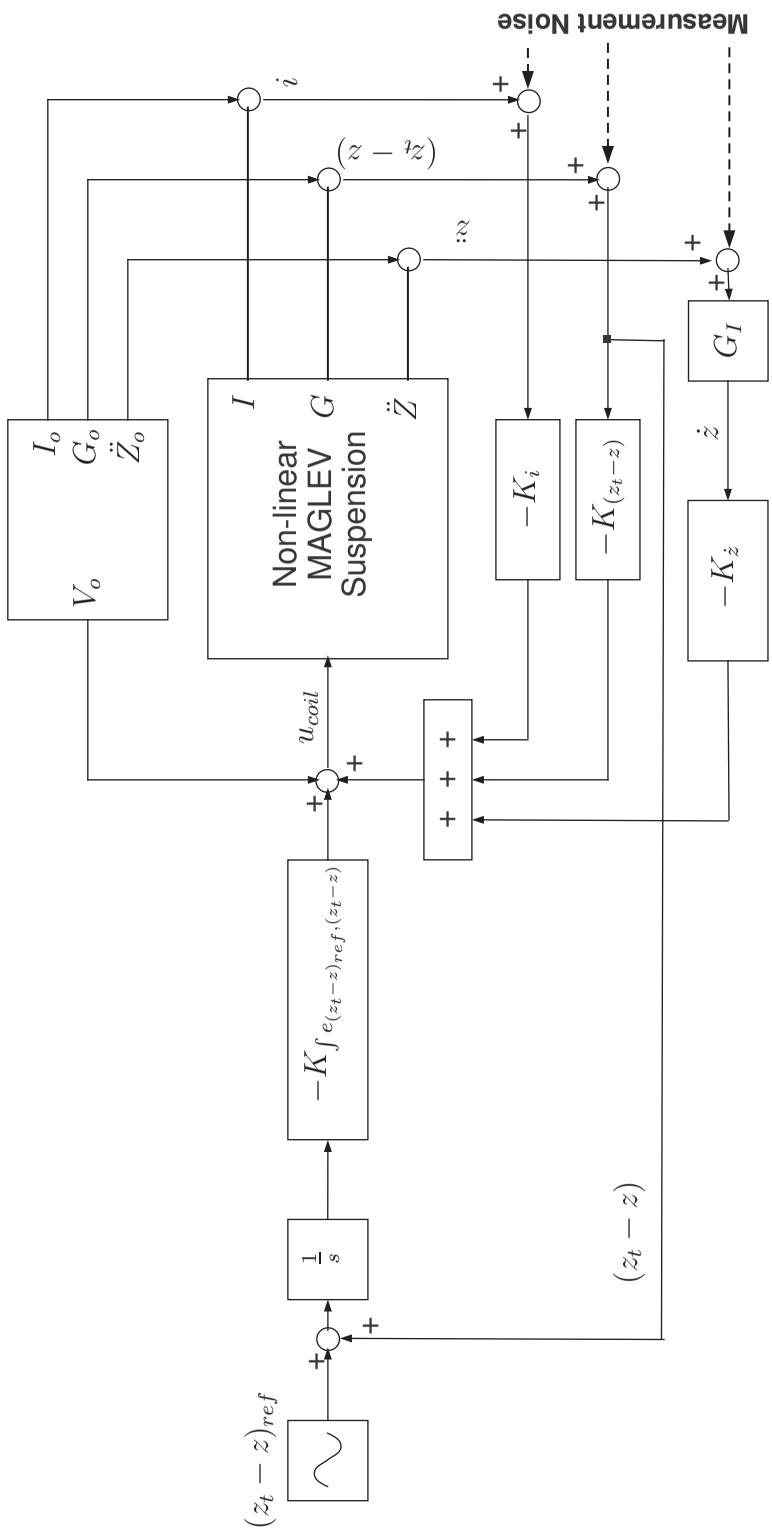

Figure 9.15: State feedback control of the $25kg$ MAGLEV suspension rig.

$$Q = diag(q_i, q_{\dot{z}}, q_{(z_t-z)}, q_{\int e_{(z_t-z)mea,(z_t-z)}}) \quad R = 1/r_{u_{coil}} \tag{9.8}$$

The state feedback tuning is done using three objective functions given as

$$\phi_1 = \int_0^t |(z_t - z)_{ref} - (z_t - z)|dt \tag{9.9}$$

$$\phi_2 = \int_0^t |u_{coil}|dt \tag{9.10}$$

$$\phi_3 = u_{coil_{noise}} \tag{9.11}$$

where, ϕ_1 is the IAE between the reference and the measured air gap signals, ϕ_2 is the integral of the input voltage and ϕ_3 is the level of the noise on the input voltage. The constraints for this problem setup are listed in Table 9.4. From the optimum Pareto front of the objectives (not shown

Table 9.4: MAGLEV Suspension rig constraints using state feedback control.

	Constrains	Value
g_1	Max air-gap deviation (det),$((z_t - z)_p)$	$\leq 3mm$
g_2	Input voltage, (u_{coil})	$\leq 3V$
g_3	Closed-loop Bandwidth $(f_{b_{cl}})$	$\leq 10Hz$
g_4	Closed-loop Bandwidth $(f_{b_{cl}})$	$\geq 6Hz$

here) the controller that results to the minimum noise level on the driving signal is selected $(min[u_{coil_{noise}}])$ with the following state feedback gains: $K_i = -19.17V/A$, $K_{\dot{z}} = -306.91V/ms^{-2}$, $K_{(z_t-z)} = 3.0855 \times 10^4 V/m$ and $K_{e_{(z_t-z)_{ref},(z_t-z)}} = 1.3177 \times 10^5 V/m$.

The closed-loop response to the reference signal is illustrated in Fig. 9.16. As it can be seen from Fig. 9.16(a) the electromagnet varies around the nominal air gap by $\pm 3mm$ in sinusoidal motions. However, there is a small error between the reference and the actual air gap. The driving signal is

depicted in Fig. 9.16(b) while a demo is uploaded on Youtube by Michail [2008b] (web link).

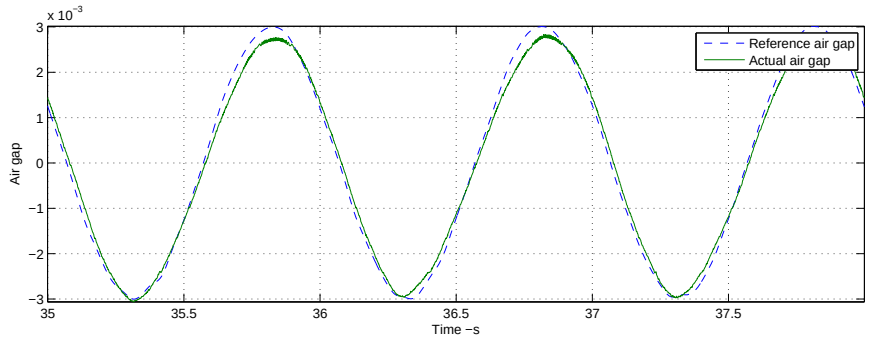

(a) Actual and reference air gap signals using state feedback control.

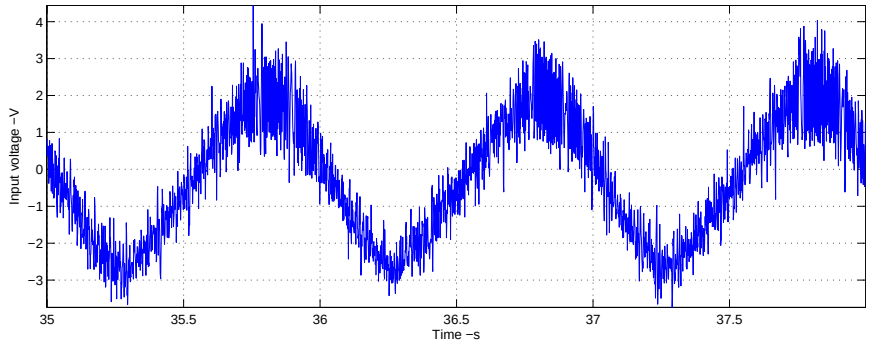

(b) Coil's driving signal using state feedback control.

Figure 9.16: Closed-loop response of the MAGLEV suspension using the optimally tuned state feedback control gains.

Linear Quadratic Gaussian control tuning and implementation

During the first part, the LQR weights are optimally tuned using the NSGA-II in order to achieve an optimum Pareto front of controllers that represents the trade-off between the objective functions. From the optimum Pareto front of the resulting controllers the one that results to the desired closed-loop response is selected. The state feedback gains that results to the minimum level of the noise on the input voltage are selected ($min[u_{coil_{noise}}]$) and given as $K_i = -19.17V/A$, $K_{\dot{z}} = -306.91V/ms^{-2}$, $K_{(z_t-z)} = 3.0855 \times 10^4 V/m$ and $K_{e_{(z_t-z)_{ref},(z_t-z)}} = 1.3177 \times 10^5 V/m$. This represents the 'ideal' or reference

closed-loop response for the Kalman estimator tuning.

The block diagram of the sensor optimisation via LQG for the MAGLEV suspension is depicted in Fig. 9.17. Two self-zeros integrators are required, one for the flux and one for the acceleration in order to produce the flux density and the velocity respectively. The Kalman estimator is optimally tuned to achieve the 'ideal' closed-loop response for every feasible sensor set. As described in Chapter 6 the V and W matrices have to be tuned to properly estimate the states. V is constructed from the noise covariance of the measurements, it is not straightforward calculating the sensors' output noise covariance in practical situations. Datasheets give information on noise but not considering external interference and therefore in this case the noise covariance is calculated from the time history response by stabilising the MAGLEV suspension using either classical or state feedback. The noise covariance for each sensor is assumed to be $V = diag(V_i, V_b, V_{z_t-z}, V_{\dot{z}}, V_{\ddot{z}})$ where $V_i = 7.44 \times 10^{-3}$, $V_b = 2.27 \times 10^{-6}$,$V_{(z_t-z)} = 2.50 \times 10^{-3}$,$V_{\dot{z}} = 7.04 \times 10^{-5}$,$V_{\ddot{z}} = 1.00 \times 10^{-3}$. The tuning of the Kalman filter is done by assuming the process noise affects the states, hence $W = diag(W_i, W_{\dot{z}}, W_{z_t-z})$.

Three objective functions to be minimised ensure proper state estimation, i.e

$$\phi_1 = \int_0^t |x_{o_i} - x_{a_i}|dt \tag{9.12}$$

$$\phi_2 = \int_0^t |x_{o_{\dot{z}}} - x_{a_{\dot{z}}}|dt \tag{9.13}$$

$$\phi_3 = \int_0^t |x_{o_{(z_t-z)}} - x_{a_{z_t-z}}|dt \tag{9.14}$$

where, as from Chapter 6, x_o is the vector of the monitored states of interest of the closed-loop with the LQR state feedback (e.g. 'ideal' closed-loop response) and x_a the monitored states of interest of the closed-loop with the overall LQG controller, e.g. actual closed loop (prior to adding sensor noise).

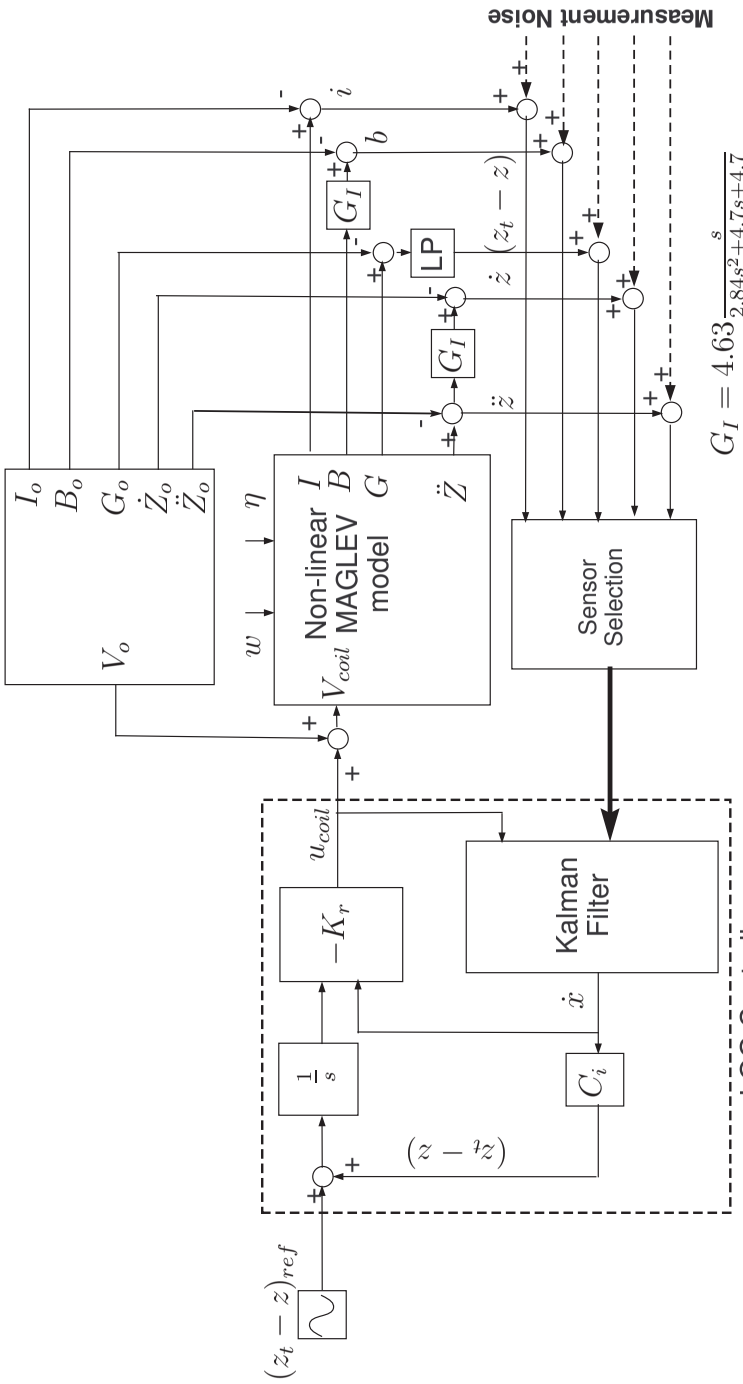

Figure 9.17: Sensor optimisation via LQG for non-linear control of the MAGLEV suspension

To ensure the estimation is correct, three constraints (one for each state estimate) have been assigned as follows:

$$g_1 \equiv \int_0^t |x_{o_i} - x_{a_i}| dt \leq 5\% \tag{9.15}$$

$$g_2 \equiv \int_0^t |x_{o_{\dot{z}}} - x_{a_{\dot{z}}}| dt \leq 15\% \tag{9.16}$$

$$g_3 \equiv \int_0^t |x_{o_{(z_t - z)}} - x_{a_{(z_t - z)}}| dt \leq 5\% \tag{9.17}$$

$$g_4 \equiv u_{coil_{rms}} \leq 10V \tag{9.18}$$

For the NSGA-II optimisation process the parameters' values are listed in Table 9.5.

Table 9.5: NSGA-II parameters for the LQG tuning of the $25kg$ suspension.

Maximum generation	100
Population size	20
Crossover probability	0.9
Mutation probability	$1/n_r$ $(n_r = 3)$

The sensor optimisation algorithm using the LQG for the MAGLEV suspension rig results in 20/31 sensor sets that satisfy the required performance (based on ideal LQR closed-loop response). Some randomly selected sensor sets are listed in Table 9.6. As it can be seen, the current and acceleration measurements are sufficient to controlling the maglev suspension but the flux measurement fails to control. Note that for the systematic framework, in Chapter 6, the current measurement had some constraint violation (settling time) but within this problem setup it can estimate the states in a satisfactory manner. The flux density measurement was able to satisfy the required performance while here it is not possible. However, the problem setup and the performance requirements are slightly different in the systematic framework presented and in the practical implementation.

The practical implementation of the Kalman estimator is presented next.

Table 9.6: Sensor optimisation results with LQG for the MAGLEV suspension rig.

	Sensor set	Ω
id:1	i	✓
id:2	b	x
id:3	$\ddot{z}$	✓
id:4	i, b	✓
id:5	$i, \ddot{z}$	✓
id:6	$b, (z_t - z)$	x
id:7	$i, b, (z_t - z)$	✓
id:8	$i, b, \ddot{z}$	✓
id:9	$b, (z_t - z), \dot{z}$	x
id:10	$b, (z_t - z), \ddot{z}$	✓
id:11	$i, (z_t - z), \dot{z}, \ddot{z}$	✓
id:12	$i, b, (z_t - z), \dot{z}, \ddot{z}$	✓

To test the estimation of the states the MAGLEV suspension rig is stabilised by the state feedback control (note that the states can be measured) while the selected sensors are fed to the Kalman estimator. In this way the measured and the estimated states can be compared. Introducing three of the estimated states simultaneously in the closed-loop response cause instability therefore, the states are introduced one-by-one using software switches as depicted in Fig. 9.18. As it can be see from the diagram, using switches the measured states can be replaced by the estimated states via switches. With this method it was found that the current and velocity states were successfully used to stabilise the MAGLEV suspension but as soon as the air gap estimate was introduced stability degraded (driven unstable). For unknown reasons the estimated air gap signal cause instability. Hence, two of the states were used along with the air gap measured state to demonstrate the state estimations using id:1 and id:8 (one or three measurements). The states estimation is compared with the measured states using single (i.e current) and triple measurements (current, flux density, acceleration) in Fig. 9.19 and Fig. 9.20 respectively. In both cases the current state estimation is sufficient. The estimated velocity state is not precisely the same as the measured one

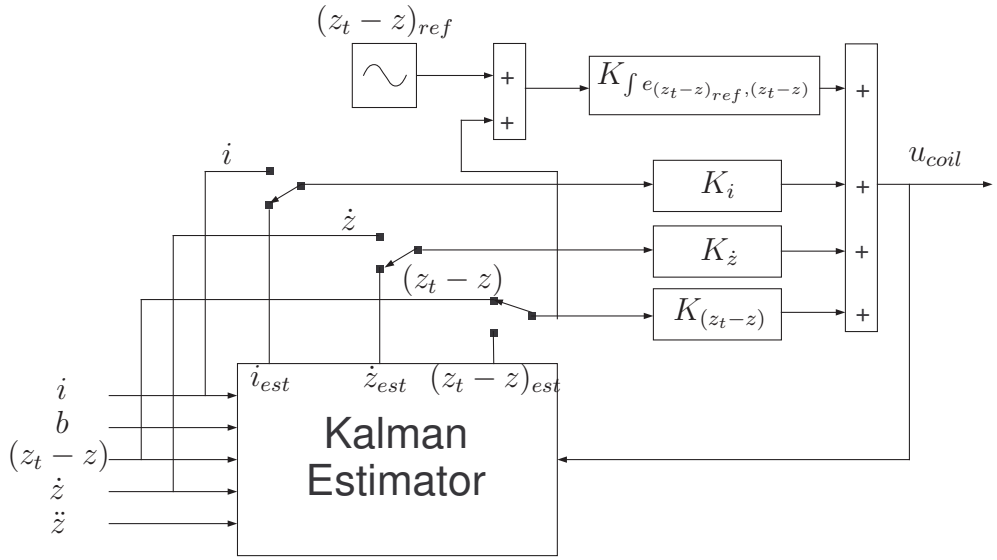

Figure 9.18: Switching between measured and estimated states

however, it is sufficiently used to stabilise the suspension. There were some problems faced in using the air gap estimate in the practical implementation although further manual tuning of the Kalman filter improved the estimation. This is an interesting issue for further investigation.

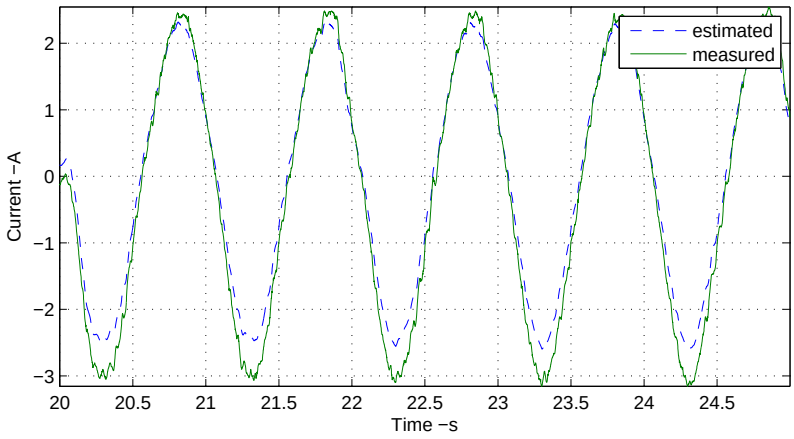

(a) Estimated and measured current state.

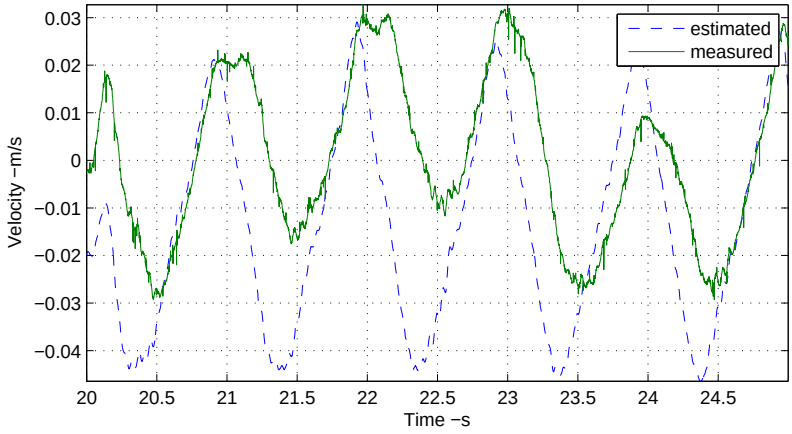

(b) Estimated and measured velocity state.

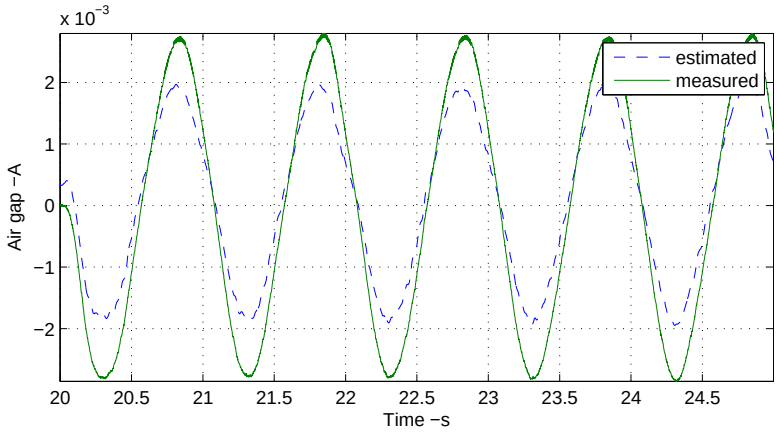

(c) Estimated and measured air gap state.

Figure 9.19: Estimated and measured states using the current measurement (id:1).

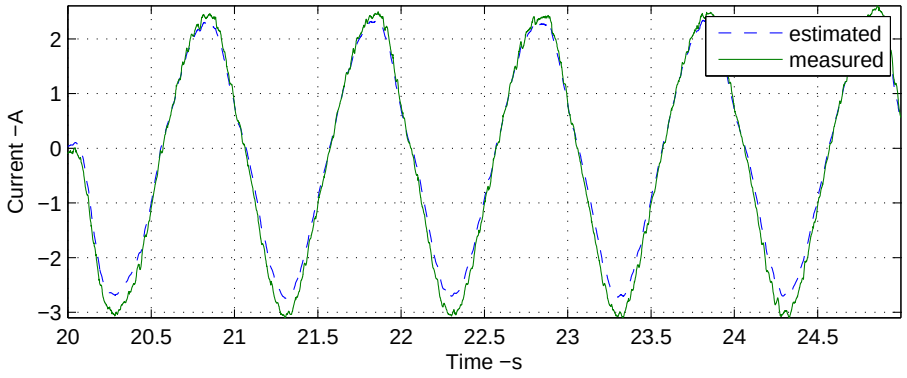

(a) Estimated and measured current state.

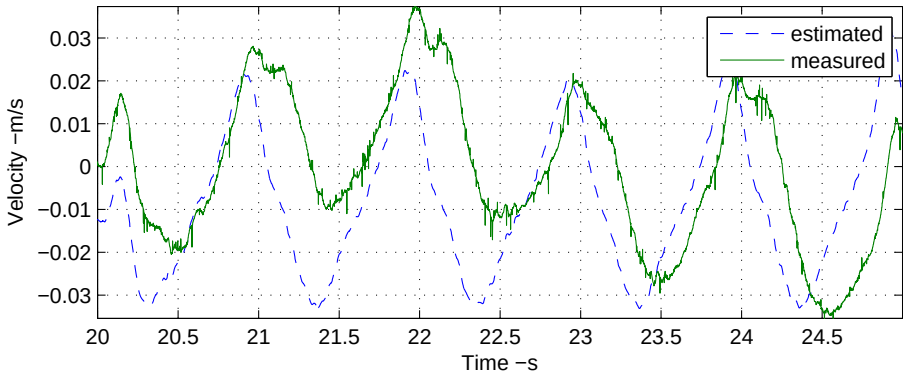

(b) Estimated and measured velocity state.

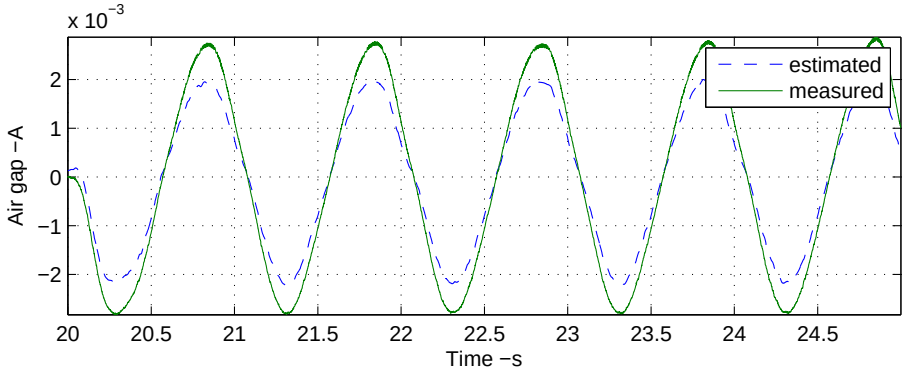

(c) Estimated and measured air gap state.

Figure 9.20: Estimated and measured states using the current, flux and acceleration measurements (id:8).

9.4 Summary

A $25kg$ MAGLEV rig suspension is designed and constructed aiming to practically test the sensor optimisation frameworks. The design of the mechanical parts was easier compared to the electronic circuits implementation. Particularly, the switching mode power amplifier was difficult to implement and there was a lot of problems related to MOSFET ringing which appears on the measurements as a form of noise. However, the problems were accommodated and the power amplifier worked properly. All five measurements are successfully implemented giving relatively clear measurements with correct scaling and polarity. The scaling as well as the polarity of the measurements are very critical and they were carefully verified.

The classical control strategy optimally tuned using the NSGA-II was successfully implemented with the required performance. The electromagnets are successfully suspended $5mm$ below the track while instructed oscillations around the operating point are followed as expected.

The sensor optimisation framework via LQG is successfully applied on the 25kg EMS system and tuned 20 out of 31 sensor sets that found to satisfy the required constraints. From the 20 sensor sets two were selected from practical test on the MAGLEV rig, i.e. Id:1 and Id:8 that include single and triple sensors were tested. The results show that the state estimation can be satisfactory and the suspension is stabilised under the estimated current and velocity states, and the measured air gap state.

Further experiments can include deterministic and stochastic inputs from the track using a shaker(although this was not possible in the current setup due to time constraints).

Chapter 10

Conclusions, discussion and future work

10.1 Conclusions and discussion

A novel systematic framework is presented (and extended for a series of control approaches) to produce optimised sensor configurations for control and fault tolerance applied to a MAGLEV suspension system. The modern control strategies, evolutionary algorithms, fault tolerant control and the MAGLEV suspension are combined in order to demonstrate the optimised sensor configurations for control and fault tolerance. For optimal tuning of the performance genetic algorithms have been merged with the sensor optimisation framework. In Particular, the recently developed Non-Dominated Sorting Genetic Algorithm-II is found to be a very powerful optimisation tool and it is incorporated into the sensor optimisation framework successfully. In fact, the NSGA-II successfully recovers the Pareto-optimality between the assigned objective functions for every feasible sensor set.

Genetic algorithms have been widely used in control systems. Many applications have be encountered using MOGA but fewer for the more recent NSGA-II. GAs are very useful for problems where multiple objectives have to be minimised especially when they are subject specific constraints.

Penalty functions are used to avoid the infeasible area of the solution. To demonstrate the NSGA-II properties and validity of the code two examples where presented, while the efficacy of NSGA-II is shown where sensor optimisation is demonstrated.

The non-linear equations of the EMS (Electromagnetic Suspension) system are derived using Newton's and Kirchoff's laws. An LTI state space model is used for the linear controller design purposes which is derived from the non-linear equations. Moreover the EMS suspension system has non-trivial practical requirements due to the multiobjective nature of the problem that is posed subject to number of design constraints. In particular, such a system should be able to support a very large load with a small air gap (in the region of mm), follow the track gradients and reject the unintended changes of the track due to irregularities. Generally, for the multiobjective optimisation process of each sensor set the problem is posed as follows: *"minimise the vertical acceleration and coil's excitation current from the stochastic inputs to the suspension subject to enhancing the deterministic inputs to the suspension from gradients onto the track"*. Furthermore, the MAGLEV suspension, being an unstable and safety-critical system, is sensitive to faults. Particularly, one sensor fault can lead to disaster if not accommodated on time. Under single or multiple sensor fault conditions the suspension will either fall off or stick to the track if no remedial actions are taken. In order to satisfy optimum performance and sensor fault tolerance five measurements are available, i.e the current, flux density, air gap, vertical velocity and vertical acceleration. Using combinations of the measurements 31 feasible sensor sets are available to select from by using the proposed framework.

A $25kg$ MAGLEV suspension was constructed and the classical control structures that are optimally tuned using GAs were successfully demonstrated. An attempt on implementing sensor optimisation framework via LQG controller design was considered. The optimal tuning for the performance using the non-linear model was successfully done for 23/31

sensor sets found to satisfy the constraints. Control of the suspension was achieved using two estimated states while the air gap signal was measured instead of feeding the estimated signal (the estimated signal was driving the system unstable).

Two sensor configurations via classical control strategies were studied, with inner feedback structure. The proposed genetic algorithm (NSGA-II) has been proved to be very useful as it recovers optimum Pareto fronts in both sensor configurations, i.e air gap(outer)/flux density(inner) and air gap(outer)/current(inner). Both structures were optimally tuned and compared from the performance point of view. The air gap(outer)/flux density(inner) configuration proved superior to the air gap/current structure. In the classical (inner loop) feedback structure the notion of multiple sensor configurations is rather restricted as two feasible structures are investigated and also relate to realistic implementations. The major outcome in this sense was the use of NSGA-II tuning and procedure given an insight for the furthering of the methodology. In particular employing modern control strategies for sensor optimisation, increases complexity and computational effort. To simplify the sensor set selection in the sensor optimisation frameworks a metric to identify which sensor set is able to satisfy the required performance is introduced. This refers to the overall constraint violation function Ω used to indicate if a sensor set satisfies the constraints or not. This function is efficient not only for constraint handling but also for the selection of the best controller(s) for a sensor set.

It was found that measurement noise appears on the input voltage. Although the MAGLEV suspension has low pass filter characteristics and the amplitude of the noise is largely attenuated, it has to be kept as low as possible. The proposed sensor optimisation frameworks accommodate this issue by adding an extra objective function.

At first the proposed systematic framework employs modern control approaches using Linear Quadratic Gaussian control. The particular sensor

optimisation algorithm is performed in two parts. The first part is the Linear Quadratic Regulator tuning where an optimum Pareto front of controllers is recovered (note here state feedback is used) between the objective functions. The selected closed-loop response of the LQR is used as the 'ideal' reference for the sensor optimisation in the second part. The selection of the controller is done using the user's controller selection criteria f_{c_i} and f_u. The state feedback gain, K_r, that results to the best ride quality from the stochastic input track profile is selected (The overall constraint violation function (Ω) has to be zero in order to ensure that no constraint violation occurs). The next step is where the sensor information becomes important with the Kalman estimator in the loop (note the importance of sensor selection directly related to the Kalman filter design). The Kalman estimator is optimally tuned to achieve a closed-loop response similar to the 'ideal' for every feasible sensor set, i.e the desired closed-loop response (with both closed-loop deterministic and stochastic inputs) using LQR control. On completion of the sensor optimisation process a number of optimally tuned controllers are available for each sensor set. In order to select the best controller, the overall constraint violation function (Ω) and precision of the states estimation (S_f) are used. It was found that 24/31 sensor sets satisfy the closed-loop response requirements (same as 'ideal' response with LQR). Two single measurements (vertical acceleration or flux density) are found to satisfy the performance requirements while similar performance can be achieved using more sensors. From a control point of view one measurement can be selected under these circumstances, i.e either vertical acceleration or flux density (but with hardware redundancy if no switching with other sensors is employed). Robustness tests to load variation and perturbed operating point using the acceleration measurement ($\ddot{z}$) and current, flux density and acceleration ($i, b, \ddot{z}$) have been done. The results show that both stability and performance are maintained for both sensor sets under uncertain and load variation conditions.

The sensor optimisation framework is extended to accommodate multi-objective (M.O.) $\mathcal{H}_\infty$ robust control design methodologies. It was found that

incorporating the $\mathcal{H}_\infty$ norm was sufficient but this can be extended in an $\mathcal{H}_\infty/\mathcal{H}_2$ format. M.O. $\mathcal{H}_\infty$ robust control design is combined with NSGA-II to recover the optimum Pareto front between the objective functions for every feasible sensor set of the MAGLEV suspension. The optimum Pareto front is represented by 50 (population number) optimally tuned controllers. This means that according to $N_c = Pop_{num} \times N_s$ at the completion of the sensor optimisation framework 1550 optimally tuned controllers are reported. In order to select the desired closed-loop response for each sensor set the conditions are taken into account: (i) The overall constraint violation function (Ω) that is used to chose controllers that don't violate any constraint (for each sensor set). Of course, the controller selection using Ω, may result to a group of closed-loop responses that do not violate any constraint. Optimally tuned controllers were found to satisfy the closed-loop response required constraints for 29 out of 31 feasible sensor sets. Single measurements including flux density, air gap or vertical acceleration were found to satisfy all constraints. In order to select the best controller for each of the corresponding sensor sets a second condition is considered. (ii) The best controller selection is done using the user's controller selection criteria f_{c_i} and f_u. Using these two criteria the best controller is chosen that results to a desired closed-loop response. In fact, the proposed framework gives to the user the flexibility to select the desired closed-loop response for each sensor set. Finally, 18 out of 31 sensor sets found to satisfy Ω, f_{c_i} and f_u. For control purposes a single measurement can be used. The closed-loop response to load variation and operating point perturbations have been tested under deterministic and stochastic track inputs for the acceleration measurements and sensor set that includes current, flux and acceleration. Results show that under those conditions stability is maintained as well as performance.

Next, the proposed framework is extended towards using the $\mathcal{H}_\infty$ loop shaping design procedure (LSDP) with similar flowchart but with some code modifications. LSDP requires the air gap as a standard measurement leading to 16 sensor sets. In this case, for loop shaping, one weighting filter is required per sensor, with the number of variables dynamically updated in order to

increase the framework efficiency. The number of maximum generations is dynamically updated between 150-200. Particularly, it was found that for 1,2 and 3 sensors 150 generations are sufficient to recover the optimum Pareto front while for 4 and 5 sensors a maximum of 200 generations is enough. Nevertheless, if weighting filters of increased complexity are used the problem could require higher number of generations with larger population resulting to much more completion time for the framework. Moreover, if a model is considered with more sensors (i.e 10 sensors) and subsequently 10 weighting filters are used the completion of the framework may need very large computational time. There exist 16 feasible sensor sets to optimise while the optimum Pareto front between the objectives for each sensor set is created from 50 optimally tuned controllers. After the completion of the optimisation framework there exist 800 optimally tuned controllers according to $N_c = Pop_{num} \times N_s$. The best controller selection for each sensor set is done in the same manner as before. The controller(s) that result to the satisfaction of the constraints are selected and then the controller that satisfy the user's controller selection criteria (f_{c_i}, f_u) is chosen. Eleven out of 16 sensor sets are found to satisfy the constraints and user's controller selection criteria. The proposed framework using LSDP concludes that the minimum number of sensors that can be used for control is 2 (air gap and vertical acceleration). In the LSDP approach is the air gap measurement is constantly used and therefore no air gap sensor failure can be afforded. In such case, triple redundancy of the air gap sensor overcomes the problem but in the expense increase cost in the control system. Robustness tests to load variations and perturbed operating point are performed under stochastic and deterministic inputs of the suspension concluding that the closed-loop response to such inputs do not affect stability and performance.

The most important points from the proposed systematic framework extensions are highlighted in Table 10.1. Using LQG and M.O. $\mathcal{H}_\infty$ robust control 31 feasible sensor sets exist whereas using the LSDP 16 feasible sensor sets exist. Employing genetic algorithms into the framework is time consuming but efficient strategy for the multiobjective constraint

optimisation of each sensor set. Using the M.O. $\mathcal{H}_\infty$ design 29 out of 31 sensor sets are found to satisfy the constraints while 24 out of 31 sensor sets for the LQG and 11 out of 16 for the LSDP. Single measurements are found for the M.O. $\mathcal{H}_\infty$ and the LQG control strategies while for the LSDP 2 sensors are the minimum that can be used to control the suspension. Because each one of the control strategies has different problem formulation, the completion time differs for each approach. M.O. $\mathcal{H}_\infty$ robust control requires the highest (175 hours) while for LQG and LSDP 54 and 42 hours respectively.

Table 10.1: Systematic frameworks overview.

	LQG	M.O. $\mathcal{H}_\infty$	LSDP
Number of feasible sensor sets	31	31	16
Sensor sets found to satisfy Ω	24/31	29/31	11/16
Sensor sets found to satisfy user's controller selection criteria	24/31	18/31	11/16
Minimum number of sensors that can be used for control	1 b or $\ddot{z}$	1 b or $\ddot{z}$ or $(z_t - z)$	2 $(z_t - z)$ and $\ddot{z}$
Completion time for framework	54 hours	175 hours	42 hours

b-Flux density, $\ddot{z}$- Vertical acceleration, $(z_t - z)$- Air gap

Two sensor fault tolerant approaches were studied in this thesis. One approach involves a combination of classical control strategy and analytical redundancy to recover performance for an air gap sensor failure and the other one using LQG control aims to recover performance with to multiple sensor faults. In the former case the air gap sensor failure is masked using the estimated and the calculated air gap signals. This approach avoids air gap sensor redundancy however is restricted to single sensor failure (air gap sensor). Considering the optimised sensor configurations via LQG multiple sensor faults can be accommodated using active fault tolerance approaches. In fact, the sensor selection is considered with fault tolerant extensions were the best sensor set is selected that ensures optimum performance under any possible fault conditions via controller reconfiguration

Table 10.2: Sensor fault conditions with current, flux density and acceleration.

Sensor set	Healthy Sensors	Faulty Sensors	Kalman estimator	Successful performance recovery
$i, b, \ddot{z}$	$i, b, \ddot{z}$	-	$K_{i,b,\ddot{z}}$	
	i, b	$\ddot{z}$	$K_{i,b}$	✓
	$b, \ddot{z}$	i	$K_{b,\ddot{z}}$	✓
	$i, \ddot{z}$	b	$K_{i,\ddot{z}}$	✓
	i	$b, \ddot{z}$	K_i	x
	b	$i, \ddot{z}$	K_b	✓
	$\ddot{z}$	i, b	$K_{\ddot{z}}$	✓

(active fault tolerant control design). Investigating the optimised sensor configurations via LQG control it is possible to locate the best possible sensor set that could be used for multiple sensor fault tolerance so that the minimum numbers of sensors are used. As described in Chapter 8, for the MAGLEV suspension, it was found that the current, the flux density and the acceleration measurements are good options since they can recover the optimum performance under multiple sensor faults. Table 10.2 tabulates the possible sensor fault conditions that can be accommodated. Only two conditions cannot be accommodated. One is when all sensors fail and when the current and flux fail. In such case, the stability cannot be maintained during transition from the state change. Although is not likely for two sensors to fail at the same moment, sensor redundancy can be used for one of the two sensors so that the possibility for the current measurement to remain alone is very low.

Throughout this thesis the linearised model of the MAGLEV suspension has been used in order to design linear controllers. However the MAGLEV suspension is non-linear therefore to accommodate non-linearities and ensure optimum performance and stability the controllers are tuned via simulations using the non-linear model of the suspension. In this way, stability and optimum performance of the closed-loop response are both ensured.

To summarise, the following items have been encountered in this work

- optimisation of classical control strategies for controlling a quarter car of a MAGLEV train via genetic algorithms proves the efficancy of the NSGA-II and gives an insight of the optimised sensor configurations concept
- the proposed framework via LQG control produce 31 optimised sensor configurations where 24 satisfy the constraints among them single measurements that can be used to optimally control the MAGLEV suspension.
- the proposed framework via M.O. $\mathcal{H}_\infty$ robust control design found 29/31 optimised sensor configurations that satisfy the required performance among them single measurements that can be used to optimally control the suspension.
- the proposed framework using LSDP has successfully recover 11 out of 16 sensor sets that satisfy the required performance while the minimum number of sensors to be used are two (i.e the air gap and acceleration). However, this method is that the air gap measurements can not be avoided and hence hardware redundancy for this sensor is unavoidable if sensor fault tolerance is a requirement.
- Robustness to load variations and uncertain model parameters has been tested for the three aforementioned modern control approaches maintaining stability and sufficient closed-loop performance with the corresponding sensor sets even with single measurements.
- optimised sensor configurations with LQG were investigated from a fault tolerant point of view. The results reveal that using the selected sensor set optimum, performance is maintained under most of sensor fault conditions using the minimum number of sensors.
- optimally tuned classical control strategies were successfully implemented on a $25kg$ MAGLEV suspension as well as optimally tuned

state feedback controllers. In addition the Kalman filter proved useful for a number of sensor combinations, although there were some issues with the air gap state estimation.

References

Abuzeid, M., Shen, G., Ren, L., and Pratt, I. (2006). Modelling and suspension parameter optimisation of a high speed maglev train. In *International Control Conference*, pages 138–143.

Anderson, B. D. O. and Moore, J. B. (1990). *Optimal control: Linear quadratic methods*. Prentice-Hall Inc.

Balas, G. J., Chiang, R., Packard, A., and Savonof, M. (2005). Robust control toolbox version 3, the mathworks inc.

Balas, G. J. and Young, P. M. (1999). Sensor selection via closed-loop control objectives. *IEEE Transactions on Control Systems Technology*, 7(6):692–705.

Beaven, R. W., Wright, M. T., and Seaward, D. R. (1996). Weighting function selection in the h_∞ design process. *Control Engineering Practice*, 4(5):625–633.

Blanke, M., Frei, C. W., Kraus, F., Patton, R. J., and Staroswiecki, M. (2001a). What is fault-tolerant control? *Fault Detection, Supervision and Safety for Technical Processes 2000 (SAFEPROCESS 2000), Proceedings volume from the 4th IFAC Symposium*, pages 40–51.

Blanke, M., Izadi-Zamanabadi, R., Bogh, S. A., and Lunau, C. P. (1997). Fault-tolerant control systems - a holistic view. *Control Engineering Practice*, 5(5):693–702.

Blanke, M., Kinnaert, M., Lunze, J., and Staroswiecki, M. (AUG 2003). *Diagnosis and Fault-Tolerant Control*. Springer-Verlag Berlin and Heidelberg.

Blanke, M., Staroswiecki, M., and Wu, N. E. (2001b). Concepts and methods in fault-tolerant control. *Proceedings of the American Control Conference*, 4:2606–2620.

Calderon-Espinoza, G. (2003). Model-based fault diagnosis techniques: an overview and a proposal.

Campos-Delgado, D. U., Martinez-Martinez, S., and Zhou, K. (2005). Integrated fault-tolerant scheme for a dc speed drive. *IEEE ASME Transactions on Mechatronics*, 10:419–427.

Chellaboina, V. and Ranga, M. K. (2005). Reduced order optimal control using genetic algorithms. In *Proceedings of the American Control Conference*, volume 2, pages 1407–1412.

Chilali, M. and Gahinet, P. (1996). h_∞ design with pole placement constraints: an lmi approach. *IEEE Transactions on Automatic Control*, 41(3):358–367.

Coello, C. A. C. (1999a). A comprehensive survey of evolutionary-based multiobjective optimisation techniques. *Knowledge and Information Systems*, 1(3):269–308.

Coello, C. A. C. (1999b). A survey of constraint handling techniques used with evolutionary algorithms. Technical report, Laboratorio Nacional de Informtica Avanzada.

Coello, C. A. C. (1999c). An updated survey of ga-based multiobjective optimization techniques. *Assiciation for Computing Machinery, Computing Surveys*, 32(2):109–143.

Coello, C. A. C. (2002). Theoretical and numerical constraint-handling techniques used with evolutionary algorithms: A survey of the state of the

art. *Computer Methods in Applied Mechanics and Engineering*, 191(11-12):1245–1287.

Dakev, N. V., Whidborne, J. F., Chipperfield, A. J., and Fleming, P. J. (1997). Evolutionary h_∞ design of an electromagnetic suspension control system for a maglev vehicle. *Proceedings of the Institution of Mechanical Engineers.Part I, Journal of Systems & Control Engineering*, 211(5):345–355.

Deb, K. (2001). *Multi-objective Optimization using Evolutionary Algorithms*. John Wiley and sons Ltd.

Deb, K., Pratap, A., Agarwal, S., and Meyarivan, T. (2002). A fast and elitist multiobjective genetic algorithm: Nsga-ii. *IEEE Transactions on Evolutionary Computation*, 6(2):182–197.

Debouk, R., Lafortune, S., and Teneketzis, D. (2002). On an optimization problem in sensor selection. *Discrete Event Dynamic Systems: Theory and Applications*, 12(4):417–445.

den berg, F. W. J. V., Hoefsloot, H. C. J., Boelens, H. F. M., and Smilde, A. K. (1999). Selection of optimal sensor position in a tubular reactor using robust degree of observability criteria. *Chemical Engineering Science*, 55(4):827–837.

Dreo, J., Siarry, P., Petrowski, A., and Taillard, E. (2006). *Metaheuritics for Hard Optimization*. Springer-Verlg Berlin Heidelberg, New York.

Fleming, P. J. and Fonseca, C. M. (1993). Genetic algorithms in control systems engineering: a brief introduction. *IEE Colloquium on 'Genetic Algorithms for Control Systems Engineering'*, 1:1–5.

Fleming, P. J. and Purshouse, R. C. (2002). Evolutionary algorithms in control systems engineering: A survey. *Control Engineering Practice*, 10(11):1223–1241.

Fonseca, C. M. and Fleming, P. J. (1993). Multiobjective genetic algorithms. *IEE colloquium on 'Genetic Algorithms for Control Systems Engineering'*, 1:1–5.

Fonseca, C. M. and Fleming, P. J. (1995). An overview of evolutionary algorithms in multiobjective optimization. *Evolutionary Computation*, 3(1):1–16.

Fraleigh, L. M., Guay, M., and Forbes, J. F. (2003). Sensor selection for model-based real-time optimization: relating design of experiments and design cost. *Journal of Process Control*, 13(7):667–678.

Frank, P. M. (1990). Fault diagnosis in dynamic systems using analytical and knowledge-based redundancy-a survey and some new results. *Automatica*, 26(3):459–474.

Friedland, B. (1986). *Control System Design - an introduction to state space methods*. McGraw Hill.

Friedland, B. (1996). *Advanced Control System Design*. Prentice-Hall Inc.

Frisk, E. (1996). Model-based fault diagnosis applied to an si-engine. Master Thesis, Reg nr: LiTH-ISY-EX-1679, Vehicular Systems, Linkoping University (SE).

Goldberg, D. E. (1989). *Genetic algorithm in Search, Optimisation and Machine Learning.* Addison-Wesley, USA.

Goodall, R. M. (1989). Electromagnetic suspension control without airgap measurement. *Transactions of the Institute of Measurement and Control*, 11(2):92–98.

Goodall, R. M. (1994). Dynamic characteristics in the design of maglev suspensions. *Proceedings of the Institution of Mechanical Engineers, Part F: Journal of Rail and Rapid Transit*, 208(1):33–41.

Goodall, R. M. (2000). On the robustness of flux feedback control for electro-magnetic maglev controllers. In *Proceedings of 16th International Conference on MAGLEV Systems and Linear Drives*, pages 197–202.

Goodall, R. M. (2004). Dynamics and control requirements for ems maglev suspensions. In *Proceedings on international conference on Maglev*, pages 926–934.

Goodall, R. M. (2008). Generalised design models for ems maglev. In *Proceedings of MAGLEV 2008 - The* 20^{th} *International Conference on Magnetically Levitated Systems and Linear Drives*.

Goodall, R. M. (Sep 1985). The theory of electromagnetic levitation. *Physics in Technology*, 16(5):207–213.

Gu, D. W., Petkov, P. H., and Konstantinov, M. M. (Jun 2005). *Robust Control Design with MATLAB*. Springer-Verlag London Ltd.

Hu, J., Bohn, C., and Wu, H. R. (2000). Systematic h_∞ weighting function selection and its application to the real-time control of a vertical take-off aircraft. *Control Engineering Practice*, 8(3):241–252.

Huixing, C., Zhiqiang, L., and Wensen, C. (2006). Fault tolerant control research for high-speed maglev system with sensor failure. In *Sixth World Congress on Intelligent Control and Automation*, volume 1, pages 2281–2285.

Ingimundarson, A., Hagglund, T., and Astrom, K. J. (2003). Criteria for design of pid controllers. In *Proceedings of the 2nd IFAC conference Control System Design*.

Izadi-Zamanabadi, R. and Blanke, M. (1999). A ship propulsion system as a benchmark for fault-tolerant control. *Control Engineering Practice*, 7(2):227–239.

Jager, B. D. and Wal, M. V. D. (1999). Efficient selection of inputs and outputs for robust control. In *Proceedings of the IEEE Conference on Decision and Control*, volume 5, pages 4517–4522.

Jager, B. D., Wal, M. V. D., and Kamidi, R. (1998). Large-scale rigorous actuator and sensor selection. *Proceedings of the IEEE Conference on Decision and Control*, 4:4314–4319.

Joines, J. A. and Houck, C. R. (1994). On the use of non-stationary penalty functions to solve nonlinear constrained optimization problems with ga's. In *Proceedings of the First IEEE Conference on Evolutionary Computation*, volume 2, pages 579–584.

Jones, D. F., Mirrazavi, S. K., and Tamiz, M. (2002). Multi-objective meta-heuristics: An overview of the current state-of-the-art. *European Journal of Operational Research,*, 137(1):1–9.

Kicinger, R., Arciszewski, T., and Jong, K. D. (2005). Evolutionary computation and structural design: A survey of the state-of-the-art. *Computers and Structures*, 83(23-24):1943–1978.

Konak, A., Coit, D. W., and Smith, A. E. (2006). Multi-objective optimization using genetic algorithms: A tutorial. *Reliability Engineering and System Safety*, 91(9):992–1007.

Krohling, R. A., Jaschek, H., and Rey, J. P. (1997). Designing pi/pid controllers for a motion control system based on genetic algorithms. In *Proceedings of the 1997 IEEE International Symposium on Intelligent Control*, pages 125–130.

Kwok, D. P., Leung, T. P., and Sheng, F. (1993). Genetic algorithms for optimal dynamic control of robot arms. In *Proceedings of the 19th International Conference on Industrial Electronics, Control and Instrumentation*, volume 1, pages 380–385.

Lane, D. J., Gray, W. S., and Murphy, K. M. (1997). Linear h_∞ optimal control of a two degree of freedom magnetic suspension system. In *Proceedings of the American Control Conference*, volume 3, pages 1687–1691.

Lee, H.-W., Kim, K.-C., and Lee, J. (2006). Review of maglev train technologies. *IEEE Transactions on Magnetics*, 42(7):1917–1925.

Lin, C. L., Jan, H. Y., and Shieh, N. C. (2003). Ga-based multiobjective pid control for a linear brushless dc motor. *IEEE/ASME Transactions on Mechatronics*, 8(1):56–65.

Long, Z., Xue, S., Zhang, Z., and Xie, Y. (2007). A new strategy of active fault-tolerant control for suspension system of maglev train. In *IEEE International Conference on Automation and Logistics, ICAL 2007*, pages 88–92.

Maciejowski, J. M. (1990). *Multivariable Feedback Design*. Addison-Wesley.

MacLeod, C. and Goodall, R. M. (1996). Frequency-shaping lq control of maglev suspension systems for optimal performance with deterministic and stochastic inputs. *IEE Proceedings: Control Theory and Applications*, 143(1):25–30.

Mansfield, A. N. (2007). *Electromagnets - Their Design and Contruction*. Wexford College Press.

McFarlane, D. C. and Glover, K. (1990). *Robust controller design using normilized coprime factor plant descriptions, lecture notes in control and information sciences*, volume 38. Springer-Verlag.

McFarlane, D. C. and Glover, K. (1992). A loop-shaping design procedure using h_∞ synthesis. *IEEE Transactions on Automatic Control*, 37(6):759–769.

Michail, K. (2008a). Control of the 25kg single degree of freedom maglev rig suspension using classical control strategies. http://www.youtube.com/watch?v=kXodf7WKiFs.

Michail, K. (2008b). Control of the 25kg single degree of freedom maglev rig suspension using full state feedback control. http://www.youtube.com/watch?v=TsgoF13KvYk.

Michail, K. (2008c). Demo for the 25kg single degree of freedom maglev rig suspension. http://www.youtube.com/watch?v=Y_WG4YStMxs.

Michail, K., Zolotas, A., and Goodall, R. M. (July 6-11, 2008a). Optimised sensor configurations for a maglev suspension. *Proceedings of the* 17^{th} *World Congress The internetional Federation of Automatic Control*, pages 8305–8310. http://hdl.handle.net/2134/3351.

Michail, K., Zolotas, A., Goodall, R. M., and Pearson, J. T. (2008b). Sensor optimisation via h_∞ applied to a maglev suspension system. In *WASET ICCAS 2008: International Conference on Control and Automation Systems*. http://hdl.handle.net/2134/3526.

Michail, K., Zolotas, A. C., Goodall, R., and Pearson, J. T. (2009a). Sensor optimisation via h_∞ applied to a maglev suspension system. *International Journal of Computer Systems Science and Engineering*, 5(1):43–49. http://hdl.handle.net/2134/5109.

Michail, K., Zolotas, A. C., and Goodall, R. M. (2008c). Optimised sensor configurations for a maglev suspension system. *Journal Facta Universitatis (FU) Series Mechanics, Automatic Control Robotics (MARC), Invited paper for the Special Issue on Advance Controls and Signal Processing in Active Robotic Systems*, 7(1):169–184. http://hdl.handle.net/2134/5258.

Michail, K., Zolotas, A. C., and Goodall, R. M. (2009b). Ems systems: Optimised sensor configurations for control and sensor fault tolerance. *Japan Society of Mechanical Engineers, International Symposium on Speed-up, Safety and Service Technology for Railway and Maglev Systems*. http://hdl.handle.net/2134/5061.

Michail, K., Zolotas, A. C., Goodall, R. M., and Pearson, J. T. (2008d). Maglev suspensions - a sensor optimisation framework. In 16^{th} *Mediterranean Conference on Control and Automation*, pages 1514–1519. http://hdl.handle.net/2134/3350.

Michail, K., Zolotas, A. C., Goodall, R. M., and Pearson, J. T. (2009c). Fault tolerant control for ems systems with sensor failure. 17^{th}

Mediterranean Conference on Control and Automation, pages 712–717. http://hdl.handle.net/2134/4997.

Mohamed, A. M., Matsumura, F., Namerikawa, T., and Lee, J.-H. (1997). Q-parameterization/ μ control of an electromagnetic suspension system. In *Proceedings of the 1997 IEEE International Conference on Control Applications*, pages 604–608.

Morishita, M. (1996). Robust controller design for maglev transport vehicles with a guide-effective electromagnetic suspension system. In *Proceedings of the 35th IEEE Decision and Control*, volume 2, pages 1242–1244.

Morishita, M., Azukizawa, T., Kanda, S., Tamura, N., and Yokoyama, T. (1989). New maglev system for magnetically levitated carrier system. *IEEE Transactions on Vehicular Technology*, 38(4):230–236.

Mushini, R. and Simon, D. (2005). On optimization of sensor selection for aircraft gas turbine engines. In *Proceedings of the* 18^th *International Conference on Systems Engineering, IICSEng 2005*, pages 9–14.

Neumann, D. and Araujo, H. X. D. (2004). Mixed h_2/h_∞ control for uncertain systems under pole placement constraints using genetic algorithms and lmis. In *Proceedings of the 2004 IEEE International Symposium on Intelligent Control - 2004 ISIC*, pages 460–465.

Niemann, H. and Stoustrup, J. (2005). Passive fault tolerant control of a double inverted pendulum - a case study. *Control Engineering Practice*, 13(8):1047–1059.

Obika, M. and Yamamoto, T. (2005). An evolutionary design of robust pid controllers. In *IEEE International Conference on Mechatronics and Automation, ICMA 2005*, pages 101–106.

Obinata, G. and Anderson, B. D. O. (2001). Model reduction for control system design.

Ortega, M. G. and Rubio, F. R. (2004). Systematic design of weighting matrices for the h_∞ mixed sensitivity problem. *Journal of Process Control*, 14(1):89–98.

Paddison, J. E. (1995). Advanced control strategies for maglev suspension systems. PhD Thesis, Loughborough Univeristy (UK), Department of Electronic and Electrical Engineering.

Panagopoulos, H., Astrom, K. J., and Hagglund, T. (2002). Design of pid controllers based on constrained optimisation. *IEE Proceedings Control Theory and Applications*, 149(1):32–40.

Patton, R. J. (1993). Robustness issues in fault-tolerant control. *IEE Colloquium on Fault Diagnosis and Control System Reconfiguration*, pages 1–25.

Patton, R. J. (1997a). Fault-tolerant control: The 1997 situation. volume 3 of *In IFAC Symposium on Fault Detection Supervision and Safety for Technical Processes*, pages 1029–1052.

Patton, R. J. (1997b). Robustness in model-based fault diagnosis: The 1995 situation. *Annual Reviews in Control,*, 21:103–123.

Pereira, G. J. and Araujo, H. X. D. (2004). Robust output feedback controller design via genetic algorithms and lmis: The mixed h_2/h_∞ problem. In *Proceedings of the 2004 American Control Conference (AAC)*, volume 4, pages 3309–3314.

Pollard, M. G. (1984). Maglev - a british first at birmingham. *The Institute of Physics*, 15:61–72.

Postlethwaite, I., Tsai, M. C., and Gu, D. W. (1990). Weighting function selection in h_∞ design. In *IFAC Symposia Series - Proceedings of a Triennial World Congress*, volume 3, pages 127–132.

Rohloff, K. R., Khuller, S., and Kortsarz, G. (2006). Approximating the minimal sensor selection for supervisory control. *Discrete Event Dynamic Systems: Theory and Applications*, 16(1):143–170.

Schaffer, J. D. (1985). Multiple objective optimization with vector evaluated genetic algorithms. In *Proceedings of the 1st International Conference on Genetic Algorithms*, pages 93–100.

Seron, M. M., Zhuo, X. W., Dona, J. A. D., and Martinez, J. J. (2008). Multisensor switching control strategy with fault tolerance guarantees. *Automatica*, 44(1):88–97.

Shin, J. Y. and Belcastro, C. M. (2006). Performance analysis on fault tolerant control system. *IEEE Transactions on Control Systems Technology*, 14(5):920–925.

Sinha, P. K. and Pechev, A. N. (2004). Nonlinear h_∞ controllers for electromagnetic suspension systems. *IEEE Transactions on Automatic Control*, 49(4):563–568.

Skogestad, S. and Postlethwaite, I. (2005). *Multivariable Feedback Control Analysis and Design*. John Wiley and Sons,Ltd.

Srinivas, N. and Deb, K. (1994). Multiobjective optimization using nondominated sorting in genetic algorithms. *Journal of Evolutionary Computation*. 2(3):221-248.

Sun, C. C., Chung, H. Y., and Chang, W. J. (2003). Ga-based robust h_2 controller design approach for active suspension systems. In *Proceedings of IEEE International Conference on Robotics and Automation*, volume 2, pages 2330–2335.

Sung, H. K., Lee, S. H., and Bien, Z. (2005). Design and implementation of a fault tolerant controller for ems systems. *Mechatronics,*, 15(10):1253–1272.

Venkatasubramanian, V., Rengaswamy, R., and Kavuri, S. N. (2003a). A review of process fault detection and diagnosis part ii: Qualitative models and search strategies. *Computers and Chemical Engineering*, 27(3):313–326.

Venkatasubramanian, V., Rengaswamy, R., Kavuri, S. N., and Yin, K. (2003b). A review of process fault detection and diagnosis part iii: Process history based methods. *Computers and Chemical Engineering*, 27(3):327–346.

Venkatasubramanian, V., Rengaswamy, R., Yin, K., and Kavuri, S. N. (2003c). A review of process fault detection and diagnosis part i: Quantitative model-based methods. *Computers and Chemical Engineering*, 27(3):293–311.

Vidyasagar, M. (1985). *Control system synthesis - a coprime factorisation aproach*. MIT Press.

Wai, R.-J., Lee, J.-D., and Liao, C.-C. (2005). Model-free control design for hybrid magnetic levitation system. In *The 14th IEEE International Conference on Fuzzy Systems, FUZZ '05.*, pages 933–938.

Wal, M. V. D. and Jager, B. D. (1996). Selection of sensors and actuators for an active suspension control problem. In *Proceedings of the 1996 IEEE International Conference on Control Applications*, pages 55–60.

Wal, M. V. D. and Jager, B. D. (1998). Input/output selection for robust control. In *UKACC Internetional Conference on Control*, pages 1023–1028.

Wal, M. V. D. and Jager, B. D. (2001). A review of methods for input/output selection. *Automatica*, 37(4):487–510.

Wal, M. V. D., Philips, P., and Jager, B. D. (1998). Actuator and sensor selection for an active vehicle suspension aimed at robust performance. *International Journal of Control*, 70(5):703–720.

Wal, M. V. D., Willems, F., and Jager, B. D. (2002). Selection of actuators and sensors for surge control. *Journal of Propulsion and Power*, 18(1):84–92.

Wang, Q., Spronck, P., and Tracht, R. (2003). An overview of genetic algorithms applied to control engineering problems. In *International*

Conference on Machine Learning and Cybernetics, volume 3, pages 1651–1656.

Wu, N. E. (2001a). Reliability of fault tolerant control systems: Part i. In *Proceedings of the 40th IEEE Conference on Decision and Control*, volume 2, pages 1460–1465.

Wu, N. E. (2001b). Reliability of fault tolerant control systems: Part ii. In *Proceedings of the 40th IEEE Conference on Decision and Control*, volume 2, pages 1466–1471.

Wu, N. E., Thavamani, S., Zhang, Y., and Blanke, M. (2006). Sensor fault masking of a ship propulsion system. *Control Engineering Practice*, 14(11):1337–1345.

Yan, L. (2004). Suggestion for selection of maglev option for beijing-shanghai high-speed line. *IEEE Transactions on Applied Superconductivity*, 14(2):936–939.

Yang, C. D., Tai, H. C., and Lee, C. C. (1994). Systematic approach to selecting h_∞ weighting functions for dc servos. In *Proceedings of the 33rd IEEE Conference on Decision and Control*, volume 2, pages 1080–1085.

Zames, G. (1981). Feedback and optimal sensitivity: Model reference transformations, multiplicative seminorms, and approximate inverses. *IEEE Transactions on Automatic Control*, 26(2):301–320.

Zamzuri, H. (2008). Intelligent model-based robust control for tilting railway vahicles. PhD Thesis, Loughborough University (UK), Department of Electronic and Electrical Engineering.

Zhao, F. and Thornton, R. (1992). Automatic design of a maglev controller in state space. In *Proceedings of the* 31^{st} *IEEE Conference on Decision and Control*, volume 3, pages 2562–2567.

Zhenyu, Y. and Pedersen, G. (2006). Automatic tuning of pid controller for a 1-d levitation system using a genetic algorithm - a real case study. In *IEEE International Symposium on Intelligent Control*, pages 3098–3103.

Zhou, K. and Doyle, J. C. (1998). *Essentials of robust control*. Prentice Hall International Editions.

Zhou, K., Doyle, J. C., and Glover, K. (1996). *Robust and Optimal Control*. Prentice Hall.

Zitzler, E., Deb, K., and Thiele, L. (2000). Comparison of multiobjective evolutionary algorithms: Empirical results. *Evolutionary Computation*, 8(2):173–195.

Zolotas, A. C. (2002). Advanced control strategies for tilting trains. PhD Thesis, Loughborough University (UK), Department of Electronic and Electrical Engineering.

Zou, X., Chen, Y., Liu, M., and Kang, L. (2008). A new evolutionary algorithm for solving many-objective optimization problems. *Systems, Man, and Cybernetics, Part B: Cybernetics, IEEE Transactions on*, 38; 38(5):1402–1412.

Please note: All URLs included in this thesis were operational when this thesis was produced. The author accepts no responsibility in case any of the referenced URLs does not either operate properly or for some reason its operation is terminated in the future.

Appendices